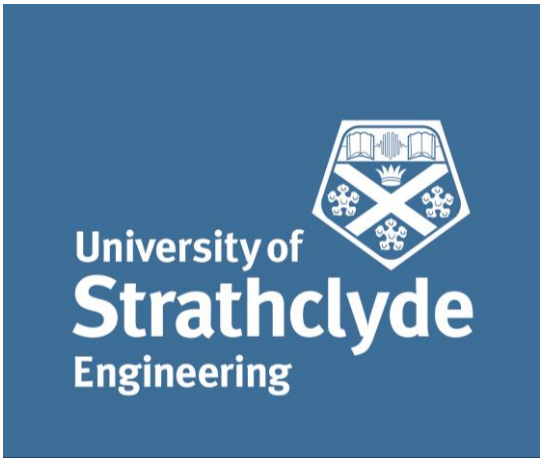

Atmospheric Non-Thermal Plasma Discharges for Cleaning And Bio-Decontamination

SIRUI LI，BEng (Hons), MSc

Thesis submitted in accordance with the requirements of the University of Strathclyde for the degree of

Doctor of Philosophy 2016

Department of Electronic and Electrical Engineering
University of Strathclyde
Glasgow, UK

DECLARATION OF AUTHENTICITY AND AUTHOR'S RIGHTS

This thesis is the result of the author's original research. It has been composed by the author and has not been previously submitted for examination which has led to the award of a degree.

Signed:

Date:

ACKNOWLEDGEMENT

First, I would like to thank my family, especially my parents and my wife for their unconditional support.

Special thanks to my supervisor Dr. Igor Timoshkin, also Dr. Michelle Maclean, Dr. Tao Wang and all the amazing people in Strathclyde HVT group.

Last but not the least, I would like to thank my baby daughter Yujia, who will read this thesis someday.

ABSTRACT

It has been shown that non-thermal plasma has great potential for chemical oxidation and bacterial inactivation. However, the mechanism of plasma-induced oxidation and bactericidal effects is not fully understood, and optimisation of the non-thermal plasma treatment is required to improve the efficiency of this technology.

This research presents an investigation into the oxidation and bio-decontamination capabilities of steady-state corona discharges and impulsive transient plasma discharges in atmospheric air. Degree of decolorisation of blue dye by plasma discharges was obtained and used for evaluation of the oxidation efficiency of these discharges. The Gram-positive and Gram-negative bacteria, *Staphylococcus aureus* and *Escherichia coli,* respectively, were used for investigation of the bio-decontamination capability of the plasma discharges. It has been shown that conditions such as air humidity, electrode topology, and voltage levels may affect the efficiency of plasma treatment. The obtained results show that the oxidation and inactivation effects depend on the amount of charge delivered by the plasma. The charge-dependent decolorisation and inactivation rates of plasma discharge treatment, which indicate the oxidation efficiency and inactivation efficiency, were obtained and analysed. Different decolorisation and inactivation rates were achieved with various electrode topologies and energisation polarities.

This study also investigated the production of reactive species by atmospheric plasma discharges. Ozone concentration was measured during the decolorisation and inactivation tests. The production of OH radicals by the plasma discharges have also been obtained in this study using terephthalic acid as the chemical probe. The obtained results confirm that the reactive oxygen species play a major role in the plasma discharge treatment. In addition, an attempt of using TiO_2 as a catalyst to enhance oxidation and bio-decontamination effects of the plasma discharge treatment has been made. TiO_2 was revealed to have the potential to improve the oxidation efficiency of atmospheric plasma discharges.

The results obtained and presented in this thesis will help in optimisation of non-thermal plasma systems for chemical and biological decontamination.

PUBLICATIONS

Journal Papers:

[1] S. Li, I. V Timoshkin, M. Maclean, S. J. Macgregor, M. P. Wilson, M. J. Given, J. G. Anderson, and T. Wang, "Steady-State Corona Discharges in Atmospheric Air for Cleaning and Decontamination," IEEE Trans. Plasma Sci., vol. 41, no. 10, pp. 2871–2878, 2013.

[2] S. Li, I. V Timoshkin, M. Maclean, S. J. Macgregor, M. P. Wilson, and M. J. Given, "Fluorescence Detection of Hydroxyl Radicals in Water Produced by Atmospheric Pulsed Discharges," IEEE Trans. Dielectr. Electr. Insul., vol. 22, no. 4, pp. 1856–1865, 2015.

[3] S. Li, I. V Timoshkin, M. Maclean, S. J. Macgregor, M. P. Wilson, M. J. Given, J. G. Anderson, and T. Wang, "Oxidation and Bio-decontamination Effects of Impulsive Discharges in Atmospheric Air," IEEE Trans. Plasma Sci., vol. PP, no. 99, pp. 1–11, 2016.

Conference Papers

[4] S. Li, I. V Timoshkin, M. Maclean, S. J. Macgregor, M. P. Wilson, M. J. Given, J. G. Anderson, T. Wang, and C. Mcgarvey, "Impulsive Streamer Discharges in Atmospheric Air for Cleaning and Decontamination," in IEEE Pulsed Power Conference, 2015, pp. 1–4.

[5] S. Li, I. V Timoshkin, M. Maclean, S. J. Macgregor, M. P. Wilson, M. J. G. T. Wang, and J. G. Anderson, "Direct and Indirect Steady-State Corona Discharges for Cleaning and Decontamination," in 4th Euro-Asian Pulsed Power Conference, 2012, pp. 1–4.

Presentations

[6] S. Li, I. V Timoshkin, M. Maclean, S. J. Macgregor, J. G. Anderson, M. P. Wilson, M. J. Given, and T. Wang, "Corona Discharges in Air for Microbial

Decontamination," accepted for oral presention at 2012 Technological Plasma Workshop, 2012.

[7] S. Li, I. Timoshkin, M. Maclean, M. Wilson, M. Given, S. Macgregor, T. Wang, and J. Anderson, "Investigation on OH Production of Pulsed Streamer Discharges in Ambient Air Targeting Liquid Surface," accepted for post presention at 12th UK Technological Plasma Workshop, 2014.

LIST OF SYMBOLS

Symbol	Definition
T_e	Temperature of electron
T_i	Temperature of ions
T_0	Temperature of neutral particles
K_B	Boltzmann constant
E_0	External electric field
E'	Localised electric field caused by space charge
α	Townsend primary ionisation coefficients
γ	Townsend secondary ionisation coefficients
β	Electron attachment coefficient
V_{cr}	Critical corona ignition voltage
U_{TS}	Breakdown voltage
U_0	Output voltage from the power supply
T_t	Period of the transient spark pulses
R_{cl}	28 MΩ current limiting resistor
R_{cv}	1 kΩ current viewing resistor
$T\%$	Differential transmittance
T_a, T_b	Transmittance of sample A and B
ε	Molar absorptivity of the media
c	Molar concentration of the media
ℓ	Depth of the media
c_u, c_t	Concentration of dye for sample solutions untreated/treated by plasma
$c_{0,}$	Initial molar concentration of dye

$T_{0,}\ T_t$	Measured transmittance of untreated/treated sample solution
$K(D)$	Normalized concentration of dye
$C_t(D)$	Actual concentration of the dye in water
D	Total delivered charge
μ	Rate of the decolorisation process
S	Normalised bacterial population
P_n	Survived bacteria population
P_0	Initial population of bacteria
N_n	Number of bacteria colonies on the plasma treated sample plate
N_0	Number of bacteria colonies on the control plates
$S(D)$	Charge-dependent normalised population
λ	Rate of the inactivation process
H	Concentration of HTA
Y	Integral intensity of fluorescence signal
C_{OH}	Concentration of OH radicals
γ	Production rate of OH radicals
ΔP	Change of blue value in the sample area
$B_{SB,}\ B_{SA}$	Average blue value of the sample area in picture B and picture A (before /after the discharge treatment)
ΔC	Change of blue value in the colour map caused by the light condition difference
$B_{cB,}\ B_{cA}$	Blue value in calibration area in picture B and picture A (before /after the discharge treatment)
ΔB	Actual change in blue value caused by the discharge treatment
M	The enhancement of decolorisation by using tio_2
$\Delta B_{T,}\ \Delta B_C$	Actual change in blue value caused by discharge treatment with and without tio_2 as catalyst

LIST OF ABBREVIATIONS

HV	High Voltage
TS	Transient Spark
PBS	Phosphate Buffered Saline
ROS	Reactive Oxygen Species
RNS	Reactive Nitrogen Species
OES	Optical Emission Spectroscopy
UV-VIS	Ultraviolet-Visible
DBD	Dielectric Barrier Discharge
TBARS	Thiobarbituric Acid Reactive Substances
RH	Relative Humidity
SOD	Superoxide Dismutase
PVC	Polyvinyl Chloride
AOPs	Advanced Oxidation Processes
E. coli	*Escherichia coli*
NCTC	National Collection of Type Cultures
CFU	Colony-Forming Units
S. aureus	*Staphylococcus aureus*
TA	Terephthalic Acid
HTA	2-Hydroxyterephthalic Acid
HPLC	High-Performance Liquid Chromatography
CVP	Chemical Vapour Deposition
PECVP	Plasma Enhanced Chemical Vapour Deposition
MSW	Municipal Solid Waste

CBW	Chemical and Biological Warfare
APPJ	Atmospheric Pressure Plasma Jet
nsPEF	Nanosecond Pulsed Electric Field
ACDAP	Afterglow Corona Discharge Air Plasma
TiO_2	Titanium Dioxide

CONTENT

CHAPTER 1

Introduction

Plasma, as the fourth state of matter, has been studied over many decades. Generally, plasma refers to a partial or fully ionizioniseded gas which consists of ions (positively or negatively charged), electrons, and neutrals. Plasmas are usually categorised into two major groups: thermal plasma and non-thermal plasma. In the case of thermal plasma, thermal equilibrium or near equilibrium can be formed between electrons, ions, and neutrals. Generation of thermal plasma typically is associated with thermal ionization and Joule heating. Thermal plasma can be used in several practical applications, including reduction of environmental pollution by the destruction of toxic substances, and thermal (municipal) treatment of industry wastes (plasma gasification). However, the high temperature of thermal plasma may be undesirable in many situations. In addition, the maintenance of thermal plasma systems and energy costs is generally quite high. Alternatively, non-thermal plasmas are generated through ionization processes which deliver energy primarily to the energetic electrons instead of heating up the gas. This type of plasma also can be applied in heat-sensitive situations, and the maintenance cost is low. Therefore, non-thermal plasma has attracted significant attention in recent years.

The non-thermal plasma generated by electrical discharges in atmospheric air has been investigated by many researchers worldwide, and its cleaning and decontamination effects have been confirmed in various published papers such as [1]-[4]. As a result, a number of practical applications of non-thermal plasma are now being developed, including non-thermal plasma discharges for gas treatment, water purification, bio-decontamination, and wound healing [5], [6]. Although the great potential of non-thermal plasma technology has been proved, the exact mechanisms of the chemical and microbiological effects of atmospheric plasma discharges still are not fully understood. It is believed that plasma agents generated by atmospheric discharges such as chemically reactive species, UV radiation, and intensive electric fields make a significant contribution to those processes. The reactive chemical species generated by plasma discharges are considered the most important plasma agents. Species such as OH radicals, ozone, hydrogen peroxide, singlet oxygen, nitric dioxide, peroxynitrites, and many others have been detected and studied in multiple

papers including [7]–[10]. Different types of plasma discharges or even different discharge conditions can result in varying rates of production of these chemically active species and, thus, can result in a different degree of chemical or anti-microbial activity. For further development of practical applications of the non-thermal plasma discharges, it is necessary to investigate the oxidation and microbiological decontamination efficacy of different types of discharges and their dependency on discharge parameters, such as the magnitude and polarity of the applied voltage, the charge delivered during the plasma treatment, and the discharge topologies.

The present research project is aimed at the investigation of the oxidation and microbiological decontamination efficacy of atmospheric steady-state and impulsive plasma discharges. Two important types of atmospheric non-thermal plasma discharges that are commonly used are steady-state corona discharges and transient plasma discharges. The main objectives of this project are to

- Investigate oxidation and decontamination efficacy of the steady-state corona discharges and transient plasma discharges
- Investigate the difference in oxidation and decontamination efficacy caused by discharge parameters
- Investigate the production of reactive oxygen species with high redox potential (ozone and hydroxyl radicals) and their relation to oxidation and bio-decontamination effects of plasma
- Provide analysis and discussion on the optimisation of non-thermal plasma discharge technology

Factors that affect the oxidation and decontamination efficacy of atmospheric plasma discharge were studied in this research project. These factors include the discharge topologies and the total charge delivered by the discharge. It is believed that ozone and hydroxyl radicals play a dominant role in the process of oxidation and decontamination. The production of ozone and hydroxyl radicals is directly related to the plasma bio-decontamination and oxidation efficacy. However, the contribution of other species cannot be ruled out. Another important approach which was investigated in this research is to use TiO_2 to enhance the oxidation and decontamination effects of atmospheric plasma discharges. Preliminary tests demonstrated potential enhancement

effects which depend on the way TiO_2 is introduced into the plasma treatment system in practical situations.

A brief description for each thesis chapter is provided in the following paragraphs：

Chapter 2 ("Background and Literature Review") provides background information on the non-thermal plasma discharges and their use for surface cleaning and bio-decontamination. Electrical properties of corona discharges and transient spark discharges are discussed in this chapter along with their chemical and bio-decontamination effects. Generation of important reactive chemicals and possible mechanisms of bacterial inactivation are also presented.

Chapter 3 ("Development of Steady-State and Transient Plasma Treatment Systems") describes the development of plasma systems and equipment used in this research project. The plasma systems developed and used in this project include a DC steady-state corona discharge system and an impulsive transient plasma discharge system. Experimental conditions are presented, and the topologies of plasma reactors are discussed. The results of electrostatic simulations of the electric field in the plasma reactors and electrical characteristics of both types of discharges are also presented.

Chapter 4 ("Oxidation Capability of Atmospheric Non-Thermal Plasma Discharges") presents the experimental study of chemical oxidation capability of atmospheric plasma discharges. In this study, indigo carmine was used as an indicator to investigate the oxidation capability of both steady-state corona discharge and transient plasma discharge under different conditions (polarity, voltage level, humidity, and reactor topology). Decolorisation rates of indigo carmine solutions were evaluated in plasma reactors with different electrode topologies. The results of this experiment were analysed and are discussed in this chapter to present information on optimisation of the plasma systems.

Chapter 5 ("Bio-Decontamination Capability of Atmospheric Non-Thermal Plasma Discharges") presents an experimental study of bio-decontamination efficiency of steady-state corona discharges and transient plasma discharges. *E. coli* and *S. aureus* were used as test bacteria and were inactivated by both types of discharges under different conditions. The obtained results are presented in this chapter along with their

analysis and discussion. The mechanisms of plasma-induced bactericidal effects and their efficiency are discussed.

Chapter 6 ("OH Radicals Produced by Atmospheric Non-Thermal Plasma Discharges") describes experimental work on the detection of OH radicals produced by plasma discharges. Terephtalic (TA) acid was used as a sensor to detect OH radicals and to produce HTA acid, which gives the fluorescence signal. Thus, concentration of OH radicals produced by plasma discharges can be obtained. The concentration of OH radicals generated by both types of discharges under different conditions was detected, and results are discussed in this chapter.

Chapter 7 ("TiO_2 as A Potential Catalyst for Improving The Efficiency of Non-Thermal Plasma Treatment") presents several attempts of using TiO_2 as a catalyst to enhance the decolorisation and bio-decontamination effects of the plasma discharges. A six-needle corona discharge reactor was used to generate plasma discharges. Different approaches of introducing TiO_2 into the plasma discharge treatment system were tested, and results are presented and discussed.

Chapter 8 ("Conclusion and future work") summarises the results and achievement of this research project. The bio-decontamination and oxidation capabilities of the steady-state corona and transient plasma discharges under different conditions are analysed. OH radical production is also discussed to provide insight into the mechanisms of plasma-induced chemical and biological effects. The obtained results and analysis from each chapter are combined in this chapter to provide information and discussion on optimisation of plasma discharge treatment systems. Recommendations for future work are also provided.

CHAPTER 2

Background and Literature Review

2.1 General

In this chapter, a background study and a comprehensive literature review on chemical and bio-decontamination effects of non-thermal plasma discharges has been conducted. Fundamentals and principles of plasma are described, and related theories and applications are presented to provide theoretical support for the research of oxidation and decontamination effects of non-thermal plasma discharges. The following topics are included in this review:

- Plasma basics
- Atmospheric pressure non-thermal plasma discharges
- Chemical effect of non-thermal plasma
- Bactericidal effect of non-thermal plasma

Practical applications of the non-thermal plasma discharges, including plasma catalytic processes, are also discussed.

2.2 Basics of Plasma

2.2.1 What is plasma?

The term “plasma” was first used by Noble prize winning chemist Irving Langmuir to describe ionised gas in 1927 [11]. The matter in our universe is classified into four states: solid, liquid, gas, and plasma. It is known that the bonding force which holds the particles together is different in solid, liquid, and gas states (solid>liquid>gas). The random kinetic energy of the atoms or molecules and the bonding energy determine which state the matter has. If sufficient energy is provided, for example through heating of solid or liquid substances, the kinetic energy of atoms and molecules increases, atoms and molecules overcome the bonding force, and phase

transition will occur. In the case of a substance in the gas phase, when enough energy is provided (for example, by heating up the gas), the kinetic energy will exceed the molecular bonding potential energy and result in dissociation of gas molecules. Furthermore, if the kinetic energy in an atomic gas increases to a level that overcomes the bonding force of orbital electrons, ionised gas or plasma is formed.

Plasma refers to fully ionised or partially ionised gases. The ionisation degree of plasma can vary from very low value (for example 10^{-4} to 10^{-6}, partially ionised) to 1 (fully ionized) [12]. Typically, plasmas are electrically neutral, and they consist of ions (positively or negatively charged), electrons, and neutrals. The visible universe is mostly in plasma form; examples include the sun, interstellar medium, and solar wind. Plasmas are also very common on earth: polar auroras, flames, and lightning are all plasmas. With modern technology, artificial plasmas are commonly created and used in multiple practical applications including bio-decontamination and chemical oxidation such as in [13] and [14].

2.2.2 Plasma Temperature

The temperature of plasma is described by the temperatures of each particle, including electron temperature T_e, ion temperature T_i, and temperature of neutral particles T_0. Assuming that plasma is an ideal gas, the average kinetic energy of a particle can be written as in (2.1) based on the Maxwell-Boltzmann distribution:

$$E = \frac{3}{2} K_B T \qquad (2.1)$$

where K_B is the Boltzmann constant $1.38 \cdot 10^{-23}$ J/k.

Generally, for ionising molecules, the energy required is greater than ~10 eV. It is also very common to use $K_B T$ to express temperature in an energy unit of eV, which indicates the energy acquired by an electron through a potential change V, $eV = K_B T$.

Hence, 1 eV equals a temperature of 11,600 K. Examples of plasmas with different electron temperatures and densities are shown in Figure 2.1.

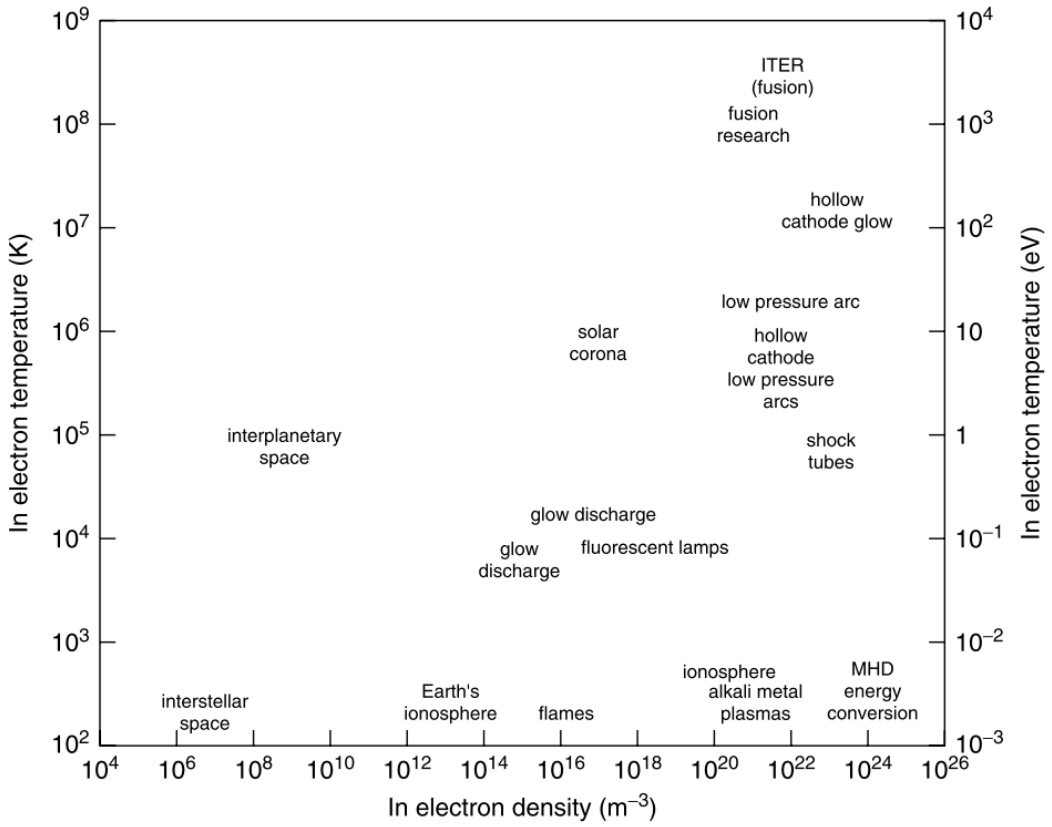

Figure 2.1. Plasmas with different electron temperatures and densities (graph from [15]).

2.2.3 Classification of Plasmas

In laboratory research, plasmas generally are classified into two major categories: equilibrium plasma and non-equilibrium plasma. Equilibrium plasma, also known as thermal plasma, typically has a high temperature that results in thermal equilibrium. The species (ions, electrons, and neutrals) in this type of plasma have the same temperature $T_e \approx T_i \approx T_0$. Thermal equilibrium could be formed in a localised area. In non-equilibrium (or non-thermal) plasma, electrons have a much higher temperature, $T_e >> T_i \approx T_0$, and thermal equilibrium is not formed. Based on the electron

temperature, plasmas can also be further classified into cold plasma ($T_e \leq 10^5$ K) and high-temperature plasma ($T_e > 10^6$ K) [15], [16]. Many other types of plasma classifications exist. They are based on parameters other than temperature, such as ionisation degree and gas temperature. In this thesis, research was focused on non-thermal atmospheric plasma which was generated by high-voltage discharges in ambient and bottled air.

2.3 Non-Thermal Atmospheric Plasma Discharges

2.3.1 Introduction

As mentioned in Section 2.2.3, plasmas are typically categorised into two major types: thermal plasma and non-thermal plasma. Each of these types has its features and can be used for practical applications. In the case of thermal plasma, thermal equilibrium or near equilibrium can be formed between electrons, ions, and neutrals. Thermal, fully ionised plasma is hot (10s of thousands of degrees K) and difficult to control. Despite this characteristic, thermal plasma can be applied to many areas, such as material processing [17], solid waste treatment [18], and many others [19]. However, the high temperature of thermal plasma may be undesirable in many situations. In addition, the costs of energy and the maintenance of thermal plasma systems are generally quite high.

Alternatively, non-thermal plasmas are generated through ionisation processes which deliver energy primarily to the energetic electrons instead of heating up the gas. Those energetic electrons with high electron temperature $T_e \approx 10^4 \sim 10^5$ K can produce radicals, ions, and electrons by impact with gas molecules. Chemically active species produced in this way can degrade organic molecules and kill microorganisms, resulting in oxidation, cleaning, and bio-decontamination effects. The temperatures of ions and neutrals are low (close to room temperature in most cases). Therefore, non-thermal plasma discharge could be applied to heat-sensitive material such as

biological tissues and polymers. Additionally, the maintenance and energy cost of non-thermal plasmas are much lower compared with those of thermal plasmas.

Electric discharges in air are one of the most common ways to generate non-thermal plasma. As reported in [12], various chemical non-equilibrium conditions can be achieved by modifying the discharge parameters such as gas content, electrode configuration, and pressure. Therefore, gas discharge plasma is considered highly potential in many environmental applications. In this research, non-thermal plasmas generated by atmospheric discharges were investigated.

2.3.2 Ionisation and Charged Particles

Gases in a non-ionised state and under normal environmental conditions (temperature, pressure) are electrical insulators. Gas molecules are electrically neutral. Charged particles in gases are generated through ionisation, and this process may involve the collision of species and photoionization. Atoms can be excited and transferred into an excited state after receiving energy through absorption of a photon or collision with electrons or other energetic particles. When enough energy is provided to an atom (amount equal to the electron bond energy), the electron will no longer be bound to the atom and will separate from the atom. Thus, this atom will be ionised. The minimum energy which is required to release an electron from an atom is called the ionisation potential. For different atoms and molecules, the ionization potentials are different: for example, 13.6 eV for H, 12.07 eV for O_2, 13.77 eV for CO_2, 14.5 eV for N, and 15.6 eV for N_2 [20].

Charged particles and free electrons can also return to neutral atoms or molecules through recombination. The main mechanisms of ionisation and recombination can be written in the following equations:

$$A + e \leftrightarrow A^+ + e + e \tag{2.2}$$

$$A + B \leftrightarrow A^+ + e + B \tag{2.3}$$

$$A + h\nu \leftrightarrow A^{+} + e \quad (2.4)$$

where A and B represent neutral atoms or molecules. These equations describe ionization by (2.2) electron collision with neutral species; (2.3) neutral species colliding with each other; and (2.4) photoionization.

Ionisation occurs not only with ground state neutral species, but also with excited atoms and metastable particles, which can be ionised or de-activated through the impact of other particles such as electrons and neutrals. Excited atoms take less energy to be ionised compared with ground state atoms. Reactions caused by collisions of metastable species and neutrals can be written as:

Penning dissociation: $M^{*} + C_2 \rightarrow 2C + M$ (2.5)

Penning ionisation: $M^{*} + A \rightarrow A^{*} + M + e$ (2.6)

where M^{*} are metastable particles, and C_2 represents neutral molecules such as O_2 and N_2.

In addition, negative ions can be produced through another reaction which is caused by attaching electrons to heavy molecules. These attachment reactions are shown in (2.7) and (2.8):

Dissociative attachment: $C_2 + e \rightarrow C^{-} + C$ (2.7)

Triple collision attachment: $C_2 + e \rightarrow C_2^{-}$ (2.8)

As discussed in [21], other reactions can take place in the non-thermal plasma environment:

Charge exchange: $A^+ + B \rightarrow B^+ + A$ (2.9)

Ion-ion recombination: $A^+ + B^- + M \rightarrow AB + M$ (2.10)

Generation and disappearance of the charged particles are important events in the mechanism of gas discharges, and the reactions between species also result in the production of chemically reactive species which directly and indirectly work on pollutants and bacteria.

2.3.3 Plasma Streamers

A plasma streamer is a form of transient discharge event which is developed from an electron avalanche in dielectric media. The concept of streamer was introduced by Raether, Meek, and Loed around 1940 to describe the electric breakdown phenomenon in gas [22]. The formation of the streamer is based on the distortion effect of space charges created during electron avalanches. Under the effect of an applied external electric field, gas molecules are ionised, and the electron avalanche occurs. The numbers of electrons and positive ions increase exponentially in the process of electron avalanche. Due to the difference in mobility, electrons move to the anode with a higher speed, while positive ions move to the cathode slowly. Electrons are accumulated in the front area, and the positive ion zone is in the “tail” part, creating additional localised electric fields. Therefore, distortion of the electric field occurs due to the existence of space charges. An example is shown in Figure 2.2; the electric field is enhanced near the head (electron zone) and tail (positive ion zone) of the avalanche; while inside the avalanche, the electric field is reduced.

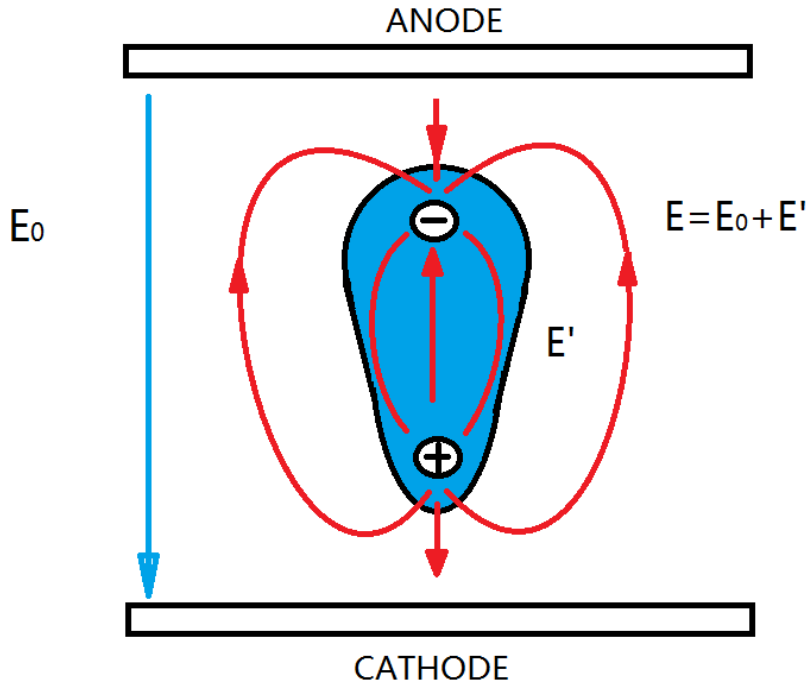

Figure 2.2. Distortion to the electric field caused by the effect of space charges. E_0 is the external electric field; E' is the localised electric field caused by space charges.

When the primary electron avalanche is not very strong, the number of electrons in the avalanche head is less than 10^{18}-10^{20}, and the concentration of charge is not sufficient to distort the electric field between the electrodes. In this case, the avalanche ends after it propagates through the gap (electrons reach the anode and ions reach the cathode). When the primary electron avalanche is strong, the number of electrons in the head is $>10^{20}$, and space charges can create an intensive localised electric field, E'. Under the effect of this localised electric field, the growth of further avalanches is enhanced in a direction conditioned by the external electric field. As a result, an ionised, thin conductive region propagates in that direction, forming single or multiple discharge channels as "the streamers". The densities of electrons and ions are roughly the same in the ionised streamer channel, and the external electric field is screened by the thin space charge layer. In the area in front of the streamer head, an electric field is enhanced by the space charge.

Streamers are categorised as positive streamers or negative streamers. Streamers which grow from the anode to the cathode are known as the cathode-directed streamers or positive streamers. The negative streamers (anode-directed streamers)

move in the direction of electron drift (from cathode to anode), as shown in Figure 2.3.

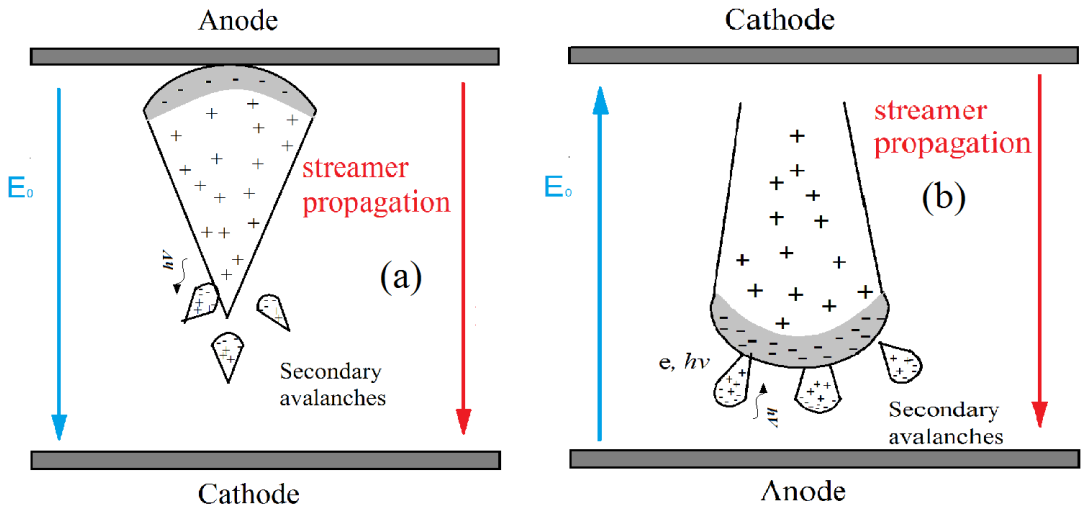

Figure 2.3. Positive streamers (left) and negative streamers (right) propagate in the gap.

In the case of negative streamers, photons emitted from the primary avalanche generate electrons in the area near the head of the primary avalanche, and those electrons (together with electrons from the primary avalanche that are moving in front of the primary avalanche head) would start secondary avalanches under the effect of a strong electric field. Tails of secondary avalanches (positive ions) then will be neutralised by the head of the primary avalanche (electrons).

In the case of positive streamers, photons emitted from the primary avalanche generate electrons which may cause many secondary avalanches in the area near the tail of the primary avalanche, where the electric field is enhanced. Electrons from secondary avalanches are then pulled into the tail of the primary avalanche and create a quasi-neutral plasma channel. The streamer propagates from the anode to the cathode, with a growth velocity of 10^8 cm/s [23].

A streamer is a weakly conductive and short-lived cold plasma discharge. However, when it bridges the gap between the anode and cathode, the discharge current increases significantly, and the streamer channel becomes highly conductive and thermalised. Thus, the spark channel is formed in this way.

Several differences, including diameter, length, and propagation velocity between positive and negative streamers, could be observed. In [24], Luque *et al.* used models to simulate the propagation of positive and negative streamers in ambient air in a needle-plane discharge system stressed by high voltage; the radius of the needle was 0.26 mm. They claimed that positive and negative streamers have similar behaviours when the voltage is above 60 kV, while differences in streamer behaviours were observed for voltages below 40 kV. Positive streamers are faster, longer, and thinner. Under 23 kV, positive streamers propagating through an 11.5 mm gap used ~15 ns, while negative streamers used ~25 ns. The authors explained this phenomenon: they believe that the electron drift in negative streamers does not strongly help in streamer propagation, but leads to an increase of the streamer head diameter and dilutes the field enhancement effect. In the case of positive streamers, the growth depends more on the local electric field; it is thinner, so the field is more enhanced, and positive streamers propagate faster [24]. This was supported by experimental results from another study [25] in which the propagation, formation, and diameters were compared between positive and negative streamers. In their research, the authors claimed that positive streamers are thinner and can be ignited and propagate easily, while thicker negative streamers require higher ignition voltage. Streamers were generated in ambient air at 1 bar using a pair of needle-plane electrodes with a gap length of 40 mm. It was reported that in the voltage range of 5 kV to 40 kV, positive streamers were observed. The diameter of the positive streamer head and the propagation speed increased from 0.2 mm, 10^5 m/s (at 5 kV) to 1 mm, 10^6 m/s (at 40 kV). When the voltage is increased to 40 kV, negative streamers appeared. As the voltage increased from 40 kV to 96 kV, the diameters of positive and negative streamers are similar, 1–3 mm. The propagation velocity of positive streamers increased from 10^6 m/s to $4 \cdot 10^6$ m/s, while the propagation velocity of negative streamers can only be measured above 56 kV, and is 25% lower than in the positive streamer case. The authors of this research also reported similar energy of primary streamers with positive or negative polarities (20-50 mJ). However, they also believed that the total energy delivered by the positive discharges is higher than the negative discharges.

Streamers in ambient air promote multiple reactions including excitation dissociation and ionisation. O and N based neutral molecule, positive and negative ions participate in those reactions as reported in [26]. An optical study in [7] reported the existence of

OH radicals, ozone, and NO molecules in streamer discharges. Streamer-based discharges are often considered as good sources to generate non-thermal plasma. They can provide good performance with low costs to meet the requirement of many applications such as plasma medicine [27].

2.3.4 Corona Discharge

Corona discharge is a type of self-sustained discharge which normally occurs in gas and is generated by a highly divergent, intensive electric field in areas around sharp, high-voltage (HV) electrodes. During the corona discharge, a weak, light emission of bluish color can be observed near the high-voltage electrode. The corona discharge is a common type of non-thermal plasma discharge, and it has been observed in many gases, including air at different conditions. For example, the St. Elmo's fire is a form of corona discharge which appears at the end of the mast on a ship during storms. With the development of electrical engineering, corona discharges are more widely seen in the modern world; they may appear around high-voltage transmission lines, or near lightning rods or high-power antennae.

Mechanisms of Corona Discharge

When a high voltage is applied, a highly intensive divergent electric field is generated in the area near a sharp (highly curved) electrode. If this field exceeds the critical value, electron avalanches start to develop, and the ionisation process in the high field area becomes intensive enough to generate the corona discharge. The region near the stressed electrode where the electric field is intensive and the ionisation take place is the "ionisation region". Light emission can be observed from this region. Outside the ionisation region is the "drift region". In this region, the intensity of the electric field is low, and ions or electrons generated in the ionisation region drift to opposite electrodes through the region. The ions or electrons may interact with neutral molecules, but ionisation is not caused due to insufficient energy. If the applied voltage would increase sufficiently, breakdown of the entire inter-electrode gap could happen, and corona discharge would be transformed into a spark [23].

Corona discharges can be classified as positive corona and negative corona discharges: if the sharp electrode is stressed with negative high voltage, corona discharge generated in this case is negative. Alternatively, if a positive high voltage is applied to the sharp electrode, generated corona discharge is positive. Although both types of corona discharges rely on the development of electron avalanche, the mechanisms of positive and negative corona discharges are quite different.

In the case of positive corona discharge, electrons produced by exogenous ionisation move toward the curved electrode which is positively charged. In the region where the electric field is sufficiently high, electron avalanche is then triggered. More electrons produced from ionisation move toward the curved positive electrode, while positive ions move to the flat electrode (cathode). Photons emitted from ionisation then radiate into the gas and generate electrons; those electrons move toward the curved electrode under the effect of the electric field and trigger secondary avalanches. The mechanism of positive corona discharge can be described as a cathode-directed streamer.

In the case of negative corona discharge, electrons generated from the ionisation process move away from the curved cathode, and positive ions move toward the cathode. Contrary to the positive corona case, those electrons do not contribute to further avalanches in the negative corona. However, electrons can be generated at the surface of the curved electrode by the photoelectric effect or the impact of positive ions. These electrons then start further avalanches under the effect of the intensive electric field. As the electrons move away from the curved electrode, they attach to neutral molecules and form negative ions. Those negative ions will then move to the anode.

Characteristics of Corona Discharge

Due to the different mechanisms of positive corona and negative corona discharges, the ignition conditions for these discharges are described in different ways. Fridman *et al.* discussed the ignition of corona discharge in [23] and [28]. In the case of negative corona, the ignition follows the same criterion of Townsend breakdown, as shown in (2.11):

$$\int_0^{x_{max}}[\alpha(x)-\beta(x)]dx = \ln(1+\frac{1}{\gamma}) \quad (2.11)$$

where α(x) and γ are the Townsend primary and secondary ionisation coefficients, and β (x) is the attachment coefficient.

At the position which is a distance x_{max} from the cathode, the electric field is low enough, the balance between ionization and attachment is reached, and $\alpha(x_{max}) = \beta(x_{max})$. Thus, no additional electron multiplication occurs. The critical distance x_{max} defines not only the ionization-attachment balance but also the excitation zone (i.e., the visible size of the corona discharge).

In the case of the positive corona, the process is described as the formation of the cathode-directed streamer. Therefore, the ignition process can be described by the streamer breakdown criterion (Meek breakdown criterion) as in equation (2.12):

$$\int_0^{x_{max}}[\alpha(x)-\beta(x)]dx \approx (18-20) \quad (2.12)$$

Although mechanisms of development of positive and negative corona discharges are different, the critical ignition field is only slightly higher in the positive case.

Additionally, in [23] and [28], the relationships between the corona discharge current and voltage characteristics of two parallel wires have been deduced. In a more general case with different electrode geometry, the corona discharge current and voltage have a relation as written in (2.13):

$$I = CV(V - V_{cr}) \quad (2.13)$$

where C is a constant, I is the discharge current, V is the applied voltage, and

V_{cr} is the critical corona ignition voltage.

Therefore, the power released in the corona discharges can be expressed by equation (2.14):

$$P = VI = CV^2(V - V_{cr}) \quad (2.14)$$

The power released from continuous corona discharge is limited by the low discharge current (tens or hundreds of μA in atmospheric air). However, if the applied voltage is increased, the spark channel can be formed. This becomes a problem in many applications. To increase the power delivered to the corona discharge without forming a spark, pulsed corona discharges and continuous corona discharges with pulse-periodic regimes are considered in many applications.

Pulse-Periodic Regime of Continuous Corona Discharges

As mentioned previously, corona discharge can be transformed into spark discharge if the applied voltage increases to a level that is sufficiently high. Therefore, to avoid undesirable sparks, the applied voltage level used to generate the continuous corona discharge is limited. The pulsed power supply has been used in many cases to generate corona discharges with high power while avoiding transformation into a spark [29], [30].

However, periodic current pulses can be observed even if the corona discharges are produced by a constant voltage. This pulse-periodic regime that is sustained by continuous constant voltage is known as "flashing corona" in the case of positive energisation and "Trichel pulses" in the case of negative energisation. According to [31], the frequency of flashing corona current pulses can reach up to 10^4 Hz. The frequency of Trichel pulses can reach a higher frequency, up to 10^5 to 10^6 Hz. Although increase in the voltage can still result in a transition to spark, the discharge current and power of these self-pulsing corona discharges is still limited; the pulse-periodic regime can increase power delivered by corona discharge under

constant voltage conditions. An example is given in [31], in which the author calculated the maximum power of corona discharge generated in a point-plane electrode system: the radius of the stressed sharp electrode is 3–50 μm, and the gap between electrodes is 1 cm. Results showed that the maximum corona power with the continuous regime is 0.4 W; the maximum power is much higher during the pulse-periodic regime (~3 W). Therefore, the pulse-periodic regime is crucial and must be discussed in the study of steady-state corona discharge.

Flashing Corona

In the case of positive corona discharges generated by application of DC constant voltage, flashing corona (positive current periodic pulse) is caused by the effect of positive space charge. The process can be explained briefly as follows: during positive corona discharge, a cathode-directed streamer is formed along with the generation of electrons and positive ions. Under the effect of an external electric field, electrons with a higher speed move to the anode, and their number decreases quickly. At the same time, positive ions with low speed remain in the gap. The accumulation of positive ions in the gap results in a local electric field which is in an opposite direction of the external field, and this prevents the formation of new streamers. Therefore, the positive discharge current is suppressed. Those positive ions in the gap move slowly under the effect of an external electric field and eventually reach the cathode, then the gap is cleared up, and new streamers can be formed. Periodic-pulses in discharge current appear due to the repetition of this process.

Examples of flashing corona discharge current waveforms are shown in Figure 2.4.

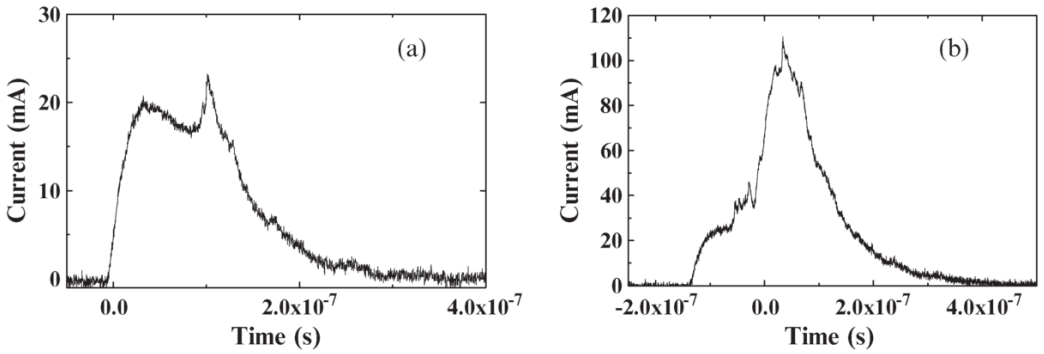

Figure 2.4. Examples of positive flashing corona discharge current waveforms, at 0.2-bar gauge pressure: (a) +22 kV, (b) +26 kV [32].

The pulses in discharge current exist when the applied voltage/electric field is in a certain range. Increasing the applied voltage would result in an increase in the electric field. Discharge current becomes stable as the electric field provides enough ability to clear up the space charge in the gap. For example, a positive corona discharge generated in a point-plane reactor is described in [33] and [31]. The radius of the stressed point electrode was 0.17 mm, and the gap distance was 3.1 cm. The observed corona ignition voltage $V_{cr} \approx 5$ kV, and the flashing corona was operated in the voltage range from the ignition voltage to $V_1 \approx 9.3$ kV. The maximum frequency of discharge current pulses was ~6.5 kHz; it was achieved at an applied voltage level in the middle of V_{cr} to V_1. The voltage was increased to $V_2 \approx 16$ kV, at which pulses in the discharge current disappeared. As the voltage further increased to $V_t \approx 29$ kV, spark discharges with a frequency of 4.5 kHz were achieved. The mean values of discharge current were 1 μA, 10 μA, and 100 μA at V_{cr}, V_1, and V_t, respectively. The regimes of positive corona discharge are shown in Figure 2.5.

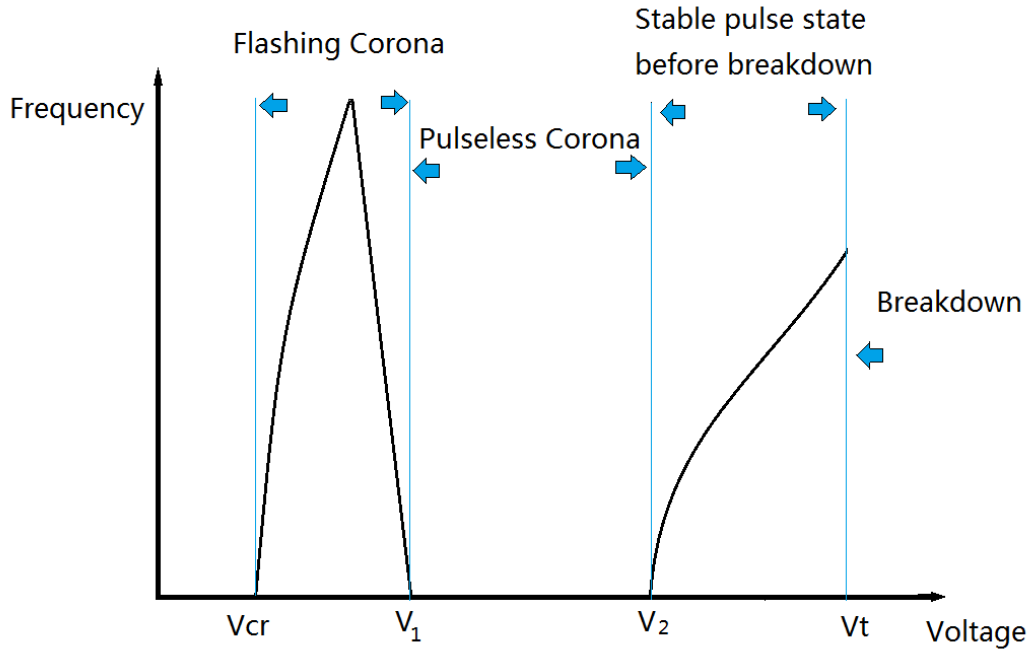

Figure 2.5. Positive corona discharge regimes with voltage and pulse frequency [33].

Trichel Pulses

Periodic pulses in discharges can also be achieved in negative corona discharges; this effect is known as "Trichel pulses". Trichel pulses are also caused by the effect of space charge. When corona discharge is ignited in electronegative gases such as air and oxygen, electrons released from ionisation can form negative ions in the gap. Under the effect of an external electric field, positive ions move to the stressed cathode, and negative ions move to the anode. Two layers are formed near the stressed electrode: a layer of positive ions close to the electrode and an outside layer of negative ions. As the number of negative ions grows, they produce a local electric field which is in the opposite direction of the external field. Therefore, the ionisation process is suppressed, and the discharge current is suppressed as a result. When the negative ions move to the anode (far from the cathode), the suppression brought by space charge effect is decreased; then, the negative corona discharge is ignited again. Periodic pulses are produced by repetition of this process [34], [35]. However, in the case of corona discharge in electropositive gases such as argon and nitrogen, electrons

can move to the anode rapidly without forming negative ions. In this case, the electric field near the cathode is not suppressed as much, and Trichel pulses are not generated [36]. Examples of discharge current waveforms with Trichel pulses are shown in Figure 2.6.

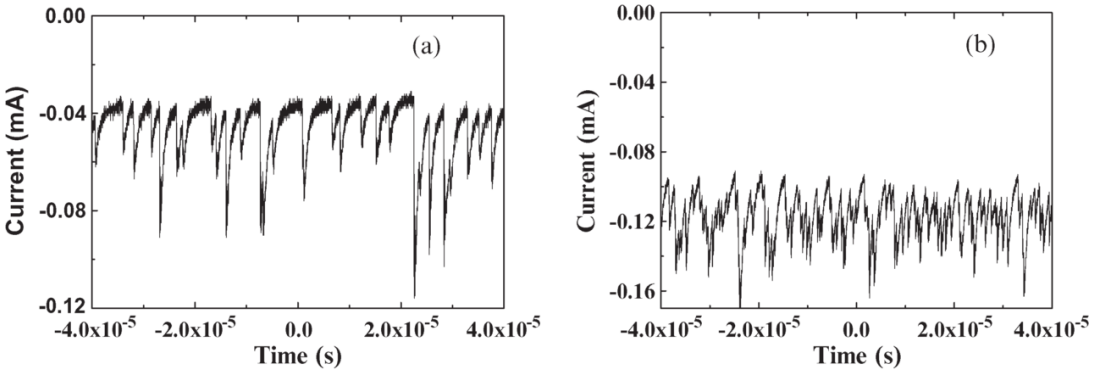

Figure 2.6. Examples of negative corona discharge current waveforms with Trichel pulses, at 0.2-bar gauge pressure: (a) +22 kV, (b) +26 kV [32].

Compared with flashing corona, Trichel pulses disappear at a high constant voltage level, and the steady-current state exists until the voltage increases to a certain level that is enough to transform the corona into a spark. An example is given in [37]: the characteristics of negative corona discharges under different regimes are shown in Figure 2.7.

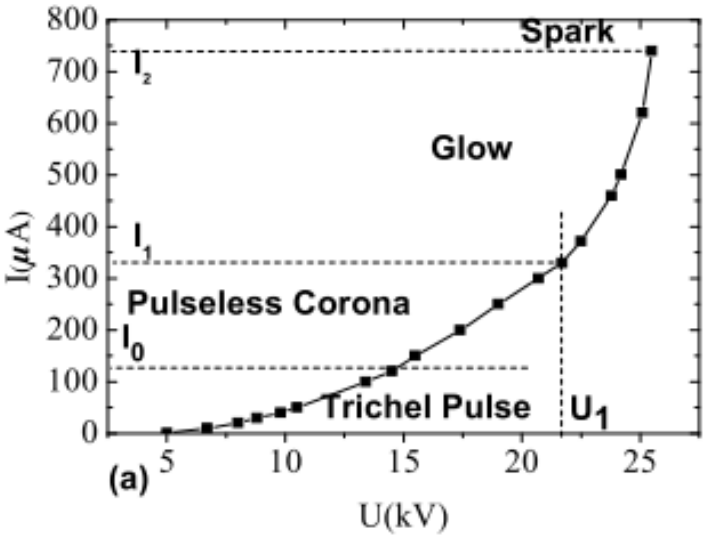

Figure 2.7. Characteristics of negative corona discharges under different regimes (graph from [37]).

As described in [37], a pair of needle-plane electrodes was supplied with a high-voltage DC power supply. The stressed needle electrode had a radius of 0.1 mm, and the distance from the tip to the plane electrode was 15 mm. The observed ignition voltage of negative corona discharge was 5 kV; the Trichel pulses in discharge current were observed immediately after the ignition. As the voltage increased, the time-averaged current and the pulse frequency increased, while the amplitude of the Trichel pulses decreased. As the voltage and time-averaged current increased to ~14.1 kV and ~120 μA, corona discharge with Trichel pulses was converted into the pulseless state, and it became glow corona with further increase of voltage and current. Finally, a spark was formed as the discharge current increased to ~740 μA. Also in [37], the author suggested that the gap distance between electrodes has less influence on the magnitude of Trichel pulses. However, by using a needle electrode with a bigger radius, a higher discharge current can be achieved before corona discharge with Trichel pulses convert into the pulseless state. In another study [38], the author believes that the frequency of Trichel pulses depends on the radius of the cathode, air pressure, and gap distance, and this frequency increases with the voltage.

Production of Reactive Species by Corona Discharges in Air

Multiple practical applications have been developed based on the corona discharges: examples include ozone generation [39], [40], removal of industrial flue gases [41], and decontaminating microorganisms [32]. These processes are based on the reactive species produced by corona discharges. Considering corona discharges in the atmospheric air, which mainly consist of nitrogen (78.09%) and oxygen (20.95%), reactions take place under the effect of electron impact, and parent species (O_2 and N_2) are transformed into reactive species. In addition, water molecules can be considered as one of the parent species if discharges are generated in humid air.

By breaking the chemical bonds in the molecules of the parent species (such as H-OH bond and O=O bond), primary chemical species are produced. These primary species include H, OH radicals, O_2^*, N_2^*, H_2O*, O, N, and positive/negative ions. Then, these primary species react with each other or with the parent species to form secondary species. The secondary species include reactive oxygen species such as O_3, OH radicals, H_2O_2, and so on. Reactive nitrogen species such as NO, NO_2, and ONOOH also are produced as secondary species. These species could react with liquid to produce H^+, NO_2^-, and NO_3^- through further reactions. This chemical production process of corona discharge in the atmospheric air has been proposed in [42] and [43]. The entire process is illustrated in Figure 2.8.

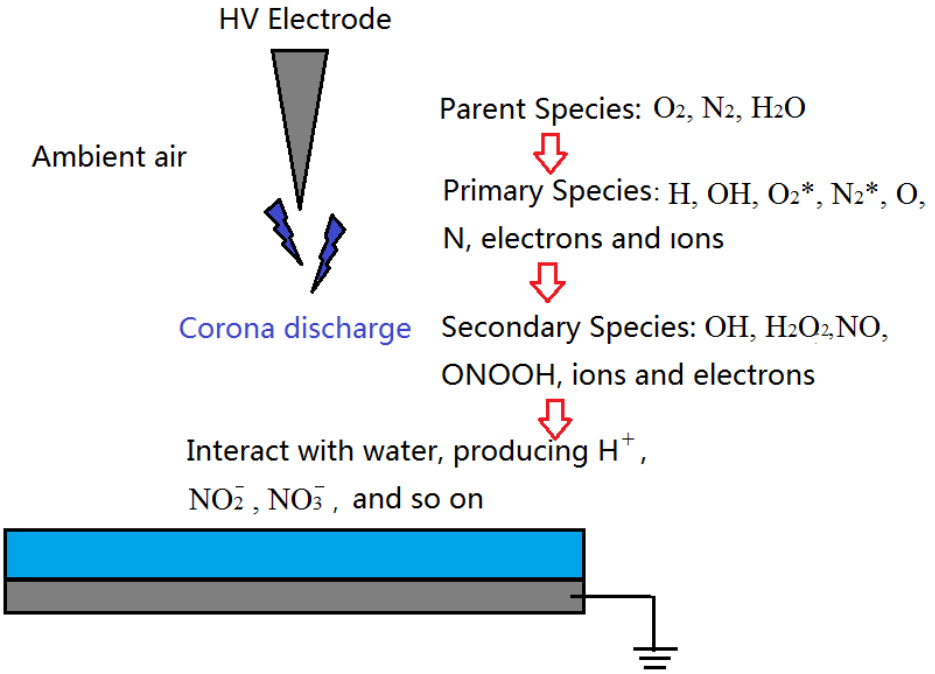

Figure 2.8. Chemical production process of corona discharge.

Evidence of reactive species production by corona discharge has been reported in many studies. For example, in studies [44], [45], the OH radical produced by corona discharge was measured using the laser-induced fluorescence technique. Ozone is considered to be the most important component among the reactive species generated by corona discharge by many studies [46], [47]. Ozone concentration was measured in [48], which showed the formation of ozone during corona discharge through the following two steps:

First, the oxygen atoms are formed by dissociation of the oxygen molecule, as shown in (2.15):

$$O_2 + e^- \rightarrow 2O + e^- \qquad (2.15)$$

Then, the atomic oxygen and oxygen molecules react with a third species to create ozone molecules:

$$O + O_2 + M \rightarrow O_3 + M \quad (2.16)$$

M refers to a third species, such as O_2 and N_2.

In the case of nitrogen molecules, bonds can be broken by electron impact to form atomic nitrogen, and atomic nitrogen and nitrogen molecules react with oxygen atoms to form NO:

$$N_2 + e^- \rightarrow 2N + e^- \quad (2.17)$$

$$N_2 + O \rightarrow NO + N \quad (2.18)$$

$$N + O \rightarrow NO \quad (2.19)$$

NO further reacts with O_2 and O_3 to form NO_2:

$$2NO + O_2 \rightarrow 2\,NO_2 \quad (2.20)$$

$$NO + O_3 \rightarrow NO_2 + O_2 \quad (2.21)$$

NO and NO_2 can be dissolved in water and trigger further reactions with H_2O and OH to produce NO_2^-, NO_3^-, and ONOOH.

Under the same discharge conditions, including the geometry of electrodes, gap length, and so on, negative and positive corona discharges have different abilities to produce reactive chemical species. Due to the differences in the mechanisms, negative corona discharge produces more energetic electrons and has a larger plasma region than positive corona discharge [49], [50]. As a result, negative corona discharge has a higher electron impact rate and produces more excited molecules. Therefore, more ozone can be produced by negative corona discharge. Chen *et al.* [40] compared models of positive corona and negative corona with experiment results that showed the dependence of discharge polarity [49], [50]. In their study, corona discharges were generated near a 100 μm-radius wire with a current per unit of I=2.55 μA/cm.

Negative corona generated plasma was reported to be 200 μm thicker than the plasma generated by positive corona discharge. Additionally, the total number of electrons in negative corona plasma was more than 50 times higher than in positive corona generated plasma. Consequently, ozone production rate in the negative corona was reported as $6.1 \cdot 10^{-3}$ mg/s-m, which was 6.6 times of the production rate in the positive corona ($9.2 \cdot 10^{-4}$ mg/s-m). This research also suggested that the ozone production rate increases with discharge current, electrode radius, and the decrease of temperature. Higher ozone production in negative corona discharge has been observed in many research. In [51] and [52], the authors reported that the ozone production rate of the negative corona is 5-8 fold as opposed to positive corona under the same condition in a wire-cylinder/plate discharge system.

The production of ozone could make a significant contribution to the chemical and bio-decontamination effect of corona discharges. However, other chemical species such as OH radicals and reactive nitrogen species can be generated by corona discharges and play a role in corona-induced oxidation and bio-decontamination reactions. Furthermore, the bio-decontamination effect of non-thermal plasma is caused by multiple agents generated in discharges; this will be discussed in a later section.

2.3.5 Transient Spark Discharge

As mentioned in the previous section discussing streamer mechanisms, once the streamers propagate through the gap and reach the opposite electrode and form a conductive plasma channel which bridges both cathode and anode, a breakdown in the gap occurs and a spark can be formed. In a spark discharge, the spark channel is thermalized, and gas typically is heated up to a high temperature (10^4 of degrees K). Considering practical environmental applications of plasma discharges in atmospheric air, high plasma temperature is not desirable. Therefore, attempts were made to avoid thermalisation of plasma in the case of the streamer-to-spark transition while maintaining a high production rate of chemically active species in the plasma.

Different approaches, including using sub-microsecond or nanosecond high-voltage pulses to generate transient plasma discharges [29], [53]–[57], using prevented-spark discharge regimes as discussed in [58], and employing dielectric barrier discharge topologies [59]–[61], have been used to achieve this goal. However, one of the most effective ways to develop transient chemically rich atmospheric pressure plasma is to use a novel type of discharge, the transient spark (TS) discharge, which is described by Machala et al. in [62] and [63].

Transient spark discharge is a type of transition discharge which is initiated by a streamer and followed by a short current pulse (~10-100 ns). Despite using a DC high-voltage stress, this discharge has a self-pulsing nature due to charging and discharging of the reactor which has an internal capacitance. High-current pulses with magnitude of ~1–10 A can be generated by the transient spark discharges with a high repetition rate of up to 20 kHz [62], [64]. As confirmed by optical emission studies [63], [65]–[67], the plasma produced by transient spark discharge is in a non-equilibrium condition. At a 1 kHz pulse frequency, it is reported that the gas temperature and rotational temperature is 550 ± 100 K, while the vibrational temperature is much higher than 3000 K [65]. This type of discharge is different than that of a typical spark discharge in which a much hotter plasma is produced and local thermodynamic equilibrium can be reached. Transient spark discharge is capable of producing cold plasma.

An example of a transient spark discharge system is given in [64]. In the research, a DC high-voltage power supply was connected to a needle electrode through a current limiting resistor R (3.5–9.84 MΩ) and a separating resistor r (0–110kΩ). A simplified schematic diagram is shown in Figure 2.9.

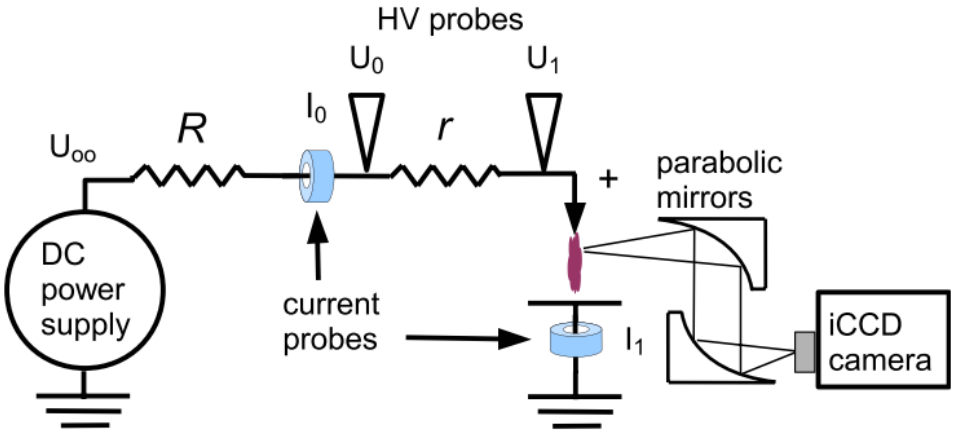

Figure 2.9. Simplified schematic diagram of a TS discharge system [64].

A high-voltage power supply with output voltage V_0 was used to stress the needle electrode. The streamer was formed first in the reactor chamber. When the voltage across the gap V reached the breakdown voltage V_{TS}, the streamer transformed to a short pulse spark. The discharge current can be expressed as in (2.22) [64]:

$$I(t) \approx -C\frac{dU(t)}{dt} \tag{2.22}$$

where C is the capacitance of the discharge system, including the internal capacitance of the discharge reactor, and the capacity of the cable and so on.

The discharge current increased to the peak value and then decreased to zero. Then C was recharged by the increasing voltage U (t). This voltage can be expressed by charging time t, resistance R, capacitance C, and voltage of the external power supply U_{00} [64]:

$$U_1(t) = U_{00}[1 - \exp\left(\frac{-t}{RC}\right)] \tag{2.23}$$

According to this equation, the breakdown voltage can be expressed as in (2.24) [64]:

$$U_{TS}(t) = U_{00}[1 - \exp\left(\frac{-T_t}{RC}\right)] \tag{2.24}$$

where T_t is the period of the TS pulses.

The pulse repetition frequency is then shown in (2.25) [64]:

$$f = \frac{1}{T_t} = \frac{1}{RCln[\frac{U_{00}}{U_{00}-U_{TS}}]} \tag{2.25}$$

It can be seen from equation (2.25) that with certain R and C, the pulse frequency can be increased by increasing the voltage level of the external power supply.

Typical transient spark discharge current and voltage waveforms from [64] are shown in Figure 2.10.

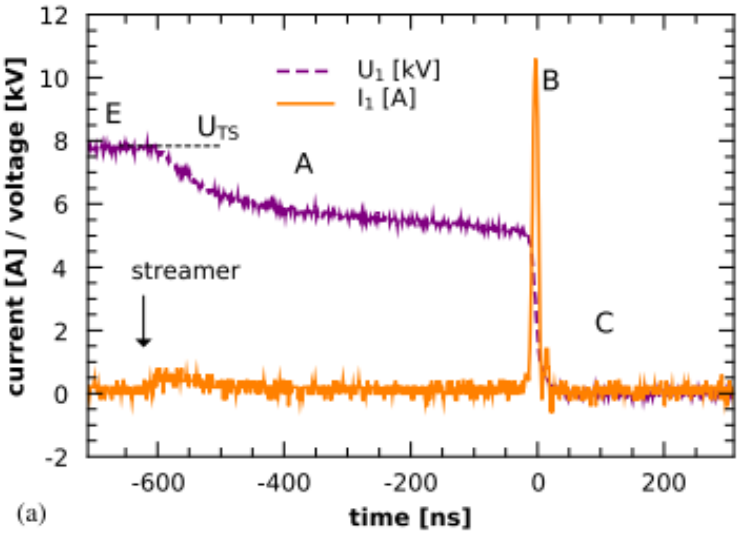

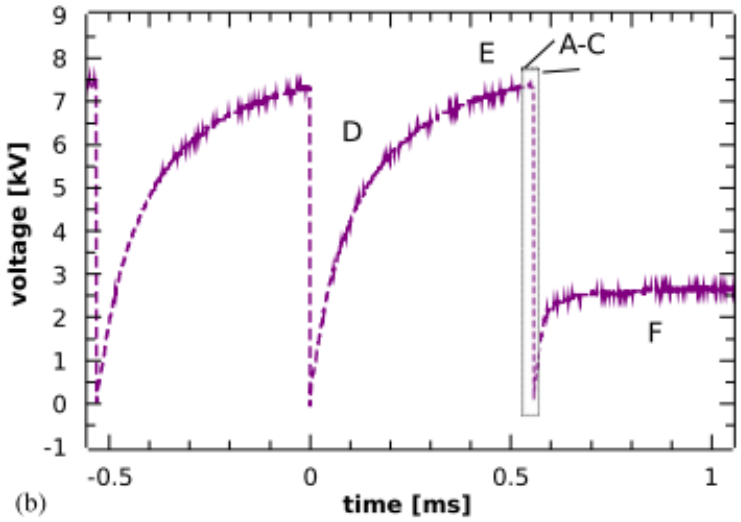

Figure 2.10. Typical current and voltage waveforms of transient spark discharge a) in ns scale; (b) in ms scale [64].

As shown in Figure 2.10 (a), the streamer transformed to pulse from phase A to B, and the current decreased to zero in phase C. Through recharge phase D in Figure 2.10 (b), the voltage reached a certain level, and corona and pre-breakdown appeared in phase E. As the voltage increased to the breakdown level, the transition re-occurred (back to phase A).

In addition, the plasma generated by transient spark discharge is highly reactive. This type of discharge can produce reactive species such as ozone, OH radicals, excited ions, and others. Because of this feature, good performance in terms of chemical oxidation and bio-decontamination can be achieved with this type of discharge. As reported in [68], suspensions of *E. coli* were treated by transient spark discharges, and up to 7-log reduction in population was obtained. This research also reported that H_2O_2, NO_2^-, and NO_3^- were detected in the treated liquid sample. In another study [69], transient spark discharges and streamer corona discharges were used to inactivate *S. typhimurium*. Results showed that time required to achieve 90% inactivation (D-value) is in a range from 110 s to 326 s when transient spark discharges were used, which is much shorter than the time using streamer corona

discharges (529 to 1947 s). Transient spark discharges can be used to inactivate bacterial cells, and they also have cytotoxic effects on mammalian cells. In research work [70], transient spark discharges in air were used to treat *E. coli* contaminated water, and a strong bactericidal effect was observed (3-5 log reduction in population was obtained). Also in this research, HeLa cells suspended in 5 ml phosphate buffered saline (PBS) with a population of approximately $5 \cdot 10^5$ cells/ml was directly exposed to transient spark discharges, and maximum cytotoxicity of 94% was observed in samples treated by transient spark discharge with a frequency of 4 kHz for 20 minutes.

As one of the most important factors that leads to a strong chemical and bio-decontamination effect, the formation of the reactive species in transient spark discharges has been investigated in many studies. In the case of transient spark discharge generated in atmospheric air, reactive oxygen species (ROS) and reactive nitrogen species (RNS) are considered the main reactive species produced. A study [67] that conducted optical emission spectroscopy (OES) investigation on the UV-VIS (ultraviolet-visible) spectra proved that N, O atoms, N^+ ions, and N_2 excited species could be generated by TS discharge in air. This research also suggested that TS discharge with low-frequency, intensive and shorter current pulses generates more radicals per pulse. Research [65] also used OES in the UV-VIS region to identify the reactive species generated by TS discharges. Results confirmed the existence of OH, NO radicals, N_2^+ ions, and atomic O, N, and H. The OH radicals were considered to be formed from water vapors in air, and the NO radicals were from dissociation of O_2 and N_2 by electron impact. The presence of atomic O, N, and H would participate in further chemical processes that produce other reactive species such as ozone O_3 and peroxyl radicals (HO_2). The authors also claimed that no UV-C radiation was detected during the TS discharges.

In a gas-liquid environment, transient spark discharge produces chemical effects in both the gas phase and the liquid phase. It is believed that chemicals generated in the gas phase and at the gas-liquid interface could be induced to liquid, initiate further reactions, and result in bactericidal and chemical effects. For example, hydrogen peroxide, which contributes to the bactericidal effect, can be generated in liquid by TS

discharge in the gas-liquid environment. As suggested in [71], the most straightforward pathway of generating H_2O_2 by plasma discharge in the gas-liquid environment is:

$$H_2O \rightarrow OH^{\cdot} + H^{\cdot} \quad (2.26)$$

$$OH^{\cdot} + OH^{\cdot} \rightarrow H_2O_2 \quad (2.27)$$

$$H^{\cdot} + O \rightarrow OH^{\cdot} \quad (2.28)$$

The generation of H_2O_2 could take place in the gas phase and then be induced to liquid, or it could occur directly in the liquid phase. However, the author of the research [71] observed a very low concentration of H_2O_2 (<0.1 mol%) in the liquid sample treated by plasma discharges with the absence of water molecules in the gas phase (gas with RH=0% was fed to the reactor). The concentration of H_2O_2 increased with increased gas humidity during discharges. The researchers believed that H_2O_2 was formed through dissociation of water molecules in the gas phase instead of in liquid. However, the contribution of liquid phase reaction cannot be totally ruled out. It is possible that OH radicals are partially produced in liquid phase, and H_2O_2 can be formed through (2.26)-(2.28) or through other reactions such as described in (2.29) [72]:

$$O_3 + H_2O(l) \rightarrow H_2O_2(l) + O_2 \quad (2.29)$$

Reactive nitrogen species play an important role in the case of plasma discharge in contact with the liquid. During plasma discharge in the gas phase, dissociation of N_2 and O_2 take place, and nitrogen oxides are formed through reactions in the gas phase. Then the NO_x dissolute in liquid which exposed to plasma discharge, forming NO_2^-

and NO_3^-. The pH of the liquid solution is decreased by this process. Equation (2.30) and (2.31) describes the dissolution of NO_x:

$$NO_2 + NO_2 + H_2O \rightarrow NO_2^- + NO_3^- + 2H^+ \quad (2.30)$$

$$NO + NO_2 + H_2O \rightarrow 2NO_2^- + 2H^+ \quad (2.31)$$

Furthermore, nitrites converts into nitrates under acid condition, as in equation (2.32):

$$3NO_2^- + 3H^+ + H_2O \rightarrow 2NO + NO_3^- + H_3O^+ \quad (2.32)$$

This route was proposed in [68] and [73] as the major reason for having a higher concentration of nitrates (≈0.9–1 mol/L) than nitrites (≈0.2 mol/L) in water treated by transient spark discharge. It also was suggested in this paper that the conversion from nitrites to nitrates through equation (2.32) was accelerated at low pH level (pH<3.5). This reaction occurred even after the plasma discharge turned off, so the reaction also was indicated as a "post-discharge reaction".

In the liquid phase under acid condition, proxynitrous acid (O=NOOH) or peroxynitrites ($O=NOO^-$) can be formed via reaction route in (2.33):

$$NO_2^- + H_2O_2 + H^+ \rightarrow O = NOOH + H_2O \quad (2.33)$$

Peroxynitrites are strong oxidants and can react directly with cells and chemicals or form highly reactive species such as $NO_2^{\cdot}$ and OH radicals via decomposition

reactions under acid conditions. The decomposition route is complex and can be shown briefly as:

$$O = NOOH \leftrightarrow [ONO^{\cdot\cdot}OH]cage \quad (2.34)$$

$$[ONO^{\cdot\cdot}OH]cage \leftrightarrow OH^{\cdot} + NO_2{}^{\cdot} \quad (2.35)$$

$$[ONO^{\cdot\cdot}OH]cage \rightarrow HNO_3 \rightarrow NO_3{}^{-} + H^{+} \quad (2.36)$$

First, O=NOOH homolyzes to form a geminated pair of $NO_2{}^{\cdot}$ and $OH^{\cdot}$, as described in (2.34). Then, ~30% of the geminated pairs convert to $NO_2{}^{\cdot}$ and $OH^{\cdot}$ through equation (2.35), and ~70 % of the geminated pairs collapse to HNO_3, which forms NO_3^- and H^+ by dissociation [73], [74], as in (2.36).

In addition, more reactions take place under acid condition in water treated by plasma discharges. For example, nitrous acid (HNO_2) formed via dissolution of nitrites is not stable and may decompose:

$$2HNO_2 \rightarrow NO^{\cdot} + NO_2{}^{\cdot} + H_2O_2 \quad (2.37)$$

The products of this reaction, $NO^{\cdot}$ and $NO_2{}^{\cdot}$, are known for their strong cytotoxic effects under acid condition [73], [75], [76]. The oxygen dissolved in water may react with $NO^{\cdot}$ and $NO_2{}^{\cdot}$ as:

$$4NO^{\cdot} + O_2 + 2H_2O \rightarrow 4NO_2{}^{-} + 4H^{+} \quad (2.38)$$

$$4NO_2^{\cdot} + O_2 + 2H_2O \rightarrow 4NO_3^{-} + 4H^{+} \quad (2.39)$$

In general, the bactericidal and chemical effect in liquid is induced by atmospheric plasma discharge (TS discharge) through multiple chemical processes. Hydrogen peroxide and nitrites under acid condition may make a significant contribution, and the existence of products in the liquid phase such as ONOOH, OH radicals, and NO radicals is critical. The simplified overall chemical processes at the gas/liquid interface and in bulk liquid are shown in Figure 2.11.

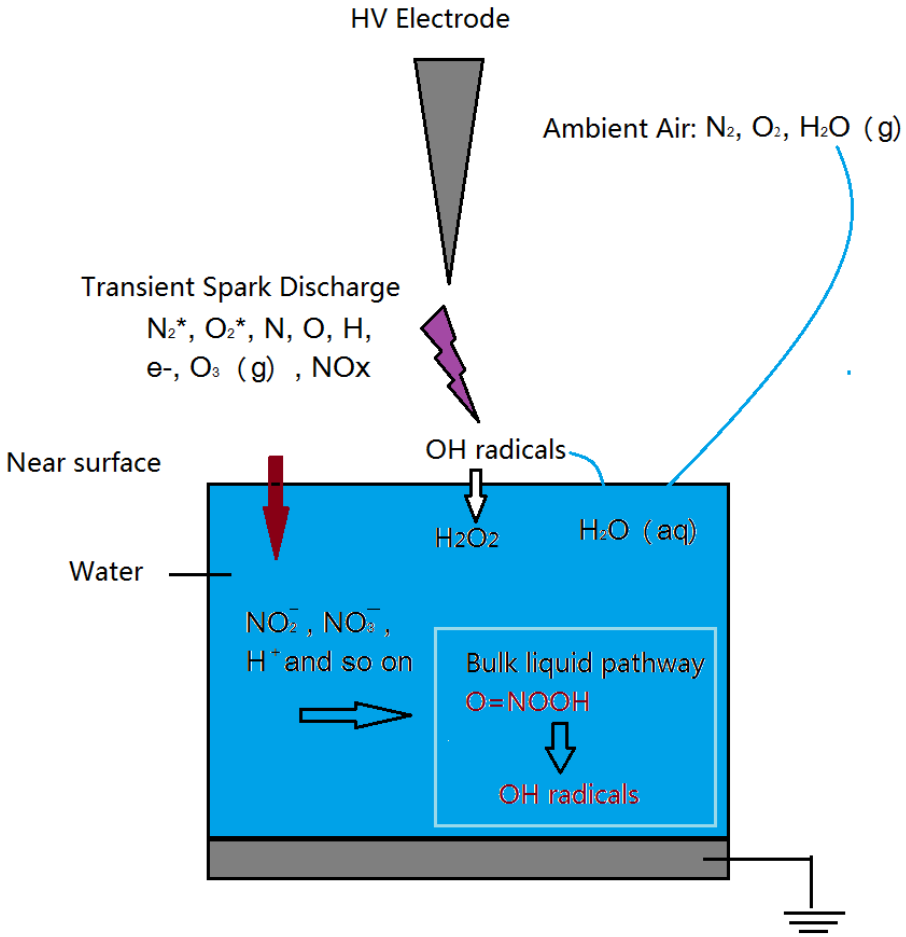

Figure 2.11. Chemical process of plasma discharge in contact with liquid (a) at the gas/liquid interface; (b) in the bulk liquid.

The role of ozone in the liquid phase chemical process is debatable. Lukes *et al.* discussed the contribution of ozone through experimental study. In [73], they claimed that ozone did not contribute to the aqueous-phase chemical process induced in water by plasma discharge in air. The authors believed that this was because ozone was eliminated by radicals such as $NO^{\cdot}$ and $NO_2^{\cdot}$ in the plasma zone, or in liquid through the reaction shown in (2.40):

$$NO_2^- + O_3 \rightarrow NO_3^- + O_2 \qquad (2.40)$$

According to [77], ozone reacted with NO_2^- rapidly, and the rate constant was ~$3.7 \cdot 10^5$ $M^{-1}s^{-1}$.

2.4 Non-Thermal Plasma Treatment for Microbial Inactivation

It has been shown that non-thermal plasma discharges have a great potential in inactivation of microorganisms over a wide range [78]–[80]. The bactericidal effect of non-thermal plasma discharge depends on discharge type, discharge parameters (intensity of voltage and current), temperature, humidity, gas pressure, and many other factors. However, due to the complexity of the physical and chemical processes during a non-thermal plasma discharge, the mechanism of bacterial inactivation remains unclarified. In this section, a background study of plasma-microbial cell interaction is presented. This section of literature investigation provides important information to optimise the bacterial inactivation effect of non-thermal plasma discharges.

2.4.1 Basic Structure of Biological Cells

Biological cells are the fundamental working units of life. Bio-cells can be classified as eukaryotic cells and prokaryotic cells. Eukaryotic cells contain a nucleus and other membrane-bounded organelles which prokaryotic cells do not have. Plant cells and animal cells are eukaryotic cells, while bacteria are prokaryotic cells. Both types of cells have a semi-permeable outer cell membrane which plays an important role in plasma-cell interactions. The membrane is composed of a lipid bilayer with an embedded protein. The lipid layer acts as a barrier, and the protein determines functions such as pumps and gates. In addition to the membrane, bacterial cells also have a cell wall. Depending on the structure of the cell wall, bacteria are classified as Gram-positive or Gram-negative.

Gram-positive bacteria have a cell wall with a thicker peptidoglycan layer outside the membrane. This type of bacteria appears purple in the Gram stain test.

Gram-negative bacteria have a cell wall that contains a thinner peptidoglycan layer between the plasma membrane and the outer membrane. This type of bacteria appears pink in the Gram stain test.

Structural differences in the cell wall between Gram-positive and Gram-negative bacteria are shown in Figure 2.12.

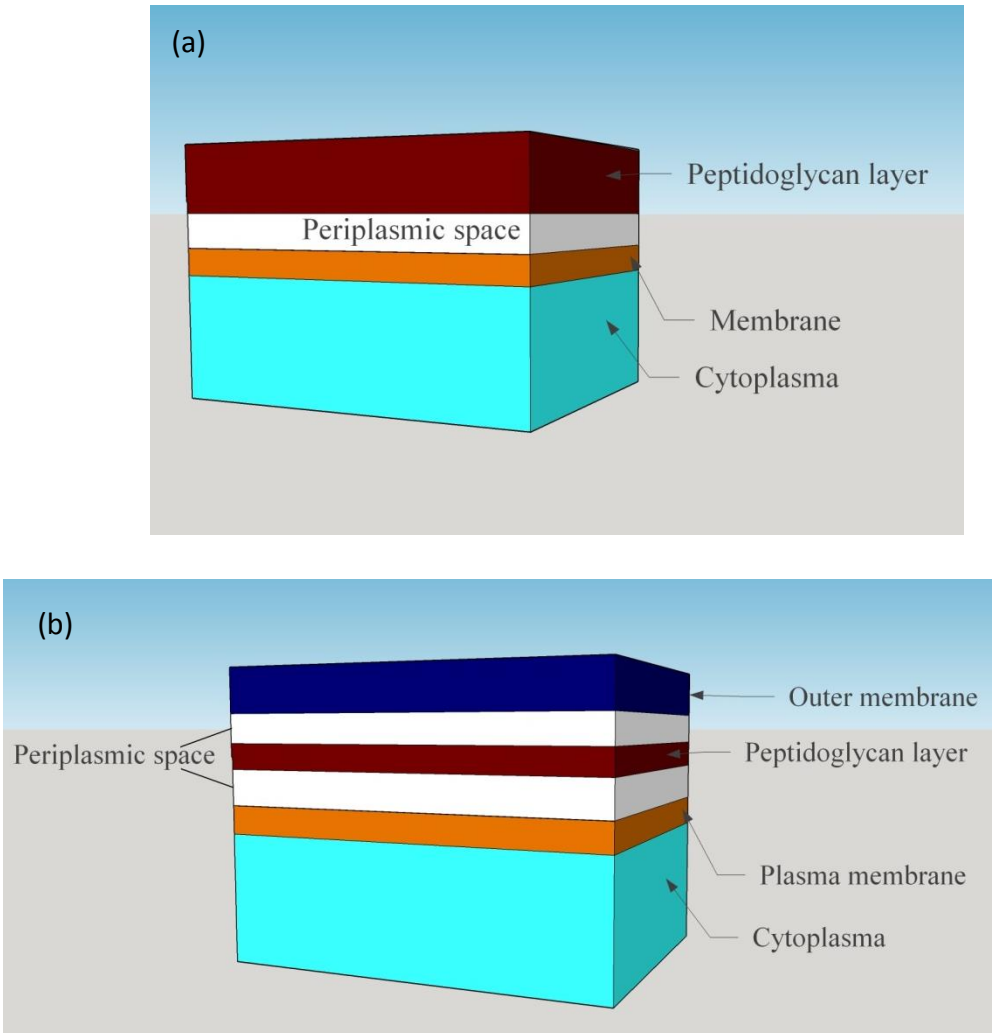

Figure 2.12. Cell wall structure of (a) Gram-positive bacteria and (b) Gram-negative bacteria.

Cell death is of two types: necrosis and apoptosis. Both types of cell death can be caused by non-thermal plasma discharge treatment.

Apoptosis is a process of natural programmed cell death. It typically occurs in multicellular organisms. Biochemical events in cells can cause morphology changes such as cell shrinkage, nuclear fragmentation, DNA fragmentation, etc., and lead to cell death.

Apoptosis is a common and necessary process in organisms of human, animal, and other life forms. However, plasma-induced cell apoptosis has been reported in many studies. As reported in [81] and [82], plasma-induced cell apoptosis can be achieved. Reactive species generated by plasma discharges could result in cell apoptosis. In [83], the concentration of H_2O_2 was reported to have a strong influence on cell apoptosis. Reactive species generated by plasma discharges could bring DNA damage which leads to a potential apoptotic process. In [84], plasma-induced reactive oxygen species are proved responsible for DNA damage in cells treated by dielectric barrier discharge (DBD) plasma. Another possible factor which may cause plasma-induced apoptosis is the intensive electric field; this has been proved by research [85] with a high-intensity pulsed electric field. Plasma-induced apoptosis is potentially important for the development of plasma medicine in many areas such as cancer treatment.

Necrosis is a process of unorganised cell death which typically is caused by external factors such as toxins, trauma, and infections. Unlike apoptosis, this type of cell death is not a natural process and is not necessary for organisms. Necrosis caused by non-thermal plasma discharges has been widely investigated. Inactivation of microorganisms, as an example, is one of the major topics of plasma discharge research. Many factors are potentially responsible for plasma-induced necrosis, especially regarding microbial inactivation using plasma discharge treatment.

2.4.2 Mechanisms of Bio-inactivation by Non-Thermal Plasma

Non-thermal plasma has been proved to have significant potential for inactivation of a wide range of microorganisms. Because of complicated mechanisms which result in the death of microorganisms due to the action of non-thermal plasma, these mechanisms are still not fully understood. It is known that the inactivation effect depends on the plasma chemical composition, plasma temperature, type of microorganisms, and their present environment [86]. Although a complete theory of plasma inactivation mechanisms has not been established, many attempts have been made to identify reasons that lead to cell death in plasma treatment [87], [88].

According to Akishev et al. [89], the most probable mechanisms of plasma inactivation are:

(1) Damage or irreversible alteration to the cell wall and membrane, causing an increase of the substance transport, leading to cell lysis and death
(2) Damage or irreversible alteration of intercellular components, causing dysfunction of the cell
(3) Irreversible damage to DNA (breaking the chain)

Under the effect of the non-thermal plasma, microorganisms would be attacked by plasma agents and eventually inactivated through the possible mechanisms listed.

From the non-thermal plasma point of view, the plasma agents are responsible for the microbial inactivation and must be investigated. As reported by papers [3] and [90]–[96], four major factors could result in microbial inactivation: (1) thermal effect, (2) chemically reactive species, (3) charged particles and electric field, and (4) ultraviolet radiation. Papers [97] and [98] specify these inactivation plasma agents. The effect of each plasma agent and their importance are discussed in this section.

Thermal Effect

The most frequently used method of microial inactivation is thermal heating. The heat can damage the cell membrane, cell wall, nucleus, and other components, making them lose their functions and leading to cell death. Many heat-based inactivation methods have been established, and different temperatures are required for inactivation, depending on bacterial heat tolerance and air humidity. For example, in the case of sterilisation using moist heat in an autoclave (steam sterilisation), the temperature required is 121 ℃ at atmospheric pressure, and the process takes 15 minutes. For the case of sterilisation using dry heat, 160 ℃ for 120 minutes and 170 ℃ for 60 minutes are recommended in [90] and [99].

Gas temperature remains at room temperature level in most cases of atmospheric pressure non-thermal plasma. Many studies have measured the temperature during non-thermal plasma discharges in various ways, such as in [95], but no significant increase in temperature was reported. Although minor change (increase) in

temperature could be caused in the exposed target objects (samples), the thermal effect on microbial inactivation is not likely to be a major contributor to cell death. However, exceptions exist if the microorganism has a low tolerance for heat, and temperature higher than room temperature in the gas can be achieved during some types of gas discharge (70-100 ℃).

Reactive Species

During non-thermal plasma discharges, chemically reactive species are generated through dissociation of molecules or many other pathways. As discussed in [100], ionic species and neutral species are produced in atmospheric plasma discharges through ion-molecule reactions and ion evolutions. Some of those reactive species have a high oxidising potential, which indicates a strong oxidation ability; examples are listed in Table 2.1.

Table 2.1. Oxidising potential of chemicals generated by non-thermal plasma discharges [101], [102].

Oxidizing species	**Oxidation Potential (V)**
Hydroxyl radical	2.80
Oxygen (atomic)	2.42
Oxygen (molecular)	1.23
Hydrogen peroxide	1.78
Ozone	2.08

It is believed that the reactive species generated by non-thermal plasma discharge play a dominant role in the bacterial inactivation process [65], [69], [86], [103]. In the case of non-thermal plasma discharge in ambient air, reactive oxygen species (ROS) and reactive nitrogen species (RNS), such as atomic oxygen (O), Ozone (O_3), hydroxyl

radicals (OH^-), and nitrogen dioxide (NO_2), are produced [3], [95]. These reactive species react with unsaturated fatty acida and protein molecules, causing damage to the cell wall and membrane; in this way, cell lysis can be caused. Furthermore, reactive species can penetrate through the cell wall and membrane, break the biochemical balance in the cytoplasm, and bring heavy damage to inner components, leading to cell death.

As suggested in [86], [88], and [103], the reactive oxygen species play the most important role in microbial inactivation. In the research studies [104]–[106], better inactivation effect was achieved by plasma discharge with the presence of oxygen; this indicated the importance of ROS. In [107], ROS-caused lipid peroxidation was reported as the main mechanism of bacterial inactivation, while DNA damage of plasma-treated mammalian cells caused by ROS also was reported in some studies [93]. Research work by Machala et al. using optical emission spectroscopy and thiobarbituric acid reactive substances (TBARS) absorption spectroscopy confirmed the peroxidation of the membrane caused by reactive oxygen species [69].

In atmospheric non-thermal plasma discharges, ozone is one of the most commonly produced products [108], [47], and it could be the dominant product among all reactive oxygen species [47], [46]. Its high bactericidal effect has been recognised and widely used as a sterilising agent [109]–[112]. Ozone can react with all major bacterial components and cause membrane lysis and damage to DNA and RNA [113]–[115]. Although ozone has been considered as a highly bactericidal agent, its importance in microbial inactivation by plasma discharge has been argued by many studies. Dobrynin et al. reported that the same *E.coli* inactivation efficiency was achieved with and without ozone produced from DBD plasma. Therefore, they believe that ozone generated by plasma discharge is not the main factor responsible for bacterial inactivation [92]. In [116], the author proved that even modest concentration of ozone (20 ppm) produced from plasma is enough to provide an inactivation effect on *Botrytis* fungal spores. As in [117] and [118], ozone plays a “‘largely indisputable” role in the inactivation of microorganisms by plasma discharges.

The hydroxyl radical is one of the reactive species produced by plasma discharge that also has a great potential for microbial inactivation. As suggested in [97] and [119],

hydroxyl radicals generated in moist air are expected to attack the outer structure of the bacteria and make a significant contribution to bacterial inactivation. Hydrogen peroxide produced by plasma discharge is also toxic to biological cells. Other reactive species such as NO, NO_2, and O can be generated by atmospheric plasma discharge, and bring inactivation effect to microorganisms. For example, generation of nitric oxide by air plasma jet has been discussed along with the related microbial inactivation mechanism in [120]. Further research is needed to identify the reactive species produced by plasma discharges and reveal their roles in microbial inactivation.

Charged Particles and Electric Field

Non-thermal plasma discharges are normally accompanied by a highly intensive electric field, and many studies have investigated the bactericidal effect of this electric field. In [88], the global electric field in plasma discharge was isolated from other plasma agents and tested on cells, and no noticeable inactivation effect was achieved. In [121], cell apoptosis was observed by introducing a nanosecond pulsed electric field. As described in [122]–[126], the intensive pulsed electric field can be used for sterilisation, cell adhesion, or introduction of molecules into cells.

As suggested in [127], charged particles produced by plasma discharges could play a significant role in bacterial inactivation. Those charged particles could accumulate on the outer surface of the cell membrane, create an electric field, and generate an electrostatic force that could overcome the tensile strength of the membrane, causing rupture of the cell. This type of mechanism works better in the case of Gram-negative bacteria due to its more irregular membrane surface. This was confirmed by Laroussi *et al.* in [97], where the rupture of the bacteria cell wall was only observed in *E. coli* but not *Bacillus subtilis.* It is believed that *B. subtilis* cells (Gram-positive bacteria) have a much smoother membrane. In [87], the effect of charged particles and the external electric field was discussed, and the electrophysical effect was responsible for ~12% of total inactivation of *Staphylococcus aureus* and *Pseudomonas aeruginosa* by positive corona discharge. Research [87] also proposed that different cell components have different sensitivities to this mechanism. As reported in [128],

in the case of cells immersed in dielectric media with a pulsed electric field with $E>10^4$ V/cm, their membrane could be easily broken, while in [87], a field with this intensity was not always considered to be destructive to intercellular components.

In addition to the electrophysical effect, some charged particles (such as superoxide ion O_2^-) can be oxidative and bring chemical damage to the cell as well. It is believed that under the electrophysical effect, ions and reactive species can get into the cell more easily through the opened pore and attack intercellular components.

UV Radiation

Another important plasma agent for the microbial inactivation is the UV radiation generated during discharges. UV radiation has been widely used for sterilisation, and its effect is unquestionable. The germicidal wavelength range of UV is 220 nm to 280 nm, while the most effective wavelength range for microbial inactivation is 250-280 nm, with a peak at 260 nm [117]. UV radiation can cause damage to the DNA and prevent the reproduction process of the cell [129]. It can also cause damage to protein and generate hydrogen peroxide and ozone, which are toxic to cells. Some studies have listed UV radiation as a dominant factor for microbial inactivation by plasma discharges, such as in [130] and [131].

Alternatively, many studies have reported that UV plays a minor role in microbial inactivation [88], [132], [133]. This concept has been supported by [92], [134], and [104], where UV radiation is not considered the primary factor for bacterial inactivation. In studies [86] and [93], the author used a quartz window to isolate UV radiation from other plasma agents and worked on targeting cells to investigate the contribution of UV radiation to inactivation. The results also showed that the role of UV could be negligible.

In [135] and [136], UV radiation is considered to play the most important role in microbial inactivation by low-pressure plasma discharges. However, in the case of atmospheric pressure plasma, UV photons are generally reabsorbed by plasma itself, and are not delivered to target microorganisms [95], [137], [138]. In most of the atmospheric plasma discharge cases, UV emission is not able to satisfy those

conditions. Although shorter-wavelength UV can be generated, it is not able to cause lethal damage to the exposed cell. Therefore, UV radiation would not be expected to make the main contribution to microbial inactivation [97]. Experimental measurement from the research of Laroussi and Leipold [95] showed that DBD in air produced no significant UV signal below 285 nm, and the power density in the region of 200 nm to 300 nm was below 50 $\mu W/cm^2$.

It was established in [87] that the inactivation effect of UV radiation depends on the intensity of the radiation, and the sensitivity of microorganisms. The geometric size of bacteria does have a strong influence on its sensitivity to UV. Experiments in this study showed that *Staphylococcus* with a smaller size are more sensitive to UV than *Pseudomonads*. The surface-to-volume ratios are also compared in this study, and inactivation of UV radiation is more effective on small cells rather than large cells.

The production of UV radiation in plasma discharge depends on many factors, such as gas composition, electric parameters, and exposure time. Therefore, a general conclusion on the role of UV in microbial inactivation cannot be made easily. It is also important to know that UV may work synergistically with other plasma agents such as reactive species so that better inactivation effects can be achieved.

2.5 Important Factors of Non-Thermal Plasma Discharge Treatment

In the previous sections, the characteristics of non-thermal plasma discharges were discussed. Without a doubt, non-thermal plasma discharges have great potential in many practical areas, and numerous applications have been developed based on this technology. One of the most important challenges in non-thermal plasma research is to optimise the treatment effect (inactivation effect, oxidation effect, etc.) and increase the efficiency. Due to the complexity of chemical reactions in non-thermal plasma discharges and plasma-cell interactions, it is difficult to identify the mechanism of plasma inactivation clearly. However, many important factors are reported to have an influence on non-thermal plasma discharge treatment.

2.5.1 Discharge Types and Electrical Parameters

It is important to note that different types of non-thermal plasma discharges have different abilities in producing reactive species and other plasma agents. Therefore, their treatment effects, including microbial inactivation and chemical oxidation, are different. For example, dielectric barrier discharge (DBD) is known for its ozone production ability and has been widely used in the laboratary and in industry [5], [59], [139]–[141]. Electrical properties of non-thermal plasma discharges could determine the treatment effects of non-thermal plasma discharges. It is important to monitor and manipulate the electric parameters to achieve the proper results from the non-thermal plasma discharge treatment. These important parameters include voltage, current, electric field intensity, frequency of pulsation (in the case of impulsive treatment), total exposure time, and total delivered charge. This provides a wide range of choices to applied non-thermal plasma discharge to specific situations.

2.5.2 Direct and Indirect Plasma Exposure

Microorganisms, biological materials, or any other target can be exposed to non-thermal plasma discharges in two ways: direct exposure and indirect exposure (remote exposure). In the case of direct exposure, targets are directly exposed to plasma, and all the plasma agents are able to come in contact with the sample, including UV light, electric field, charged particles, and reactive species. In the case of indirect exposure, targets are at a distance from the plasma, or in a modified configuration. Short-lived species, charged particles or even UV could not make contact with the sample.

Direct exposure provides better effects due to a greater number of plasma agents participating in the inactivation process. This was proved by experimental study in [142]. Moreover, it has been supported by research [143], as faster inactivation was achieved using the direct exposure method. However, the presence of reactive neutral species is normally considered to be the main factor for inactivation of microorganisms. Therefore, indirect exposure could also provide a significant

inactivation effect. The investigation into the difference in the inactivation effect between direct and indirect exposure could identify the role of charged particles, UV, or electric field. More importantly, two types of exposure configurations provide choices to specific practical applications.

2.5.3 Gas Conditions

As the media of non-thermal plasma discharges, gas is very important to the plasma inactivation process. The condition of gas directly or indirectly determines the generation of plasma agents. Gas compositions as one of the major aspects were tested in many studies to achieve better effects of non-thermal plasma treatment. For example, in a study [144], non-thermal plasma discharge in a specific mixture of 65% O_2, 30% CO_2, and 5% N_2 produced better inactivation effects on *Bacillus atrophaeus* than another mixture with 90% N_2 and 10% O_2. Research conducted by Bo Yang et al. reported that even a small variation of oxygen content (0% to 1% b/v) in the carrying gas could result in a significant difference in the inactivation of *Bacillus* spores; discharges in gas with a higher percentage of oxygen are more effective [145]. As mentioned in the previous section, the reactive species generated by non-thermal plasma discharges plays a dominant role in most situations. Different types or amounts of reactive species could be generated if the gas composition is different. In [146], the fluorescence measurement research of Takamatsu et al. showed that different OH radicals and singlet oxygen were produced by plasma discharges in various gases. Also, generation of other plasma agents such as UV radiation could also be influenced by gas composition. Reineke et al. reported that plasma jet using argon mixed with 0.135% b/v oxygen and 0.2% b/v nitrogen have more than four-fold production of UV photons than using pure argon [147].

Another important gas condition is its humidity, especially in the case of plasma discharge in air, which has a certain gas composition. Many studies confirmed that humidity has a strong influence on the treatment effect of non-thermal plasma discharges. Trompeter et al. showed that the germicidal effect of plasma discharge can be increased by adding water vapour into the gas stream [148]. This has been

confirmed by experimental results from [144] and [149], which showed that higher relative humidity results in a higher inactivation effect.

The humidity affects the plasma discharge treatment effect in two different ways. First, humidity influences the characteristics of plasma discharges and affects the production of reactive species. Second, humidity does have an influence on the inactivation effects of some reactive species such as ozone. For example, as reported in [112] and [150], the germicidal efficiency of ozone and other species such as OH radicals is strongly influenced by relative humidity.

It was reported in [151] that changes in humidity do have a strong effect on the ozone generation of DC corona discharges. Chen and Wang used a corona discharge model to evaluate the ozone production rate of corona discharges in air with different humidities. A wire with a radius of 100 μm was used in this model as an electrode to generate corona discharges. In the case of positive corona, the ozone production rate in dry air (relative humidity RH=0%) is $9.2 \cdot 10^{-4}$ mg/s·m (expressed per unit length of wire); this number decreased to $1.49 \cdot 10^{-4}$ mg/s·m when humidity increased to RH=50%. When the humidity increased to RH=100%, the ozone production rate was $9.93 \cdot 10^{-5}$ mg/s·m, almost 10 × lower than in the dry air. In the case of negative corona, the ozone production decreased from $6.1 \cdot 10^{-3}$ mg/s·m (RH=0%) to $1.54 \cdot 10^{-3}$ mg/s·m (RH=100%). This influence of humidity on ozone production was supported by experimental results in [152] and [153]. Also, the electrical characteristics changed with the changes in humidity. The role of water vapour was investigated in many studies. Humidity could affect the mobility of charge carriers, as reported in [154] and [155], and the plasma chemistry could also be changed [156], [157], [158]. The key components of chemically reactive species are ozone and the OH radicals, and the production of both chemicals could be affected by humidity. In [153], it was reported that the production of ozone decreases with an increase in humidity, and this decrease is not linear. This research also suggested that OH radicals are responsible for the O_3 destruction in humid air. Ozone production in humid air is low due to the removal of atomic oxygen by water molecules. This has been proposed in [153] and [159], as shown in (2.41)-(2.43) .

$$O + H_2O \rightarrow 2OH^* \quad (2.41)$$

$$OH^* + O_3 \rightarrow HO_2 + O_2 \quad (2.42)$$

$$HO_2 + O_3 \rightarrow OH^* + 2O_2 \quad (2.43)$$

where OH^* is highly unstable.

Alternatively, with the presence of water molecules, OH radicals and H_2O_2 can be generated. An example is shown in [160], in which increasing humidity resulted in an increase in OH formation and a decrease in density of ozone.

The hydroxyl radical can be formed through different mechanisms, including direct electronic excitation of water molecules and dissociative recombination of excited water molecules [161], [162], [163]:

$$H_2O + e^- \rightarrow OH + H + e^- \quad (2.44)$$

$$H_2O^+ + e^- \rightarrow OH + H \quad (2.45)$$

$$H_2O^+ + H_2O \rightarrow H^+(H_2O) + OH \quad (2.46)$$

Other mechanisms of formation of the hydroxyl radical in plasma-treated water solutions can involve formation and subsequent dissociation of peroxynitrous acid and/or peroxynitrite, as discussed in [73] and [68]. These complex processes of formation of OH radicals through chemical reactions involving nitrites, nitrates, hydrogen peroxide, and ozone are not fully understood, and further investigations are

needed. OH radicals are highly reactive, and they can quickly form H_2O_2 or other products by further recombination or oxidation reactions.

2.5.4 Acidity

In many studies, non-thermal plasma discharges have been generated in a gas-liquid hybrid environment to treat the target liquid sample. With the presence of liquid, hydroxyl radicals and H_2O_2 can be formed and play important roles in microbial inactivation and chemical degradation, as described in the previous section. Furthermore, plasma-induced acidification in the target liquid has been reported in [43] and [164]–[169]. This process is considered to be an important method to affect the non-thermal plasma discharge treatment. The process also provides information on the chemical production of various plasma discharges. Therefore, extra attention has been paid by many researchers to plasma-induced acidification. As reported in [170], two major possibilities are considered to be the cause of plasma acidification: plasma generated nitric/nitrate acid and an acid consisting of hydrogen cation (H^+) and superoxide anion (O_2^-). The first possibility was confirmed by Takamatsu et al. in [146]. In their research, plasma in air resulted in the largest pH decrease among all the gases tested, and the highest concentrations of nitrite and nitrate were correspondingly observed. The process is described in the following steps: NO and NO_2 are first generated in air by plasma discharge, and then NO_3^- and NO_2^- are generated (through the dissolution of NO_2 and NO into water). NO, NO_2, and ions (NO_3^- and NO_2^-) react with water, forming HNO_2 and HNO_3. Hence, the pH is decreased [171]. A similar conclusion was made in [167] and [172].

On the other hand, pH of plasma-treated liquid can also become acid even without the production of nitric/nitrate acid. In [165], the author observed a decrease in pH of the sample liquid after treatment by discharge without nitrogen. They proposed that H_3O^+ might be one possible source of the acidification. In [170], it is believed that the superoxide anion O_2^- is partially responsible for the decrease of pH in plasma-treated liquid. The researchers added superoxide dismutase (SOD) enzyme to plasma acid and observed an increase in pH.

As known, non-thermal plasma produces not only neutral species but also charged particles. Both types of products could have an effect on target liquid pH. For example, NO and NO_2 lead to the formation of nitric/nitrate acid, while charged particles could produce H_3O^+ through a charge exchange mechanism. A study on the effects of discharge products on target pH was conducted by Brisset et al. [166]. They suggested that the acidification is mainly caused by the neutral species—especially singlet oxygen in air and oxygen plasma. They also observed pH changes caused by ions: for example, the pH increase was observed under the effect of cations.

The acidification of the target liquid induced by plasma discharge treatment could have an influence on the effect of plasma treatment itself. In [146], low pH was considered an important factor for effective inactivation of microorganisms. When pH was below 3.8, inactivation of *E. coli* was very efficient. As reported in [42], lowering pH can enhance the oxidising ability of hydrogen peroxide, which is also a product of plasma discharge. The supporting effect of plasma-induced acidification in microbial inactivation has also been reported in many other papers [173], [174]. From another point of view, low pH could cause harm to cells such as disruptions of the plasma membrane. However, some studies proved that this activity was not considered the main reason for plasma inactivation. According to results from [171], the contribution of low pH can be neglected in comparison with other factors produced by electric discharges. A similar conclusion was made in [175]; plasma-induced acidification was not considered to be the primary cause of bacteria cell death. However, its assistance cannot be ruled out completely.

2.5.5 Catalysts

Plasma catalysis, is an interesting research topic that has been studied for decades. The plasma-catalyst hybrid system has been found to provide better performance than plasma or catalyst alone in many situations [176]–[178]. Non-thermal plasma discharges were discussed in previous sections; plasma-catalysis is also worth consideration as a potential way to optimise the non-thermal plasma treatment. The advantages of introducing a catalyst into a plasma discharge system are many: it can

enhance the production of reactive species, accelerate chemical reactions, vary the selectivity of the system, and minimise unwanted products [179]. Also, the surface property of the catalyst may be changed by interaction with plasma discharges through ions, electrons, and photons. Conversely, the properties of plasma discharge may be altered by introducing catalysts, which will result in a change in the composition of reactive species generated [180].

The enhancement effect by adding catalytic material into a plasma reactor depends not only on the physical and chemical properties of the catalyst, but also on how the catalyst is introduced into the system. In [181] and [182], it was reported that particle size, the amount of the catalyst used, and the way it was packed can significantly influence the performance of the plasma-catalyst system. Two types of common configurations of the plasma-catalyst system are described in [179]: one-stage (direct) and two-stage (indirect) configurations. In the case of a one-stage system, the catalyst is directly exposed to non-thermal plasma discharges, and all the species produced by plasma discharge, including charged particles, electrons, and neutrals, are able to reach the catalyst surface. In a two-stage system, the catalyst can only be activated by stable and long-lived species such as neutrals, as shown in Figure 2.13.

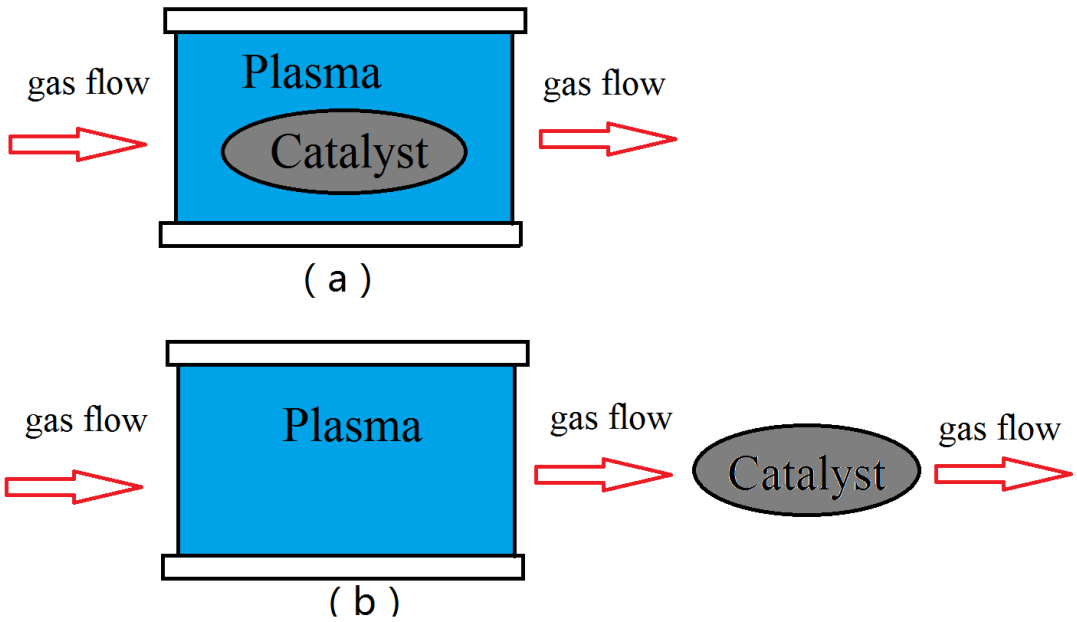

Figure 2.13. Plasma-catalyst hybrid system with (a) one-stage configuration and (b) two-stage configuration.

Many types of catalysts can be used in the plasma treatment processes. One of the most common catalysts used in the plasma-catalyst system is titanium dioxide, which has a bandgap of 3.2 eV and can be activated by UV radiation (< 385 nm). It can provide electrons and holes, leading to the production of reactive species [183]. In the case of a plasma-catalyst hybrid system, electrons produced by plasma discharge with a mean energy of ~3.5 eV are thought to activate TiO_2 as shown in (2.47) [184]:

$$TiO_2 + e^-(> 3.2eV) \rightarrow h^+ + e^- \quad (2.47)$$

h^+ represents hole provided by catalyst.

TiO_2 is also mixed with other materials that act as catalysts to achieve better performance. For example, nitrogen-doped TiO_2 nanotubes were used in [185] and achieved better results than using undoped TiO_2 nanotubes. Ag/TiO_2 was used in [186] and achieved 68% toluene destruction at 257 ℃, while using TiO_2 alone only achieved 19%. This research also suggested that temperature could have a strong influence on the performance of a plasma-catalyst system, as Ag/TiO_2 achieved 100% conversion of toluene at 400 ℃. However, this thesis will only be focused on non-thermal plasmas in gases near room temperature.

2.6 Summary

In this chapter, a literature review on non-thermal plasma was presented. Plasmas as the fourth state of matter widely exist in the universe. They are classified as thermal plasma and non-thermal plasma, depending on the thermal equilibrium. Non-thermal plasma has been studied for many years, and it has great potential in many applications including waste water treatment, bio-decontamination, and polymer surface treatment.

Discharges in atmospheric air are considered to be a good source for non-thermal plasma. During the discharge, gas can be ionised and produce chemically reactive

species. UV radiation and a strong electric field are also produced during the discharge process. Hence, the atmospheric discharges have a great potential in chemical oxidation and bio-decontamination. In this chapter, the mechanism of streamer development was presented, followed by a discussion of two types of atmospheric discharges: corona discharge and transient spark discharge. Their mechanisms, electric characteristics, and the ability of production of reactive species were discussed in this chapter.

In addition, bio-decontamination effects of non-thermal plasma discharge were addressed. This discussion includes the mechanisms of the bio-decontamination effect, the roles of different plasma agents in decontamination, and possible influences of different discharge conditions.

This chapter provides valuable information on principles and mechanisms of non-thermal plasma discharge and supports the experimental study which is presented in later chapters.

CHAPTER 3

Development of Steady-State and Transient Plasma Treatment Systems

3.1 Introduction

In the present research project, two types of atmospheric non-thermal plasma discharge were studied: DC steady-state corona discharge and transient plasma discharge. Chemical oxidation and bio-decontamination capabilities of these discharges were investigated, and measurements of the hydroxyl radicals produced by atmospheric non-thermal plasma discharges were taken. Due to the different natures of the steady-state corona discharges and the impulsive transient plasma discharges, two separate experimental plasma treatment systems were designed and constructed. This chapter presents both types of discharge systems along with the detailed experimental methodology and diagnostic equipment used to monitor electrical characteristics of the plasma discharges. Each plasma system includes:

- High voltage power sources
- Gas handling system
- Plasma discharge test cell
- Diagnostic and monitoring equipment

Electrostatic simulation of the electric field in each of the developed test cells was conducted as a part of the pre-test analysis, and the results of this modelling are also presented and discussed in this chapter.

3.2 Steady-State Corona Discharge System

As described in Chapter 2.3.4, corona discharge is one of the most commonly used sources of non-thermal plasma in atmospheric air, and it has been studied from many aspects over recent decades. This research is aimed at investigating possible factors

that can be modified to optimise the chemical oxidation and bio-decontamination efficiency of non-thermal plasma discharges. To do so, a series of experiments was performed using a steady-state corona discharge system. This system was designed and built to generate DC energised steady-state corona discharge with both positive and negative polarities in air, and it provides both direct and indirect exposure of target samples to non-thermal atmospheric plasma. In this section, a detailed description of the developed experimental system is given.

3.2.1 Corona Discharge Treatment System

The corona discharge system designed and developed in this project is shown in Figure 3.1.

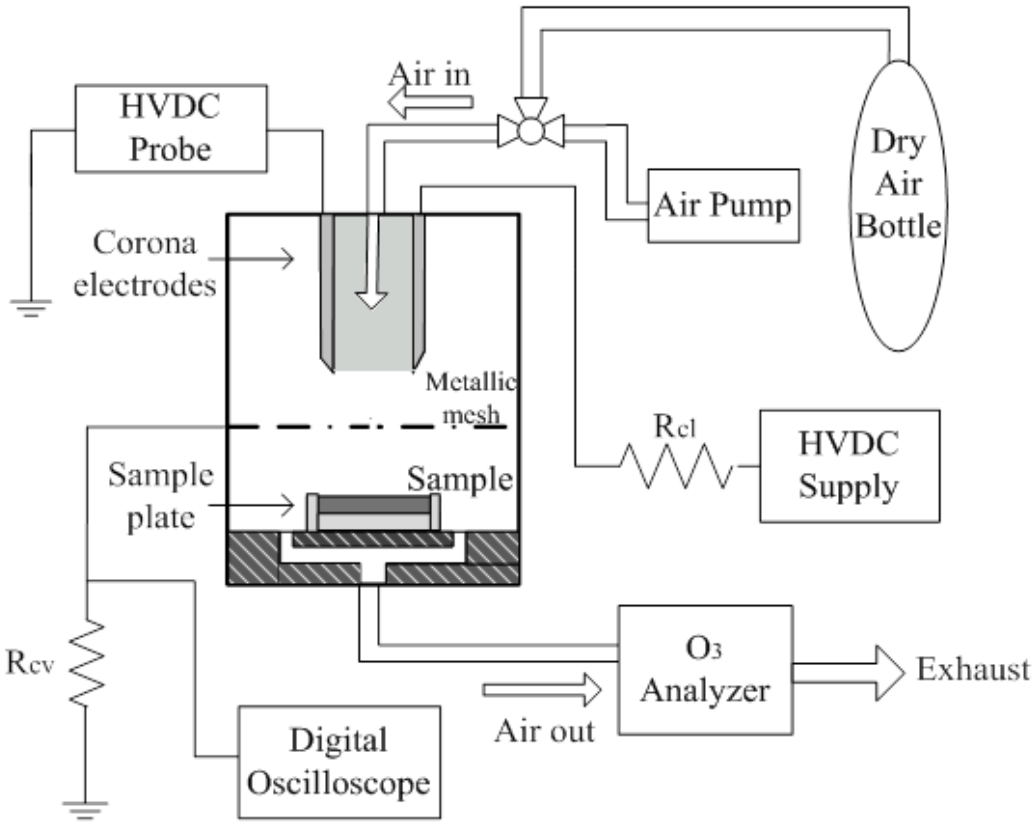

Figure 3.1. Schematic diagram of the plasma treatment system configuration.

A Glassman (WR series) 250 W regulated high-voltage DC power supply was used to energise the high-voltage corona electrode in the test cell. This power supply was connected to the test cell through a 28 MΩ current limiting resistor (R_{cl} in Figure 3.1). Output voltage and current ranges are 0–100 kV and 0–2.5 mA.

A DC high-voltage probe (Testec TT-HVP40 model) is attached to the corona electrode from the top connection port of the test cell, and the applied voltage is monitored using an ISO-TECH 705 digital multimeter. The maximum DC input voltage for the probe is 40 kV, which is suitable for the design voltage across the test cell (~30 kV).

Transient and dc corona discharge currents were monitored using a 1 kΩ current viewing resistor (R_{cv} in Figure 3.1). This resistive shunt is connected to the ground connection port of the test cell (metallic mesh in the case of indirect treatment, or conductive sample plate in the case of direct treatment). A 50 Ω BNC cable is used to connect the resistive shunt with a Tektronix TDS 2024 digital oscilloscope (bandwidth 200 MHz, sampling rate 2 G samples/s). During the discharge, the voltage drop across the resistive shunt is monitored, and waveforms are stored in the oscilloscope for further analysis.

Bottled air (obtained from BOC) and an FIAC FX 95 air compressor were used to provide bottled air flow (air with ~12.5% humidity) or ambient air flow (air with ~40% relative humidity) through the test cell during the corona discharge treatment. The air pressure inside the test cell was kept at 0.2 atm gauge, and the air flow rate was ~14 L/min. The gas outlet port of the test cell was connected to an ozone analyser (IN-2000 LoCon IN USA Inc.). Figure 3.2 shows the equipment used to generate steady-state corona discharges and to monitor the discharge voltage and current waveforms.

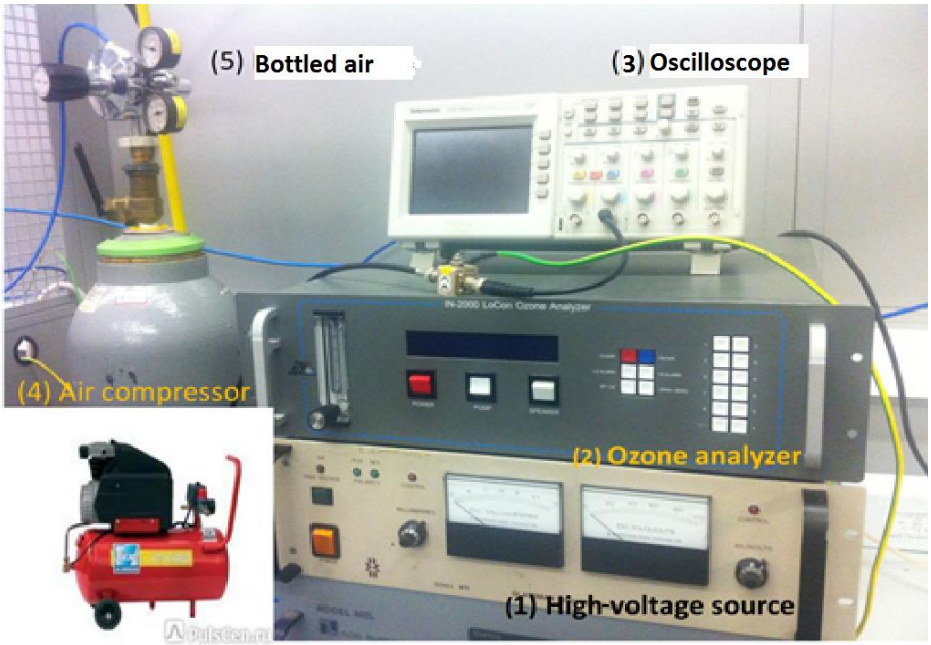

Figure 3.2. Equipment used in the steady-state corona discharge experiments:

(1) Glassman (WR series) 250 W regulated high-voltage DC power supplies

(2) IN-2000 LoCon IN USA Inc. ozone analyser

(3) Tektronix TDS 2024 digital oscilloscope

(4) FIAC FX 95 air compressor

(5) BOC bottled air

(6) Test cell

(7) 28 MΩ current-limiting resistor R_{cl}

(8) Testec TT-HVP40 DC high-voltage probe

(9) SO-TECH 705 digital multimeter

3.2.2 Corona Discharge Test Cell

The corona discharge test cells are shown in Figure 3.3. The main body of the test cell is made of a Perspex cylinder with an inside diameter of 79 mm, and thickness of the Perspex wall of 5 mm. The top and bottom of the cylinder are covered with two polyvinyl chloride (PVC) flanges. Inside the cylinder, a stainless steel tube with a sharp edge is located in the center of the top flange and connected to an external high-voltage supply through an HV connection port. This stainless steel tube acts as the high-voltage stressed electrode during corona discharge; the internal and external diameter of this tube are 20 mm and 25 mm, respectively. A gas inlet port is located in the top flange, and a gas outlet port is in the bottom flange, allowing gas flow through the test cell during the discharge.

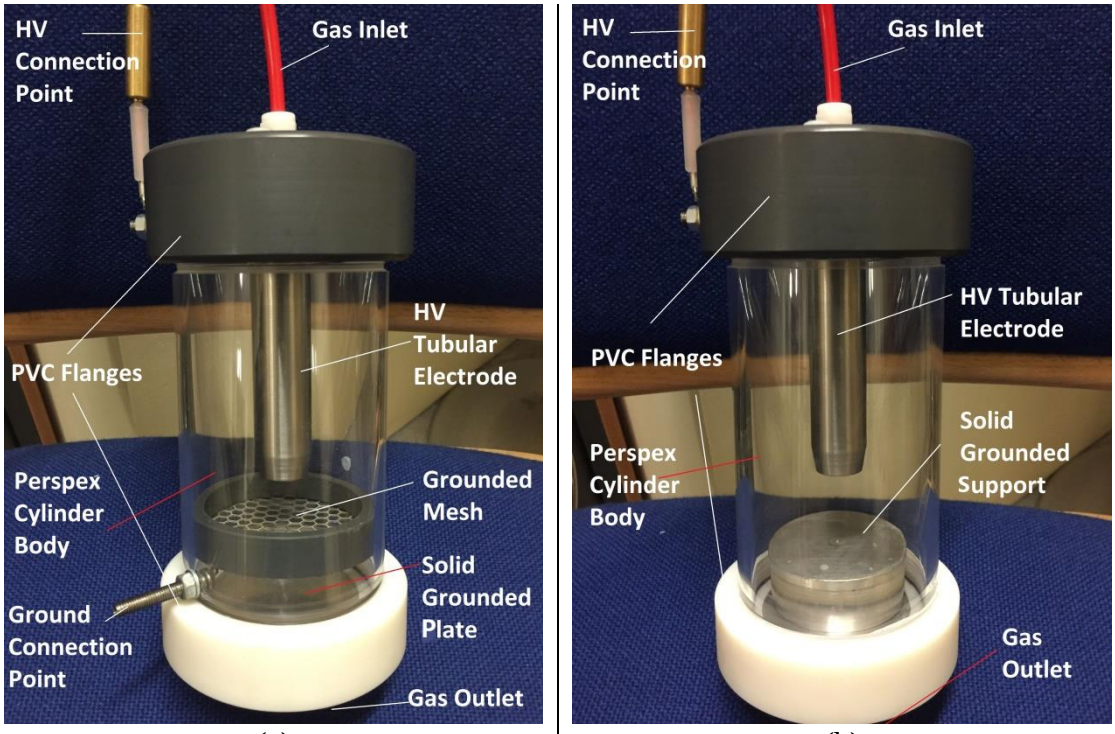

Figure 3.3. Corona discharge test cells for (a) indirect exposure and (b) direct exposure.

To perform indirect and direct corona discharge treatment on target samples, this test cell was modified into two different topologies, as shown in Figure 3.4.

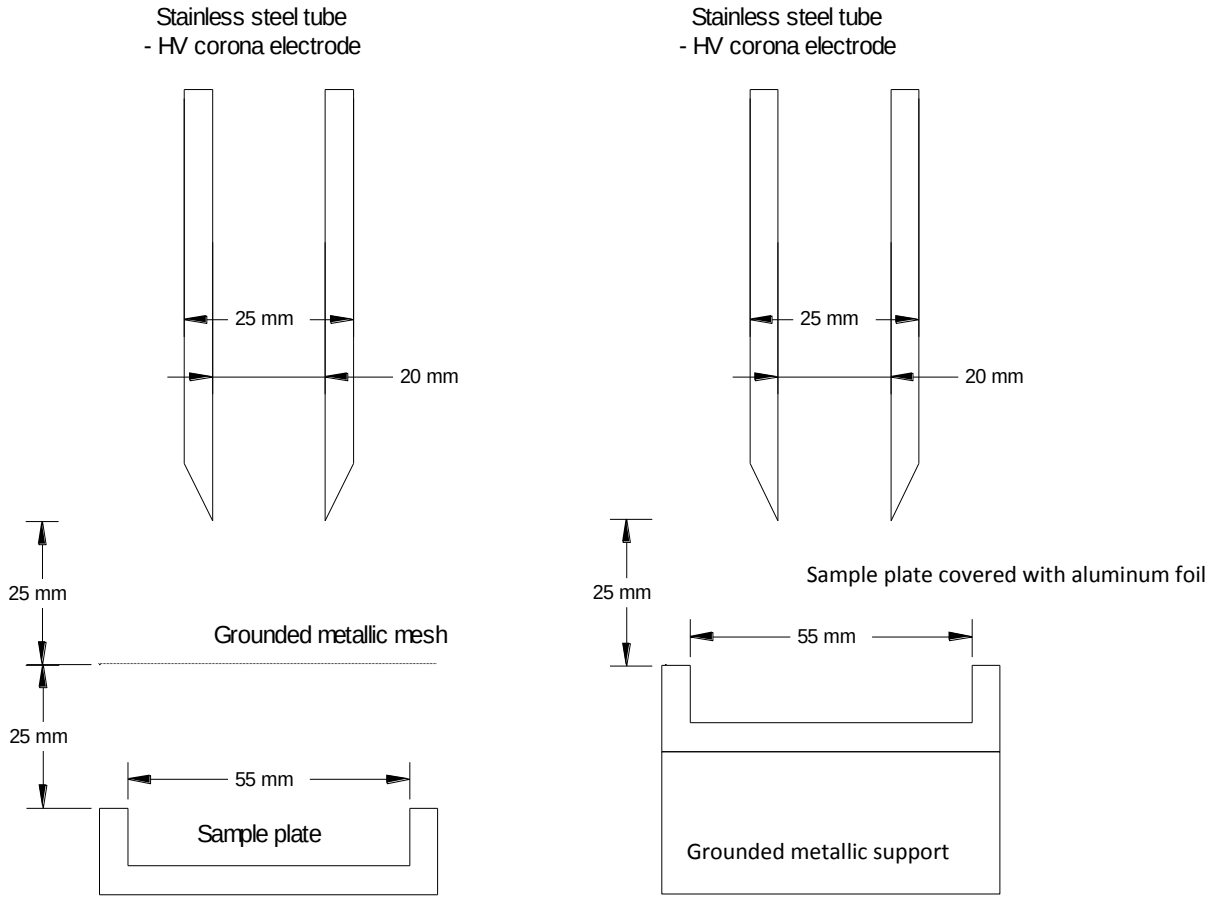

Figure 3.4. Diagrams of (left) indirect and (right) direct corona discharge treatment cells.

Two different types of corona treatment were used in the present work: direct and indirect. In the case of indirect corona discharge treatment, a grounded metallic mesh was placed under the HV tubular electrode. This mesh was made from perforated stainless steel sheet (RS Components) with 6 mm hex holes. The thickness of the mesh was 0.55 mm, and open area percentage was 79%. The distance from the edge of the tubular electrode to the mesh was 25 mm. The chemical or biological sample was held by a 55 mm plastic contact plate (Sterilin Contact Plate, Thermal Scientific) which is non-conductive, and located 25 mm under the metallic mesh. During the discharge, ions, electrons, and charged particles produced by discharges along with

the electric field can be screened by this mesh. Therefore, their effect on the target sample is reduced.

In the case of the direct corona discharge treatment, the 55 mm contact plates lined with aluminum foil (the thickness of the foil is negligible compared with other critical dimensions in the current plasma system) were used as sample plates. A picture of this conductive sample plate is shown in Chapter 4, Figure 4.4. For corona discharge tests, this sample plate with a biological or chemical sample was placed on a grounded metal support stand inside the test cell; the foil-lined plate was kept at earth potential, in this case acting as grounded electrode, 25 mm from the edge of the HV electrode. During the corona discharge treatment, a return current path was provided through the sample. Thus, ions, electrons, and charged particles, along with other neutral products from corona discharge, were able to reach the sample surface and to produce oxidation or bactericidal effects on the target sample.

3.2.3 Electrical Characteristics of Corona Discharges

The applied voltage in the present tests was 30 (±0.2) kV; positive and negative polarities were used. The discharge current was monitored using the current shunt resistor (Figure 3.1). The steady-state current values for different types of corona discharges are given in Table 3.1.

Table 3.1. Corona discharge current for direct and indirect treatment, bottled air and atmospheric air.

Treatment	Type of gas	+30 kV	-30 kV
Indirect	Atmospheric air	(80-90) µA	-(120-140) µA
Indirect	Bottled air	(68-80) µA	-(138-152) µA
Direct	Atmospheric air	(30-40) µA	-(70-90) µA
Direct	Bottled air	(33-50) µA	-(70-100) µA

The corona discharge current in the case of indirect treatment is higher than in the case of direct treatment; this is mainly due to the difference in the ground electrode and sample plate's position. Variations can also be observed due to the stochastic nature of discharges and other factors such as slight humidity and pressure change in the test cell during discharge. Examples of discharge voltage and current waveforms are shown in Figure 3.5.

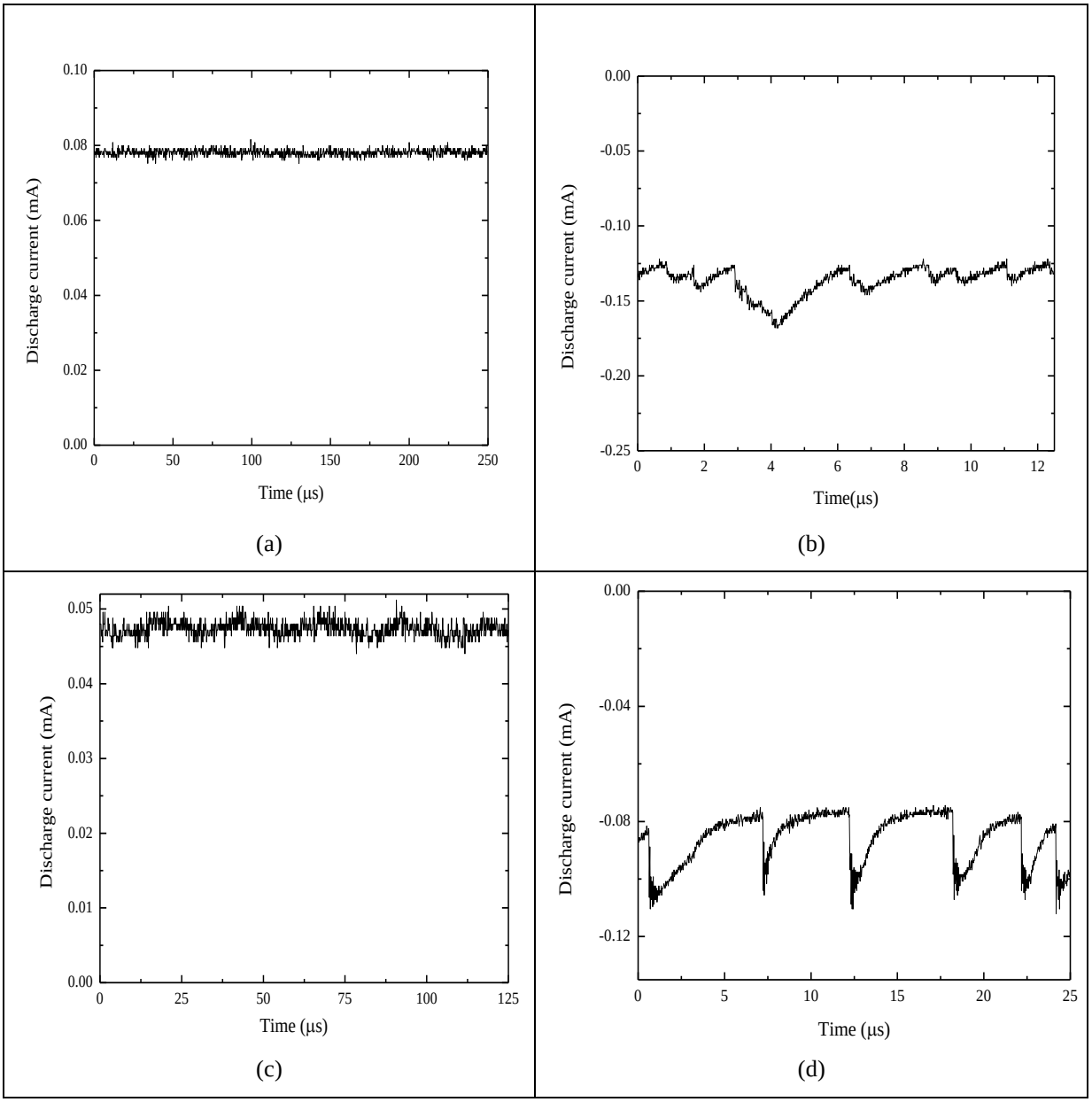

Figure 3.5. Corona current waveforms: (a) +30 kV (indirect); (b) -30 kV (indirect); (c) +30 kV (direct); (d) -30 kV (direct).

3.2.4 Electric Field Simulation

Different electrode topologies are used in the direct and indirect discharge treatment cells. Therefore, the electric field distribution and its intensity in these test cells is also different. Electrostatic models of both test cells were built using electrostatic field software, Quickfield 5.10. Simulation results are presented in this section. All models were built using axisymmetric topology, which allows analysis of the electric field in 3D. Quickfield is finite element analysis software; a mesh spacing value of 0.02 was used in all cases investigated in this work.

The applied voltage was 30 kV. Relative permittivity of different parts of the test cell used in this analysis are listed in Table 3.2.

Table 3.2. Relative permittivities used in the simulation of electric field.

Parts	Material	Relative permittivity
Top/bottom flange	PVC	3
Cylinder wall	Perspex	3.3
Contact plate	Polystyrene	2.5
Space in the test cell	Air	1
Chemical/biological sample	Water-based indigo carmine solution/ agar	80

Indirect Discharge Treatment

In the case of indirect corona discharge treatment, the electric field distribution was obtained in the topology shown in Figure 3.6.

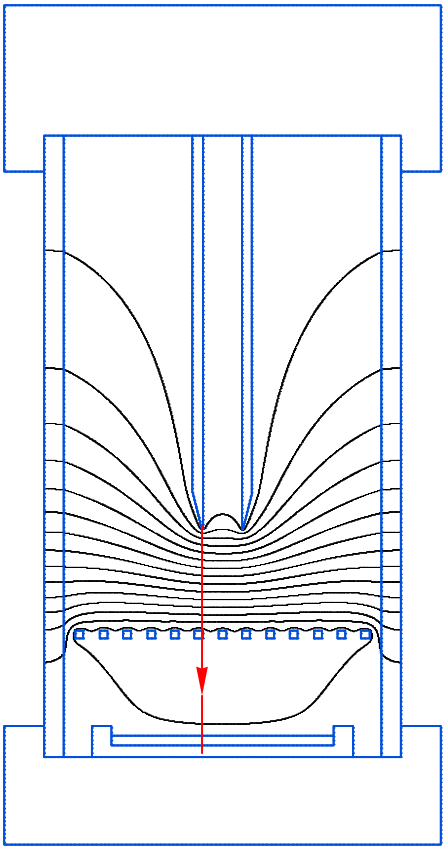

Figure 3.6. Equipotential lines in the indirect discharge treatment test cell; the field observation contour is shown as a red arrow in the vertical direction.

The magnitude of the electric field was obtained along the coutour line shown in Figure 3.6. This electric field is shown in Figure 3.7; 10 mm distance corresponds to the edge of the HV electrode. Results showed that the electric field is intensive near the edge of the HV electrode, and the screening effect of the grounded metallic mesh is obvious.

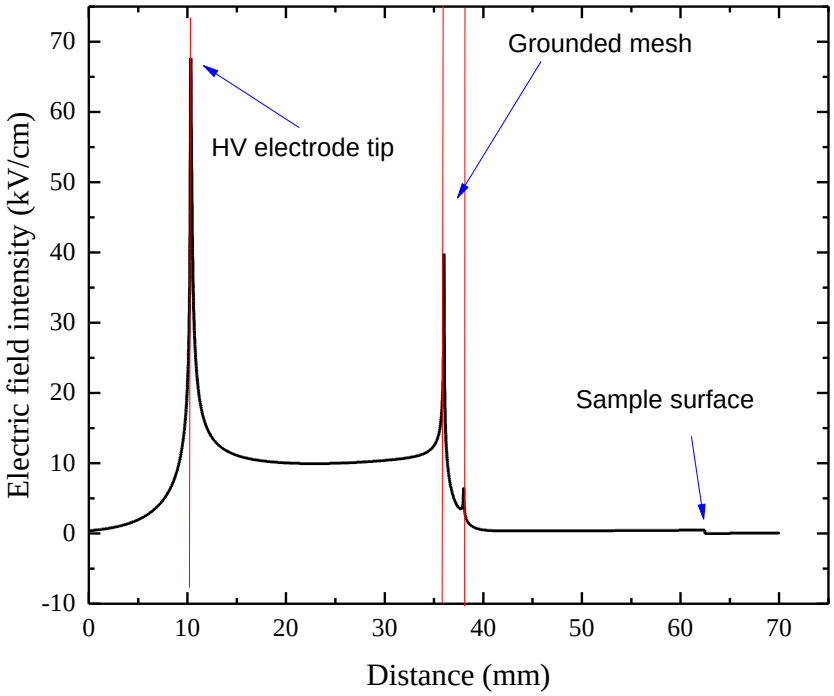

Figure 3.7. Electric field intensity along the contour in the vertical direction between high-voltage electrode and target sample during indirect discharge treatment.

In the position which is close to the edge of the high-voltage electrode tip (~10 mm from the starting point of the contour), the electric field is the strongest; the intensity is 67.69 kV/cm. As the distance between the high-voltage electrode and sample surface increases, the intensity of the electric field decreases. A small increase in intensity is observed when the position becomes closer to the grounded mesh, 39.81 kV/cm maximum. However, the intensity of the electric field behind the mesh is lower than 1 kV/cm.

The intensity of the electric field in a position which is close to the sample (0.1 mm above the sample surface) has also been monitored. Readings are taken along the contour in a horizontal direction, as shown by the red arrow in Figure 3.8.

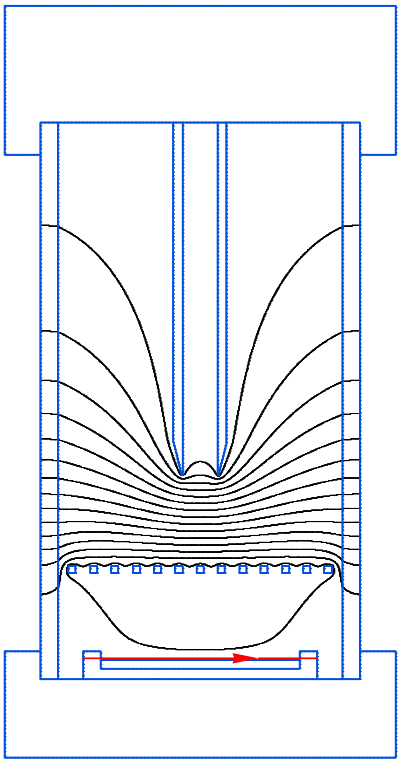

Figure 3.8. Equipotential lines in the indirect discharge treatment test cell; observation contour (red arrow) is 0.1 mm above the sample/air interface (horizontal direction).

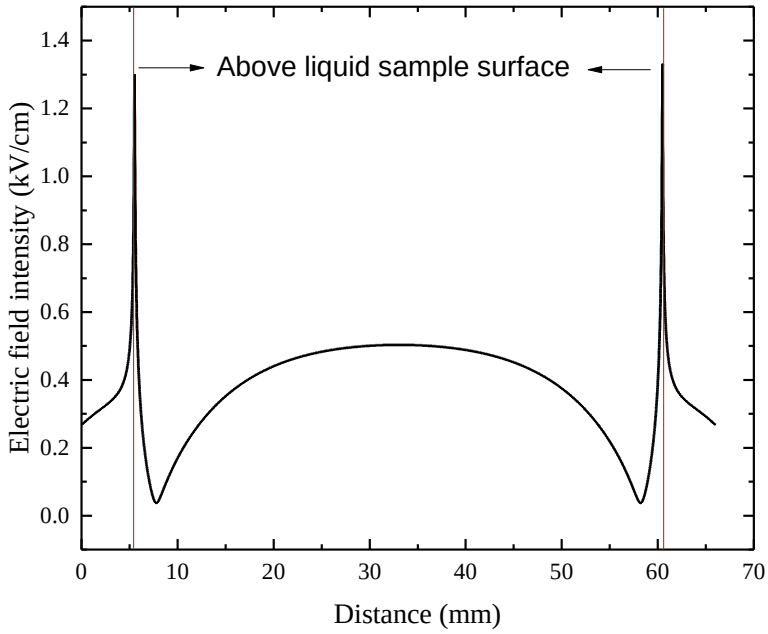

Figure 3.9. Electric field intensity at 0.1 mm above the sample surface during indirect corona discharge treatment.

As shown in Figure 3.9, at the horizontal level, which is 0.1 mm above the sample surface, the electric field has a peak of 0.50 kV/cm at the center position. Two higher peaks were observed at the polystyrene/air interface, where the the electric field is 1.30 kV/cm.

Direct Discharge Treatment

In the case of the direct discharge treatment, the electrostatic field model is built according to the structure of the indirect treatment test cell. The equipotential lines in this test cell are shown in Figure 3.10.

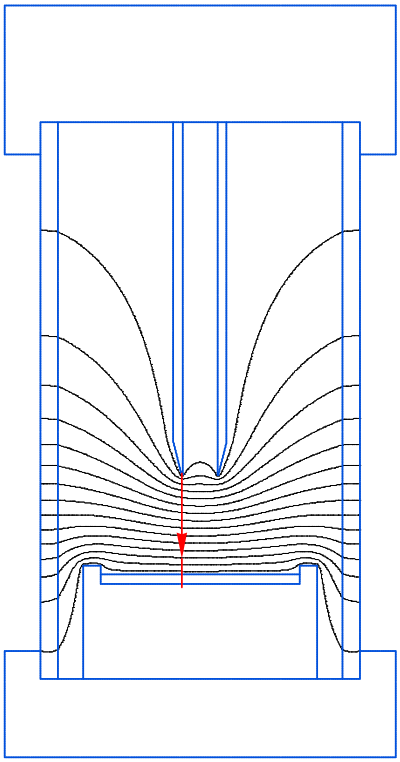

Figure 3.10. Equipotential lines in the direct discharge treatment test cell.

The intensity of the electric field along the vertical direction (indicated as the red arrow) is shown in Figure 3.11:

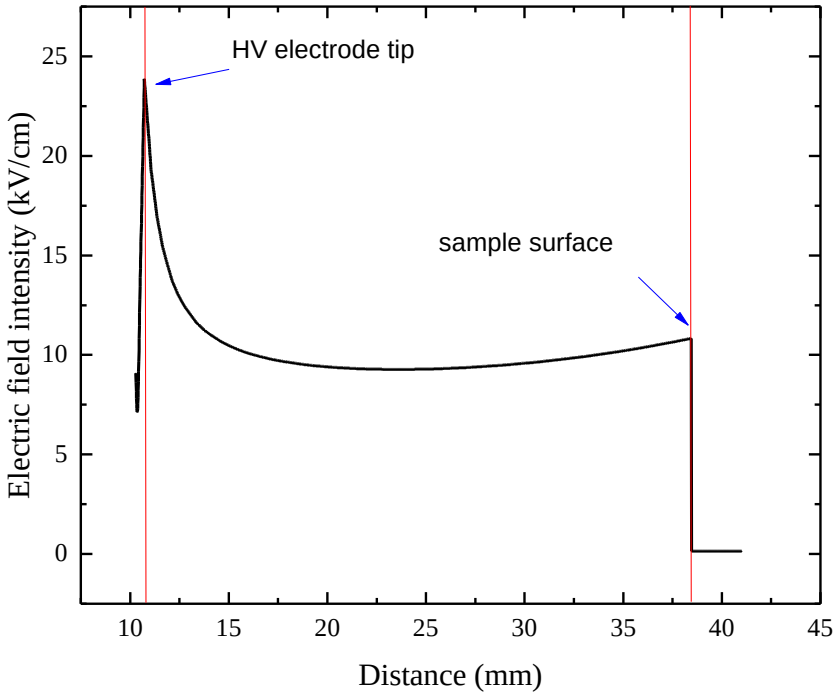

Figure 3.11. Electric field intensity along the contour in the vertical direction between high-voltage electrode and target sample during direct discharge treatment.

As shown in Figure 3.11, the electric field is intensive near the tip of the high voltage electrode; the intensity is 23.87 kV/cm. Another peak was observed at the sample/air interface with a value of 10.83 kV/cm. In comparison with the case of indirect treatment, the intensities are lower in the case of direct discharge treatment. This is primarily caused by the difference in the grounding electrodes.

The electric field intensity across the sample/air interface (as in the indirect treatment case, 0.1 mm above the sample surface) also was obtained and is shown in Figure 3.12.

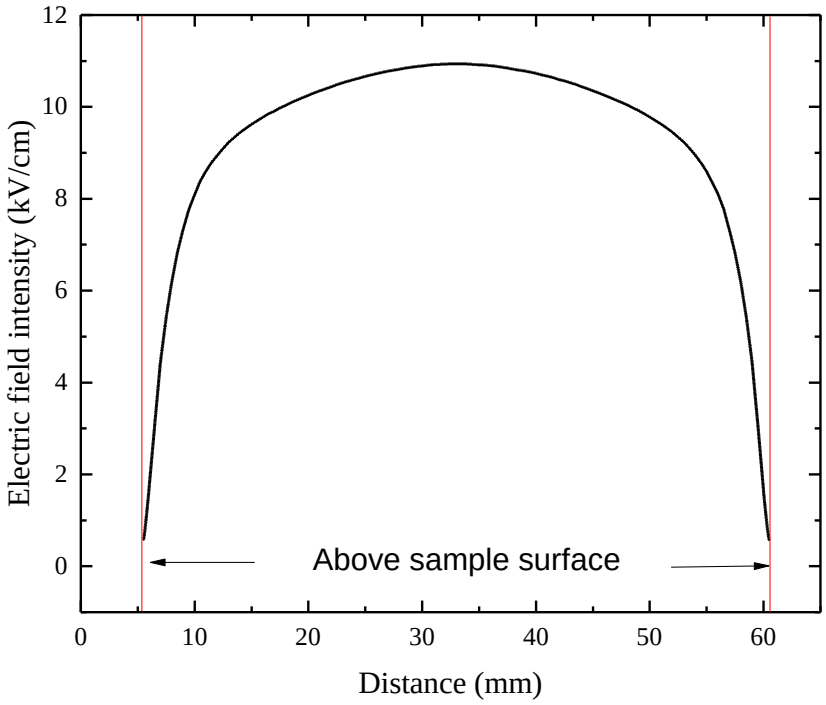

Figure 3.12. The electric field intensity along contour on the sample/air interface.

The electric field intensity has a peak value of 10.94 kV/cm, which is 20 times higher compared with the case of indirect discharge treatment. Grounded mesh does significantly reduce electric field magnitude at the sample/air interface.

3.3Transient Plasma Discharge System

As discussed in Chapter 2.3.5, transient spark discharge is a novel type of discharge which has a great potential in production of chemically reactive species and the resulting bacteridal effect. Simular to the steady-state corona discharge, many factors could be modified to provide better bactericidal and decontamination effect, such as

voltage levels, electrode configurations, and discharge polarities. Therefore, a transient plasma discharge system has been developed and tested in this series of experimental tests. In this section, the transient plasma discharge system is described.

3.3.1 System and Equipment

The schematic diagram of the transient plasma discharge system is shown in Figure 3.13.

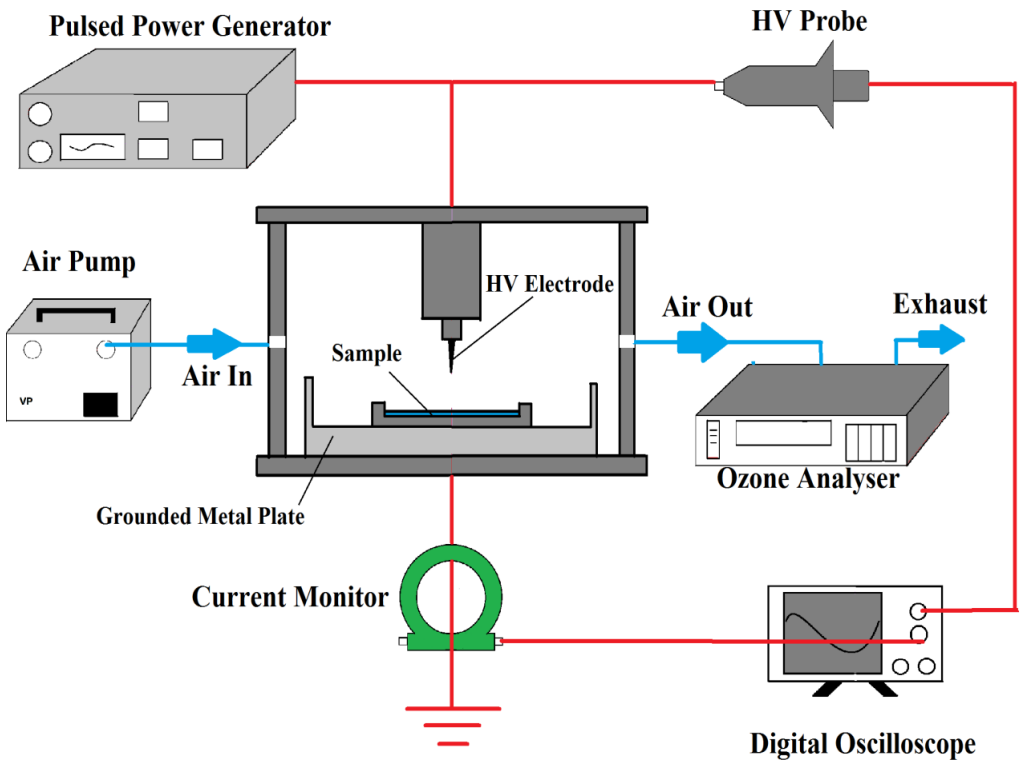

Figure 3.13. The schematic diagram of the transient plasma discharge system.

A high-voltage pulsed generator (Samtech Ltd., Scotland) was used to supply high-voltage pulses to the test cell, so the electrode inside the test cell could be energised. Transient spark discharges were produced in this way. This pulsed power generator is designed based on a high-voltage autotransformer; the voltage of pulses generated can be up to 30 kV, and the rate of rise is $(3\text{-}5)\cdot 10^2$ kV/ms. The repetition rate is also adjustable; 20 pulses per second is set for this series of experiments [187].

To monitor transient current in the discharge circuit, a Pearson current monitor (model 6585) was used. It has a bandwidth of 250 MHz, and it was installed to the wire at the ground end of the test cell. A Tektronix high-voltage probe (model P6015A) with a bandwidth of 75 MHz was used to monitor discharge voltages across the test cell. The probe can measure voltage pulses up to 40 kV, which is suitable for the current system. Both high-voltage probe and current monitor were connected to a digital oscilloscope with 50 Ω BNC cables. The digital oscilloscope used in this system is identical to the corona discharge system in the previous section (Tektronix TDS 2024, bandwidth 200 MHz, sampling rate 2 G samples/s).

An air pump (VP 1HV, KNF Neuberger Ltd.) was used to create a gentle air flow across the test cell, so that air inside the test cell could be delivered to an ozone analyser (IN-2000 LoCon, IN USA Inc.), which monitors the ozone level during discharges. Pressure and humidity in the test cell are kept the same as the ambient environment outside of the test cell (relative humidity was ~40%).

3.3.2 Transient Plasma Discharge Test cell

The transient spark test cell has a topology similar to the corona discharge test cell discussed in Section 3.2.2, but the electrodes and test cell diameter are different. The main body of the test cell is made of a Perspex cylinder with a height of 80 mm and a diameter of 150 mm. The thickness of the cylinder wall is 6 mm. Two PVC flanges cover the top and the bottom of this cylinder. Inside this cell, a single gramophone needle is used to act as the high-tension electrode. The body diameter of the needle is 1.2 mm, and the tip radius is ~36 μm. This needle electrode is installed into the top flange through a conductive screwed-in bar, which provides a connection port to the impulsive power supply. The distance between the needle tip and the sample surface can be adjusted by rotating the bar. A metal plate with a 27 mm high rounded edge is on the bottom flanges. The thickness of the plate is 10 mm; external and internal diameters are 120 mm and 100 mm, respectively. This metal plate is grounded through the earthed connection port on the bottom flange. The transient plasma discharge test cell is shown in Figure 3.14.

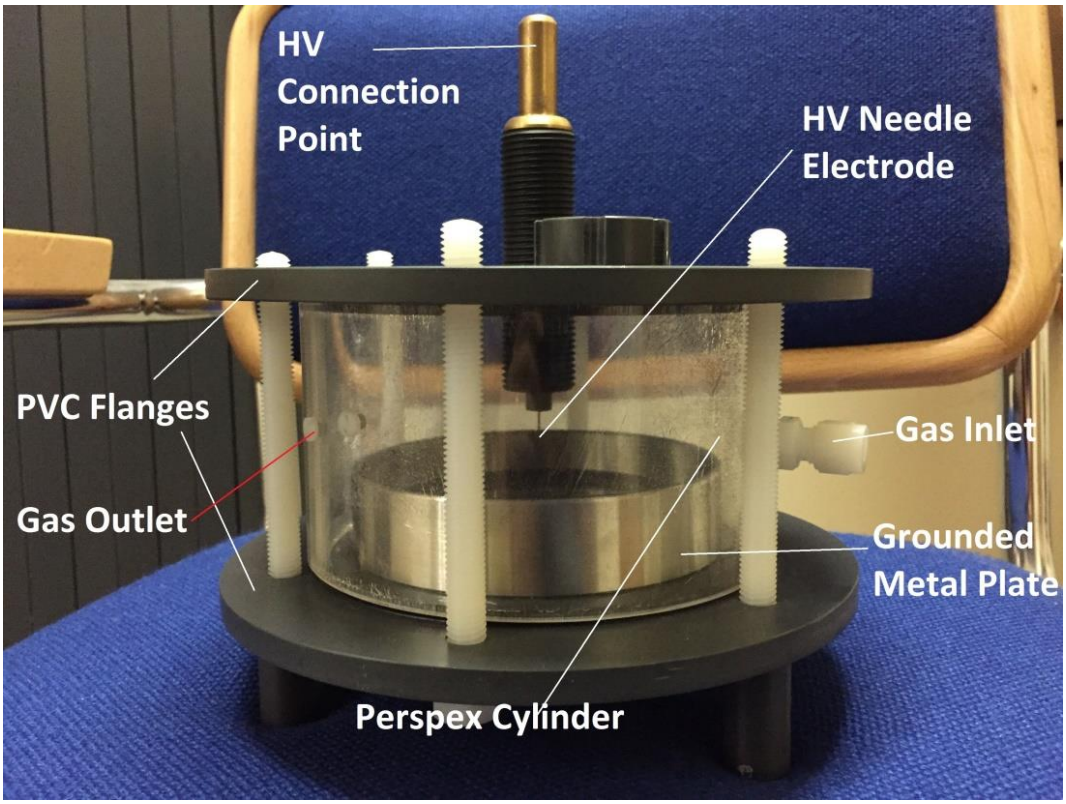

Figure 3.14. Transient plasma discharge test cell.

As in the case of the corona discharge tests, two types of sample plates were used in the impulsive discharge system: non-conductive plate (plastic contact plate), and conductive plate (plate lined with aluminum foil). By using different types of sample plates, the propagation passages of generated transient spark discharge in this system are different. The cross-section of the test cell with non-conductive and conductive sample plates are shown in Figure 3.15.

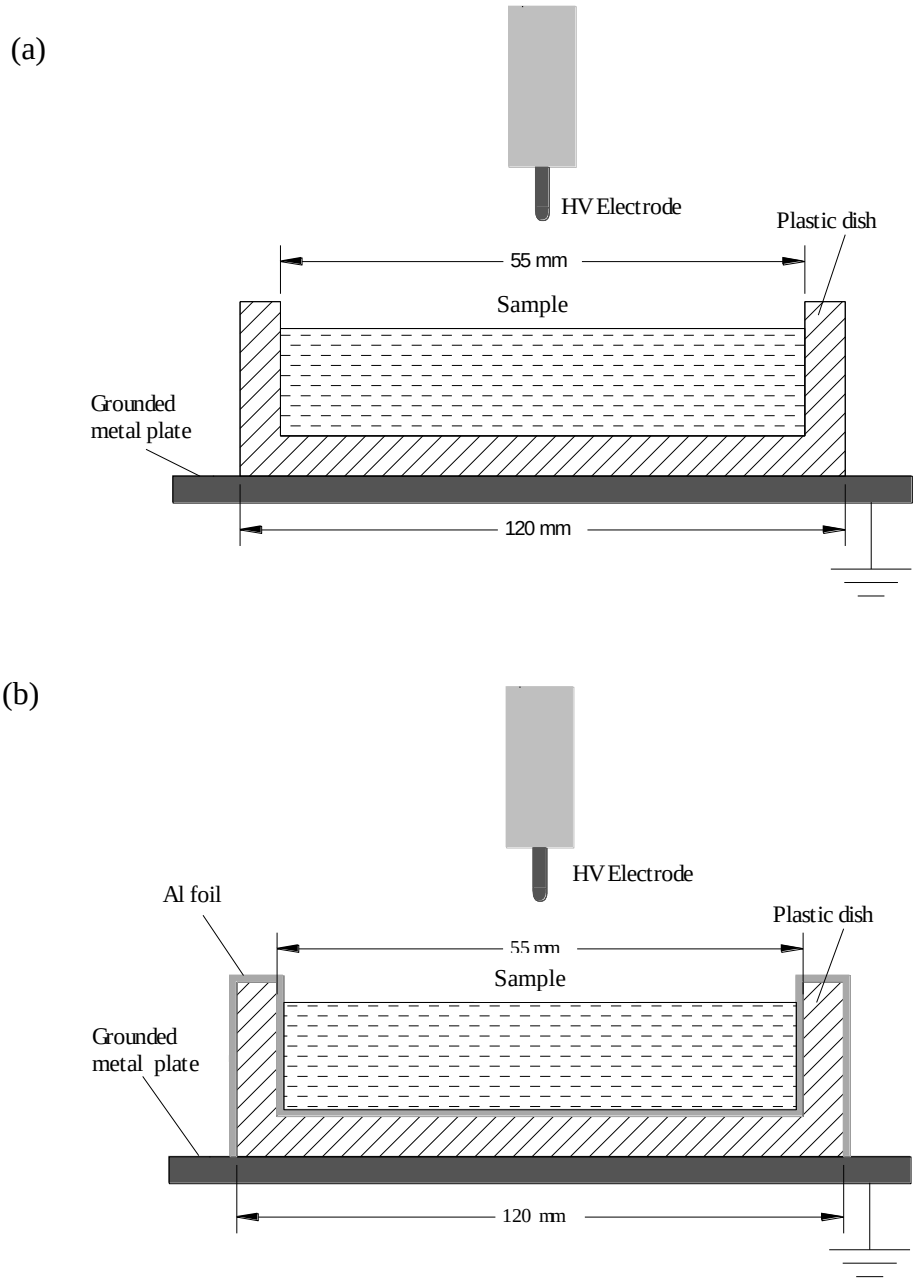

Figure 3.15. Cross-section of the treatment cells: (a). non-conductive plate (plastic plate) filled with sample, and (b). conductive plate (plastic plate lined with aluminum foil) filled with sample.

In the case of the non-conductive sample plate, as shown in Figure 3.15 (a), liquid or agar samples were held in the contact plate and placed onto the grounded metal plate. The streamer discharge produced from the high-voltage needle electrode propagated down to the surface of the sample, developed across the sample/air interface to the edge of the sample plate, and finally reached the ground.

In the case of the conductive plate, as shown in Figure 3.15 (b), the contact plate was lined with aluminum foil, and the sample was held by this conductive plate and placed onto the metal plate in the test cell. The plate was grounded in this way. The discharge produced from the high-voltage electrode propagated directly to the sample surface, and the ionic current flowed through the liquid sample toward the grounded sample plate.

As mentioned earlier, the distance between the needle and the sample surface can be adjusted. At the extreme position where the needle is in contact with the sample surface, discharges are generated at the sample/air interface, propagate along this interface to the edge of the non-conductive sample plate, and then reach the ground. In the case of the conductive sample plateplate, when the high-voltage needle electrode is in contact with the sample surface, all discharge activity and ionic conduction occurred in the liquid, and no visible discharges across the liquid/air interface were observed.

3.3.3 Electrical Characteristics of Impulsive Discharges

As mentioned in the description of the transient plasma discharge test cell, the distance from the tip of the HV needle to the sample surface can be set to different values. The breakdown voltages vary, corresponding to the different distances. Distances for breakdown voltages of 20 kV, 24 kV, and 28 kV for both polarities are listed in Table 3.3.

Table 3.3. Breakdown voltage for different distances between the HV needle electrode and liquid surface.

Peak Voltage (kV)	Non-conductive sample plate (mm)	Conductive sample plate (mm)
+20	0.53	4.98
+24	5.06	7.73
+28	7.25	11.06
-20	0.68	1.72
-24	1.37	3.32
-28	3.65	6.03

As Table 3.3 shows, for the same breakdown voltage level, the distance is shorter for the non-conductive sample plate than for the conductive sample plate. This difference in the distance could be responsible for the difference in the efficiency of the discharge treatment and will be discussed in Chapters 4-6.

In this research, transient spark discharges were generated at 20 kV, 24 kV, and 28 kV voltage levels (both polarities were used). The waveforms of discharge voltage and current were recorded by the oscilloscope. In Figure 3.16, typical discharge current and voltage waveforms are presented.

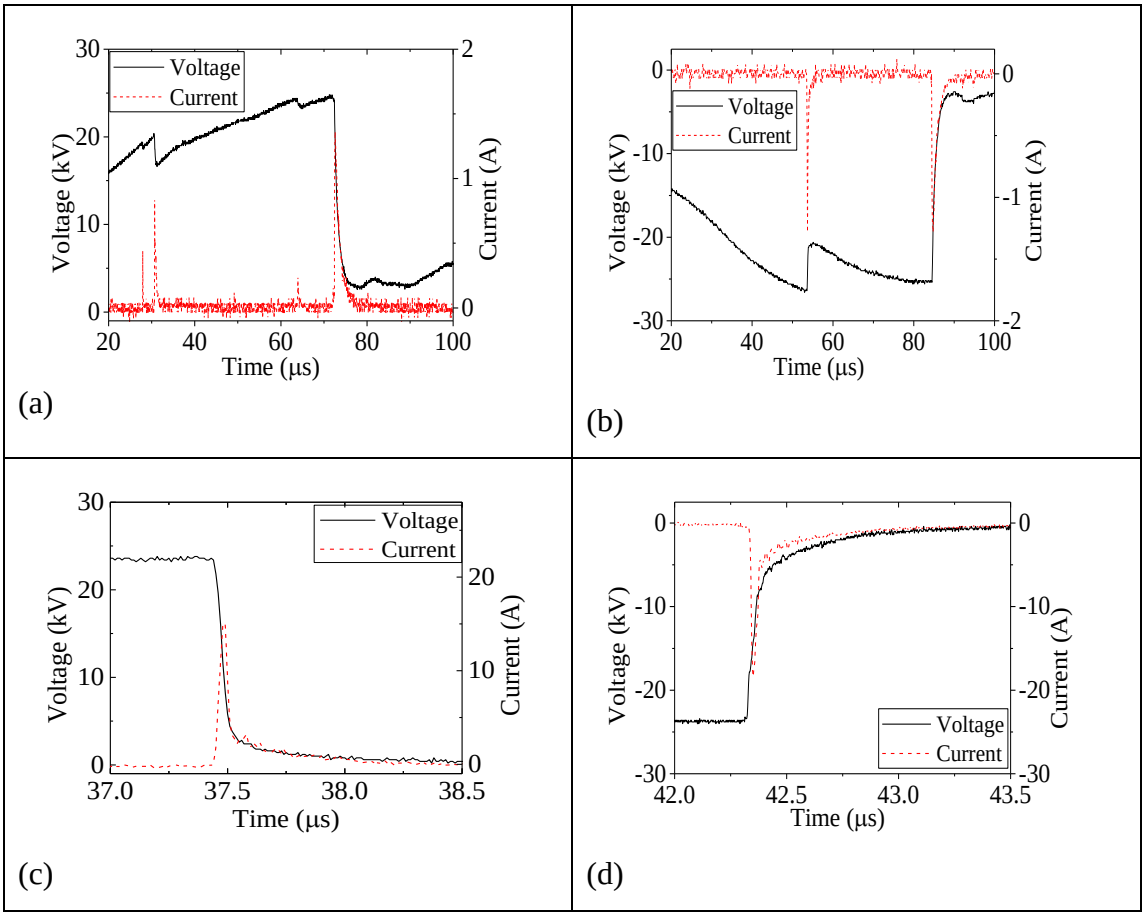

Figure 3.16. Voltage and current waveforms: (a) +24 kV non-conductive plastic plate; (b) - 24 kV non-conductive plastic plate; (c) +24 kV foil-lined conductive plate; and (d) -24 kV foil-lined conductive plate.

As shown in Figure 3.16 (a, b), when the transient spark discharge is developed in the test cell with non-conductive sample plates, multiple current peaks can be observed in the discharge current and voltage waveforms. Corresponding drops in voltage also are clearly seen in the voltage waveforms (flashes) before the complete breakdown between high-voltage electrode and ground. This complete breakdown is manifested by the voltage collapse to zero. The existence of the multiple current peaks is related to the breakdown path: the streamer propagates from the tip of the needle electrode to the sample surface, across the sample/air interface, and finally reaches the ground from the edge of the sample plate.

The discharge voltage and current waveforms obtained in the case of treatment in the conductive sample plates are presented in Figure 3.16 (c, d). Only one single current

peak is observed in each of these waveforms. The breakdown path of the transient streamer is from the tip of the needle electrode vertically down to the sample surface, and then the discharge passes through the sample to the ground.

The magnitude of breakdown current peaks is quite different between the two cases. Waveforms (a) and (c) in Figure 3.16 confirm this statement: the peak discharge current is ~1.36 A (at breakdown voltage of +24.6 kV) in the case of non-conductive sample plates. This value is much lower than in the case of conductive sample plates: ~16.1 A at breakdown voltage of +23.8 kV. In addition, the duration of discharges is also different: ~1 μs when using the conductive sample plate and ~10 μs when using the non-conductive sample plate.

Also, it was observed that the peak current increases with an increase in the applied voltage. For example, in the case of a conductive foil-lined plate, when the (negative) applied voltage was increased from -20 kV to -24 kV, the peak discharge current increased by more than 50%, and an 80% increase was observed when the voltage was increased to -28 kV. In the case of the non-conductive plastic plate, the peak discharge current was doubled when the voltage was increased from -20 kV to -24 kV, and increased by three times when the voltage was increased to -28 kV.

3.3.4 Electric Field Simulation

According to the system and tests described in the previous section, the electrostatic model of transient spark discharges was built, and the field analysis was conducted in Quickfield 5.10. Different topologies (conductive and non-conductive plates) and electrode-sample distance (as shown in Table 3.3) were considered in this series of simulations.

Non-conductive Sample Plate

In this case, the relative permittivity of the sample plate was set as 2.5 (55 mm contact plate), and the grounded electrode was the metal plate under the sample plate. The voltage of the stressed HV electrode was set as 28 kV, 24 kV, and 20 kV with related electrode-sample distances.

The electric field distribution during transient plasma discharge with a breakdown voltage of +28 kV with electrode distance of 7.25 mm is shown in Figure 3.17.

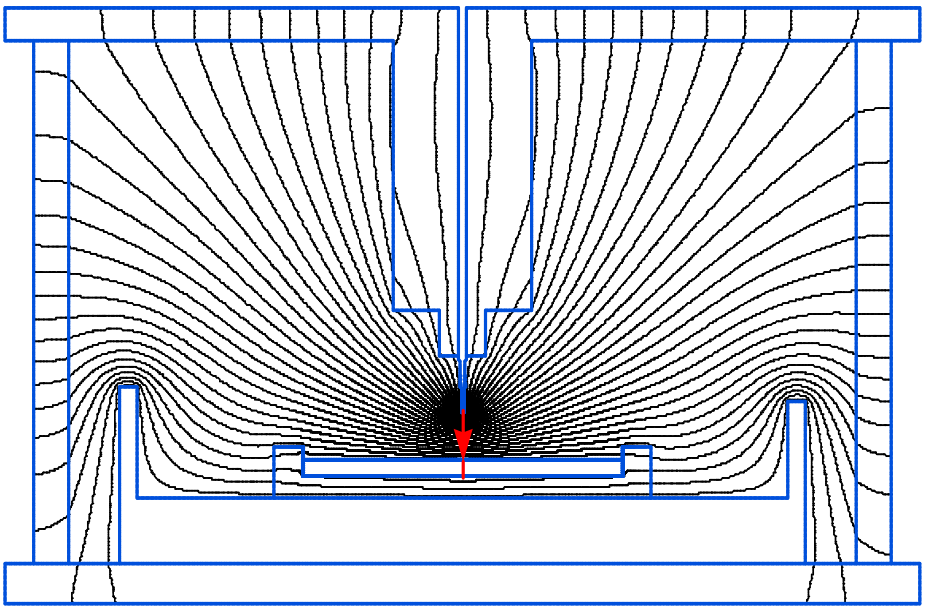

Figure 3.17. The equipotential lines during the transient plasma discharge with a breakdown voltage of +28 kV for the case of the non-conductive sample plate.

The electric field distribution under other breakdown voltage levels is similar to that shown in Figure 3.17, but the intensity of the field is different. The intensity of the electric field from the HV electrode to the sample along the vertical direction (as the red arrow points in Figure 3.17) is shown in Figure 3.18.

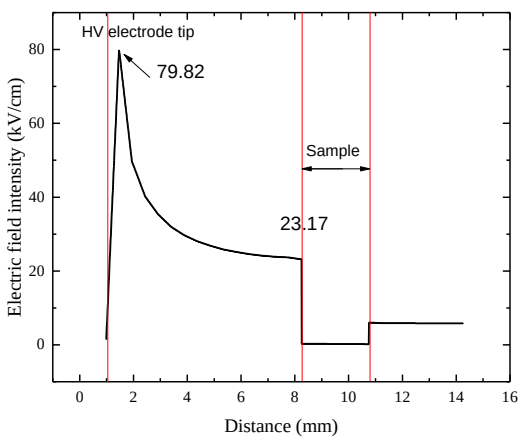

(a)

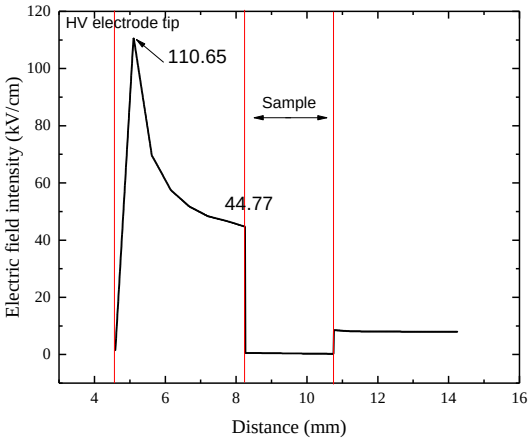

(b)

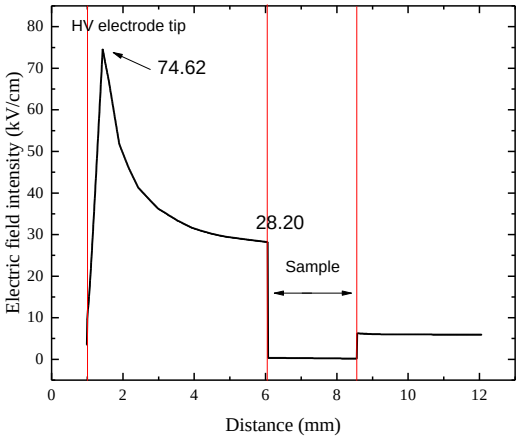

(c)

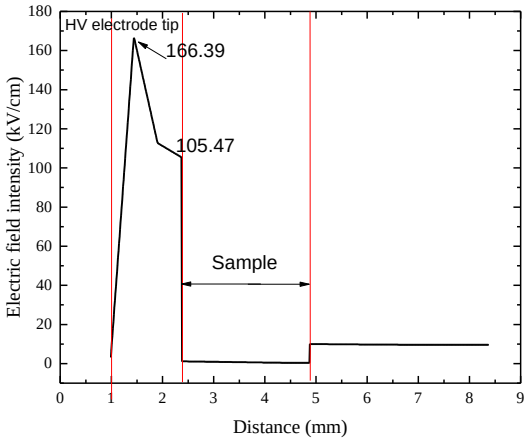

(d)

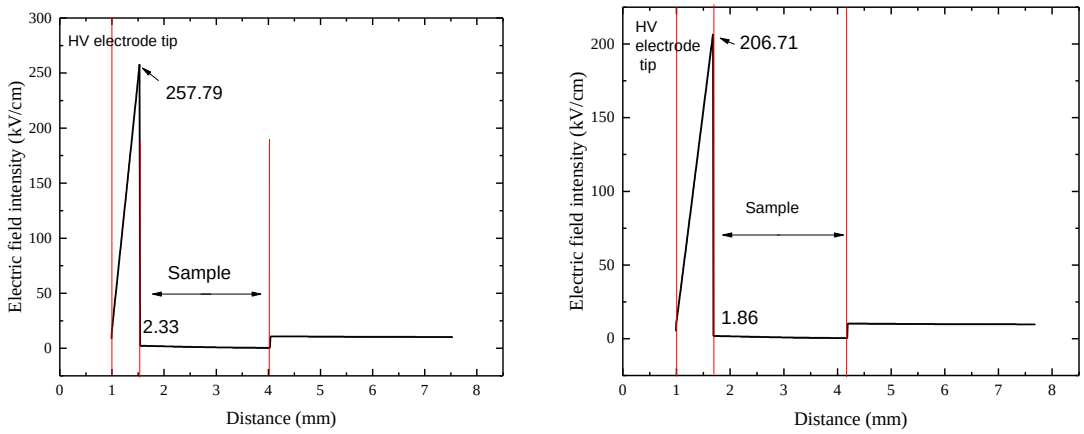

(e) (f)

Figure 3.18. Intensity of electric field along vertical direction from the electrode to the sample with breakdown voltage (a) +28 kV, (b)-28 kV, (c)+24 kV, (d)-24 kV, (e)+20 kV, and (f)-20 kV.

The intensity of the electric field in a position which is close to the sample (0.1 mm above the sample surface) has also been monitored. Results are shown in Figure 3.19.

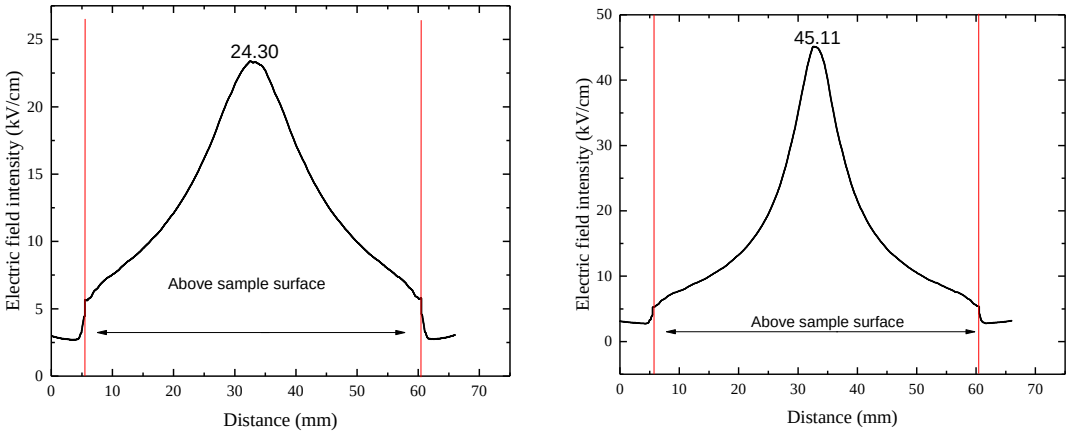

(a) (b)

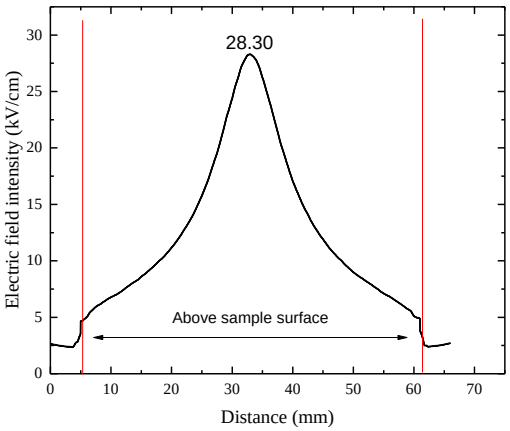

(c)

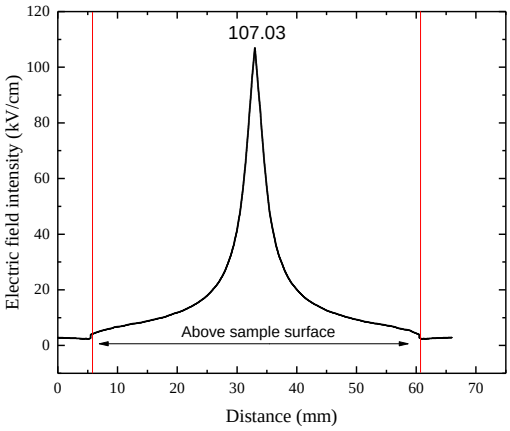

(d)

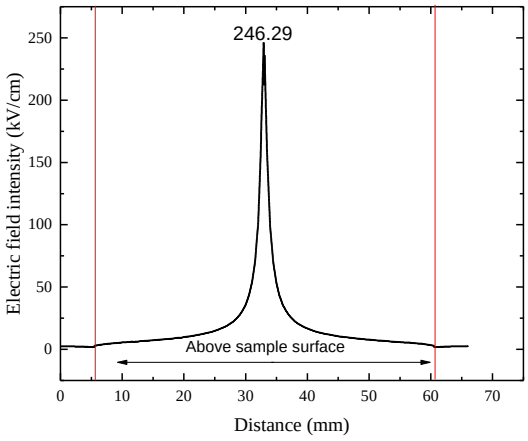

(e)

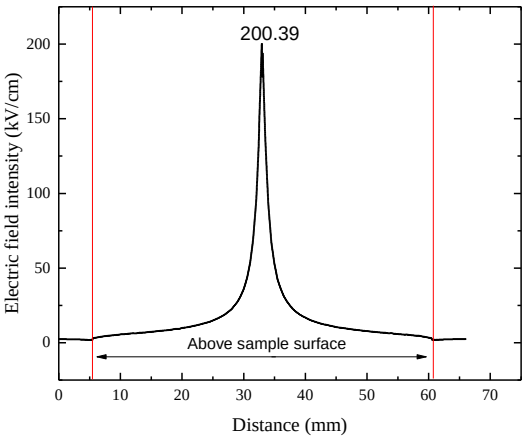

(f)

Figure 3.19. Intensity of electric field, for the case of the non-conductive sample plate, along horizontal direction 0.1 mm above sample surface with breakdown voltage (a) +28 kV, (b)-28 kV, (c)+24 kV, (d)-24 kV, (e)+20 kV, and (f)-20 kV.

Conductive Sample Plate

In the case of the conductive sample plate, the sample plate was set as the grounded electrode. The equipotential lines in this case with the breakdown voltage of +28 kV are shown in Figure 3.20.

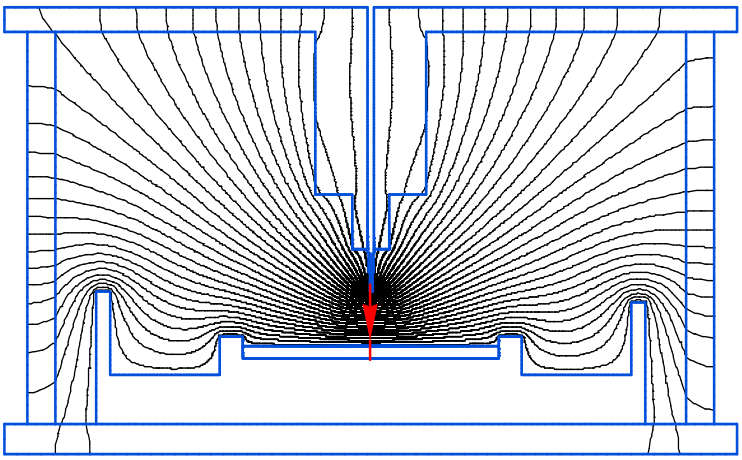

Figure 3.20. The equipotential lines of transient plasma discharge with a breakdown voltage of +28 kV for the case of the conductive sample plate.

The intensity of the electric field with different breakdown voltages is measured in a vertical direction from the electrode to the sample (as the red arrow points in Figure 3.20). Results are shown in Figure 3.21.

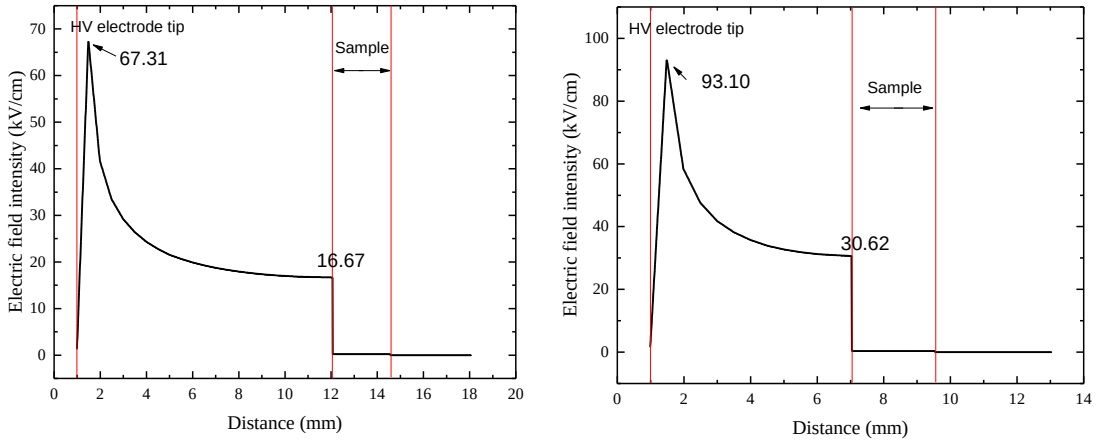

(a) (b)

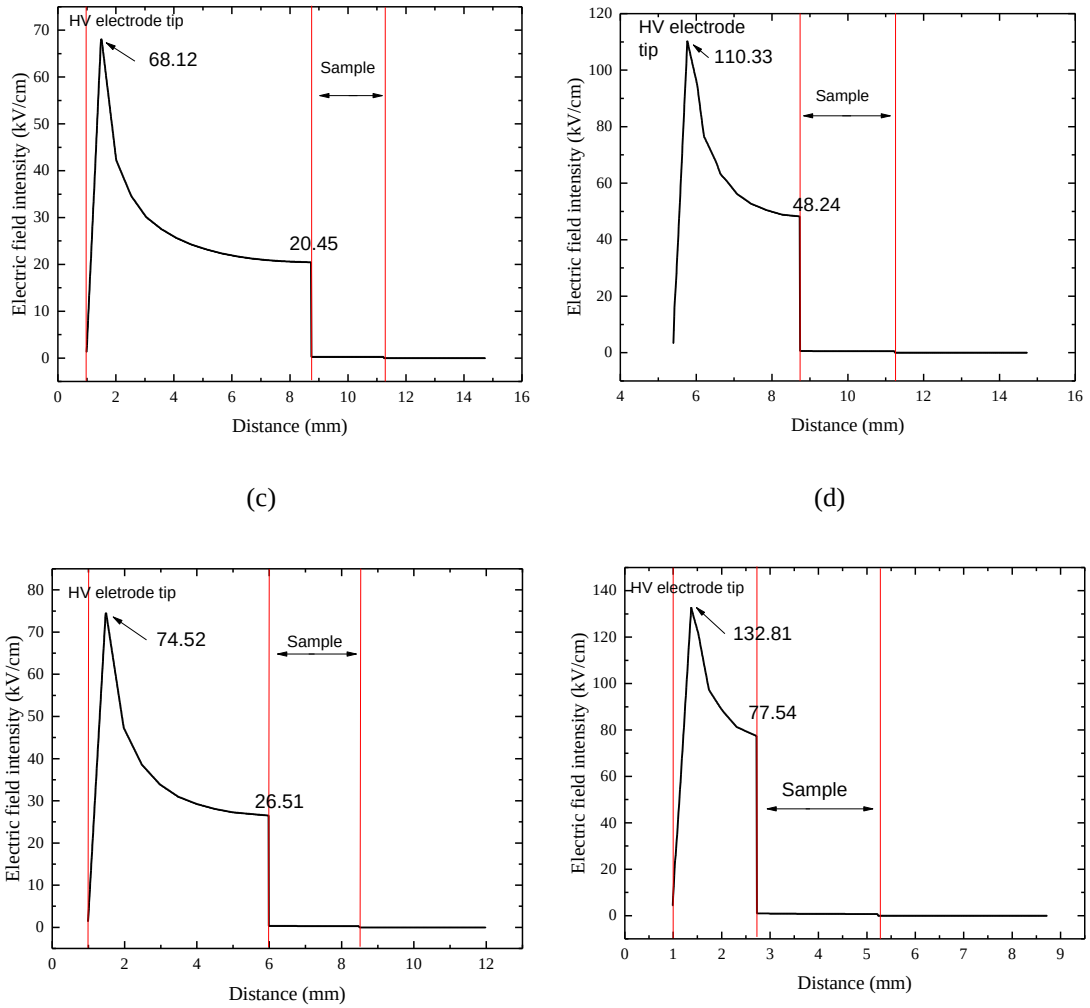

Figure 3.21. Intensity of electric field, for the case of the conductive sample plate, along horizontal direction 0.1 mm above sample surface with breakdown voltage (a) +28 kV, (b)-28 kV, (c)+24 kV, (d)-24 kV, (e)+20 kV, and (f)-20 kV.

In the horizontal direction, the electric field intensity also was measured. The results are shown in Figure 3.22.

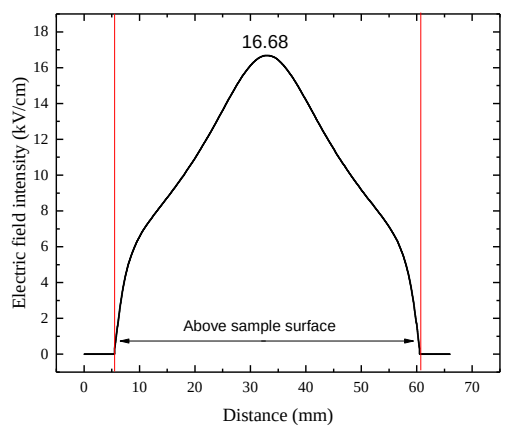

(a)

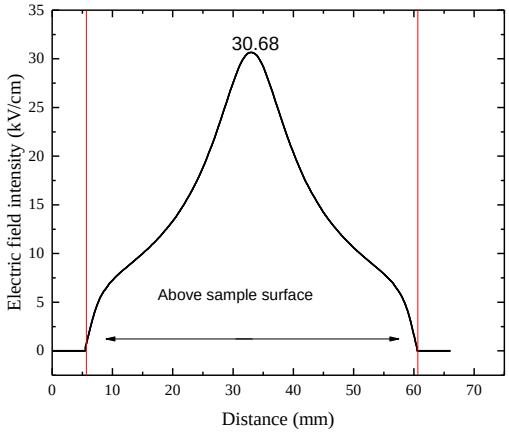

(b)

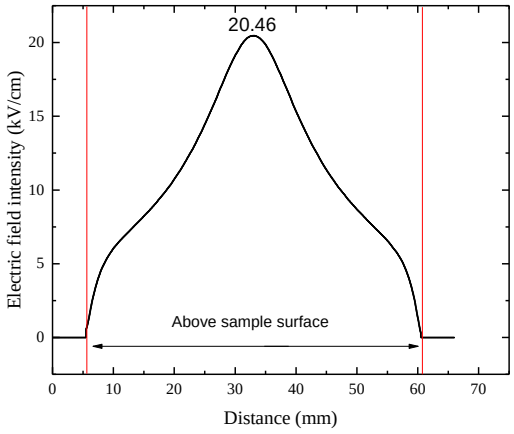

(c)

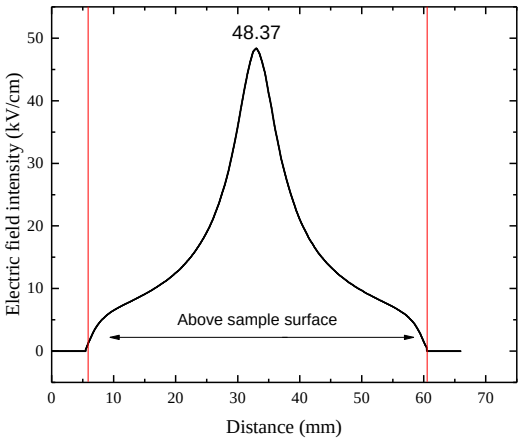

(d)

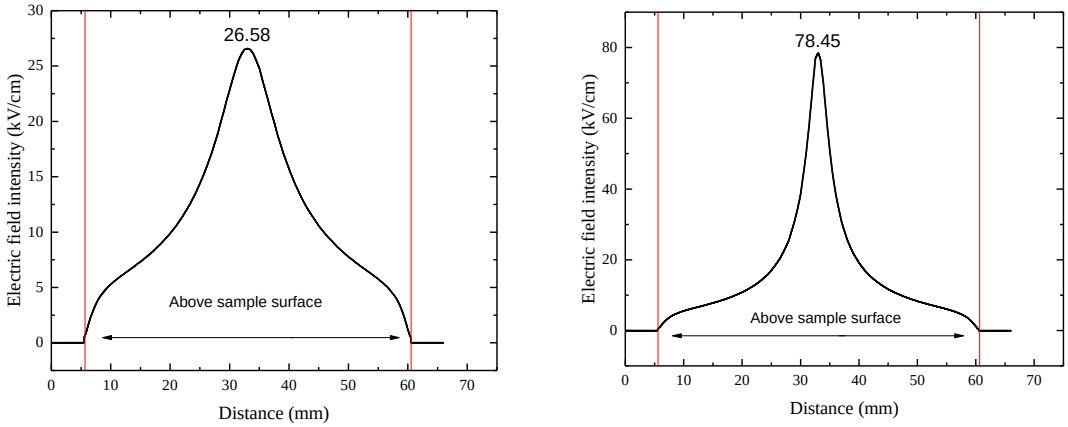

(e) (f)

Figure 3.22. Intensity of electric field, in the case of the conductive sample plate, along horizontal direction, 0.1 mm above the sample surface with breakdown voltage (a) +28 kV, (b)-28 kV, (c)+24 kV, (d)-24 kV, (e)+20 kV, and (f)-20 kV.

3.4 Summary

In this chapter, the experimental set-up designed and developed to generate the non-thermal plasma discharges was described. The systems and equipment used in this research project were listed and discussed. Designed non-thermal plasma discharge systems can perform steady-state corona discharge/transient spark dischare treatment under different conditions.

In the study of the steady-state corona discharge, both positive and negative polarities were tested, and samples were exposed to the corona discharge directly or indirectly. In the case of the transient plasma discharges, different voltage levels and configurations were applied. Also, discharges of both polarities were generated in the system.

In addition, the pre-experiment analysis of the electric field was addressed in this chapter. The electrical characteristics of the generated corona discharges and transient plasma discharges were presented and discussed, including the waveforms of dicharge voltage/current and the results of electric field simulations.

CHAPTER 4

Oxidation Capability of Atmospheric Non-Thermal Plasma Discharges

4.1 Introduction

As discussed in Chapter 2 (Literature Review), the bactericidal and chemical effects of non-thermal plasma discharges have been actively studied. Chemically reactive species are generated by non-thermal plasma discharges along with UV light and an intensive electric field. Although the chemical composition of non-thermal plasma discharges in the air is still not fully understood, it has been established that such discharges generate reactive oxygen species and nitrogen species that have high oxidation capability. In the case of bacterial inactivation, plasma discharge-induced oxidation damage to the bio-cell is considered to be the main mechanism that leads to cell death [69], [93], [107], [188]. More importantly, non-thermal plasma discharges are recognised as one of the novel technologies for advanced oxidation processes (AOPs), and applications in the area of air cleaning and wastewater remediation are actively studied [189]–[192]. Therefore, the oxidation capability of atmospheric plasma discharges should be investigated to optimise the biological and chemical effects of atmospheric non-thermal plasma discharges.

It has been reported that chemicals such as azo dye, methylene blue, phenol, and other organic compounds can be decomposed by non-thermal plasma discharges [8], [193]–[195]. Chemical degradation can be used as an indication of the oxidation capability of plasma discharges. As suggested in [8], [30], [189], and [195], ozone, hydroxyl radicals, and singlet oxygen are primarily responsible for the oxidation effect. However, multiple reactive species are generated by plasma discharges, and their contributions to the oxidation process cannot be ruled out completely. Additionally, the production of reactive chemical species by plasma discharges can vary under different conditions such as discharge voltage, energy delivered to plasma, electrode configuration, and types of discharges. In [196], Sato *et al.* used different gases and electrode topologies to decompose phenol by plasma discharges. The authors reported that the electrode shape influences the phenol decomposition rate. Also, it was

reported in [196] that discharges in argon provided better decomposition rate than in oxygen and air. Various attempts have been made to investigate the oxidation mechanisms of plasma discharges. However, still there is a gap in understanding of the mechanism and efficiency of the plasma-induced oxidation.

In the present research project, the oxidation capabilities of the steady-state corona discharges and transient plasma discharges were investigated. Indigo carmine water solution was selected as a chemical sensor and exposed to non-thermal plasma discharges. Based on the degree of decolorisation of treated indigo carmine solution, the oxidation capability of non-thermal plasma discharge was obtained. According to [190], the possible factors that could affect the plasma oxidation efficiency include gas input, energy input, plasma reactor topologies, and energisation regime. In this series of experiments, the decolorisation tests were conducted using plasma discharges under different conditions: polarity, voltage level, air humidity, and electrode topology.

In this chapter, the experimental methodology, plasma systems, and analysis of the obtained results are presented. The achieved oxidation effects for both types of discharges is discussed. Information on further optimisation of the plasma systems for efficient oxidation of liquid samples is provided.

4.2 Experimental Methodology

4.2.1 Indigo Carmine as a Chemical Sensor

To investigate the oxidation capability of non-thermal plasma discharges, including steady-state corona discharge and transient plasma discharge, in this research, indigo carmine water solution was chosen as the target sample (chemical sensor).

Indigo carmine ($C_{16}H_8N_2Na_2O_8S_2$) is a commonly used, non-toxic chemical with the formula weight of 466.35 g/mol. It is often used as PH indicator, redox indicator, cell stain, and even food colorant. Its molecular structure is shown in Figure 4.1.

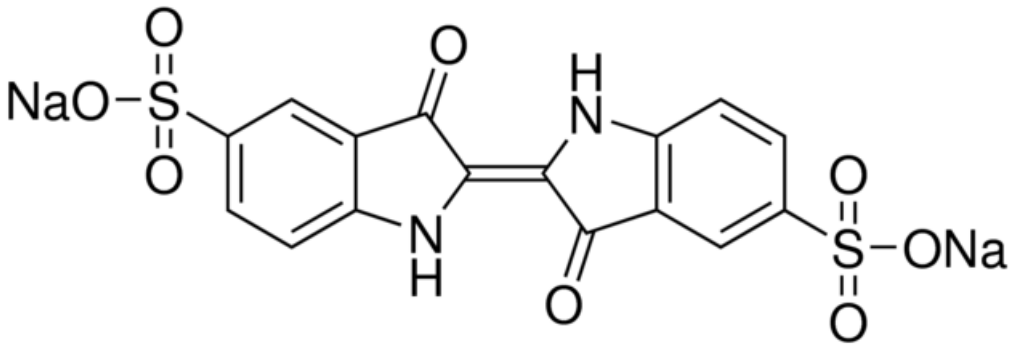

Figure 4.1. Molecular structure of indigo carmine [198].

Indigo carmine is dark blue in color and powder in form. The solution of indigo carmine is typically a blue color. However, indigo carmine can react with superoxide and form isatin sulfonic acid [197], [198]. Consequently, the concentration of indigo carmine is reduced, and the blue color of this solution turns yellowish. In many studies, this method was used to detect ozone [199], [200]. Indigo carmine also can react with other oxidative species such as OH radicals [201], [202], [203]. As discussed in the literature review, ozone and other oxygen reactive species can be generated during high-voltage discharges. Indigo carmine can be oxidized by those products, which results in a color change in the solution. This color change is much easier to recognize compared with other complex methods such as emission spectrum analysis of discharges. Therefore, the indigo carmine solution is selected as a target sample to indicate the oxidation capability of non-thermal discharges.

It is also important to note that the color of indigo carmine solution can be affected by the change in pH. Generally, indigo carmine solution appears to be blue in solutions with a pH below 11.4. It is known that pH in the target sample solution is affected by the production of reactive species during discharges. Thus, it is necessary to monitor pH of the target sample solution before and after the discharge treatment experiment. If a significant pH change is observed, then the color change of the indigo carmine solution could be a result of oxidation, pH change, or both. Further experiments would be required in such case.

Preparation of Indigo Carmine Solution

Indigo carmine dye in the form of dry powder was purchased from Sigma-Aldrich (product code 131164) and used to make aqueous solution samples. The purity of this dye powder is >85%. Figure 4.2 shows the original powder dye and the aqueous solution.

Figure 4.2. Indigo carmine original powder (left) and aqueous solution (right).

A 59 mg indigo carmine sample was weighed using a digital analytical balance (Ohaus® Adventurer® balance AR 1530); the effective dye content is 50 mg. Next, the powder was dissolved in 200 ml distilled water to create a solution with a concentration of ~0.25 g/L. This solution was stored in a 250 ml bottle and kept in a cool, dark place.

The pH of this sample solution is between 5.0 and 5.2, as measured using the Hannah pH210 Microprocessor pH meter with Sentek miniature probe (see Figure 4.3). This pH meter also has been used to measure the pH of sample solutions after exposure to plasma discharges.

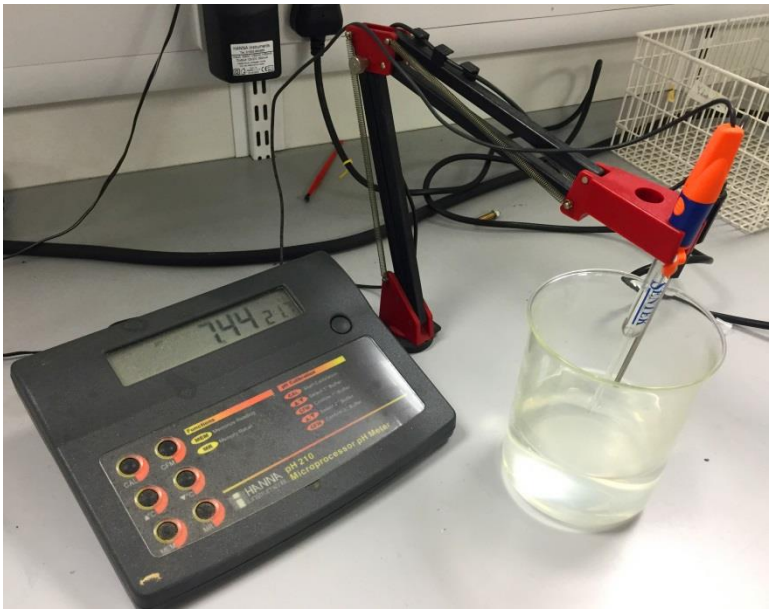

Figure 4.3. Hannah pH210 Microprocessor pH meter and Sentek miniature pH probe.

Before the plasma treatment, a 5 ml sample solution was transferred onto a non-conductive or conductive sample plate, as shown in Figure 4.4. Clean, 4 ml plastic transfer pipettes (Thermo Scientific™ Sterilin™) were used during the process to avoid any contact with the solution sample. Then, the sample solution together with the sample plate was put into the test cell and exposed to high-voltage discharges.

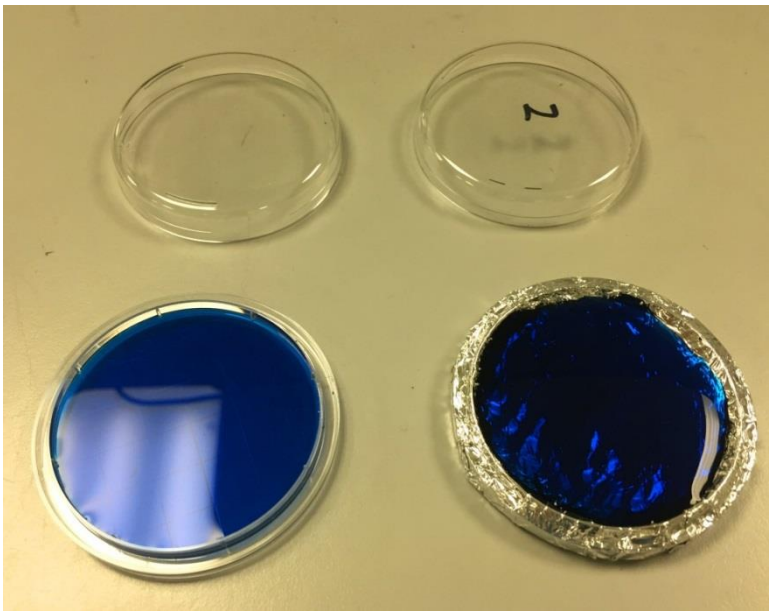

Figure 4.4. The 5 ml sample solution in the non-conductive sample plate (left) and in the conductive sample plate (right).

4.2.2 Optical Transmittance of Indigo Carmine Solutions

As mentioned earlier, the intensity of blue color of the indigo carmine solution will be changed as a result of the plasma oxidation effect (the solution will be decolorized). However, this change in color may not be recognised easily by the naked eye, and an analytical method should be used to monitor any changes in optical properties of the treated indigo carmine solutions.

In this series of experiments, the indigo carmine sample solution was exposed to high-voltage plasma discharges, and transferred into plastic cuvettes (BrandTech, UK) and analysed by a UV-visible spectrophotometer (Biomate, Thermo-Spectronics Europe), as shown in Figure 4.5. In this way, the decolorisation of the blue indigo carmine sample solution can be registered as the change of transmittance. By measuring this change in optical transmittance, the degree of decolorisation is established and quantified, so the oxidation capability of plasma discharges can be established.

Figure 4.5. UV-visible spectrophotometer and sample cuvettes.

Differential optical transmittance

The UV–visible spectrophotometer can measure differential optical transmittance by comparing transmittances of two samples. This function is used to detect the change in transmittance of the sample solution after exposure to the plasma discharges. The basic concept of this type of measurement is explained in the following paragraphs.

Two samples were placed into the spectrophotometer: Sample A is the control sample and is referred to as the original sample solution that has not been exposed to plasma discharges; Sample B is a target sample, which has been exposed to the plasma discharges. The differential transmittance is defined as:

$$\mathrm{T}\% = \frac{T_b}{T_a} \cdot 100\% \qquad (4.1)$$

where T_a is the transmittance of sample A (unexposed sample);

T_b is the transmittance of sample B (exposed sample).

The differential transmittance directly indicates the change in transmittance of the indigo carmine sample solution after exposure to high-voltage plasma discharges.

Differential transmittance of the samples was measured in the range from 200 nm to 1000 nm. This range covers the wavelength of near UV, visible light, and IR. Noise was observed at the UV wavelength range due to the nature of the sample and equipment. Therefore, the actual wavelength with information is from 350 nm to 1000 nm.

First, the unexposed original sample solution was measured as an example. In this case, distilled water was used as the control sample. The differential transmittance of the unexposed sample compared to distilled water is shown in Figure 4.6.

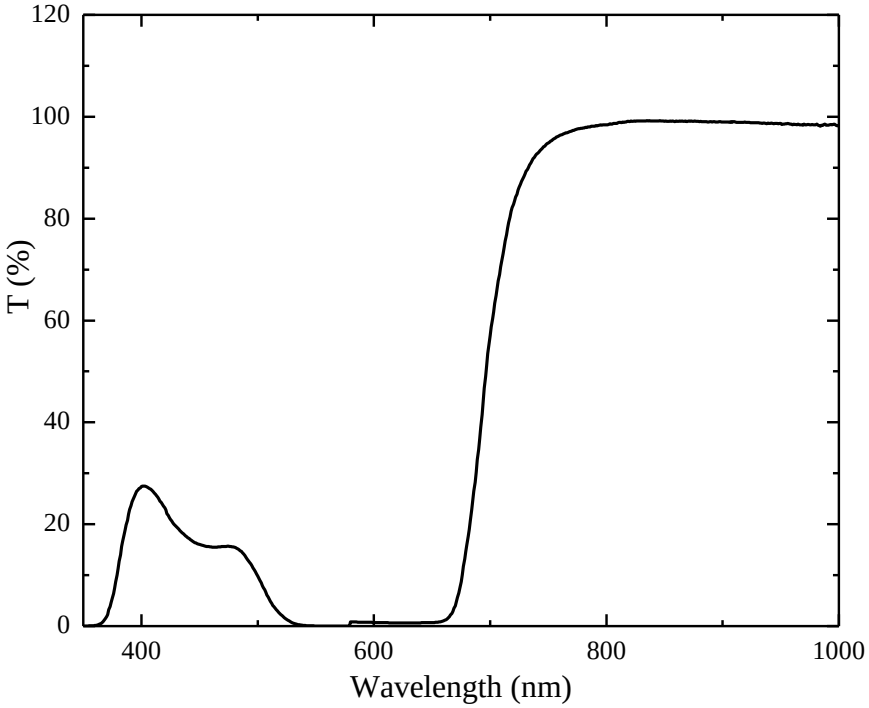

Figure 4.6. Differential transmittance of unexposed sample compared to distilled water.

It is clear that in the wavelength range from 350 nm to 700 nm, the differential transmittance (T%) is less than 100%. This means the indigo carmine solution has a lower transmittance compared to distilled water. In other words, the indigo carmine sample solution absorbs much more visible light.

The original unexposed indigo carmine solution is then used as the control sample (sample A); the exposed sample solution is used as the target sample (sample B). The differential transmittance spectrum is measured. Figure 4.7 and Figure 4.8 are two examples of the differential transmittance spectrum of "exposed sample to unexposed sample". Measurements were taken after the sample was exposed to positive indirect corona discharges for 2 minutes (Figure 4.7) and for 10 minutes (Figure 4.8).

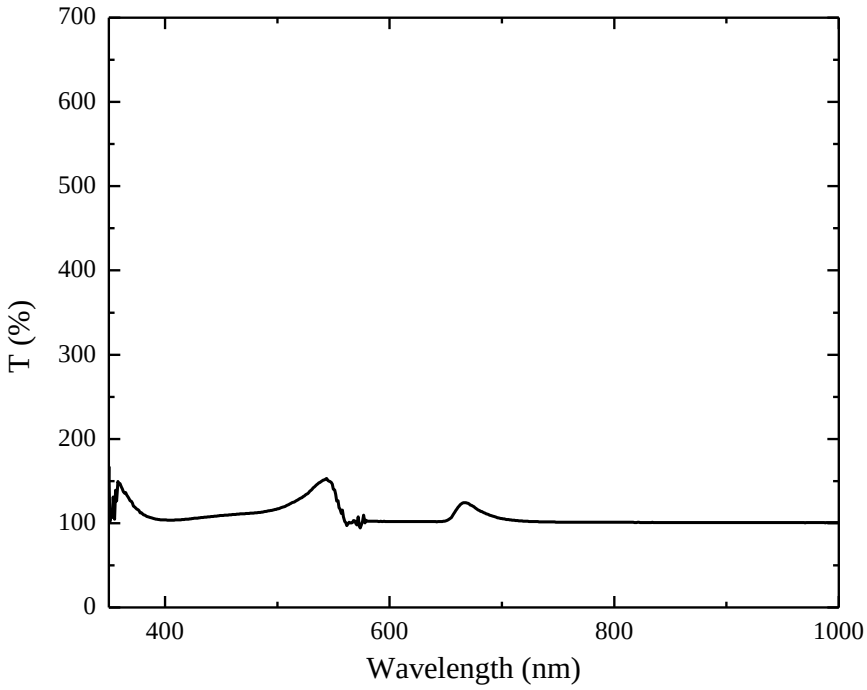

Figure 4.7. Differential transmittance spectrum of the sample after exposure to positive indirect corona discharges for 2 minutes.

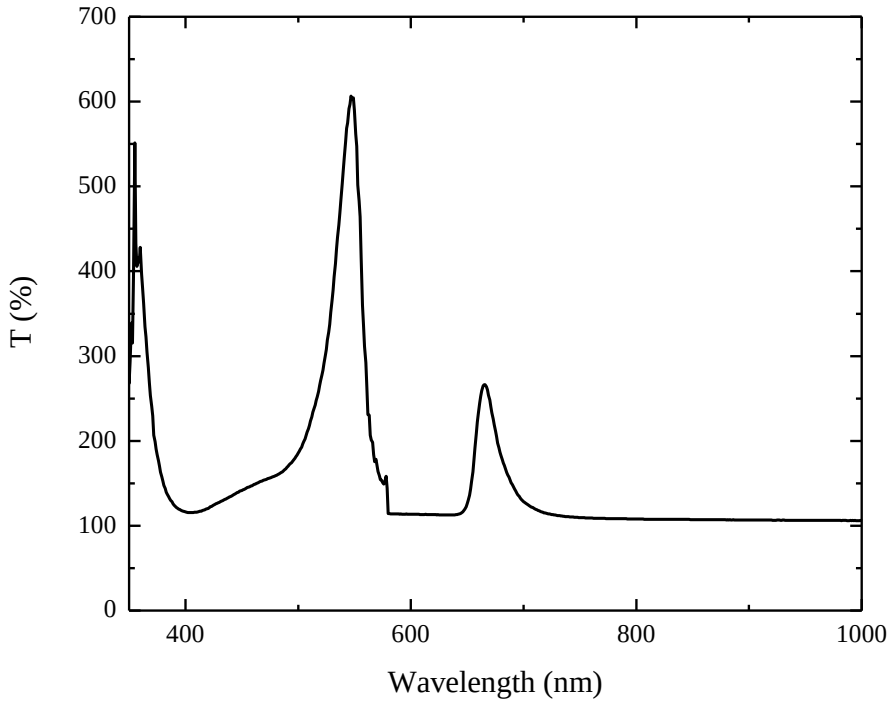

Figure 4.8. Differential transmittance spectrum of the sample after exposure to positive indirect corona discharges for 10 minutes.

As mentioned in the previous section, oxidation effects or pH changes can make the indigo carmine solution change color from blue to yellow. Therefore, in the differential spectrum, the changes in the wavelength ranging from 450 nm to 590 nm should be investigated, because this is the wavelength range for blue to yellow light.

Three main peaks can be observed in each spectrum, and these peaks indicate that the differential transmittance is above 100%. This means that the transmittance of the sample solution exposed to plasma has increased compared to that of the original unexposed sample solution. The major peak is observed at 550 nm. This wavelength matches the wavelength range of green light (495–570 nm), which is between the wavelength range of blue light (450–495 nm) and yellow light (570–590 nm). As discussed in the previous section, the oxidation effect or pH increment leads to the change in color of the indigo carmine solution, from blue to yellowish. Therefore, the peak at 550 nm in the differential transmittance spectrum is the most representative peak which can be used to obtain the magnitude of the color change. This peak was selected as an indicator to show the oxidation capability of plasma discharges. The values of the 550 nm peak in all the differential transmittance spectrums will be presented in Section 4.3 and Section 4.4.

Examination of Figure 4.7 and Figure 4.8 demonstrates that a longer exposure under the corona discharges results in a larger increment in the transmittance. After 2 minutes of exposure, the differential transmittance at 550 nm is 170%. However, after 7 minutes of exposure to plasma discharges, this peak increased to more than 600%.

4.2.3 Concentration of Indigo Carmine in Solution

The change in the optical transmittance of the sample solution exposed to plasma discharges is related to the oxidation capability of atmospheric non-thermal plasma discharge. Through comparison of the differential transmittance spectrum at 550 nm, the oxidation effect of discharges can be estimated indirectly. The change of transmittance is caused by the change of concentration of indigo carmine dye in the solution samples. The oxidation process reduces the concentration of indigo carmine molecules in the sample solution. Therefore, the change in concentration of indigo

carmine molecules in the solution directly shows the oxidation capability of the plasma discharges to which the sample was exposed.

Based on the peak in each differential transmittance spectrum, the actual concentration of indigo carmine in the treated sample solution was calculated by applying the Beer-Lambert law. The general concept of this calculation is discussed next.

Beer-Lambert Law

For a situation in which monochromatic light is induced to the surface of the homogeneous medium, and travels through this medium with a certain depth, the Beer-Lambert law defines the transmittance as:

$$T = \frac{I}{I_0} = 10^{-\varepsilon \ell c} \tag{4.2}$$

where Tis the transmittance

ε is the molar absorptivity of the media (m^2/mol)

c is the molar concentration of the media (mol/L)

ℓ is the depth of the media (m)

Transmittance is the ratio of the transmitted light intensity, I, to induced light intensity, I_0. According to the Beer-Lambert law, the transmittance of the media is related to its molar absorptivity, ε, molar concentration, c, and depth, ℓ.

Initial calculations were made for the original unexposed sample solution with a volume of 0.2 L:
Volume =0.2 L.
Concentration of indigo carmine in untreated sample c_u= 0.25 g/L.
Hence, the mass of indigo carmine in the sample is m=0.25 • 0.2=0.05 g (in 0.2 L).

The molar mass of the indigo carmine molecule is 466.36 g/mol; therefore, 0.2 L contains
$0.05/466.36 = 1.072.10^{-4}$ mol of indigo carmine.

Hence, the initial molar concentration of dye, c, in the fresh solution before exposure to plasma (t=0) is:

$c_0 = 1.072.10^{-4}/0.2 = 5.36.10^{-4}$ mol/L.

This value can be used in the Beer-Lambert law to calculate the molar absorptivity of indigo carmine:

$$\varepsilon = -\frac{\log(T_0)}{c_0 \ell} \tag{4.3}$$

where ℓ is the depth of the cuvette, $\ell = 0.01$ m. With known transmittance of the original unexposed sample solution, this molar absorptivity can be calculated.

For a sample solution exposed to plasma discharge for a period of t, the concentration of indigo carmine C_t can be calculated using equation (4.4):

$$c_t = -\frac{\log(T_t)}{\varepsilon \ell} \tag{4.4}$$

where T_t is the measured transmittance of the exposed sample solution; the molar absorptivity, ε, can be obtained by equation (4.3）.

Simplified Calculations Based on Differential Transmittance

In this research, the differential transmittance of the exposed and unexposed samples was measured. However, the absolute transmittance of individual exposed samples were not measured. This is because the differential transmittance can be used to

obtain the changes in transmittance of the treated samples. Equations (4.3) and (4.4) can be combined and rearranged so the concentration of indigo carmine in the exposed sample solution can be calculated.

In differential transmittance measurements, two samples with different concentrations of indigo carmine were used.

For sample A, by using equation (4.2), transmittance, T_a, can be written as:

$$T_a = 10^{-\varepsilon \ell c_a} \tag{4.5}$$

where c_a is the concentration of indigo carmine in sample A (g/L).

The same approach is taken in the case of sample B:

$$T_b = 10^{-\varepsilon \ell c_b} \tag{4.6}$$

where c_b is the concentration of indigo carmine in sample B (g/L).

Thus, the differential transmittance T% of samples A and B can be determined:

$$T\% = \frac{T_b}{T_a} = \frac{10^{-\varepsilon \ell c_b}}{10^{-\varepsilon \ell c_a}} = 10^{-\varepsilon \ell (c_b - c_a)} \tag{4.7}$$

The value of $\varepsilon \cdot \ell$ can be calculated from transformation of equation (4.5) as:

$$\varepsilon \cdot \ell = \frac{\log(T\%)}{c_a - c_b} \tag{4.8}$$

Using the differential transmittance, T%, of two samples with known concentrations of the dye, c_a and c_b, this value can be calculated.

Distilled water without indigo carmine was used as sample A, c_a=0 g/L, and a solution with dye concentration of c_b =0.025 g/L was used as sample B. The differential transmittance, in this case, is 27.74% at 550 nm. Sample B in these measurement was 1/10 dilution of the original unexposed indigo carmine sample, which has a dye concentration of 0.25 g/L. The original unexposed sample solution is unsuitable for

calculation because its differential transmittance to distilled water at 550 nm is near 0% (see Figure 4.6).

According to equation (4.8), the value of ε ℓ can be calculated as:

$$\varepsilon \cdot \ell = \frac{\log(27.736\%)}{(0-2.5\cdot 10^{-2})} = 22.300\ \mathrm{L/g} \qquad (4.9)$$

Then, the concentration of indigo carmine in the exposed sample, c_t, can also be obtained from equation (4.7) as:

$$c_t = c_0 - \frac{\log(T\%)}{\varepsilon l} \qquad (4.10)$$

Here, sample A is the exposed indigo carmine solution; sample B is the original unexposed indigo carmine solution with a concentration of dye, c_0 = 0.25 g/L. By using the differential transmittance of each exposed sample in equation (4.10), the concentration of dye in the exposed sample solution, c_t, can be calculated.

4.2.4 Analytical Method

Normalised Concentration

After calculations of dye concentration in the samples, further analysis was conducted to show the degree of decolorisation after non-thermal plasma discharge treatment. In this case, the normalised concentration K(D) was used. This normalized concentration is a ratio of the concentration of dye in the treated solution to the concentration of dye in the untreated sample. The results from this series of experiments show that this concentration depends on the total charge delivered to the sample by discharge treatment. The concentration of dye was calculated using the method described in the

previous section. A low value of K(D) indicates a high degree of decolorisation. The normalised concentration of dye is given by equation (4.11):

$$K(D)=C_t(D)/C_0 \quad (4.11)$$

where $C_t(D)$ is the actual concentration of the dye in water (g/L)

C_0 is the initial concentration of the dye (0.25 g/L in the present study)

D is the total delivered charge (C)

Charge-dependent Decolorisation Rate

According to the results obtained in this study, the normalised concentration depends on the total charge delivered by the plasma discharge treatment. Therefore, the normalised concentration of indigo carmine in the solution sample as a function of the charge delivered during the plasma treatment was fitted with a first-order kinetic function:

$$K(D)= \exp(-\mu D) \quad (4.12)$$

where D is the total charge delivered, normalised on the total surface of the sample (C)

K(D) is the dose-dependent normalised concentration

μ is the rate of the decolorisation process (C^{-1}).

Total Charge Delivered

Total charge delivered was used as a metric in this study to evaluate the efficiency of the plasma discharge treatment. The total charge delivered was calculated by integrating the transient current waveform.

The energy of this discharge is split into two separate components: the energy released in the plasma channel above the sample, and the energy released in the transient plasma channel(s) which either propagates across the sample surface or dissipates through the bulk of the samples. In the study of transient plasma discharges, the distance between the sample surface and the HV needle electrode was changed to provide the same voltage in the case of positive and negative energisation conditions. Thus, this difference in the distance may potentially result in different proportions of energy dissipated in the plasma above the sample surface.

Conversely, the total delivered charge is not affected by the experimental topology. It is related to the amount of chemically active species generated by the transient discharge, which results in the observed oxidation effects. The use of the total charge as the metric allows all charged (and potentially neutral) species produced by the transient discharges to be considered when the efficacy of the decontamination and oxidation processes is considered. Also, it was found that in the range of voltages used in the present study, the voltage magnitude does not affect the efficacy of the oxidation process.

Only phenomenological scaling relationships (pseudo first-order kinetic equations) which describe the decolorisation and inactivation processes as charge-dependent processes have been obtained. Therefore, it can be argued that the total amount of the charged species produced by the transient plasma discharges defines the efficacy of the biological inactivation and chemical oxidation plasma processes for the range of parameters used in this study.

4.3 Steady-State Corona Discharge Treatment: Decolorisation of Indigo Carmine

It was proved that the corona discharges in atmospheric air have great potential for decomposition of a wide range of chemicals, including CO_2, phenol, benzene, lignin, CF_3CL, toluene, and some other volatile organic compounds such as propane, propene, and isopropyl alcohol [204]–[210]. A mixture of ions, charged particles, and neutral reactive chemical species generated by the corona discharges include super oxide anions, hydroxyl and hydro-peroxyl radicals, reactive nitrogen species, and reactive oxygen species. These reactive chemical species can interact with the liquid or solid surface and lead to oxidation or bactericidal effects. Depending on the concentration of chemical species generated by the corona discharges, the efficiency of oxidation/bio-decontamination of these discharges may vary.

In this part of the research, the oxidation capability of the steady-state corona discharges was investigated. Indigo carmine was used as the target sensor in this study. Based on the achieved decolorisation effect, the charge-dependent chemical degradation efficiency of the corona discharges was obtained.

To provide information on optimisation of the corona discharge treatment regimes to achieve maximum oxidation effect, different conditions and topologies were used to generate corona discharges. Both direct and indirect treatment was performed in this series of experiments. In the case of indirect discharges, a grounded metallic mesh was placed between the energised electrode and the sample. Therefore, most of the ions and charged particles were not able to reach the sample surface in the indirect discharge treatment. Thus, the neutral reactive species plays the dominant role in the decolorisation process in this case. In the case of direct treatment (no grounded mesh above the sample), both charged or neutral species can reach the sample surface and contribute to the oxidation effect (more details are provided in Chapter 3). Humidity of air and polarity of the applied voltage also have been reported as important factors that could have significant influence on the oxidation effect of the corona discharges [211], [212]. Therefore, these parameters were investigated in this research.

The discharge voltage was set to a constant value of 30 ± 0.2 kV, and both positive and negative polarities were used. Two types of gas were tested: atmospheric air (~40%

relative humidity) and bottled air (~12.5% relative humidity). The pressure inside the test cell was maintained at the 0.2-atm gauge. As mentioned in the previous section, 5 ml indigo carmine sample solution with a concentration of 0.25 g/L was placed on the non-conductive or conductive sample plate, and treated by corona discharge in the test cell for 2, 5, and 10 minutes. Ozone level and discharge current were monitored during the test. The differential transmittance between treated and untreated samples was measured.

In this section, the results of decolorisation tests using the steady-state corona discharges are presented and analysed.

4.3.1 Indirect Steady-State Corona Discharge Treatment

Indigo carmine solution samples were exposed to the indirect steady-state corona discharges. The treated samples were placed in the spectrophotometer along with the untreated sample solution, and the differential transmittance was measured. Then the concentration of indigo carmine in the sample solution was calculated based on the differential transmittance. As described in Chapter 3.2, in the case of the indirect corona discharge treatment, the samples were placed under the grounded metallic mesh. Thus, ions and charged particles were screened and were not able to reach the sample surface. In addition, the discharge current does not pass through the sample.

a) Positive Energisation

Positive DC high voltage was applied to the HV electrode of the indirect corona discharge treatment test cell to generate positive steady-state corona discharges. Ozone concentration during the tests was measured and found to be ~2 ppm. The differential transmittance of the treated samples to the untreated samples was measured. Examples of the differential transmittance spectra are shown in Figure 4.7

and Figure 4.8. The major peak in the differential transmittance is at ~550 nm, as shown in Figure 4.9.

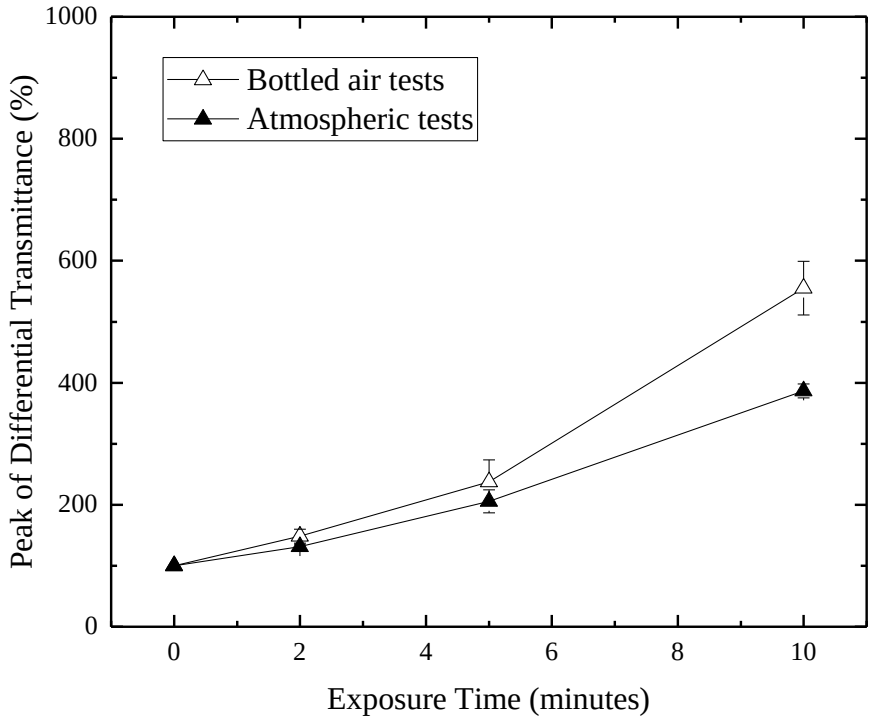

Figure 4.9. Peak of differential transmittance of sample solution as a function of exposure time. Each point in this figure represents an average of three independent tests. The error bars shows standard deviation values. Solid lines are for visual guidance only.

The measured differential transmittance was above 100% for all samples after exposure to the positive steady-state corona discharges. This indicates that the indigo carmine solution was decolorized. As shown in Figure 4.9, the peak of the differential transmittance increases with exposure time. With longer time exposure, a higher degree of decolorisation was achieved.

By applying the calculation method (as explained in Section 4.1.3), the concentration of indigo carmine in the sample solution was obtained, as presented in Figure 4.10.

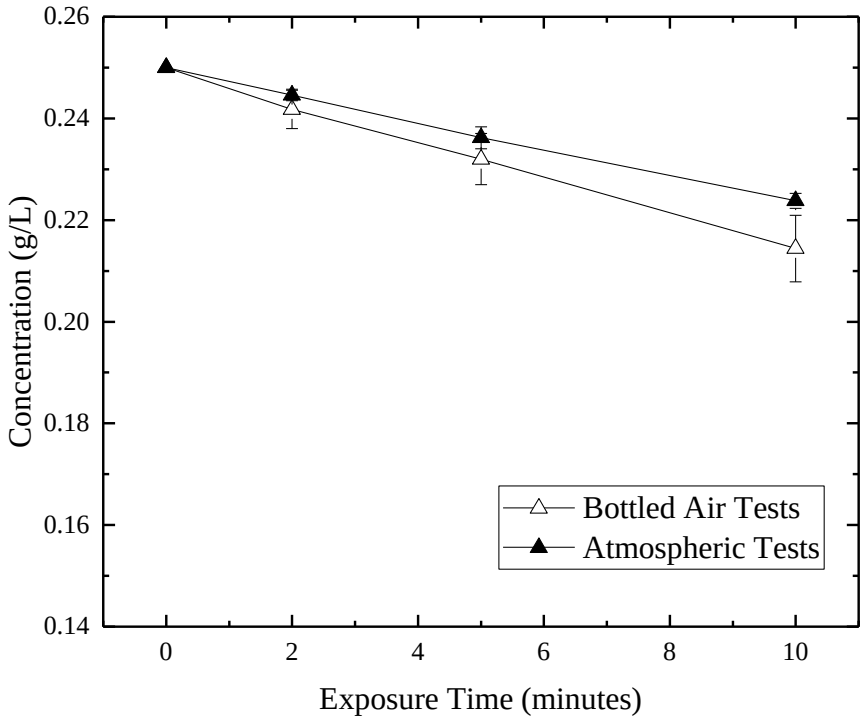

Figure 4.10. Concentration of indigo carmine in solution as a function of exposure time after exposure to indirect positive steady-state corona discharge. Each point in this figure represents an average of three independent tests. The error bars show standard deviation values. Solid lines are for visual guidance only.

Further analysis was conducted by calculation of the normalised charge-dependent concentration of the indigo carmine dye, K(D), which can be obtained by equation (4.11).

The normalised concentration of indigo carmine in the solution as a function of the charge delivered was fitted with the analytical fitting line using equation (4.12). This fitting procedure was conducted in Origin Pro 5 graphing software; the results of this fitting are shown in Figure 4.11.

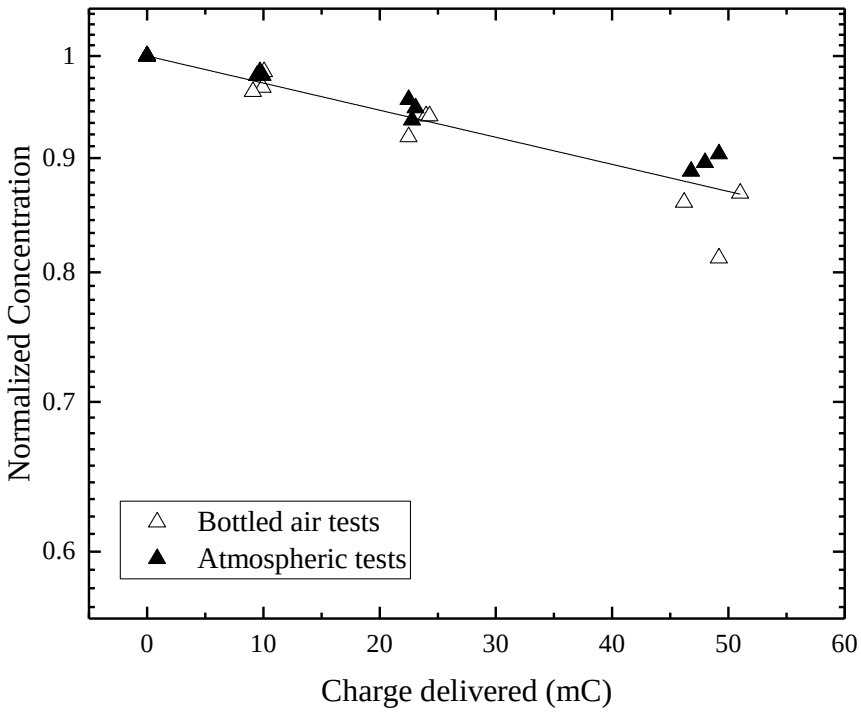

Figure 4.11. Normalised concentration of indigo carmine dye as a function of the charge delivered after treatment with positive, indirect, steady-state corona discharges. Each point in this graph represents an individual test. The straight line shows the fitting by equation (4.12).

As shown in Figure 4.11, the normalized concentration of the blue dye decreases with an increase in the charge delivered during the plasma discharge treatment. The results obtained from bottled air tests and atmospheric tests did not show a significant difference. After exposure to plasma discharges for the same period, the same total charge was delivered to the sample, and the reduction in the dye concentration was similar. This reduction in the indigo carmine concentration was not very high. For example, the concentration of indigo carmine was decreased to 0.21-0.23 g/L by 10 minutes of the positive indirect discharge treatment, which was less than 0.2 reduction in the normalised concentration.

The first-order kinetic equation (4.12) was applied to the experiment results in Figure 4.11, and the rate of the decolorisation process, μ, was found to be 2.79 C^{-1} in this case.

b) Negative Energisation

The high-voltage power supply was then switched to negative polarity, and the same 5 ml indigo carmine solution samples were placed into the indirect corona discharge test cell and exposed to negative corona discharges. Higher ozone concentration was observed in the case of negative discharges: ~40 ppm. The differential transmittance was measured, and the concentration of the dye in the solution sample was obtained. The results of this analysis are shown in Figure 4.12.

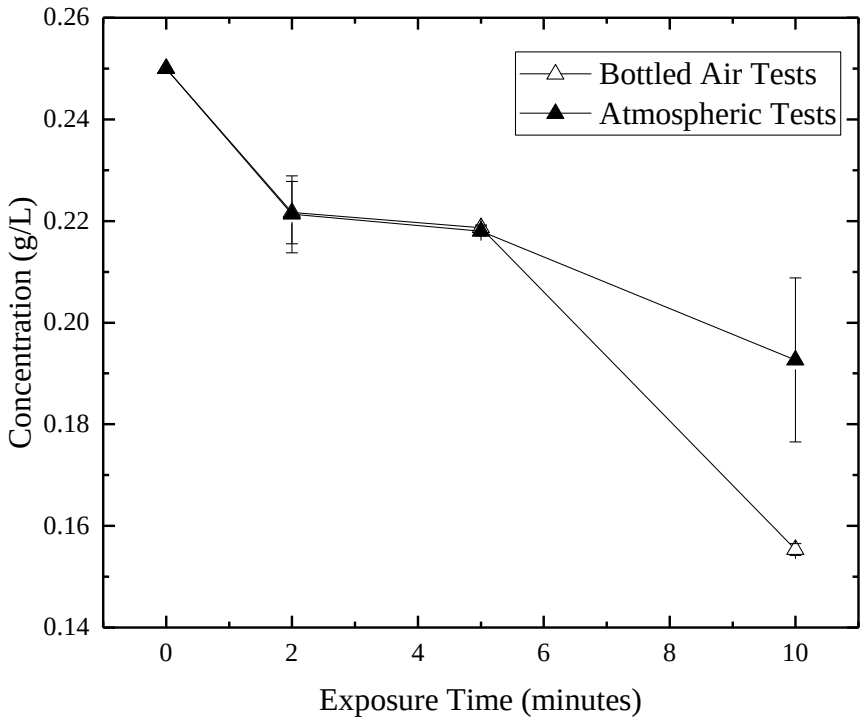

Figure 4.12. Concentration of indigo carmine solution sample as a function of exposure time after exposure to indirect negative steady-state corona discharge. Each point in this figure represents an average of three independent tests. The error bars show standard deviation values. Solid lines are for visual guidance only.

As shown in Figure 4.12, the concentration of the indigo carmine solution was decreased after exposure to negative indirect corona discharge. A high decrement was achieved after 10 minutes of exposure, particularly in the case of bottled air tests.

After 10 minutes of treatment, the concentration of indigo carmine decreased to ~0.155 g/L (bottled air tests) and ~0.19 g/L (atmospheric tests).

The normalised concentration of exposed indigo carmine solution samples is shown as a function of charge delivered in Figure 4.13.

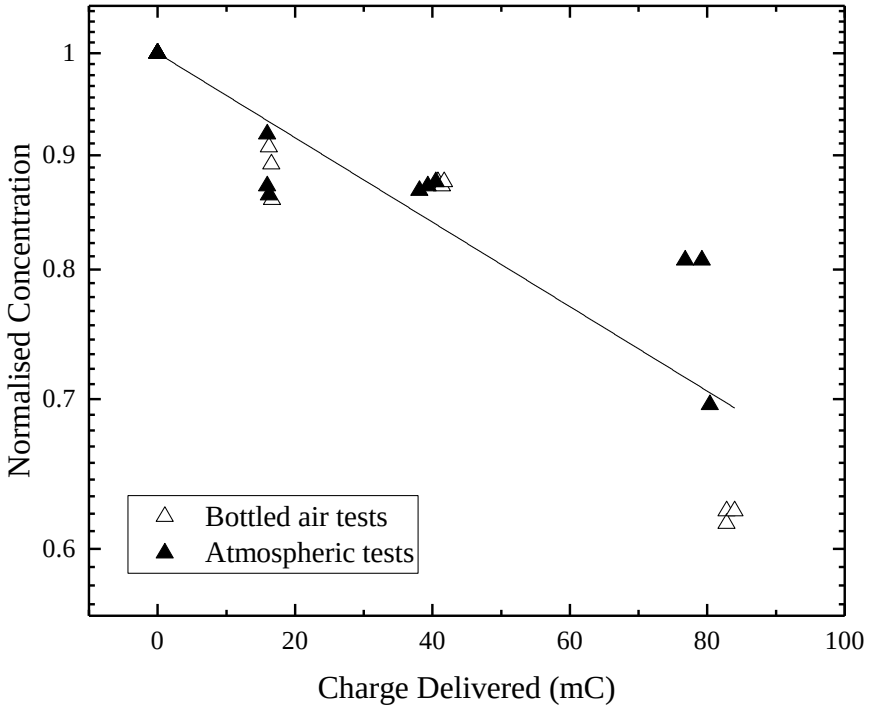

Figure 4.13. Normalised concentration of indigo carmine as a function of the charge delivered after treatment with negative indirect steady-state corona discharges. Each point in this graph represents an individual test. The straight line shows the fitting by equation (4.12).

As shown in Figure 4.13, in the case of negative indirect corona treatment, a high degree of reduction in normalised concentration was achieved. However, a much higher charge dose was delivered during the negative treatment compared with the case of the positive discharge treatment. By applying the first-order kinetic equation (4.12), the fitting curve is obtained. It is shown as a solid line in Figure 4.13, and the rate of the decolorisation process is 4.35 C^{-1}.

4.3.2 Direct Steady-State Corona Discharge Treatment

Direct steady-state corona discharge treatment also was examined in this series of experiments. The direct corona discharge treatment test cell was described in Chapter 3.2. The target sample was placed between the discharge electrodes and directly exposed to the steady-state corona discharges. Ions and charged particles were able to reach the sample surface, and the discharge current propagated through the sample.

a) Positive Energisation

Initially, the indigo carmine solution was treated by the direct steady-state corona discharges with positive polarity. The concentration of dye in the treated samples was obtained as a function of the exposure time. The results are shown in Figure 4.14.

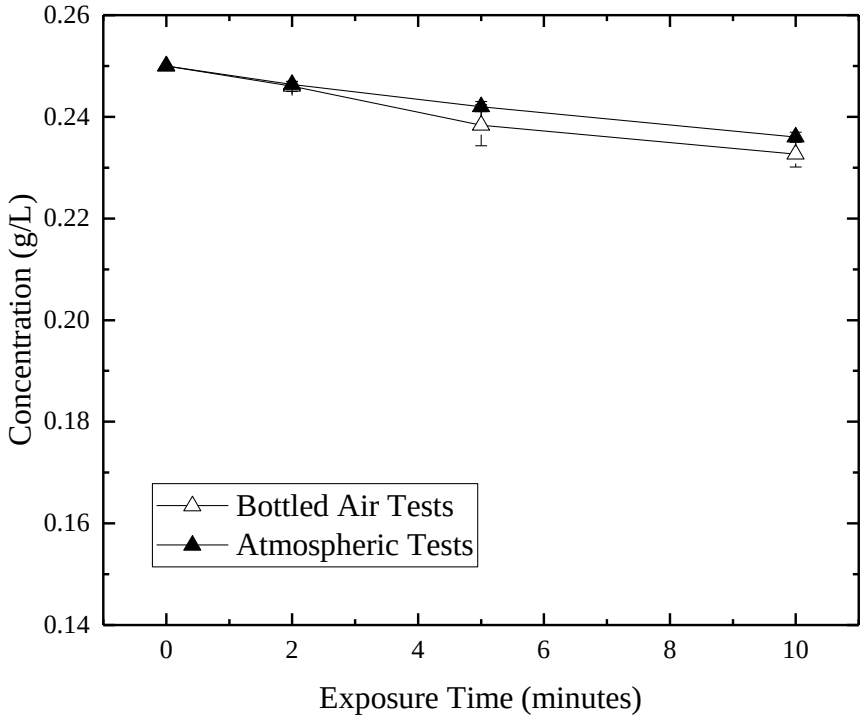

Figure 4.14. Concentration of indigo carmine solution sample as a function of exposure time after exposure to direct, positive, steady-state corona discharge. Each point in this figure represents an average of three independent tests. The error bars show standard deviation values. Solid lines are for visual guidance only.

The decrease in the concentration of indigo carmine in the treated solution samples was observed after exposure to positive direct corona discharges. However, this decrease was slightly lower than that in the case of the positive indirect treatment. The concentration was still above 0.23 g/L, even after exposure to positive direct corona discharge for 10 minutes in dry or atmospheric air.

The normalised concentration of the dye in treated solutions is presented in Figure 4.15 as a function of total delivered charge.

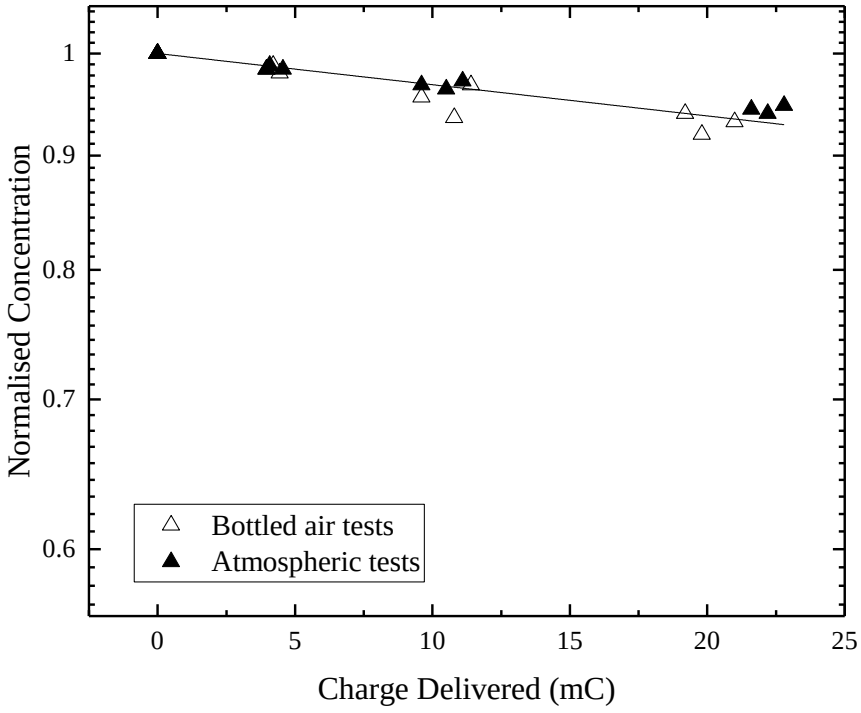

Figure 4.15. Normalised concentration of indigo carmine as a function of the charge delivered after treatment with positive, direct, steady-state corona discharges. Each point in this graph represents an individual test. The straight line shows the fitting by equation (4.12).

Low ozone concentration (~2 ppm) was observed during the discharge treatment. The normalised concentration of dye was above 0.93, even after 10 minutes of treatment. By applying the first-order kinetic fitting as in equation (4.12), the rate of the decolorisation process, μ, was obtained as 3.22 C^{-1}. Although lower reduction in dye concentration was achieved, this rate was still higher than in the case of positive

indirect corona discharge treatment. This is because the charge delivered was much lower in this case, as shown in Figure 4.15.

b) Negative Energisation

Indigo carmine solution samples also were exposed to negative corona discharges in the direct test cell. The ozone level was 20-60 ppm during the discharge treatment. The differential transmittance of the treated and untreated samples was measured, and the concentration of indigo carmine in the treated samples was calculated. The results are shown in Figure 4.16.

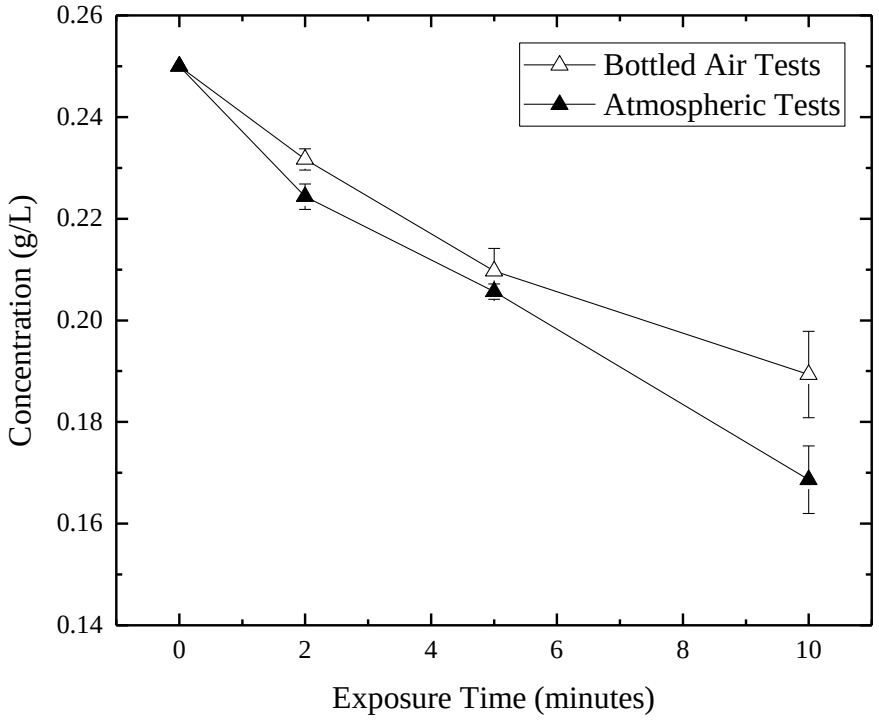

Figure 4.16. Concentration of indigo carmine solution sample as a function of exposure time after exposure to direct, negative, steady-state corona discharge. Each point in this figure represents an average of three independent tests. The error bars show standard deviation values. Solid lines are for visual guidance only.

Obvious reduction in the dye concentration was achieved in both the bottled air test and atmospheric tests. After 10 minutes of treatment, the concentration decreased to ~0.19 g/L (atmospheric tests) and ~0.17 g/L (bottled air tests).

The normalised concentration of the dye in treated samples was obtained as a function of the charge delivered; the results are shown in Figure 4.17. The first-order kinetic equation (4.12) was applied to provide a fitting curve as the solid line.

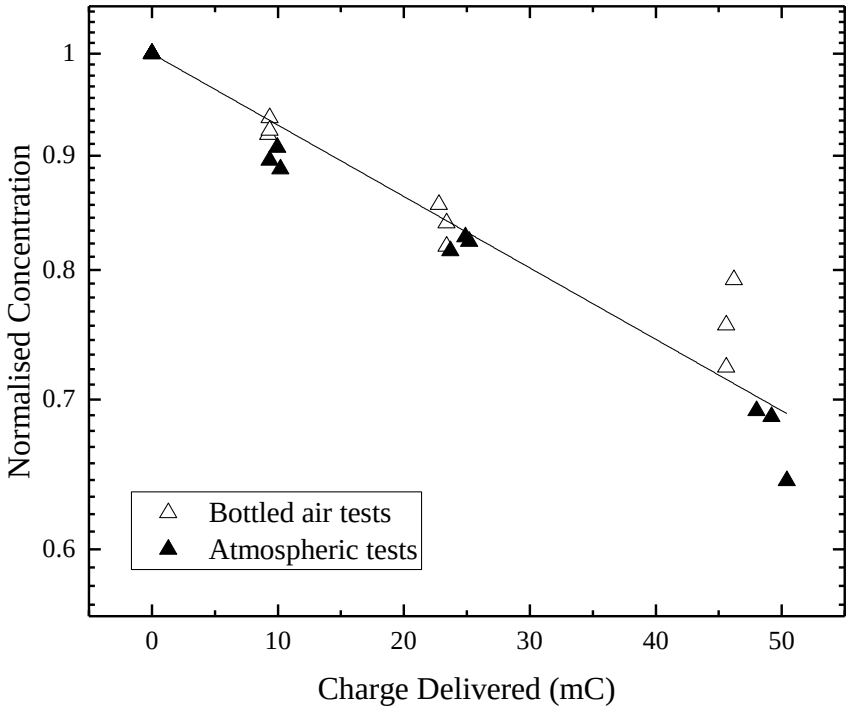

Figure 4.17. Normalised concentration of indigo carmine as a function of the charge delivered after treatment with negative, direct, steady-state corona discharges. Each point in this graph represents an individual test. The straight line shows the fitting by equation (4.12).

As shown in Figure 4.17, the reduction in the concentration of indigo carmine was proportional to the charge delivered during the discharge treatment. A charge of 45-50 mC was delivered by 10 minutes of discharge treatment, and the normalised concentration was decreased to 0.68-0.72. By applying the first-order kinetic fitting for both bottled air tests and atmospheric tests, the rate of the decolorisation process, μ, is determined to be 7.36 C^{-1}.

4.3.3 Acidity of Solution Sample after Treatment By Steady-State Corona Discharge

As mentioned in the literature review (Chapter 2.5.4), it has been proved that the acidity of liquid samples may be changed after the treatment by non-thermal plasma discharges. In this series of experiments, the pH of the indigo carmine solutions was obtained as a function of treatment time for different plasma treatment regimes. The initial value of pH of the untreated sample solutions was between 4.8 and 5.2. The pH measurements were conducted using the Hannah pH210 Microprocessor pH meter with Sentek miniature probe. The pH of the solution samples as a function of treatment time are shown in Figure 4.18.

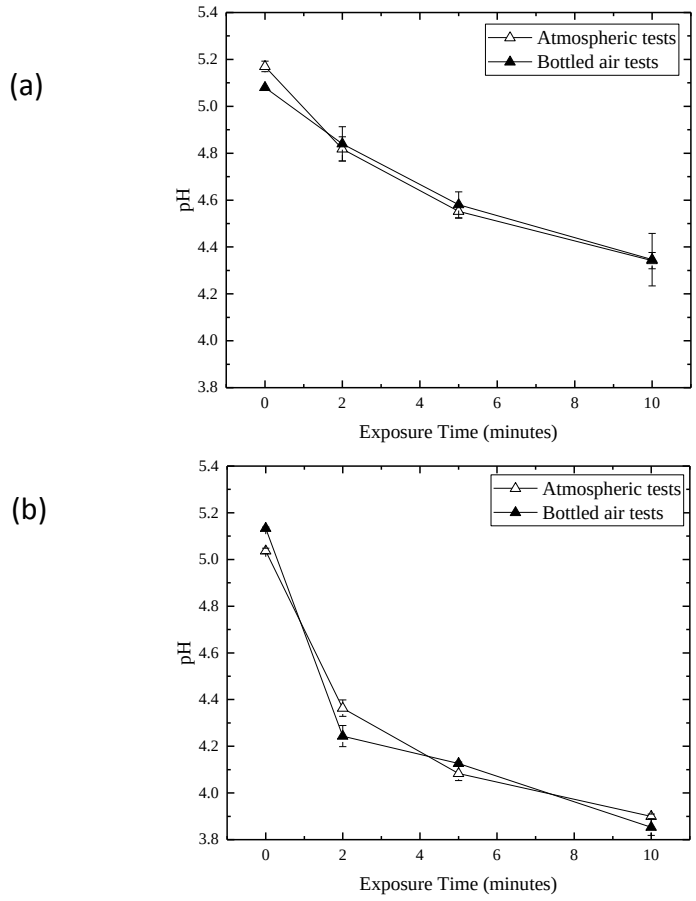

Figure 4.18. The pH of the indigo carmine solution sample after treatment by indirect steady-state corona discharge with (a) positive energisation and (b) negative energisation. Each point in this figure represent an average of three independent tests. The error bars show standard deviation values. Solid lines are for visual guidance only.

In both positive and negative energisation cases, the pH of treated solution samples decreases with an increase in the exposure time. In the case of negative energization, a higher degree of decrement was observed. This pH decrease corresponds to the decolorisation effect of the corona discharge treatment, as the negative indirect corona discharge treatment produced a higher degree of decolorisation.

In the case of direct corona discharge treatment, the pH of the solution sample was also measured and presented in Figure 4.19.

(a)

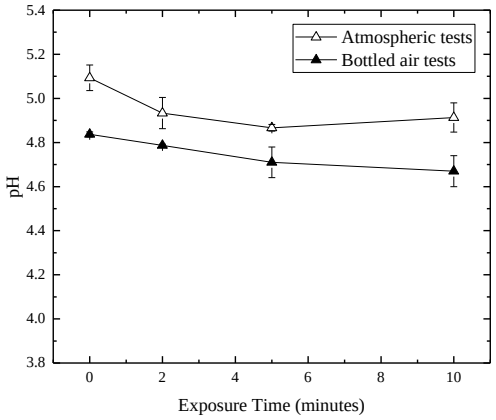

(b)

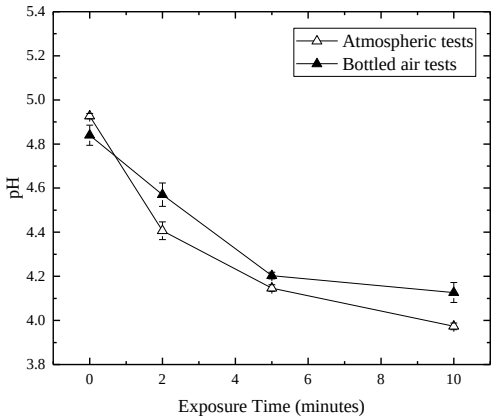

Figure 4.19. The pH of the indigo carmine solution samples after treatment by direct steady-state corona discharge with (a) positive energisation and (b) negative energisation. Each point in this figure represents an average of three independent tests. The error bars show standard deviation values. Solid lines are for visual guidance only.

As shown in Figure 4.19, the pH of the indigo carmine solution did not decrease significantly after direct positive corona discharge treatment. The decrement was less than 0.2 after 10 minutes of exposure. However, after exposure to negative direct corona discharges, the pH of the indigo carmine solution sample decreased significantly. This change in pH corresponds to the decolorisation effect: the positive direct corona discharge treatment results in a decrease in concentration of less than 0.02 g/L; negative direct corona discharge results in a much higher decrease in concentration (0.04-0.09 g/L).

4.3.4 Summary

In this section, the investigation into the oxidation effects of steady-state corona discharges was discussed. Decolorisation of indigo carmine water solutions was achieved using both indirect and direct corona discharges with positive or negative energisation mode. The concentrations of indigo carmine dye in the treated solution samples were calculated using the differential optical transmittances obtained by the spectrophotometer.

Discharges in bottled air and atmospheric air were investigated. Although a non-substantial difference was observed in oxidation effects for both types of gas, the obtained results show that humidity of the air does not significantly affect the degree of decolorisation produced by the steady-state corona discharges. As the electrical characteristics of the discharges are almost the same in bottled and atmospheric air, the humidity difference between these two types of air, 40% and 12.5% RH, was considered as insufficient to result in a significant difference in the production of the reactive chemical species. Condensation inside the test cell may compensate for the difference in air humidity.

A reduction in the concentration of the dye in the treated solutions was observed in the direct and indirect corona treatment with both bottled air and atmospheric air, and a stronger effect was observed in the negative direct and indirect treatment tests.

The results show that the oxidation capability of the steady-state corona discharges is proportional to the charge dose delivered. For longer exposure time, during which higher charge is delivered to the sample, a higher degree of decolorisation was observed. Normalised concentration of dye in the solution as a function of the charge delivered was used to indicate the decolorisation/oxidation efficiency of corona discharges. By applying the first-order kinetic equation (4.12), the rate of decolorisation was obtained. This fitting procedure was implemented in Origin Pro software. Table 4.1 summarises the decolorisation rate for different types of corona discharge treatment.

Table 4.1. Decolorisation rate (C^{-1}) for indirect and direct steady-state corona discharge.

Indirect corona discharge		Direct corona discharge	
Positive	Negative	Positive	Negative
2.79 (2.54 – 3.04)	4.35 (3.83 – 4.87)	3.22 (2.92 – 3.52)	7.36 (6.91 – 7.81)

Values in brackets indicate a 95% confidence interval.

As shown in Table 4.1, the decolorisation rates in the case of direct corona discharge treatment are higher than in the case of indirect corona discharge treatment. The main reason for this difference is considered to be the distance between the HV stressed electrode and the sample surface. The discharge current was lower in the direct treatment case: the charge was less, and the energy delivered was low. Also, charged particles may contribute to the decolorisation of the treated indigo carmine solution sample in direct corona discharge treatment.

When positive energisation was applied, the decolorisation effect in both cases, indirect and direct corona discharge treatment, was similar. The decolorisation rates in both cases were similar, as shown in Table 4.1: 2.79 C^{-1} in the indirect treatment case and 3.22 C^{-1} in the direct treatment case. However, a much more intensive decolorisation effect was observed in the case of the negative energisation mode. The rates of decolorisation are higher than in the case of positive energisation, especially in the case of negative direct corona discharge treatment, for which the number is up to 7.36 C^{-1}. This can be explained by the difference in the production of reactive species. Although the exact mechanisms of the chemical (oxidation) and bactericidal

effects of corona discharges require further investigation and analysis, as different reactive oxygen and nitrogen species make their contributions to these effects, ozone can potentially be used as an indicator of the production of ROS and the bactericidal and oxidation efficiency of corona discharges. As monitored during the discharge treatment, ozone level was ~2 ppm in the case of positive corona discharge with direct or indirect topology. The ozone level was much higher in the case of negative energisation mode: ~40 ppm in indirect corona discharge treatment and 20-60 ppm in direct corona discharge treatment.

The acidity of the sample solution was increased after exposure to steady-state corona discharges, which is in line with the results reported in many studies [73], [169], [213]. The tendency of this decrease corresponds to the decolorisation effect brought by the corona discharge treatment.

4.4 Transient Plasma Discharge Treatment for Decolorisation of Indigo Carmine

Plasma discharges with a pulsed energisation mode have been studied in chemical oxidation processing [29], [214]–[216]. The transient spark discharge with its self-pulsing feature is considered as a novel approach for generating non-thermal plasma. Transient sparks can generate a highly reactive non-thermal plasma in atmospheric air with low energy consumption of 0.1–1 mJ/pulse [62]. It has been shown in [68], [86], and [217]–[219] that ROS, RNS, and other chemical species can be produced by transient spark discharges which lead to their strong oxidation capability and ability to decompose chemicals and inactivate bacteria. However, there is still a gap in understanding of the transient spark discharge oxidation mechanisms. Furthermore, parameters such as electrode configuration and voltage levels could have a strong influence on the oxidation effect. Therefore, it is important to investigate the oxidation capability of transient plasma discharge under different conditions. In this section, an experimental study on the oxidation capability of the transient plasma discharge is presented. This impulsive transient plasma discharge is similar to transient spark discharge as described in the literature review. Information acquired from this study can be used for optimisation of the oxidation efficiency of the transient plasma discharges.

Water solutions of indigo carmine dye with a concentration of 0.25 g/L were used as a chemical indicator for analysis of the oxidation capabilities of the transient plasma discharges: depending on the decolorisation degree of these solutions, the oxidation capability of transient plasma discharges was evaluated. As described in Chapter 3.3, two types of topologies were used to provide surface discharges (which propagate across a liquid sample surface) and direct discharges (through the bulk of a liquid sample). The surface discharges were generated using non-conductive sample plates, while conductive sample plates were used to generate direct transient plasma discharge in the test cell. Three different breakdown voltage levels with both polarities were used: 20 kV, 24 kV, and 28 kV ($\pm$ 0.2 kV). The repetition rate of the high voltage pulses was set to 20 pulses per second. The discharges were generated in an atmospheric environment with humidity of ~ RH 40% and temperature ~20 ℃. Indigo carmine solution samples were exposed to transient plasma discharge for 1, 3,

5, and 7 minutes. During the transient plasma discharge treatment, ozone production was not detectable.

The change in the concentration of indigo carmine in the plasma-treated solutions was obtained and presented as a function of the charge delivered. An analysis was conducted to compare the oxidation capabilities of the transient plasma discharges under different conditions.

4.4.1 Decolorisation of Indigo Carmine Using Surface Transient Plasma Discharges

A 5 ml indigo carmine sample solution was placed on the non-conductive sample plate and exposed to transient plasma discharge. As described in Chapter 3.3, transient plasma streamers propagated from the tip of HV needle electrode to the sample/air interface; then the streamers propagated along the sample surface to the side of the sample plate, where they reached the grounded metal plate. The discharge current did not pass through the sample directly.

a) Positive Energisation

First, the high-voltage pulsed generator was switched to the positive mode and connected to the test cell. Transient plasma discharges with positive polarity were generated, and samples of dye solution were treated by these discharges. By adjusting the distance between the HV needle electrode and the sample surface, the breakdown voltage level was set as 20 kV, 24 kV, and 28 kV. The concentration of the dye in solutions after exposure to surface transient plasma discharges was obtained and is presented as a function of the exposure time in Figure 4.20.

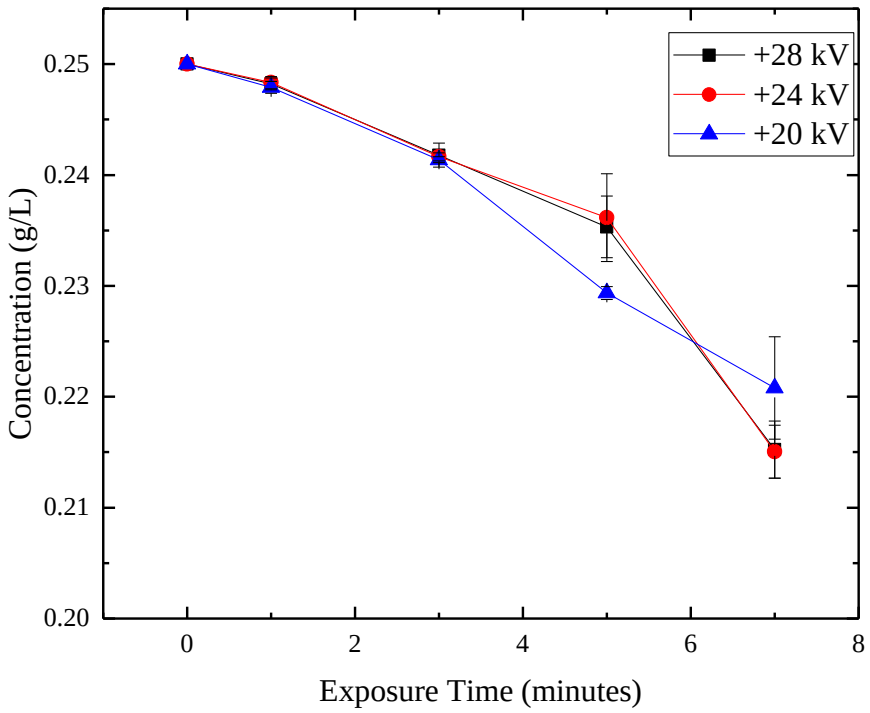

Figure 4.20. Concentration of indigo carmine in solution after exposure to positive surface transient plasma discharge. Each point in this figure represents an average of three independent tests. The error bars show standard deviation values. Solid lines are for visual guidance only.

As shown in Figure 4.20, the concentration of indigo carmine dye decreased after exposure to the surface transient plasma discharges with positive polarity. Although three different voltage levels were tested, no difference in decolorisation rate was observed for different voltage levels. After 7 minutes of exposure to the transient plasma discharges, the concentration of indigo carmine decreased to ~0.215 g/L for all three energisation voltages.

The normalised concentration K(D) of indigo carmine in the treated solutions is presented as a function of the charge dose in Figure 4.21.

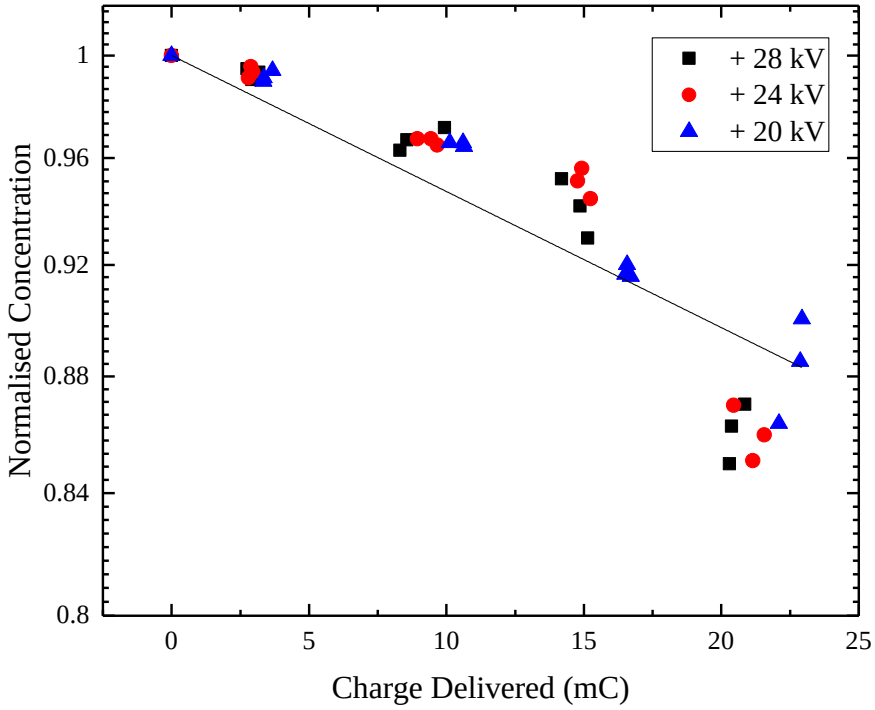

Figure 4.21. Normalised concentration of indigo carmine as a function of the charge delivered after treatment with positive surface transient plasma discharge. Each point in this graph represents an individual test. The straight line shows the fitting by equation (4.12).

By applying the first-order kinetic equation (4.12), the fitting curve of normalised concentration as a function of dose was obtained. The curve is shown as the solid line in Figure 4.21, and the rate of decolorisation μ is 5.42 C^{-1} in this case.

b) Negative Energisation

The high-voltage pulsed generator was then switched to negative energisation mode, and negative surface transient plasma discharge was generated and treated at the sample surface. The concentration of the treated solution sample was calculated based on the differential optical transmittance; the results are shown in Figure 4.22.

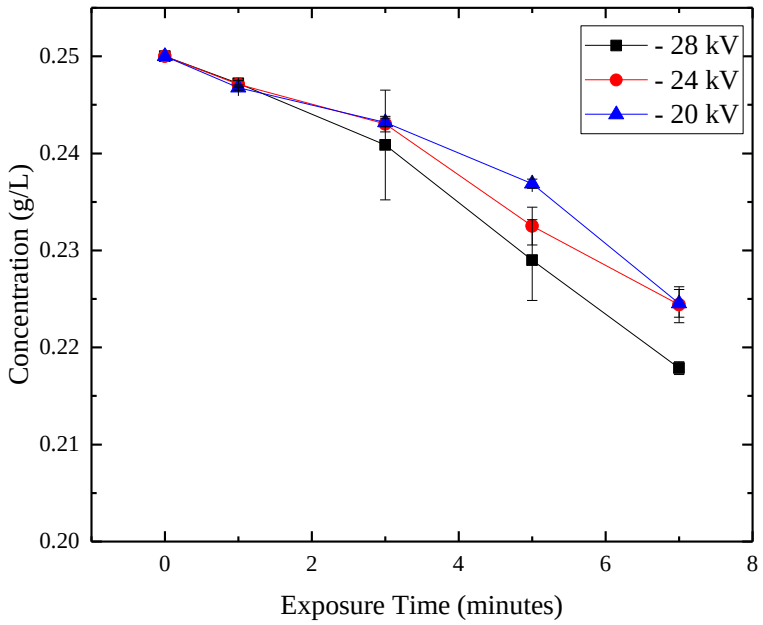

Figure 4.22. Concentration of indigo carmine solution sample as a function of exposure time after exposure to negative surface transient plasma discharge. Each point in this figure represents an average of three independent tests. The error bars show standard deviation values. Solid lines are for visual guidance only.

As shown in Figure 4.22, reduction in the concentration of the dye in the solution was achieved by treatment with negative surface transient plasma discharge. This reduction was slightly lower than in the previous positive discharge treatment case. After 7 minutes of exposure, the concentration decreased to 0.22-0.23 g/L. The normalised concentration as a function of the charge delivered obtained and is presented in Figure 4.23.

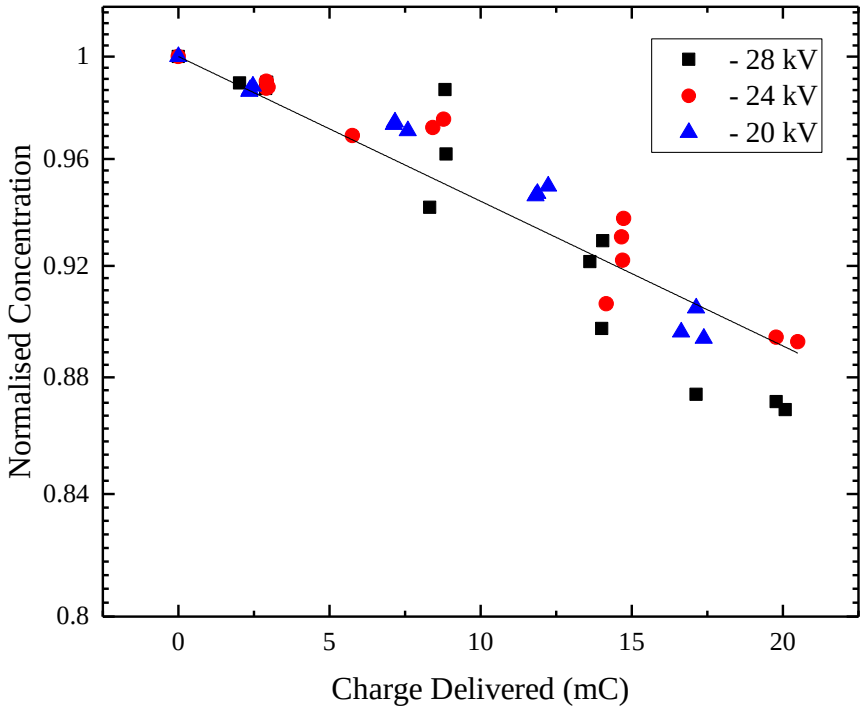

Figure 4.23. Normalised concentration of indigo carmine as a function of the charge delivered after treatment with negative surface transient plasma discharge. Each point in this graph represents an individual test. The straight line shows the fitting by equation (4.12).

The results shown in Figure 4.23 indicate that the decolorisation of the sample solution is a charge-dependent process and does not depend on the breakdown voltage level. The first-order kinetic equation (4.12) was used to fit the experimental data points. The fitting curve is shown as the solid line in Figure 4.23. The rate of decolorisation, in this case, is 5.77 C^{-1}. Although a smaller amount of charge delivered, this rate is slightly higher than that for the positive surface transient plasma discharge treatment.

4.4.2 Decolorisation of Indigo Carmine Using Direct Transient Plasma Discharge

Direct transient plasma discharges were generated in the test cell using a conductive sample plate. As described in Chapter 3.3, the transient plasma discharges were produced from the needle electrode and propagated to the sample surface. Then, the discharge current passed through the sample and reached the ground. As in the case of surface transient plasma discharge, the distance from the needle tip to the sample surface was adjusted to achieve 20 kV, 24 kV, and 28 kV breakdown voltage levels for both polarities.

a) Positive Energisation

In the positive energisation mode, the high-voltage pulsed generator supplied positive pulses to the test cell, which drove positive direct transient plasma discharges used to treat the indigo carmine solution samples. The differential optical transmittance was measured and used to calculate the change in concentration. The results are shown in Figure 4.24.

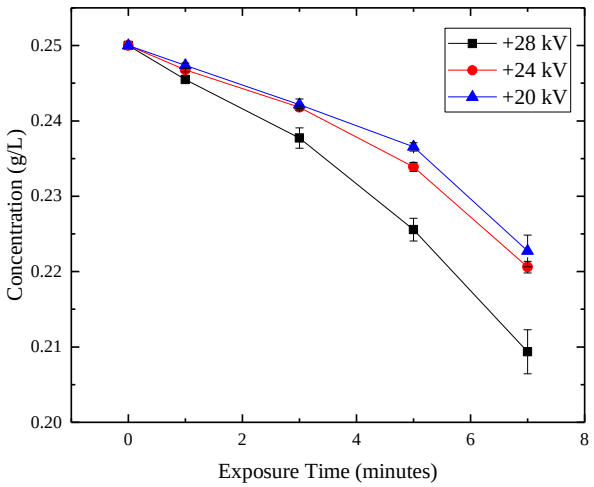

Figure 4.24. Concentration of indigo carmine solution sample as a function of exposure time after exposure to positive, direct, transient plasma discharge. Each point in this figure represents an average of three independent tests. The error bars show standard deviation values. Solid lines are for visual guidance only.

As in the previous case of the indirect TS discharges, the concentration of the indigo carmine in water solution decreased with the exposure time. However, when the breakdown voltage increased to +28 kV, the concentration was lower than the concentration in the case of +24 kV and +20 kV. This is primarily due to a higher charge that was delivered in the +28 kV case in the same period. The normalised concentration was plotted as a function of the charge dose to show this tendency. The results are presented in Figure 4.25.

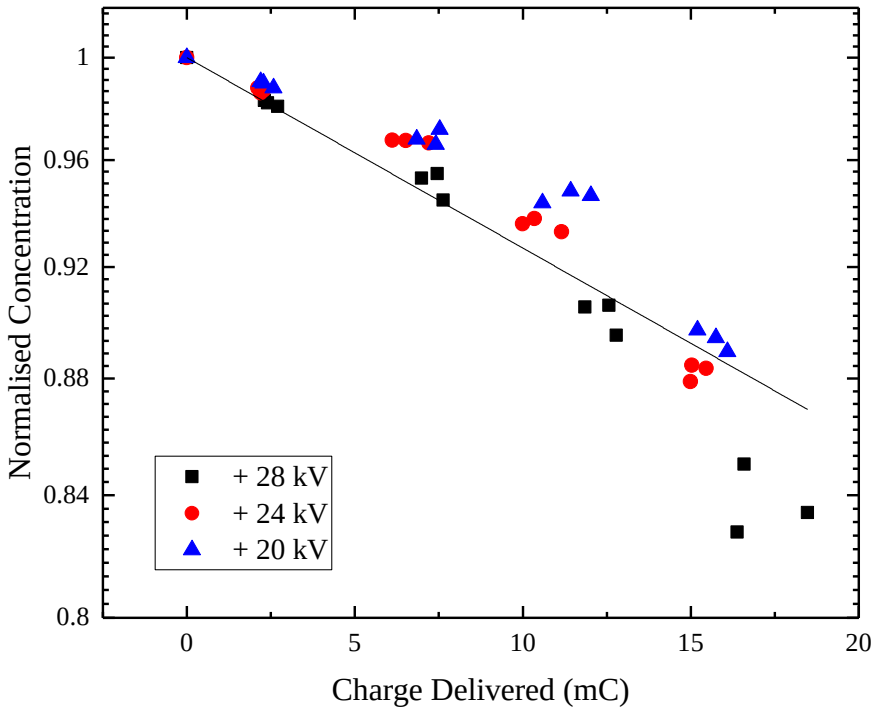

Figure 4.25. Normalised concentration of indigo carmine as a function of the dose after treatment with positive, direct, transient plasma discharge. Each point in this graph represents an individual test. The straight line shows the fitting by equation (4.12).

It is clear that the higher dose was delivered within the same period under a breakdown voltage of 28 kV. However, the general tendency of the decolorisation process is not highly dependent on the breakdown voltage level. This tendency has been obtained by applying the first-order kinetic equation; the fitting curve is shown

as the solid line in this figure. The rate of the decolorisation process is found to be 7.59 C^{-1}.

b) Negative Energisation

With negative energisation, the direct transient plasma discharges were used to treat indigo carmine solutions. The obtained change in concentration of the dye is shown in Figure 4.26.

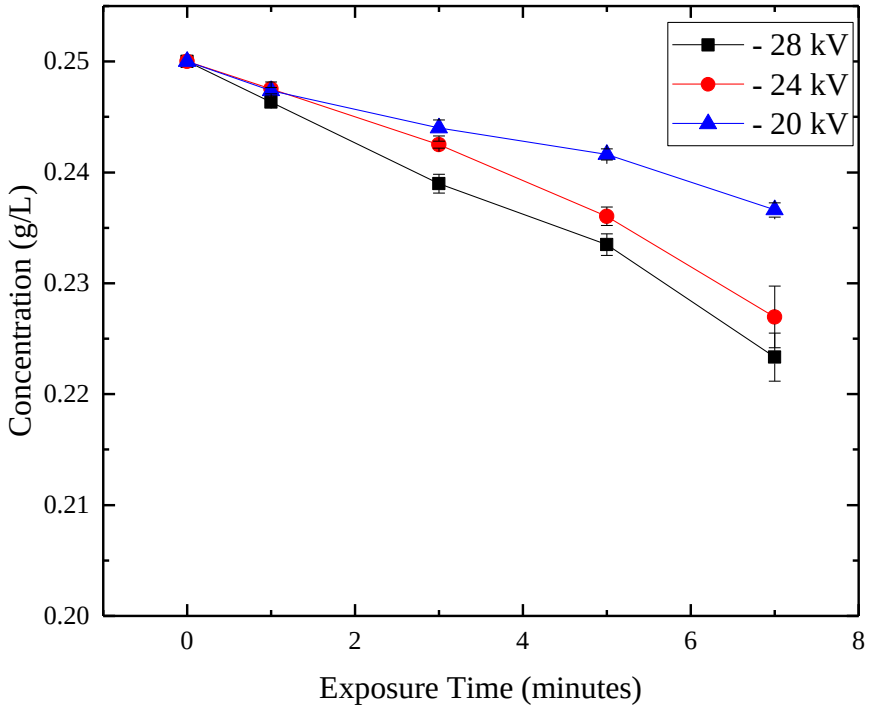

Figure 4.26. Concentration of indigo carmine solution sample as a function of exposure time after exposure to negative, direct, transient plasma discharge. Each point in this figure represents an average of three independent tests. The error bars show standard deviation values. Solid lines are for visual guidance only.

The concentration of the treated sample solution was decreased with exposure time. However, the decrement, in this case, is slightly lower than for the case of positive

energisation. Samples exposed to discharge with a breakdown voltage at 20 kV had a higher concentration; this is considered to be caused by the lower charge delivered.

The normalised concentration as a function of charge delivered is shown in Figure 4.27. By applying the first-order kinetic equation (4.12), the rate of decolorisation was 4.72 C^{-1}.

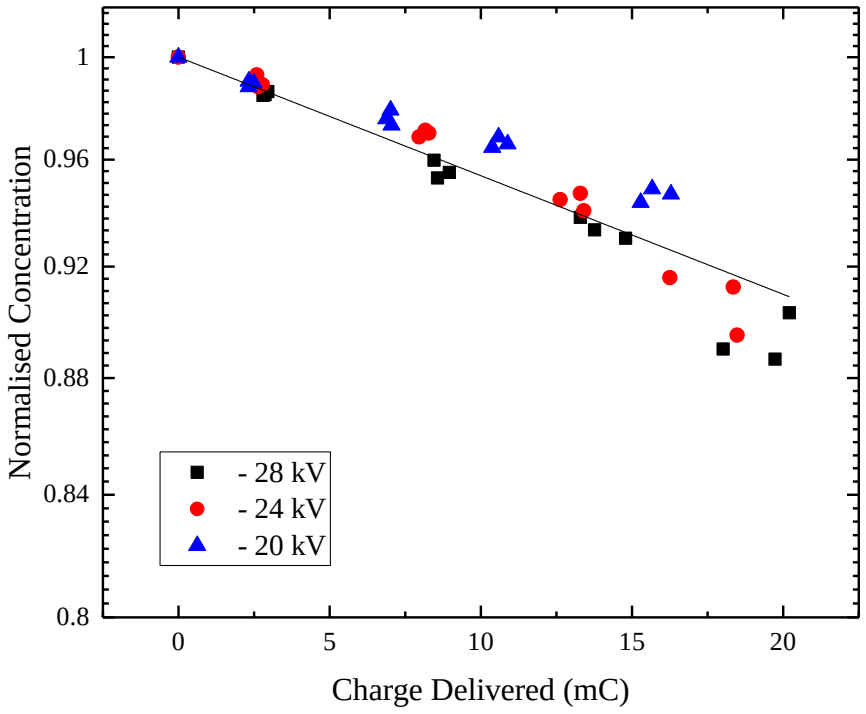

Figure 4.27. Normalised concentration of indigo carmine as a function of the dose after treatment with negative, direct, transient plasma discharge. Each point in this graph represents an individual test. The straight line shows the fitting by equation (4.12).

4.4.3 Acidity of Solutions Treated by Transient Plasma Discharge

The acidity of indigo carmine solutions also decreased after exposure to the transient plasma discharges. The initial pH of the indigo carmine samples before surface transient plasma discharge treatment was in the range of 5.2 to 5.7. After 7 minutes of exposure to the transient plasma discharges, the pH of the solution decreased to 3.22-3.42 in the positive energisation case and to 3.26-3.38 in the negative energisation case, as shown in Figure 4.28. This pH decrease corresponds to the results of the decolorisation experiment.

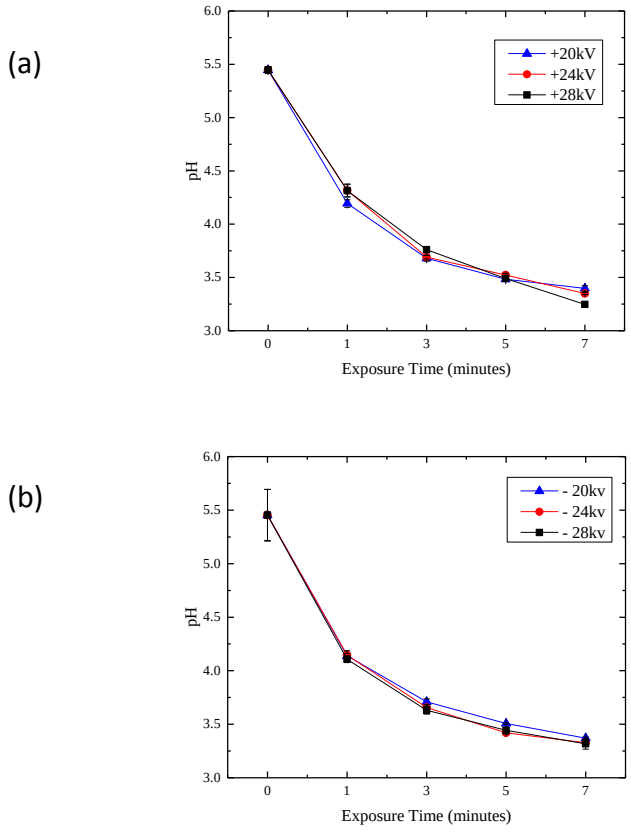

Figure 4.28. The pH of the indigo carmine solution after the surface transient plasma discharge treatment with (a) positive energisation and (b) negative energisation. Each point in this figure represents an average of three independent tests. The error bars show standard deviation values. Solid lines are for visual guidance only.

In the case of direct transient plasma discharge treatment, the pH of the treated solution samples as a function of the treatment time is shown in Figure 4.29.

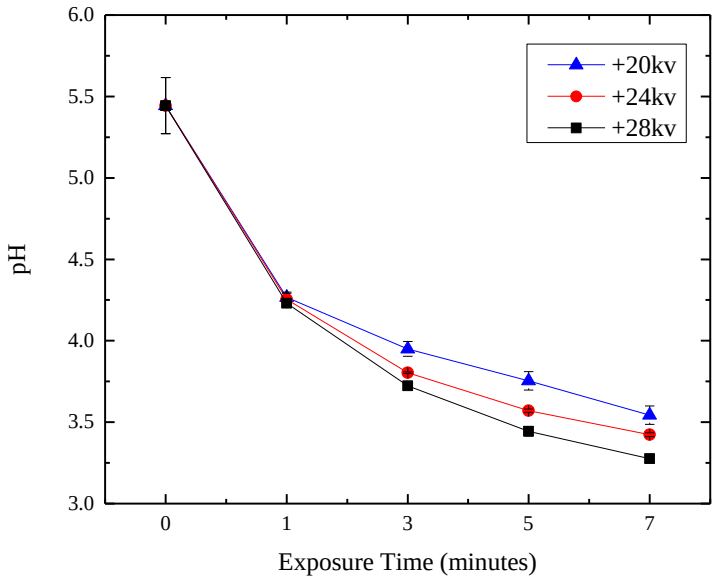

(a)

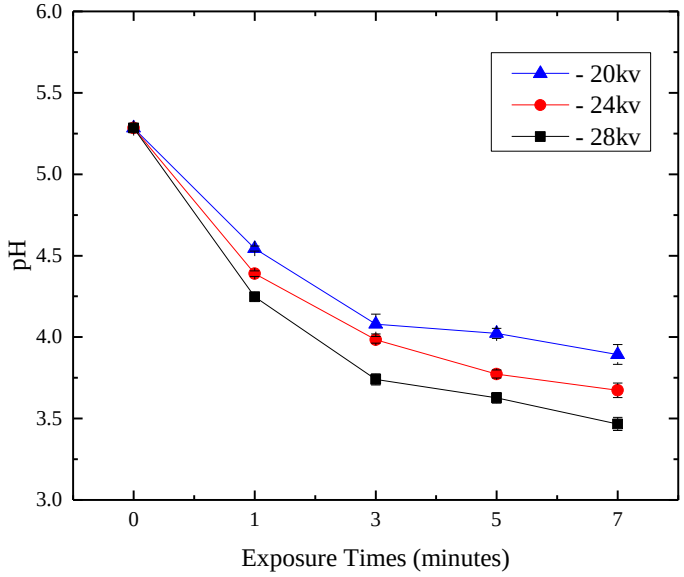

(b)

Figure 4.29. The pH of the indigo carmine solution after direct, transient plasma discharge treatment with (a) positive energisation and (b) negative energisation. Each point in this figure represents an average of three independent tests. The error bars show standard deviation values. Solid lines are for visual guidance only.

The initial pH of the indigo carmine solution is in the range of 5.20 to 5.65. Figure 4.29 reveals that after direct transient plasma discharge treatment with positive energisation, the pH reduction is higher than in the case of negative energisation. Once again, this result corresponds to the decolorisation results.

4.4.4 Summary

The oxidation capability of the transient plasma discharges was investigated in this chapter. By exposing indigo carmine solutions to transient plasma discharges, the degree of decolorisation of the treated samples was obtained. This indicates a strong oxidation effect developed by the transient plasma discharges, which is in line with previously published results [69], [195], [220].

Both positive and negative polarities were tested with different breakdown voltage levels in the case of surface and direct transient plasma discharge treatment. A decrease in the concentration of the dye in the solution samples was observed for both polarities. According to the experiment results, the degree of decolorisation is proportional to the charge delivered during the discharge treatment. Although some differences are seen in the samples treated by discharge with different breakdown voltages, it can be stated that the breakdown voltage level does not significantly affect the decolorisation process. However, a noticeable difference in the decolorisation results was still observed between surface and direct transient plasma discharge treatment. This is reflected in the rate of decolorisation, μ. This rate is obtained by fitting experiment data with the first-order kinetic equation (4.12).

Table 4.2. Decolorisation rate (C^{-1}) for surface and direct discharges.

Surface discharge		Direct discharge	
Positive	Negative	Positive	Negative
5.42 (5.02 – 5.82)	5.77 (5.44 – 6.10)	7.59 (7.11 – 8.07)	4.72 (4.46 – 4.98)

Values in brackets indicate a 95% confidence interval.

Table 4.2 summarises the decolorisation rates obtained in this study: it can be seen that in the case of surface transient discharges, the difference in the decolorisation rates for positive and negative energisation is less than 10%. Negative surface discharge resulted in a slightly higher rate.

However, positive direct discharges resulted in a higher decolorisation efficacy as compared with negative direct discharges: the difference between these two decolorisation rates is ~37%. The main reason for this is the difference in production of chemically reactive species. As mention earlier, the ozone level during both positive and negative discharge is undetectable. Therefore, it may be assumed that other chemical species were playing an important role in the decolorisation process. It was shown in [221] that polarity could have an influence on the production of reactive species during non-thermal plasma discharge. In [221] and [222], the OH density is almost the same, regardless of the discharge polarity, but positive discharges produce more NO molecules than negative discharges.

The distance between the HV needle electrode and the sample surface is also need to be considered. The longer gap means that the transient plasma discharge propagates a longer distance in air—this may have an influence on the production of reactive species. However, as the distance is longer, reactive species are generated in the air above the sample surface, and it may be more difficult for them to reach to the liquid sample. This distance was listed in Chapter 3, Table 3.2.

It was established that the acidity of indigo carmine solution has decreased after exposure to the surface and direct transient plasma discharges. The decrease in pH is not significantly different for the surface and direct transient plasma discharges with both positive and negative polarities.

4.5 Discussion and Conclusions

In this chapter, the oxidation capabilities of steady-state corona discharges and transient plasma discharges were investigated. Discharge polarities, voltage levels, and different topologies were tested in this series of experiments. Indigo carmine water solution was used as a chemical sensor to be treated by non-thermal plasma discharges, and decolorisation of the solution was measured. The concentration of the dye in the treated solution was obtained using the change in optical transmittance of the treated samples. The decolorisation process of the non-thermal plasma discharge treatment followed the first-order kinetics. The rate of decolorisation was obtained and used to evaluate the efficiency of oxidation.

In the study of steady-state corona discharges, both direct and indirect discharges resulted in a strong decolorisation effect. A higher decolorisation effect was observed in the samples treated with the negative corona discharges, especially in the case of the negative direct corona discharges. For such discharges, the rate of decolorisation was 4.35 C^{-1} for indirect treatment and 7.36 C^{-1} for direct treatment. The decolorisation effect achieved was similar for positive direct and indirect discharge treatment: the rates of decolorisation were 2.79 C^{-1} and 3.22 C^{-1}, respectively. Ozone concentration is considered to be the main reason for this result, because similar ozone concentrations of ~2 ppm were observed in positive discharge for both direct and indirect treatment. Higher ozone concentrations were observed in the case of negative indirect treatment (~40 ppm), and 20-60 ppm was observed in the direct corona discharge. This is in line with the result reported in [223]: 100% decolorisation of indigo carmine was achieved by plasma discharges in oxygen with a pulse repetition rate of 10 pps for 4 minutes (high ozone level); while 16 minutes of plasma discharge treatment in air with the same pulse repetition rate (low ozone level) only resulted in 80% decolorisation.

In the case of transient plasma discharges, decolorisation of the indigo carmine was also achieved. However, the decolorisation effect is lower compared to the steady-state corona discharges. One of the potential reasons for this could be the low

(undetectable) ozone levels produced by all types of transient plasma discharges in this study. Different breakdown voltage levels did not have a significant influence on the decolorisation tests results. The degree of decolorisation is proportional to the charge delivered to the sample surface. The obtained rates of decolorisation show that the efficiency of decolorisation in the surface discharge treatment is virtually identical, regardless of discharge polarities. In the case of the direct discharge treatment, a higher decolorisation rate was obtained. This could be caused by a higher production of reactive species by positive discharge, such as NO and other reactive nitrogen species.

The maximum energy efficiency of decolorisation of the indigo carmine obtained in the present work with the transient plasma treatment is ~5 μmol/kJ for the positive direct discharges. In the present tests, the concentration of indigo carmine is 0.25 g/L. In the case of negative direct corona discharge treatment, the maximum energy efficiency of decolorisation was much higher, it could reach to ~114 μmol/kJ. This value is higher than the efficiency of decolorisation of the indigo carmine dye achieved in [192], which was 3.7 μmol/kJ. The concentration of indigo carmine used in their tests was 0.05 g/L, which is lower than the concentration used in this study.

In both corona discharge and transient plasma discharge treatment tests, the pH measurements of the treated solutions show that the pH decreases with the treatment time, which corresponds to the decrease of the concentration of the dye in the treated indigo carmine solutions. The pH of all solutions treated with plasma discharges demonstrated a tendency to decrease. It is believed that the decrease in pH correlates with the degree of the decolorisation effect.

Compared with other studies, the decolorisation effect could be increased by changing several parameters of plasma discharge treatment. In this study, the maximum decolorisation of indigo carmine is less than 40%. As reported in [223], 16 minutes of plasma discharge treatment in air with a pulse repetition rate of 10 pps resulted in 80% decolorisation; while 8 minutes of plasma treatment with 50 pps pulse repetition rate achieved 100% decolorisation. However, the discharge current in their discharge

system has a peak of ~500 A, which is much higher than in our case (maximum current peak less than 30 A). On the other hand, in another study [224], plasma discharge was used to treat liquid spray and achieved 100% decolorisation of indigo carmine in only 2 minutes. The use of liquid spray increased the probability of reactive species (especially the short-lived, chemically active species) generated by the plasma discharge to react with the indigo carmine. However, the spray treatment system is a complex system, and the problem of electrode erosion is more serious in this case.

In this study, the oxidation capability of steady-state corona discharge and transient plasma discharge was investigated under various conditions including different polarities, electrode topologies, and voltage levels. The rate of decolorisation for each group of tests was obtained. The results and analysis provide information that can be used to optimise the oxidation capability of non-thermal plasma discharges.

CHAPTER 5

Bio-Decontamination Capability of Non-Thermal Atmospheric Plasma Discharges

5.1 General Introduction

It has been proved that non-thermal plasma discharges produce a significant bacteria decontamination effect [225], [226]. Multiple practical applications in a wide range of areas including food industry, medicine, medical device manufacturing, and environment applications are being investigated based on this effect. Although the mechanism of the inactivation process are not fully understood, there are several factors that make a significant contribution to bio-decontamination by non-thermal atmospheric plasmas: production of chemically active oxygen and nitrogen species, emission of UV light, and strong electric fields. As suggested in [69], [86], and [97], the chemically reactive species are responsible for the decontamination effect of non-thermal plasma discharges in atmospheric air. Chemically active species generated by non-thermal plasma discharges are able to induce oxidation damage to biomolecules and alter the functioning of biological membranes, which impose lethally damages on bacterial cells [227], [89]. For example, the reactive species generated O_3, OH radicals, NO_x^-, and NO by corona discharge; they play a leading role in the bacterial inactivation, as reported in [100], [78]. Other reactive oxygen and nitrogen species such as hydroxyl radicals, nitric dioxide, and singlet oxygen also have a strong effect on bacteria and should not be ignored.

In this study, the bio-decontamination capability of the non-thermal plasma discharges in the atmospheric air were investigated. Two types of discharges, steady-state corona and impulsive transient plasma discharges, were tested through a series of comprehensive inactivation experiments. The primary objective of this part of the study was to expose the bacterial sample to non-thermal plasma discharges in atmospheric air and to observe an inactivation and its dependency on plasma discharge parameters. As a result, the inactivation capability of plasma discharge was obtained and analysed.

In the case of steady-state corona discharge, both positive and negative polarities were used. Negative ions are the main charge carriers in the plasma of negative discharges, while positively charged particles are the main charge carriers in the plasma of positive discharges. This could result in a difference in generation of chemically reactive species by discharges with different polarities. Hence, the decontamination effect produced by plasma discharges could be different. In addition, two different topologies were investigated in this study. As described in Chapter 3.2, non-conductive sample plates were used in the indirect corona discharge treatment: in this case, ions and charged particles were screened by the grounded metallic mesh and could not reach the sample surface. In the case of the direct corona discharge treatment, conductive sample plates were used, and ions and charged particles were able to reach the sample surface and produce a direct bactericidal effect. Impulsive transient plasma discharges of both positive and negative polarities were also tested. By using conductive and non-conductive plates, the surface and direct transient plasma discharges were generated, and their decontamination effects were investigated. Two types of bacteria, *Escherichia coli* and *Staphylococcus aureus*, were used as model Gram-negative and Gram-positive bacteria, respectively, in the plasma bio-decontamination study.

This chapter provides a detailed description of the experimental procedures and research methodology. The obtained inactivation results are presented and analysed. Discussion on the inactivation capabilities of both steady-state corona and impulsive transient plasma discharges is presented.

5.2 Methodology

Bacterial samples of *E. coli* and *S. aureus* were used in this series of decontamination tests. In this section, the microbiological test procedures and experimental methodology are presented and discussed.

5.2.1 Microorganisms Selected for the Test

Bacteria can be categorised by their reaction to the Gram stain as Gram-positive and Gram-negative bacteria (Gram-positive bacteria become purple, and Gram-negative become pink after Gram staining). This difference is related to the difference in the cell structure of these two categories of bacteria. As described in Chapter 2.4.1, Gram-positive bacteria have a thick peptidoglycan cell wall outside of their cytoplasmic membrane. In contrast, Gram-negative bacteria have a thinner peptidoglycan cell wall. Outside this cell wall is an outer membrane.

The difference in cell structure, and especially in the membrane, may result in a difference in inactivation by non-thermal plasma discharges. Oxidation, UV light, or a strong electric field produced by non-thermal plasma discharges may cause damages to bacterial cells. With different cell structures, the effect on the membrane produced by discharges may be different, and the probability of causing cell damage may be different. Hence, the inactivation effect also may vary. To investigate the decontamination effect of the non-thermal plasma discharges, both types of bacteria should be tested. *E. coli* was selected to represent Gram-negative bacteria, and *S. aureus* was selected to represent Gram-positive bacteria in plasma inactivation tests.

Escherichia coli

Escherichia coli (*E. coli*) is a type of bacteria that commonly exists in the lower intestine of human and animal bodies. It as a "rod" shape cell. Most of the *E. coli* bacteria are non-pathogenic and even benefit their host. For example, *E. coli* can produce vitamin B and K [228], and the existence of *E. coli* in the intestine can prevent colonization of some pathogenic bacteria. However, some special types of *E.*

coli are pathogenic and may cause gastroenteritis, urinary tract infection, and serious food poisoning. For example, *E. coli* O157 is a very dangerous type of bacteria, which causes illness and even death worldwide [229].

Alternatively, *E. coli* also is one of the most popular microorganisms used in laboratory experiments. In this research, *E. coli* NCTC 9001 (National Collection Of Type Cultures, UK) was chosen as a sample of Gram-negative bacterium to investigate the effect of non-thermal plasma discharges. The reasons for choosing *E. coli* in this study are:

1) Safety considerations: the *E. coli* strain used in this study has low pathogenicity.
2) It grows fast, and forms highly recognisable colonies.
3) It grows easily, and does not require a special growing environment or conditions.
4) It is very common and representative of bacterium.

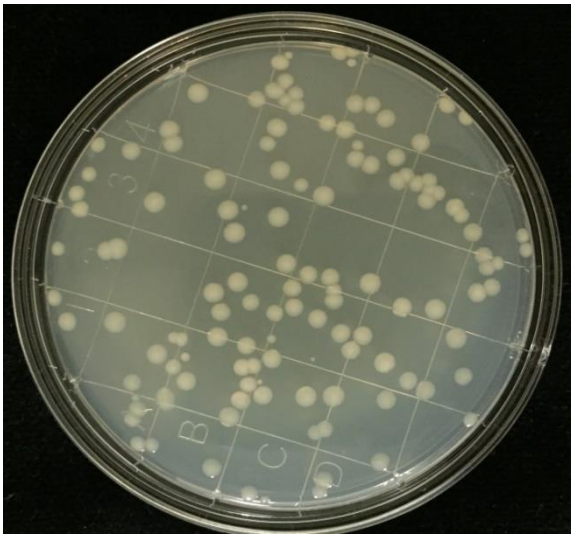

Figure 5.1. *E. coli* colony-forming units (CFU) cultured on agar plate.

E. coli colonies are white in color and grow to approximately 3-6 mm diameter, when cultured on nutrient agar for 24 hours at 37 ℃.

Staphylococcus aureus

Staphylococcus aureus (*S. aureus*) is another common type of bacteria. This type can be found in air, water, dust, human or animal skins, and waste. *S. aureus* is a

Gram-positive bacterium and has a round-shaped cell structure. Although *S. aureus* is not always pathogenic, it leads to a wide spectrum of infections including minor skin infection and respiratory infections.

S. aureus can also produce toxins and has caused many serious food poisoning cases, pneumonia, and other life-threatening diseases [230], [231]. According to [232], *S. aureus* causes nearly 241,000 cases of illness in the United States every year and has been listed as one of the major pathogens [233]. *S. aureus* is also famous for its adaptive evolution ability—it can build up resistance to human defences and the effects of antibiotics. It has been reported in [234] and [235] that *S. aureus* can even have a quick response and develop resistance to some new antibiotics such as linezolid and daptomycin. Therefore, a different and effective decontamination method must be developed, and non-thermal plasma discharge technology could be a very promising and novel method to fight these bacteria.

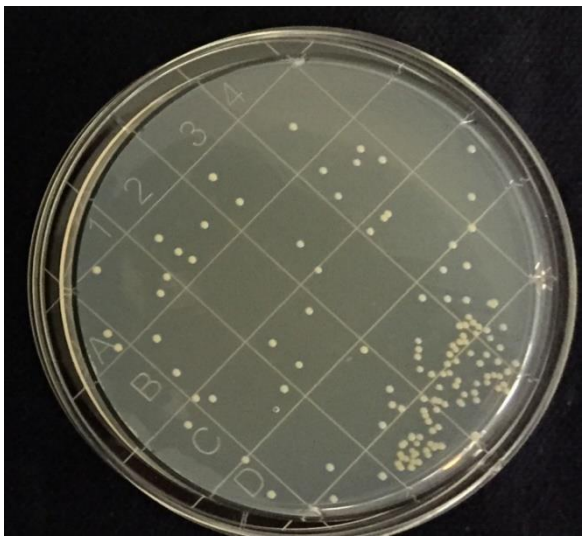

Figure 5.2. *S. aureus* colony-forming units (CFU) cultured on agar plate.

S. aureus NCTC 4135 was used for these series of tests. It grows fast and does not need special growing conditions. *S. aureus* colonies are yellow in color and have a typical size of 0.5~1.0 mm on agar plates when cultured on nutrient agar for 24 hours at 37 ℃ (see Figure 5.2).

5.2.2 Microbiological Media

To culture bacteria for experimental use, several types of media were used to provide appropriate conditions and nutrition at different stages of the experimental protocol. The media used and how they are prepared are described below:

Broth

Nutrient broth is a liquid media for culturing bacteria.

Preparation: Nutrient Broth powder (Oxoid Ltd, UK, CM0001) was weighed on a digital analytical balance (Ohaus® Adventurer® balance AR 1530), and then dissolved in distilled water and mixed well. A total of 13 g of powder should be dissolved in 1 L of distilled water, as stated by the manufacturer. Liquid broth was sterilized by autoclave and cooled down before use. As standard, the autoclave was set at 121 ℃ and 100 kPa for 15 minutes.

Diluent

Phosphate-buffered saline (PBS) is a commonly used buff solution that contains sodium dihydrogen phosphate and sodium chloride. It was used as a diluent for dilution of bacterial populations.

Preparation: Phosphate-buffered saline tablets (from Oxoid Ltd, UK, BR0014G) were completely dissolved in distilled water to make PBS solution. One tablet was dissolved in 100 ml distilled water as stated. After sterilization by autoclaving, the pH of the PBS solutions was in the range of 7.1 to 7.5 (measured at 25 ℃). Several 9 ml volumes were prepared for series dilution by using a bottle top dispenser (VITLAB simplex). Solutions of 100 ml volume were also prepared for experimental use.

Agar

Nutrient agar is a jelly-like of media which is commonly used to grow microorganisms for microbiological study.

Preparation: Nutrient agar powder (from Oxoid, Ltd, UK, CM0003) was weighed on the digital analytical balance and dissolved in distilled water. Powder (28 g) was dissolved in 1 L distilled water as stated. This solution was by autoclaving and the molten agar with the bottle was then placed in a water bath at a temperature of 48 ℃ for cooling. Next, the molten agar was poured into a sterilized petri plate/contact plate,

or tube to make agar plates or agar slopes. Prepared agar plates and slopes were incubated overnight to make sure they are free from contamination before use.

5.2.3 Microbiological Techniques

The standard procedure to obtain the bacterial population is to count bacterial colonies on the agar plates. In the microbiological study, Colony-Forming Units (CFU) are used to describe the population of bacteria. To achieve accurate counting of bacteria, several microbiological methods and techniques were employed for preparing and enumerating bacteria samples. These methods are presented in this section.

Bacteria Culture

E. coli and *S. aureus* were stored frozen on Microbank beads (Pro-Lab Diagnostics). When required, a bead was taken from the freezer and streaked onto an agar plate, and incubated at 37 ℃ overnight. A bacterial colony from the agar plate was sub-cultured to an agar slope, grown overnight at 37 ℃ and then stored at 4 ℃. This bacterial culture on the agar slope was used as the stock culture for experiments. A fresh agar slope was prepared every 4 weeks.

To prepare a bacterial culture for experimental use, a loopful of bacteria was transferred from the agar slope and inoculated into 100 ml nutrient broth. This broth was cultivated in an incubator shaker (New Brunswick Scientific Co., Inc., model C24, as shown in Figure 5.3) for 18-24 hours. The temperature was set to 37 ℃, and shaking frequency was 120 rpm.

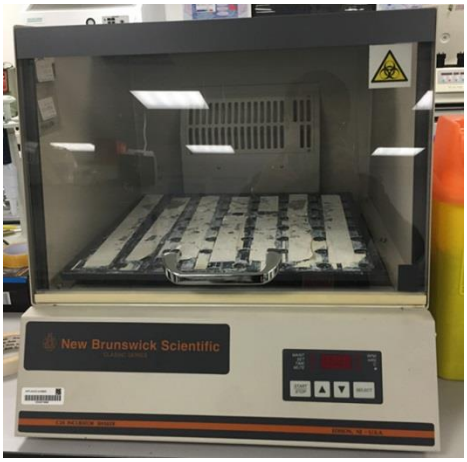

Figure 5.3. New Brunswick C24 incubator shaker.

Dilution

After incubation, the broth was centrifuged (in Heraeu Labofuge 400R Centrifuges) at 4300 rpm for 10 minutes. The cell pellets were then re-suspended in 100 ml PBS, giving a population density of ~10^9 CFU/ml. The bacterial population density required for experimental use was ~10^3 CFU/ml. To prepare suspensions with this population density the suspensions were serially diluted as follows:

Step one: 1 ml of the 10^9 CFU/ml bacterial suspension was pipetted into a volume of 9 ml PBS and mixed well. This gave a 10 ml volume with a population density of 10^8 CFU/ml.

Step two: 1 ml of the 10^8 CFU/ml suspension was transferred to another 9 ml PBS, giving a 10 ml volume of 10^7 CFU/ml.

This dilution process was continued until a bacterial population of 10^3 CFU/ml was obtained.

This serial dilution process is shown as in Figure 5.4.

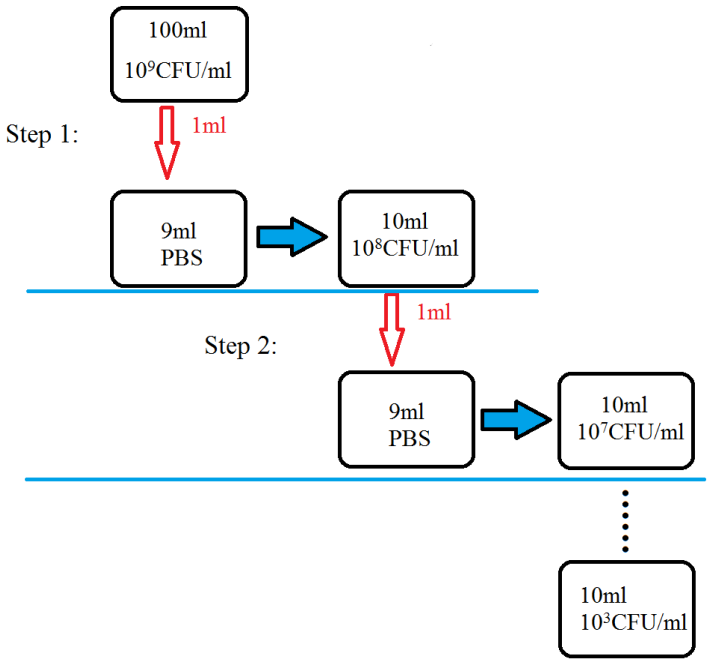

Figure 5.4. Diagram of the serial dilution method.

Plating

Using the 10^3 CFU/ml starting populations, volumes of 50 µl were pipetted onto the 55 mm agar plates, and spread evenly across the agar surface using an L-shaped spreader. The plates were then put into the discharge reactor and treated by non-thermal plasma discharges.

Incubation

After exposure, the agar plates seeded with *E. coli* or *S. aureus* were incubated at 37 ℃ for 18-24 hours. Colonies were formed on the agar surface after incubation.

Enumeration

The number of bacterial colonies formed on the agar plates were manually counted using the colony counter (BioCote), shown in Figure 5.5.

Figure 5.5. BioCote colony counter.

To establish the population density in the starting suspension, the number of colony-forming units per plate per plate grown from a 50 µl bacterial sample was multiplied by 20 to get the CFU count per mililitre (CFU/ml).

In experiments, 50 µl samples were seeded onto the agar plates and exposed to plasma discharges. These results were reported as CFU/plate. The number of colonies in each tested sample (samples treated by plasma discharges) can be compared directly

with the samples which were not treated by plasma discharges (0 minutes of plasma treatment) to present the decontamination capability.

In the present work, the inactivation results were defined in terms of normalised population, S, which represents a ratio of the survived bacterial population to the initial bacterial population:

$$S = \frac{P_n}{P_0} = \frac{N_n}{N_o} \quad (5.1)$$

where S is the normalised bacterial population

P_n is the survived bacterial population, ml^{-1}

P_0 is the initial population of bacteria, ml^{-1}

N_n is the number of bacterial colonies on the plasma-treated sample plate (CFU)

N_0 is the number of bacterial colonies on the control plates (CFU)

5.3 Steady-State Corona Discharge

The steady-state corona discharges were first used to inactivate *E. coli* and *S. aureus* bacteria. Bacteria-seeded agar sample plates were prepared as described in the previous section.

In Chapter 3.2, the steady-state corona discharge system was introduced. This system also was used in this part of the present study: bacterial samples were placed into the discharge test cell and treated by the corona discharges with different exposure times. Then, the treated samples were incubated and enumerated, and the change in the bacterial population was obtained as a result of plasma-induced inactivation.

The plasma inactivation experiments were conducted under different conditions. As mentioned in Chapter 3.2, using non-conductive and conductive sample plates, two types of corona discharge were generated, indirect and direct discharges. Based on the characteristics of the steady-state corona discharges and practical experimental environment, sample exposure time intervals were set to be 1 min, 1.5 min, 2 min, 3 min, 5 min, and 10 min. Bottled air (~12.5% RH) was fed into the test cell to create a discharge environment with different humidity. The pressure inside the test cell was kept at 0.2 bar gauge. Both positive and negative corona discharges were generated and tested at a constant voltage of 30 kV.

Both discharge current and voltage waveforms were monitored during the inactivation experiment. In addition, the concentration of ozone in the test cell during discharges was also monitored.

In this section, the results of this study, in which the populations of *E. coli* and *S. aureus* before and after exposure to steady-state corona discharges was obtained, are presented. The dependence of the surviving population on the total charge delivered during the discharge treatment also is discussed.

5.3.1 Decontamination by Indirect Corona Discharges

E. coli and *S. aureus* seeded agar samples in the non-conductive plates were exposed to the steady-state corona discharges in the indirect treatment test cell. The change in the bacterial population due to plasma treatment was monitored; these results are shown and discussed in this section.

a) Positive Energisation

Positive high-voltage DC voltage supply, Glassman WR series, was used to energise the HV electrode in the indirect treatment test cell, and to create positive steady-state corona discharges. Ozone concentration was measured during these tests and found to be ~2 ppm. The population of surviving *E. coli* after exposure to the indirect positive corona discharge is presented in Figure 5.6 as a function of the exposure time.

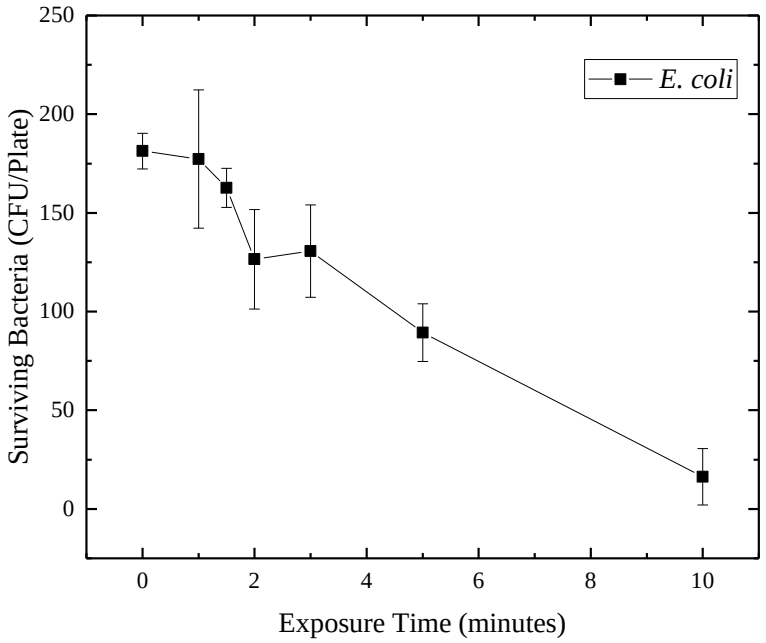

Figure 5.6. Surviving *E. coli* populations as a function of exposure time; positive, indirect, steady-state corona discharge treatment. All tests were conducted in triplicate, and each data point in this figure represents an average value. Error bars show the standard deviation. Solid lines are for visual guidance only.

The initial population before exposure to the plasma discharges was ~181 CFU/plate. Generally, with longer exposure time, less surviving bacterial colonies were observed. After 10 minutes of plasma treatment, surviving *E. coli* populations were down to less than 40 CFU/plate. In some cases, fewer than 10 CFU/plate were observed.

The surviving *E. coli* population was converted into the normalised population according to Equation 5.1. It is presented in Figure 5.7 as a function of the total charge delivered.

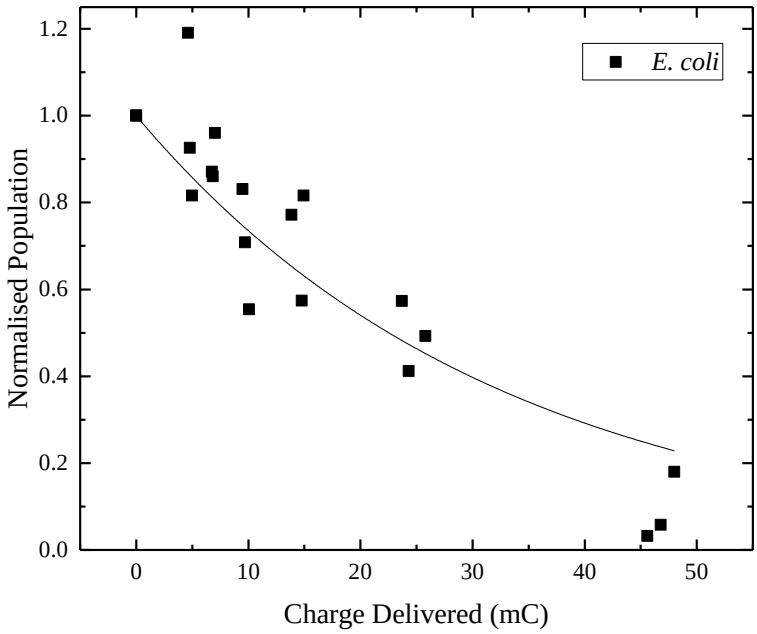

Figure 5.7. Normalised population of *E. coli* as a function of the charge delivered; positive, indirect, steady-state corona discharge treatment. The solid line is analytical fitting by equation (5.2). Each data point in this graph represents an individual test.

As can be seen from Figure 5.7, a higher level of delivered charge during the plasma treatment resulted in a lower normalised bacterial population. When the total delivered charge was ~25 mC, the normalised population was reduced to (0.40–0.55); the highest delivered charge in this group of tests, 45-50 mC, resulted in an average normalised population as low as 0.09.

The normalised population of *E. coli* as a function of delivered charge can be fitted with a first-order kinetic function:

$$S(D) = exp(-\lambda D) \quad (5.2)$$

where D is the delivered charge (mC)

S(D) is the charge-dependent normalised population

λ is the rate of the inactivation process, (mC^{-1})

In this case, the inactivation rate, λ, was found to be $0.31 \cdot 10^{-1}$ mC^{-1} ($0.25 \cdot 10^{-1}$ -$0.37 \cdot 10^{-1}$ mC^{-1}, within a confidence level of 95%). The fitting curve according to equation (5.2) was indicated by the solid line in Figure 5.7. The fitting procedure was conducted using the graphing software package, Origin Pro 2015.

In the case of Gram-positive bacterium, *S. aureus* was exposed to the indirect steady-state corona discharges under the same conditions. The surviving population of *S. aureus* as a function of the exposure time is shown in Figure 5.8.

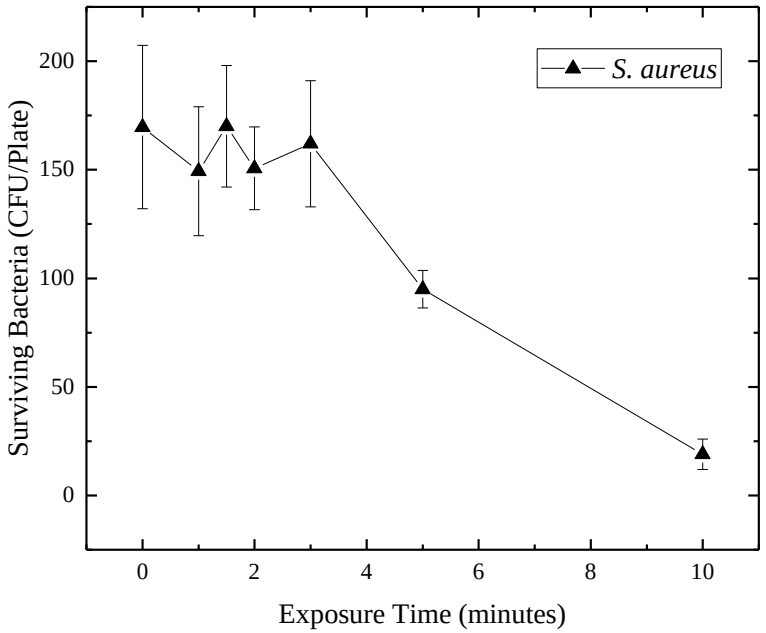

Figure 5.8. Surviving *S. aureus* populations as a function of exposure time; positive, indirect, steady-state corona discharge treatment. All tests were conducted in triplicate, and each data point in this figure represents an average value. Error bars show the standard deviation. Solid lines are for visual guidance only.

The initial population of *S. aureus* in this group of tests was ~170 CFU/plate. The surviving bacterial population was not decreased obviously after exposure to the positive indirect corona discharges for a short period of less than 3 minutes. As can be seen from Figure 5.8, surviving bacterial population remains at ~162 CFU/plate. After longer exposure time, the inactivation effect starts to become more pronounced. The surviving bacterial population was down to ~95 CFU/plate after 5 minutes of exposure, and further reduction to ~19 CFU/plate after 10 minutes of exposure was observed.

The normalised population of *S. aureus* as a function of the total charge delivered during exposure to the positive indirect corona discharges is presented in Figure 5.9.

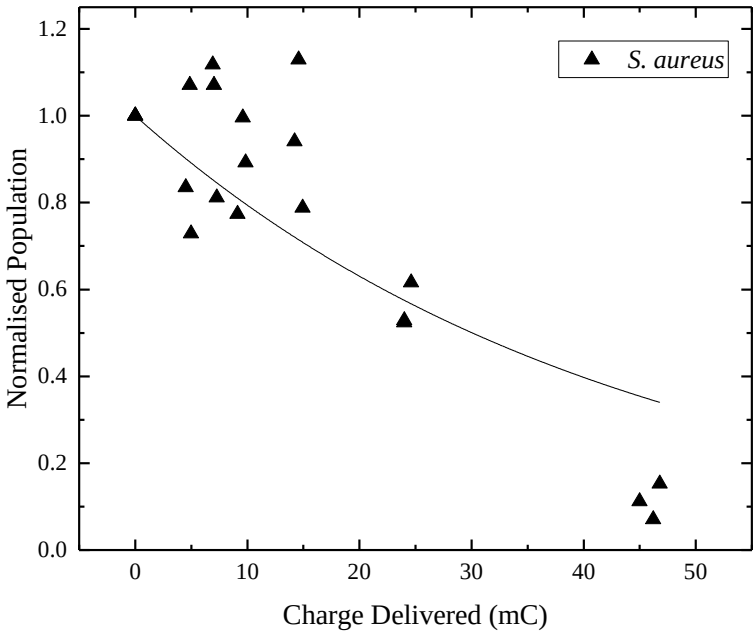

Figure 5.9. Normalised population of *S. aureus* as a function of the delivered charge; positive, indirect, steady-state corona discharge treatment. The solid line is analytical fitting by equation (5.2). Each data point in this graph represents an individual test.

When the delivered charge reached ~25 mC, the normalised population of *S. aureus* was in a range from 0.52 to 0.62. As the delivered charge increased to ~45 mC, the normalised population reduced to ~0.11.

By applying first-order kinetic fitting as in equation equation (5.2), the fitting curve was obtained using Origin Pro 2015 software. This fitting is given as a solid line in

the figure. The inactivation rate was $0.23 \cdot 10^{-1}$ mC^{-1} with a 95% confidence interval ($0.16 \cdot 10^{-1}$ - $0.30 \cdot 10^{-1}$ mC^{-1}).

b) Negative Energisation

In this section, the results of inactivation obtained using negative indirect corona discharges are presented. The DC power supply was switched to negative energisation mode. The ozone concentration was monitored during the treatment with the negative corona discharges and found to be 12–30 ppm, which is significantly higher than in the positive energisation case.

E. coli was exposed to the negative indirect corona discharges. The surviving populations of *E. coli* are a function of the exposure time, as shown in Figure 5.10.

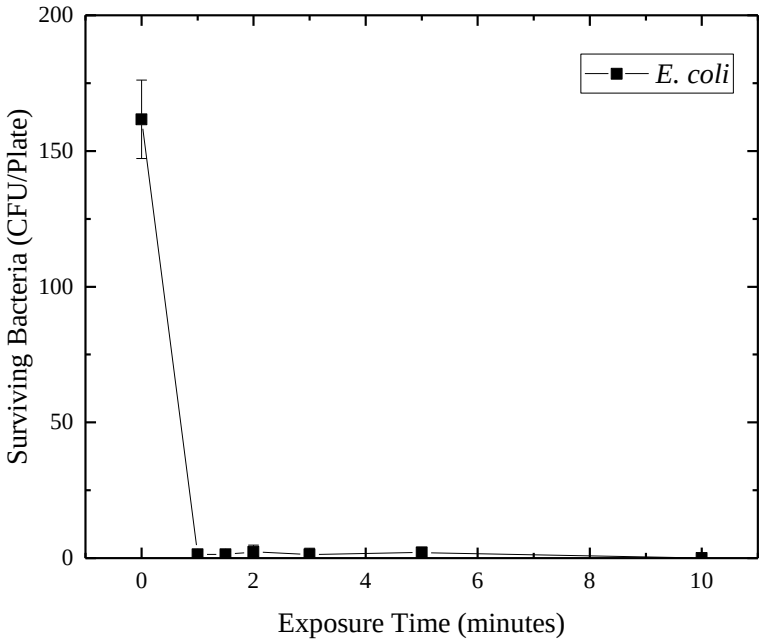

Figure 5.10. Surviving *E. coli* populations as a function of exposure time; negative, indirect, steady-state corona discharge treatment. All tests were conducted in triplicate, and each data point in this figure represents an average value. Error bars show the standard deviation. Solid lines are for visual guidance only.

The initial population of *E. coli* was ~162 CFU/plate. A significant reduction in *E. coli* population was observed, which indicates a strong inactivation effect achieved using negative indirect corona discharges. After 1 minute of exposure, surviving *E. coli* population was only ~1–2 CFU/plate. Complete inactivation of *E. coli* was achieved on the most of the sample plates.

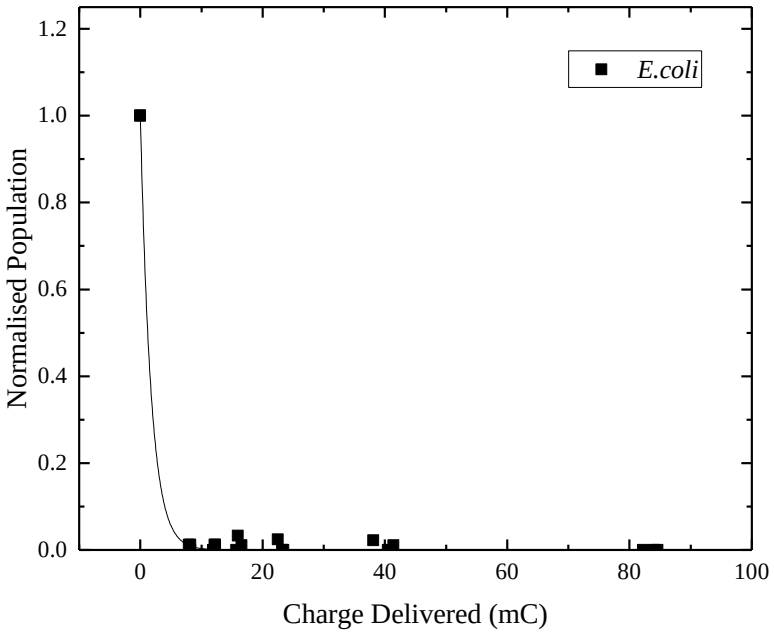

Figure 5.11. Normalised populations of *E. coli* as a function of the delivered charge; negative, indirect, steady-state corona discharge treatment. The solid line is analytical fitting by equation (5.2). Each data point in this graph represents an individual test.

In the case of the negative indirect corona discharge treatment, the normalised population of *E. coli* was reduced to 0.01 at a delivered charge level of 7–8 mC^{-1}, which shows that 99% inactivation of *E. coli* was achieved.

By applying the first-order kinetic fitting to this group of results, the inactivation rate was obtained from experimented results and found to be 0.58 mC^{-1} with a 95% confidence level (0.43–0.72 mC^{-1}).

The same procedures were applied to *S. aureus* samples, and the surviving population of these bacteria after exposure to plasma discharges is shown in Figure 5.12.

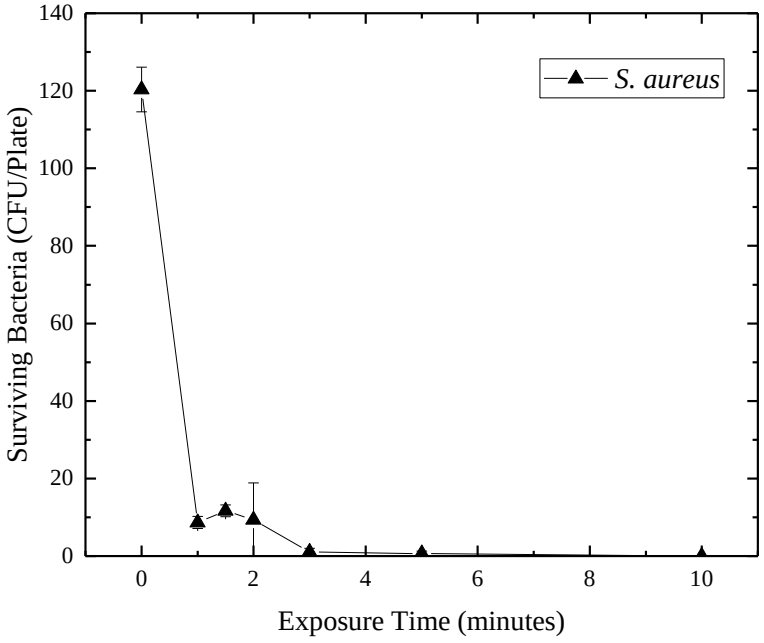

Figure 5.12. Surviving *S. aureus* populations as a function of exposure time; negative, indirect, steady-state corona discharge treatment. All tests were conducted in triplicate, and each data point in this figure represents an average value. Error bars show the standard deviation. Solid lines are for visual guidance only.

The initial population of *S. aureus* was ~120 CFU/plate. This population decreased significantly after only 1 minute of plasma treatment, resulting in ~8.7 CFU/plate. Surviving *S. aureus* population was decreased further to 0-1 CFU/plate after 3 minutes of exposure to the negative indirect corona discharges.

Normalised populations of *S. aureus* as a function of the total charge delivered after exposure of the microorganisms to the negative indirect corona discharge is shown in Figure 5.13.

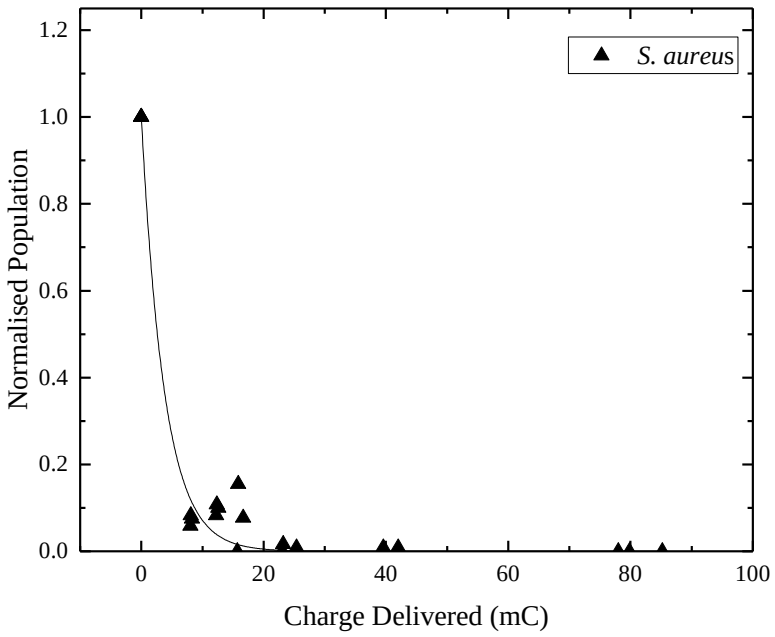

Figure 5.13. Normalised populations of *S. aureus* as a function of the delivered charge; negative, indirect, steady-state corona discharge treatment. The solid line is analytical fitting by equation (5.2). Each data point in this graph represents an individual test.

The normalised populations of *S.aureus* was decreased to below 0.2 after exposure to the negative, indirect, steady-state corona discharge with a delivered charge of 8.1 mC. As the charge delivered during the discharge treatment increased to ~23 mC, the normalised population was close to 0. The average normalised population after exposure to the negative corona discharges at the minimum delivered charge of ~8 mC was 0.072.

By applying the first-order kinetic fitting to this group of results, the rate of inactivation was found to be 0.26 mC^{-1} with a 95% confidence level (0.22–0.31 mC^{-1}).

5.3.2 Decontamination by Direct Corona Discharges

The direct corona discharge test cell was used to perform inactivation experiments, and the results are presented in this section. (The direct corona discharge system was discussed in Chapter 3.2.) In this system, bacterial samples on agar were placed in the conductive sample plates and directly exposed to corona discharge.

*a) **Positive Energisation***

A positive high-voltage DC power supply was used to energise the corona electrode and to create the positive corona discharges in the direct discharge test cell. During the discharge treatment, ozone concentration was monitored and found to be 1-2 ppm. *E. coli* was exposed to the positive direct corona discharges. The surviving population of *E. coli* are presented in Figure 5.14 as a function of exposure time.

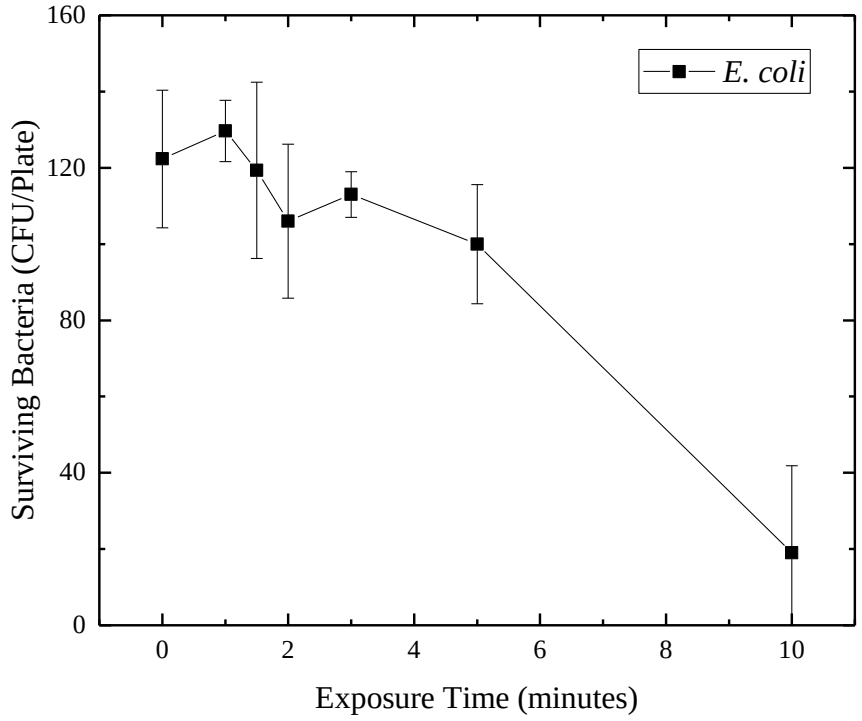

Figure 5.14. Surviving *E. coli* populations as a function of exposure time; positive, direct, steady-state corona discharge treatment. All tests were conducted in triplicate, and each data point in this figure represents an average value. Error bars show the standard deviation. Solid lines are for visual guidance only.

The initial population of *E. coli* was ~122 CFU/plate. After exposure to positive direct corona discharges for 1 minute and 1.5 minutes, no obvious decrease in the surviving population was observed. However, a minor inactivation effect was achieved after 2 minutes of exposure; the surviving bacterial population was down to ~106 CFU/plate. With longer exposure time, a higher degree of inactivation was observed: after 10 minutes of exposure, the surviving *E. coli* population was reduced to 20 CFU/plate average.

Converting the surviving population into the normalised population, the results of these tests can be presented as a function of the total delivered charge, as shown in Figure 5.15.

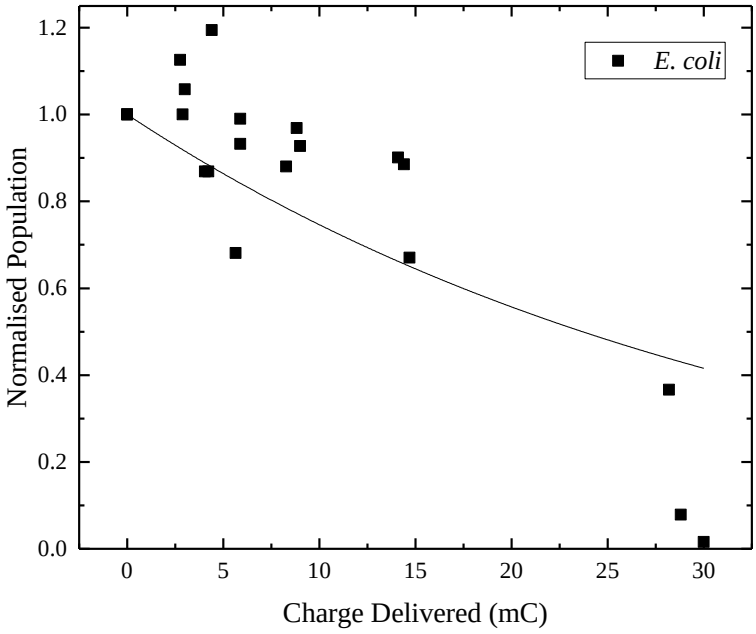

Figure 5.15. Normalised populations of *E. coli* as a function of the charge delivered; positive, direct, steady-state corona discharge treatment. The solid line is an analytical fitting by equation (5.2). Each data point in this graph represents an individual test.

As shown in Figure 5.15, the normalised populations decreased with an increase in the total delivered charge. The average normalised population was ~0.15 at the maximum delivered charge of ~30 mC.

By applying the first-order kinetic fitting to the results, the rate of the inactivation process can be obtained. For the results presented in Figure 5.15, this rate is found to be $0.29 \cdot 10^{-1}$ mC^{-1}, with a 95% confidence interval ($0.19 \cdot 10^{-1}$ to $0.39 \cdot 10^{-1}$ mC^{-1}).

S. aureus samples were exposed to the positive direct corona discharge. The surviving populations were recorded and are presented in Figure 5.16.

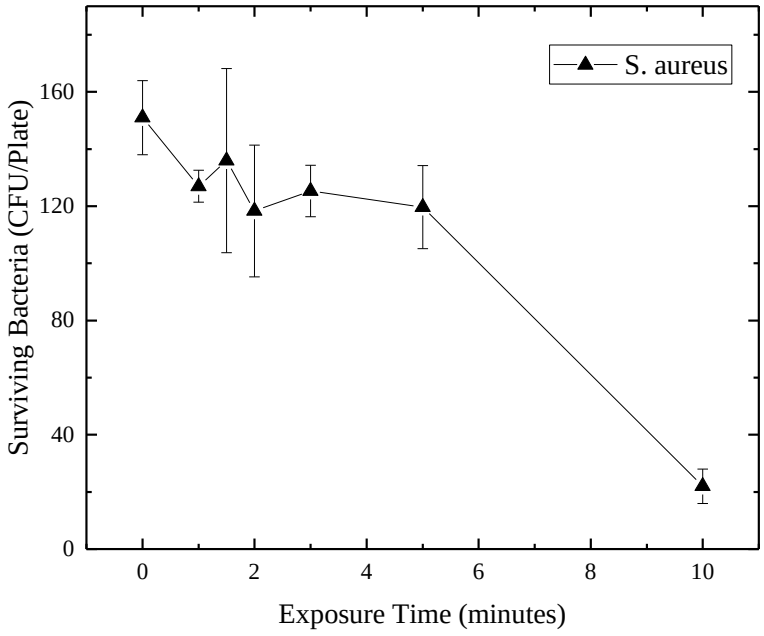

Figure 5.16. Surviving *S. aureus* populations as a function of the exposure time; positive, direct, steady-state corona discharge treatment. All tests were conducted in triplicate, and each data point in this figure represents an average value. Error bars show the standard deviation. Solid lines are for visual guidance only.

The initial population of *S. aureus* in this group of tests was ~151 CFU/plate. After exposure to the positive direct corona discharge for a short time, the population of *S. aureus* slightly decreased. After 3 minutes of exposure, the surviving population was in a range from 116 to 134 CFU/plate. Longer treatment caused futher inactivation, the surviving *S. aureus* population decreasing to ~22 CFU/plate after 10 minutes of exposure.

Normalised population and delivered charge were used to present the inactivation results, as shown in Figure 5.17.

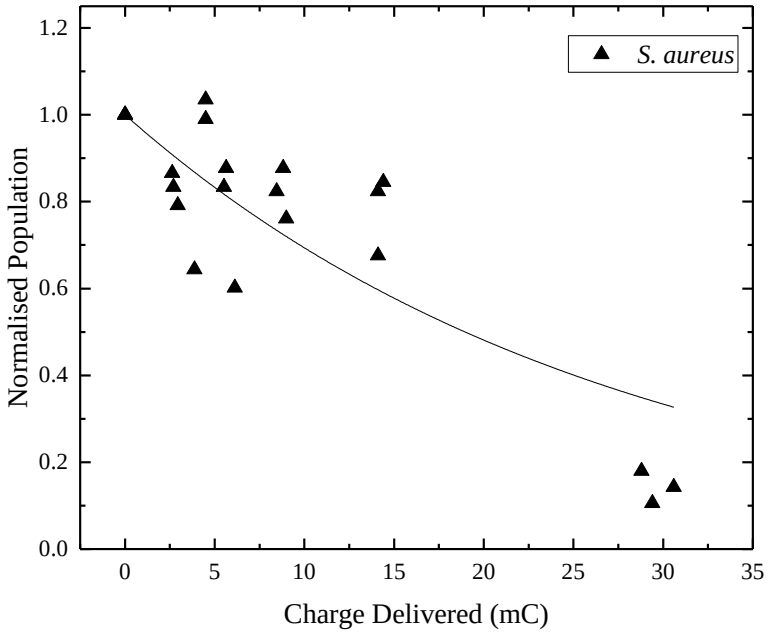

Figure 5.17. Normalised populations of *S. aureus* as a function of the charge delivered; positive, direct, steady-state corona discharge treatment. The solid line is analytical fitting by equation (5.2). Each data point in this graph represents an individual test.

As shown in Figure 5.17, a higher charge delivered results in a higher degree of inactivation. As the delivered charge increased to ~30 mC, the normalised population decreased to ~0.15.

First-order kinetic fitting was applied to this group of results, and the inactivation rate was found to be $0.37 \cdot 10^{-1}$ mC^{-1}, with a 95% confidence interval ($0.27 \cdot 10^{-1}$ to $0.46 \cdot 10^{-1}$ mC^{-1}).

b) Negative Energisation

The high-voltage DC power supply was switched to the negative mode and connected to a direct treatment test cell. Bacterial samples were exposed to the negative direct corona discharges in this case. Ozone concentration inside the test cell was 20–60 ppm during the discharge treatment.

E. coli samples were first exposed to the negative direct corona discharge. The population of the surviving bacteria as a function of the exposure time is shown in Figure 5.18.

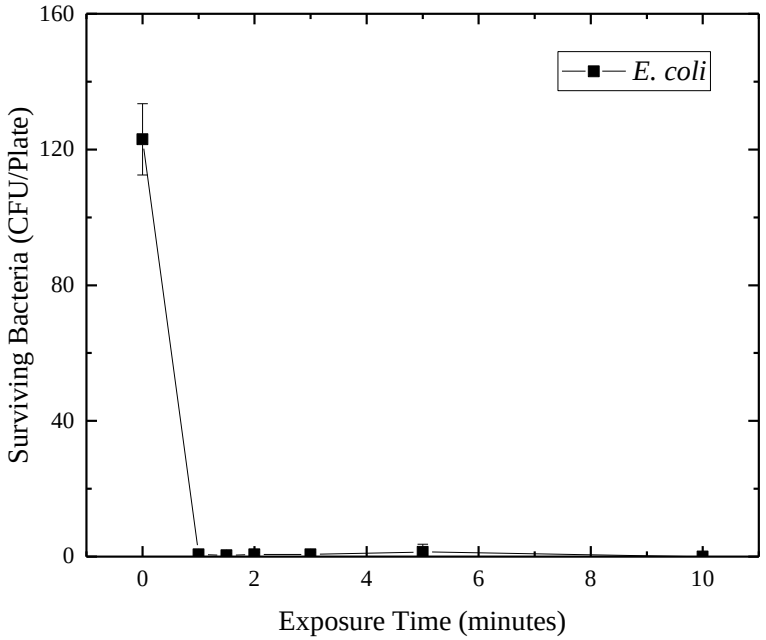

Figure 5.18. Surviving *E. coli* populations as a function of the exposure time; negative, direct, steady-state corona discharge treatment. All tests were conducted in triplicate, and each data point in this figure represents an average value. Error bars show the standard deviation. Solid lines are for visual guidance only.

The initial population of *E. coli* in this group of tests was ~123 CFU/plate. Significant inactivation was observed after exposure to negative direct corona discharges. Surviving bacterial population was close to 0 after only 1 minute of exposure, complete inactivation was achieved in sample plates after longer time exposure.

In this case, the normalised populations of *E. coli* as a function of the delivered charge is shown in Figure 5.19.

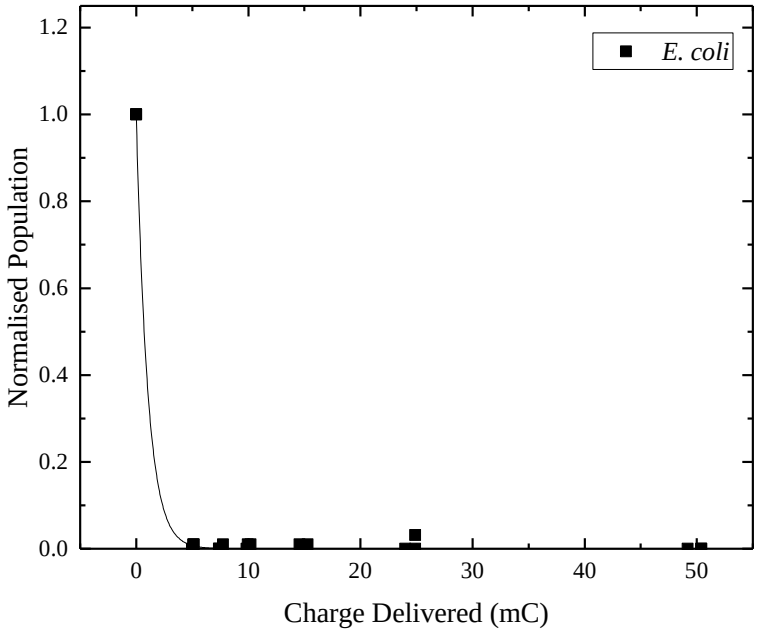

Figure 5.19. Normalised populations of *E. coli* as a function of the delivered charge; negative, direct, steady-state corona discharge treatment. The solid line is analytical fitting by equation (5.2). Each data point in this graph represents an individual test.

The minimum delivered charge in this group of experiments is 5 mC. It resulted in more than 99% inactivation of *E. coli* as the normalised population was decreased to 0.1 and less.

By applying the first-order kinetic fitting, the estimated inactivation rate was 0.98 mC^{-1} with a 95% confidence interval (0.73–1.23 mC^{-1}).

S. aureus was exposed to the negative direct corona discharges. The surviving populations of *S. aureus*, as a function of the exposure time, is shown in Figure 5.20.

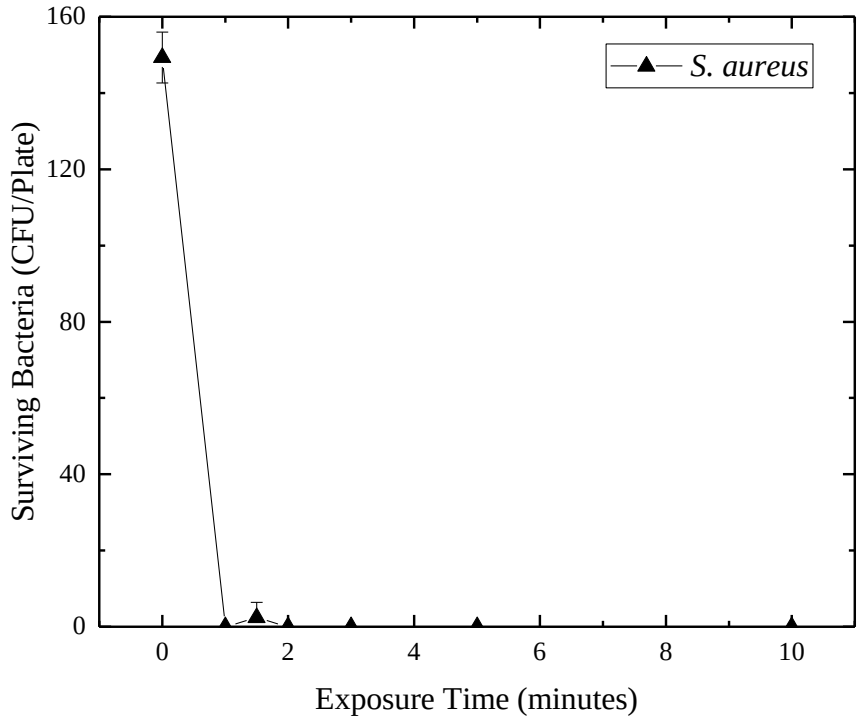

Figure 5.20. Surviving *S. aureus* populations as a function of the delivered charge; negative, direct, steady-state corona discharge treatment. All tests were conducted in triplicate, and each data point in this figure represents an average value. Error bars show the standard deviation. Solid lines are for visual guidance only.

It can be seen from Figure 5.20 complete inactivation of S. aureus on the agar surface was achieved by 1-2 minutes of negative direct corona discharge treatment.

The inactivation results were converted into the normalised populations and are shown in Figure 5.21 as a function of the total delivered charge.

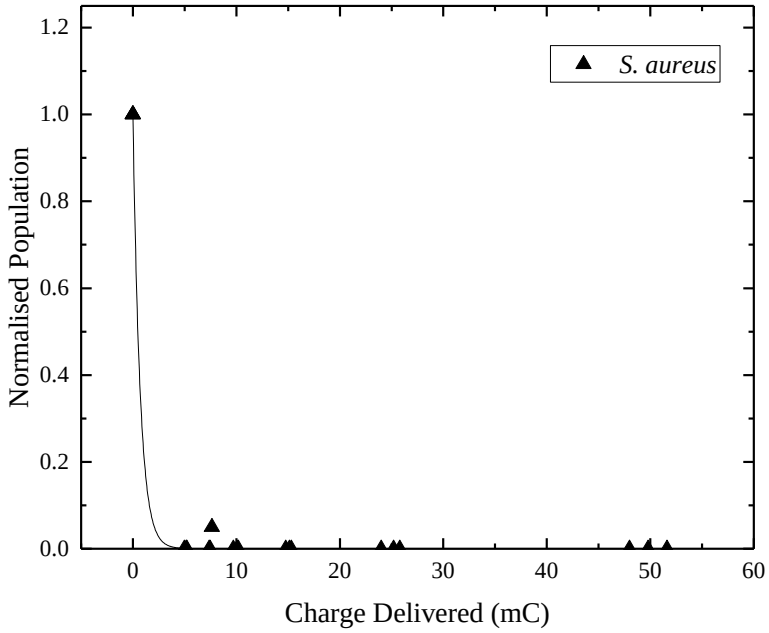

Figure 5.21. Normalised populations of *S. aureus* as a function of the delivered charge; negative, direct, steady-state corona discharge treatment. The solid line is an analytical fitting by equation (5.2). Each data point in this graph represents an individual test.

The normalised populations of *S. aureus* were reduced to zero (complete inactivation was achieved) after treatment with the negative direct corona discharges with a minimum delivered charge of ~5 mC.

The first-order kinetic fitting was applied to this group of results. The estimated rate of the inactivation process was determined to be 1.44 mC^{-1} with a 95% confidence interval (0–4.86 mC^{-1}).

5.3.3 Summary of Bacterial Inactivation by Steady-State Corona Discharge

In the experiments conducted and presented in this chapter, it was shown that the steady-state direct and indirect corona discharges have the ability to inactivate *E. coli* and *S. aureus* on surface. The degree of inactivation may vary and depends on topologies of the treatment cells and polarities of the corona discharges. However, it was shown that decontamination of bacteria on agar surface was achieved by all the types of steady-state corona discharges used in this work. The charge-dependent character of inactivation curves for both tested microorganisms were established.

Two types of corona discharge treatment test cells were used in this work: direct and indirect. In the case of the indirect corona discharge treatment, most of the charged particles were screened along with the high electric field by the grounded metallic mesh above the sample; thus, the charged particles were not able to reach the sample surface. It can be assumed that in this case neutral chemically active species such as ozone passed through the grounded mesh and acted on the bacteria on the agar surface, resulting in a decontamination effect.

During the positive corona discharge at +30 kV, the ozone concentration was ~2 ppm. At the maximum delivered charge of ~47 mC, a noticeable inactivation effect was produced by the positive indirect corona discharge: the normalised populations of *E. coli* and *S. aureus* were decreased to ~0.09 and 0.11, respectively, which means that ~91% inactivation of *E. coli* and ~89% inactivation of *S. aureus* was achieved..

In the case of the negative corona discharge treatment at -30 kV, the ozone concentration was 12–30 ppm, much higher than in the case of positive energisation. The inactivation effect was also higher according to the obtained results. After 1 minute of exposure to the negative indirect corona discharges, the normalised populations of *E. coli* and *S. aureus* were decreased to 0.01 and 0.07, respectively, which means that a 99% inactivation of *E. coli* and 93% inactivation of *S. aureus* was achieved using negative indirect corona discharges at a delivered charge level of 8 mC. As the delivered charge increased to ~16 mC, 99% inactivation of *S. aureus* was observed.

In the case of the direct corona discharge treatment, the charged particles could be delivered to the sample surface. When positive energisation was applied, the ozone concentration inside the test cell was 1–2 ppm, similar to the case of the positive indirect corona treatment. The inactivation effect produced by positive direct corona discharges was also similar to the effect produced by the positive indirect corona discharge treatment. The average normalized populations of *E. coli* and *S. aureus* were reduced to ~0.15 after exposure to the positive direct corona discharges for 10 minutes. However, the maximum charge delivered at this point was ~30 mC, which is much lower than in the case of the indirect positive discharges ~47 mC.

When the negative direct corona discharges were used to treat the bacteria samples, the ozone concentration was higher, 20–60 ppm, and significant inactivation effect was observed. The discharge treatment with a relatively low charge delivered of ~5 mC resulted in 100% inactivation of both *E. coli* and *S. aureus*.

By applying the first-order kinetic fitting to the normalised population as a function of the total delivered charge, the rate of the inactivation process was obtained in different cases. These rates are given in Table 5.1.

Table 5.1. Inactivation rate (mC^{-1}) for indirect and direct corona discharges.

Indirect discharge			
Positive		Negative	
E. coli	*S. aureus*	*E. coli*	*S. aureus*
$0.31 \cdot 10^{-1}$ ($0.25 \cdot 10^{-1}$ – $0.37 \cdot 10^{-1}$)	$0.23 \cdot 10^{-1}$ ($0.16 \cdot 10^{-1}$ – $0.30 \cdot 10^{-1}$)	0.58 (0.43–0.72)	0.26 (0.22 –0.31)
Direct discharge			
Positive		Negative	
E. coli	*S. aureus*	*E. coli*	*S. aureus*
$0.29 \cdot 10^{-1}$ ($0.19 \cdot 10^{-1}$ – $0.39 \cdot 10^{-1}$)	$0.37 \cdot 10^{-1}$ ($0.27 \cdot 10^{-1}$ – $0.46 \cdot 10^{-1}$)	0.98 (0.73 –1.23)	1.44 (0 –4.86)

Values in brackets indicate a 95% confidence interval.

In the case of positive energisation, the inactivation effect of the indirect and direct corona discharges was similar for both *E. coli* and *S. aureus.* The inactivation rates for these two bacteria were similar.

Negative energisation in both indirect and direct corona discharges produced a stronger inactivation effect compared to positive energisation. The inactivation rates in the case of negative energisation are much higher than in the case of positive energisation. The negative direct discharges produce the strongest inactivation effect: 5 mC charge resulted in ~99.9% inactivation of *E. coli*. Compared with the indirect negative corona discharges, the direct negative corona discharges produce a higher ozone concentration during the treatment: 20–60 ppm instead of 12–30 ppm. This could be the main reason that direct negative discharge treatment resulted in a higher inactivation rate.

5.4 Impulsive Transient Plasma Discharges

To compare decontamination efficiencies of different types of discharges, the decontamination capability of impulsive plasma transient discharges was investigated. The impulsive discharge system which was described in Chapter 3.3 can produce two types of discharges: surface transient plasma discharge (which propagates across the sample/air interface) and direct transient plasma discharge (which propagates through the bulk of the liquid or agar sample). In this part of the present research, both types of transient plasma discharge were tested: positive and negative energisation was used to develop the transient plasma discharegs. As in Chapter 4, the breakdown voltages were selected as 20 kV, 24k V, and 28 kV. Treatment time intervals were 1, 3, 5, and 7 minutes. Pulse repetition rate was 20 pulses per second. Bacteria were seeded on agar plates (conductive or non-conductive), and these agar plates were placed into the discharge reactor and treated by the non-thermal plasma discharges. Then the bacterial samples were incubated for 18–24 hours at 37℃, and bacterial colony numbers were enumerated. During the discharge treatment, the ozone concentration was measured and found to be less than 1 ppm; it was not detectable by the ozone analyser.

5.4.1 Decontamination by Surface Transient Plasma Discharges

a) Positive Energisation

Positive energisation was applied to the transient plasma discharge system with non-conductive sample plates to create surface transient plasma discharges. *E. coli* was treated by this discharge. The inactivatiion curves are shown in Figure 5.22.

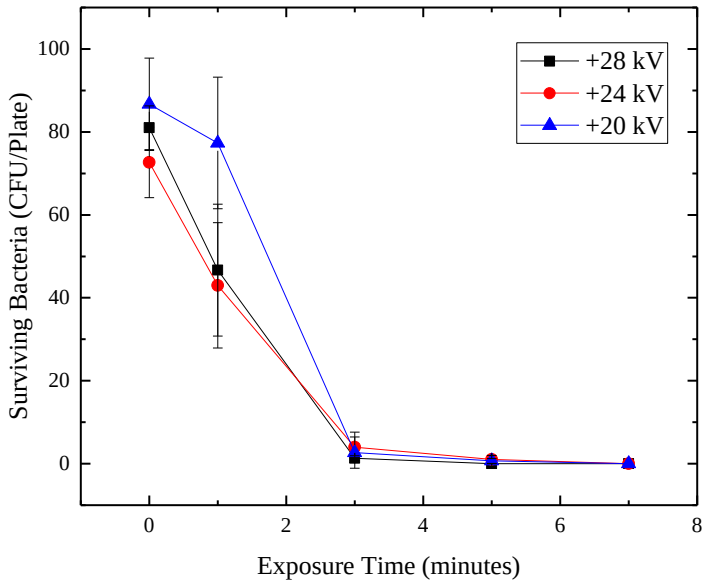

Figure 5.22. Surviving *E. coli* populations as a function of exposure time using positive surface transient plasma discharge treatment. All tests were conducted in triplicate, and each data point in this figure represents an average value. Error bars show the standard deviation. Solid lines are for visual guidance only.

The initial population of *E. coli* in these tests was in a range of 70-100 CFU/plate. An obvious decrease in population was achieved for all three applied voltages. After 1 minute of exposure to the surface transient plasma discharge with breakdown voltages of 24 kV and 28 kV, *E. coli* populations were decreased to ~(43–46) CFU/plate. The decrease was also observed in the samples exposed to the discharges with a breakdown voltage of 20 kV: the population was reduced to ~77 CFU/plate. A further decrease in the population of *E. coli* was achieved after 3 minutes of exposure for all breakdown voltages: the population was reduced to less than 10 CFU/plate. It can be seen from Figure 5.22 that all bacteria were inactivated after 5 minutes of treatment.

The surviving bacterial populations were converted into the normalised population and are presented as a function of delivered charges, as shown in Figure 5.23.

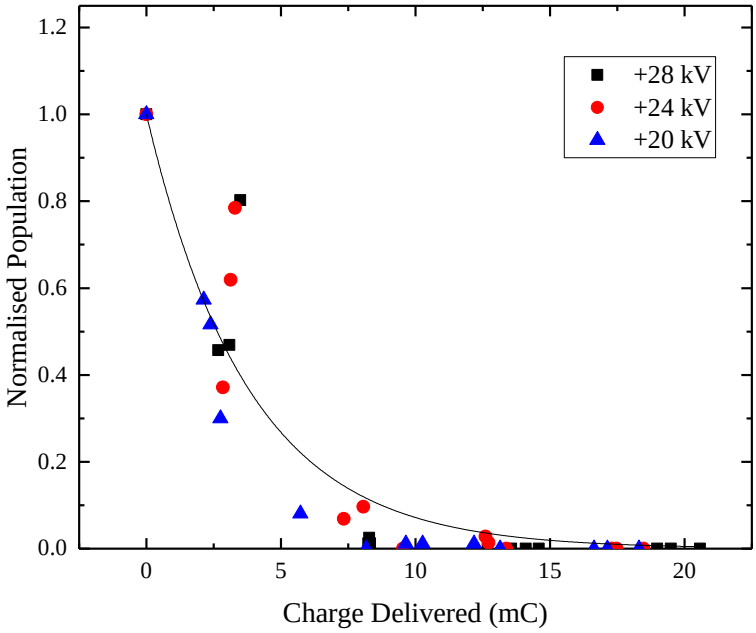

Figure 5.23. Normalised population of *E. coli* as a function of the delivered charge using positive surface transient plasma discharge treatment. The solid line is an analytical fitting by equation (5.2). Each data point in this graph represents an individual test.

It is clear that the decontamination effect is proportional to the delivered charge; as more charge is delivered to the sample surface, less *E. coli* survived on the plate treated by the discharges. The normalised population was reduced to ~0.01 as the delivered charge reached ~10 mC. In the case of the discharge treatment with a delivered charge higher than 13 mC, the normalised population of *E. coli* was decreased to 0 CFU/plate. Complete inactivation was achieved.

The rate of inactivation, λ, was found to be 0.26 mC^{-1}. This fitting is presented as the solid line in Figure 5.23.

As with *E.coli*, *S. aureus* was treated by surface transient plasma discharges with positive energisation. The surviving bacterial population as a function of exposure time is presented in Figure 5.24.

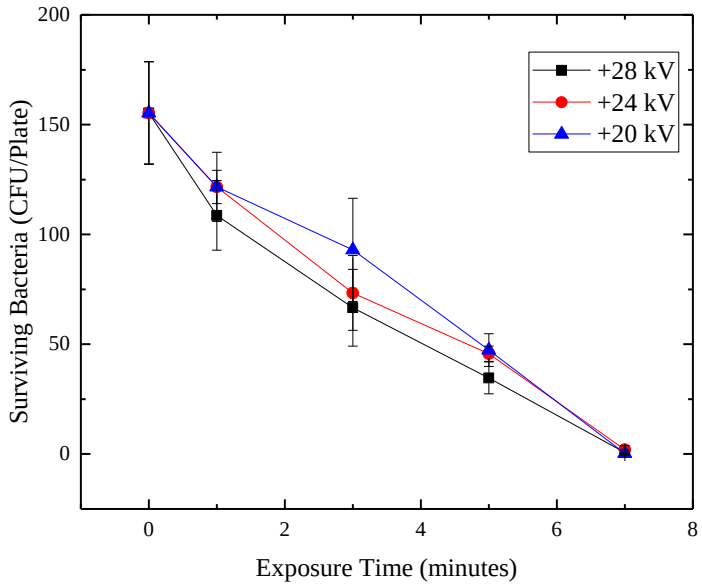

Figure 5.24. Surviving *S. aureus* populations as a function of exposure timeusing positive surface transient plasma discharge treatment. All tests were conducted in triplicate, and each data point in this figure represents an average value. Error bars show the standard deviation. Solid lines are for visual guidance only.

The initial population of *S. aureus* in these experiments was 130-176 CFU/plate. This number was reduced to 40-50 CFU/plate after 5 minutes of exposure to the positive surface transient plasma discharges. Further decrease in *S. aureus* population was observed with an increase in the treatment time: with less than five colonies of *S. aureus* were observed on agar plates after 7 minutes of exposure.

As in the case of *E. coli*, the surviving populations of *S. aureus* were converted into the normalised populations and are presented in Figure 5.25 as a function of the delivered charge.

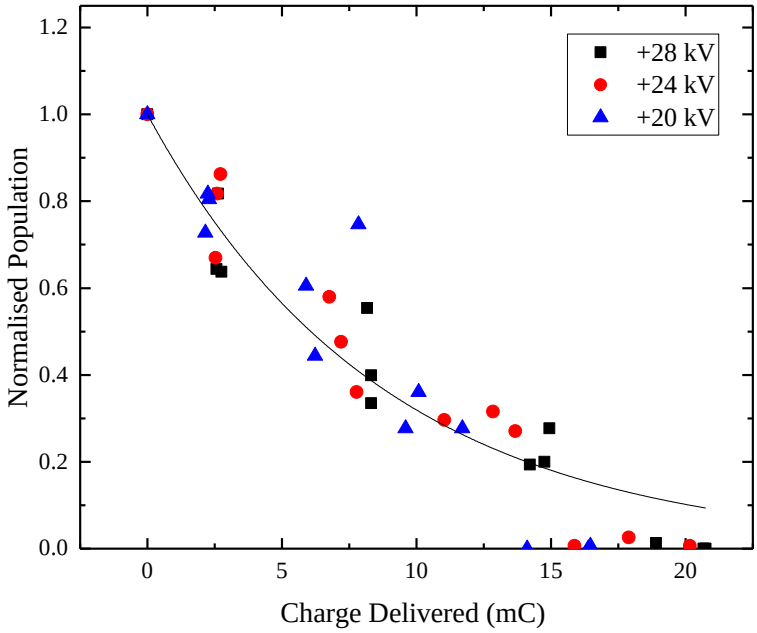

Figure 5.25. The normalised populations of *S. aureus* as a function of the delivered charge using positive surface transient plasma discharge treatment. The solid line is analytical fitting by equation (5.2). Each data point in this graph represents an individual test.

The normalised population of *S. aureus* was reduced to 0.8 after the plasma discharge treatment, with a total delivered charge of 2.5 mC. Further decreases in the population of *S. aureus* was observed with an increase in the delivered charge: as the delivered charge increased to ~20 mC, the normalised population decreased to 0.

Applying the first-order kinetic function in (equation5.2) to fit the experimental data (the normalised populations of *S. aureus* as a function of delivered charge), the fitting curve is obtained and shown as the solid line in Figure 5.20. The rate of the inactivation, λ, was found to be 0.11 mC^{-1}.

b) Negative Energisation

The negative impulsive power supply (Samtech Switching Generator) was used to energise the high-voltage electrodes in the discharge reactor. The surface transient plasma discharges were generated to treat bacteria samples.

E. coli was seeded on agar on the non-conductive plastic plates and then exposed to the transient surface plasma discharges. Surviving bacterial populations were counted and are presented as a function of the exposure time in Figure 5.26.

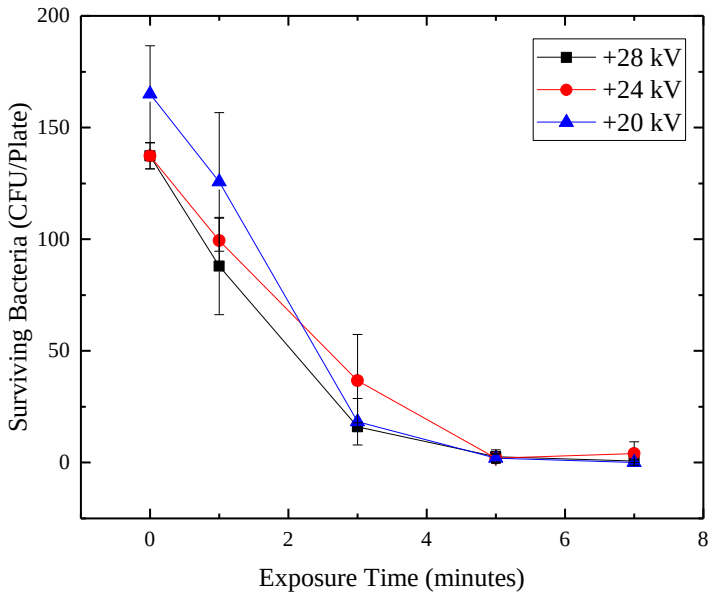

Figure 5.26. Surviving *E. coli* populations as a function of exposure time using negative surface transient plasma discharge treatment. All tests were conducted in triplicate, and each data point in this figure represents an average value. Error bars show the standard deviation. Solid lines are for visual guidance only.

The initial population of *E. coli* in these tests was in a range of 133–189 CFU/plate. After 3 minutes of exposure, the average surviving population was less than 50 CFU/plate for all three breakdown voltages. This number was reduced further to less than 5 CFU/plate after 5 minutes of exposure. After 7 minutes of exposure, 0 colonies were observed on most of the agar plates.

The normalised populations of surviving *E. coli* as a function of total delivered charge is shown in Figure 5.27.

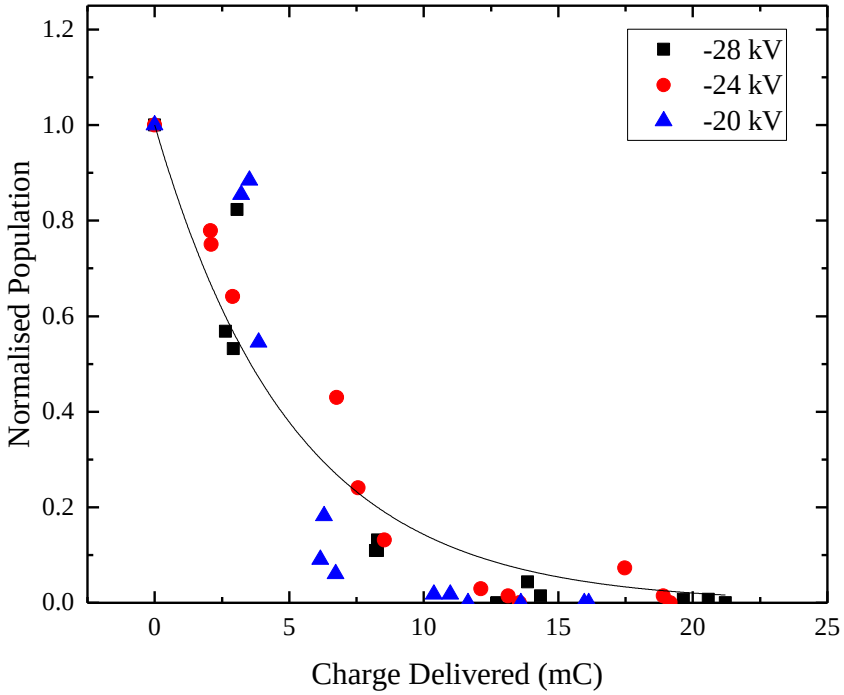

Figure 5.27. Normalised populations of *E. coli* as a function of the charge delivered using negative surface transient plasma discharge treatment. Solid line is analytical fitting by equation (5.2). Each data point in this graph represents an individual test.

The normalised population of *E. coli* was reduced to 0.01 when the delivered charge reached ~15 mC. Inactivation was achieved at the maximum charge of ~20 mC. A first-order kinetic fitting curve was obtained according to equation (5.2) using Origin Pro 2015, and the rate of inactivation, λ, was found to be 0.19 mC^{-1}.

S. aureus was then exposed to the surface transient plasma discharges with negative polarity. The same experimental procedure was applied as in the previously described *E. coli* tests. The results are shown in Figure 5.28.

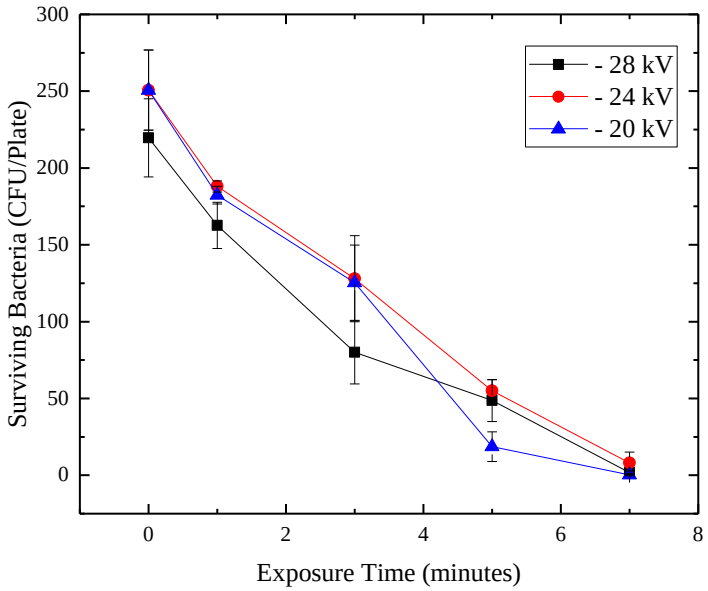

Figure 5.28. Surviving *S. aureus* populations as a function of exposure time using negative surface transient plasma discharge treatment. All tests were conducted in triplicate, and each data point in this figure represents an average value. Error bars show the standard deviation. Solid lines are for visual guidance only.

The initial population of *S. aureus* was in a range of 203–278 CFU/plate. After 3 minutes of exposure to the negative surface transient plasma discharges, the average number of surviving *S. aureus* population was less than 150 CFU/plate. After 5 minutes of exposure, the surviving bacterial population was below 60 CFU/plate. After the longest exposure, 7 minutes, complete inactivation was achieved on most of the plates; only 1 or 2 colonies were observed on the remaining plates.

The normalised population of *S. aureus* is presented as a function of charge delivered in Figure 5.29.

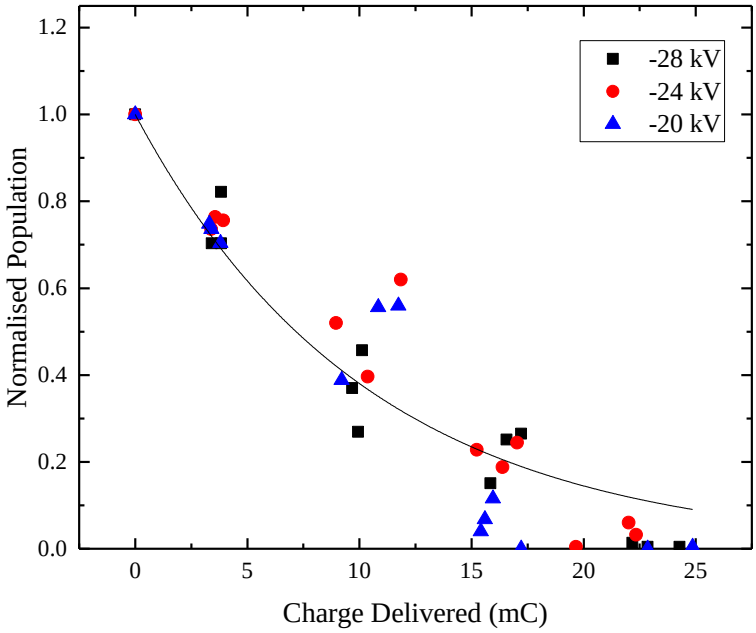

Figure 5.29. Normalised populations of *S. aureus* as a function of the delivered charge using negative surface transient plasma discharge treatment. The solid line is analytical fitting by equation (5.2). Each data point in this graph represents an individual test.

The normalised populations reduced with an increment in the delivered charge. In the case of the maximum delivered charge, 24 mC, the normalised populations were decreased to less than 0.01. The first-order kinetic fitting curved was plotted per equation (5.2) and given a solid line in Figure 5.24. The rate of inactivation, λ, is $0.97 \cdot 10^{-1}$ C^{-1}.

5.4.2 Decontamination by Direct Transient Plasma Discharges

E. coli and *S. aureus* were seeded on agar in the conductive sample plates, and treated in the discharge reactor. In this case, bacterial samples were exposed to the direct transient plasma discharges. Ozone concentration during the direct transient plasma discharge treatment was measured and found to be negligible (less than 1 ppm). The waveforms of the breakdown voltage and current were recorded for the delivered charge calculation. Bacteria on the tested sample plates were enumerated before (control) and after exposure. The results of these tests are presented in the next section.

a) Positive Energisation

The surviving populations *of E. coli* are presented as a function of the exposure time in Figure 5.30.

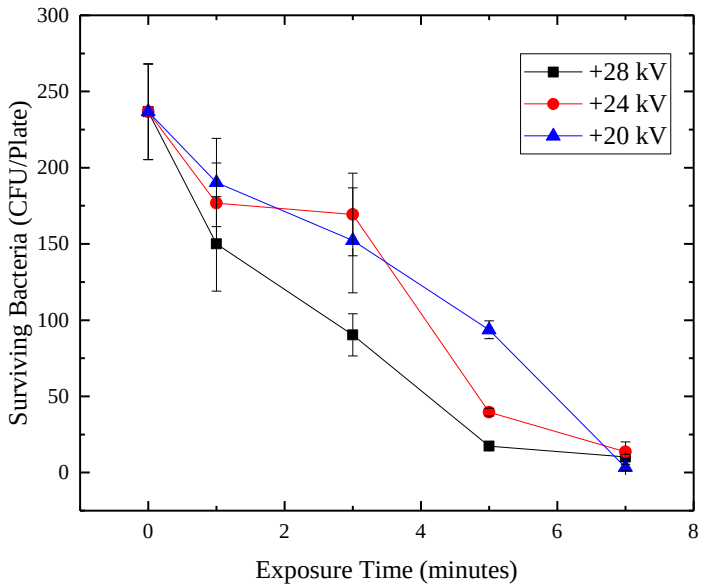

Figure 5.30. Surviving *E. coli* populations as a function of the exposure time using positive, direct, transient plasma discharge treatment. All tests were conducted in triplicate, and each data point in this figure represents an average value. Error bars show the standard deviation. Solid lines are for visual guidance only.

The initial population of *E. coli* on the agar plates was in a range of 203–265 CFU/plate. After 1 minute of exposure to the direct transient plasma discharges with a breakdown voltage of 28 kV, the surviving *E. coli* population was reduced to 150 CFU/plate. For the direct transient plasma discharges with a breakdown voltage of 24 kV and 28 kV, the average surviving populations were 190 CFU/plate and 170 CFU/plate, respectively. Further exposure resulted in a decrease in the surviving bacterial population. It was observed that the surviving *E. coli* population was reduced to less than 20 CFU/plate after exposure to the direct transient plasma discharges with different voltage levels. Inactivation was achieved by the direct transient plasma discharge treatment; however, unlike in the case of the surface transient plasma discharges, no complete inactivation (0 CFU/plate) was observed, even after 7 minutes of exposure.

The surviving *E. coli* population was converted into the normalised populations, and the delivered charge was obtained. Figure 5.31 shows the normalised populations of *E. coli* after exposure to positive, direct, transient plasma discharges as a function of delivered charge.

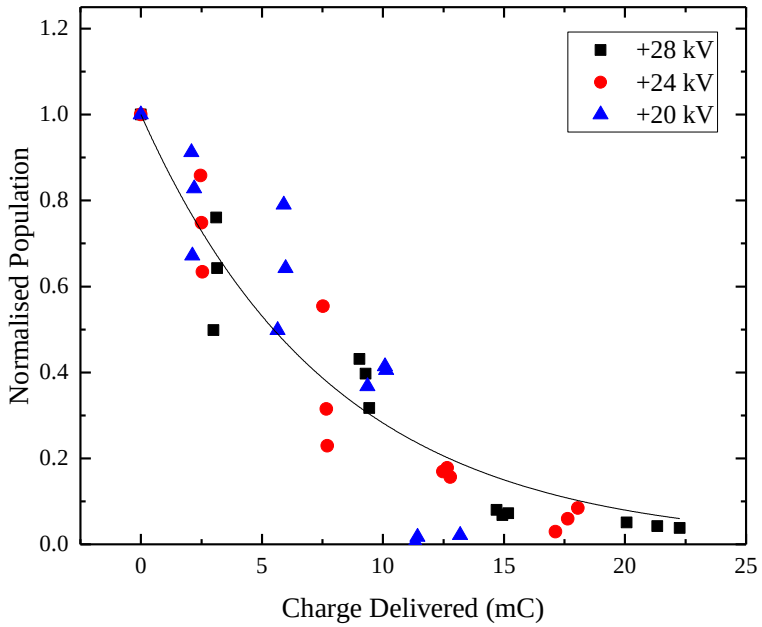

Figure 5.31. The normalised populations of *E. coli* as a function of the charge delivered using positive, direct, transient plasma discharge treatment. The solid line is an analytical fitting by equation (5.2). Each data point in this graph represents an individual test.

It is established that the normalised populations of *E. coli* is a function of the delivered charge. The highest delivered charge was 22 mC, and it resulted in a reduction of the normalised *E. coli* population to $0.38 \cdot 10^{-1}$. Different breakdown voltages do not result in a difference in the relationship between delivered charge and normalised population. The first-order kinetic fitting curve was obtained using equation (5.2). The curve is shown in Figure 5.31; the rate of the inactivation process, λ, is 0.13 mC^{-1}.

S. aureus was then treated with the positive, direct, transient plasma discharges. The surviving bacterial population is presented in Figure 5.32 as a function of the exposure time.

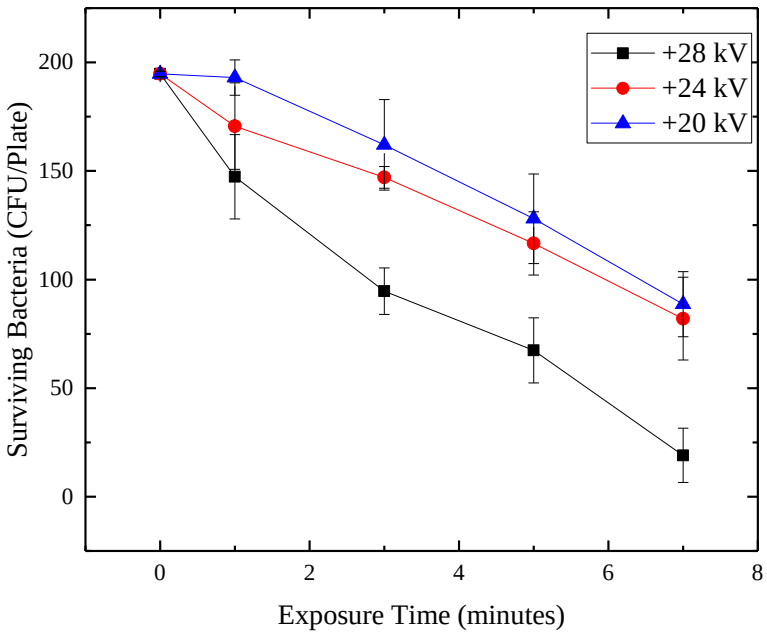

Figure 5.32. Surviving *S. aureus* populations as a function of exposure time using positive, direct, transient plasma discharge treatment. All tests were conducted in triplicate, and each data point in this figure represents an average value. Error bars show the standard deviation. Solid lines are for visual guidance only.

The initial population of *S. aureus* was in a range of 194–196 CFU/plate. After 3 minutes of exposure to the direct transient plasma discharges with a breakdown voltage of 28 kV, the surviving population was reduced to ~94 CFU/plate. Higher surviving populations of *S. aureus* were observed after exposure to the direct discharges with a breakdown voltage of 24 kV and 20 kV: 147 CFU/plate and 162 CFU/plate, respectively. After 7 minutes of exposure to the direct transient plasma discharge with a breakdown voltage of 28 kV, the surviving population was 19 CFU/plate. In the case of 7 minutes of exposure to the direct transient plasma discharges with a breakdown voltage of 24 kV and 20 kV, the surviving bacterial populations were 82 CFU/plate and 88 CFU/plate, respectively.

The surviving populations of *S. aureus* were converted into the normalised population and are shown in Figure 5.33 as a function of charge delivered.

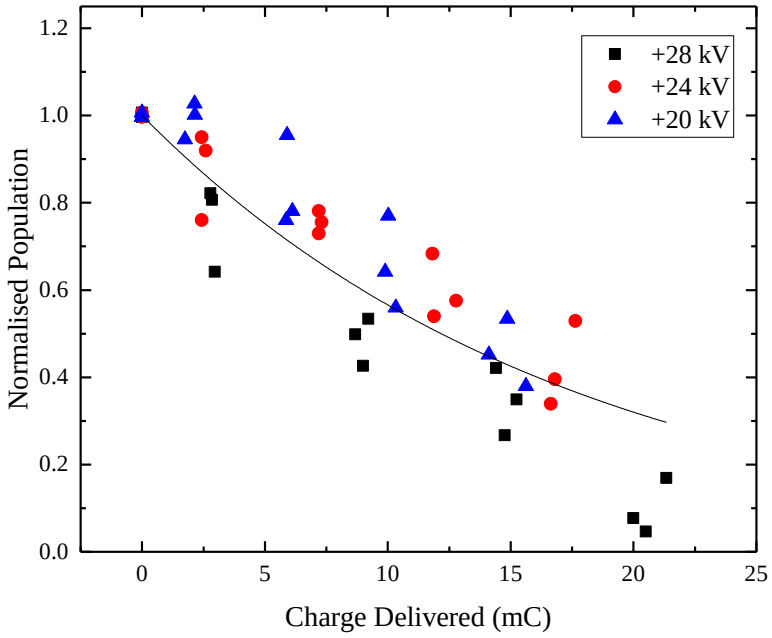

Figure 5.33. Normalised populations of *S. aureus* as a function of the delivered charge using positive, direct, transient plasma discharge treatment. Solid line is an analytical fitting by equation (5.2). Each data point in this graph represents an individual test.

At the maximum delivered charge of ~20 mC^{-1}, 0.05–0.15 normalised population was observed. The first-order kinetic fitting curve is given in Figure 5.33. The inactivation rate, λ, is $0.57 \cdot 10^{-1}$ mC^{-1}.

b) Negative Energisation

Negative pulses were generated by the pulse power supply and delivered to the discharge reactor to generate the negative, direct, transient plasma discharges. Bacteria samples were treated by the negative direct discharges, and the surviving bacterial colony were enumerated.

Figure 5.34 shows the surviving populations of *E. coli* after exposure to the negative, direct, transient plasma discharge.

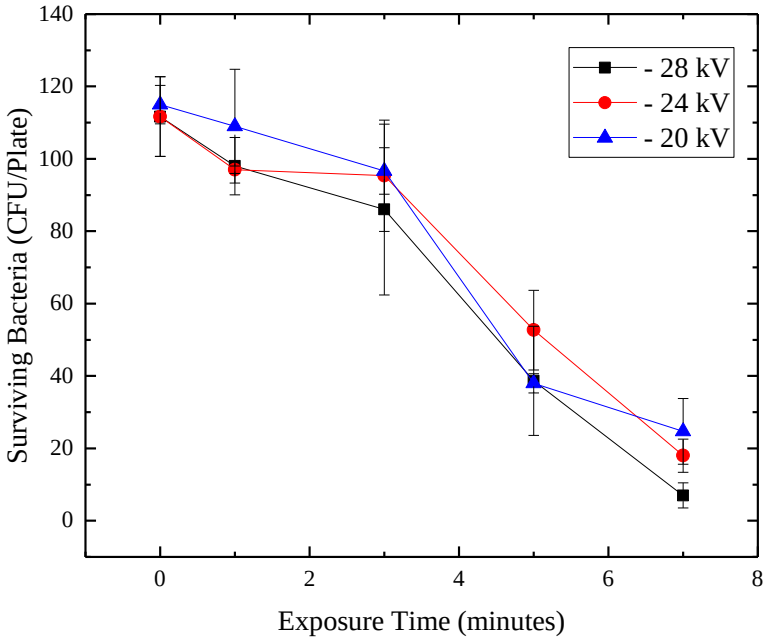

Figure 5.34. Surviving *E. coli* populations as a function of the exposure time using negative, direct, transient plasma discharge treatment. All tests were conducted in triplicate, and each data point in this figure represents an average value. Error bars show the standard deviation. Solid lines are for visual guidance only.

The initial population of *E. coli* was in the range of 101-123 CFU/plate. Inactivation was achieved by exposure of the samples to direct transient plasma discharges. As shown in Figure 5.34, after 5 minutes of exposure, the surviving bacterial population was less than 60 CFU/plate. The difference in breakdown voltage did not make a significant difference in the inactivation effect. After the longest exposure, 7 minutes, the surviving bacterial population was less than 35 CFU/plate. Some plates had a population lower than 10 CFU/plate; however, full inactivation was not achieved.

The normalised populations of *E. coli* were calculated and are presented in Figure 5.35 as a function of the total delivered charge.

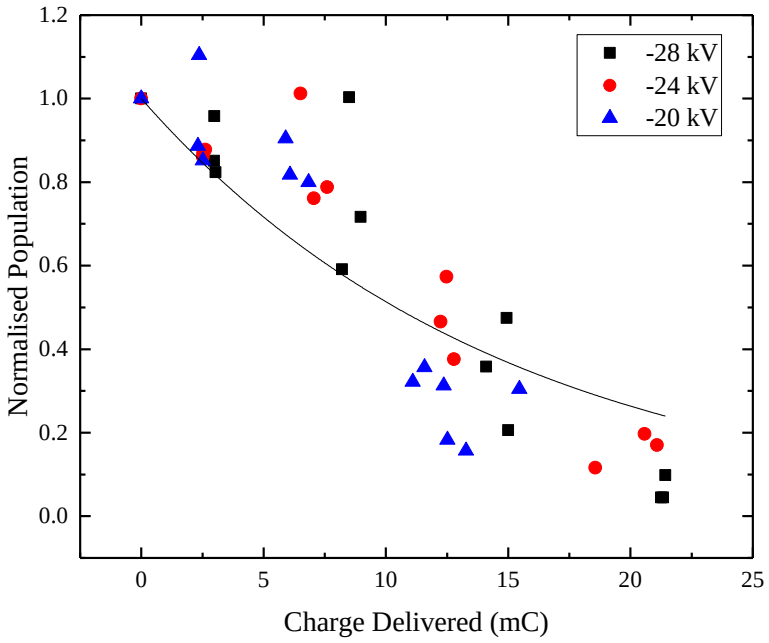

Figure 5.35. Normalised populations of *E. coli* as a function of the delivered charge using negative, direct, transient plasma discharge. The solid line is an analytical fitting by equation (5.2). Each data point in this graph represents an individual test.

The normalised population was reduced to 0.04–0.10 after the direct, transient plasma discharge treatment with a delivered charge of ~21 mC.

The first-order kinetic fitting was applied to the results. The fitting curve is shown as a solid line in Figure 5.33. The inactivation rate was found to be $0.67 \cdot 10^{-1}$ mC^{-1}.

The surviving populations of *S. aureus* as a function of the exposure time in the case of treatment with negative direct discharges are shown in Figure 5.36.

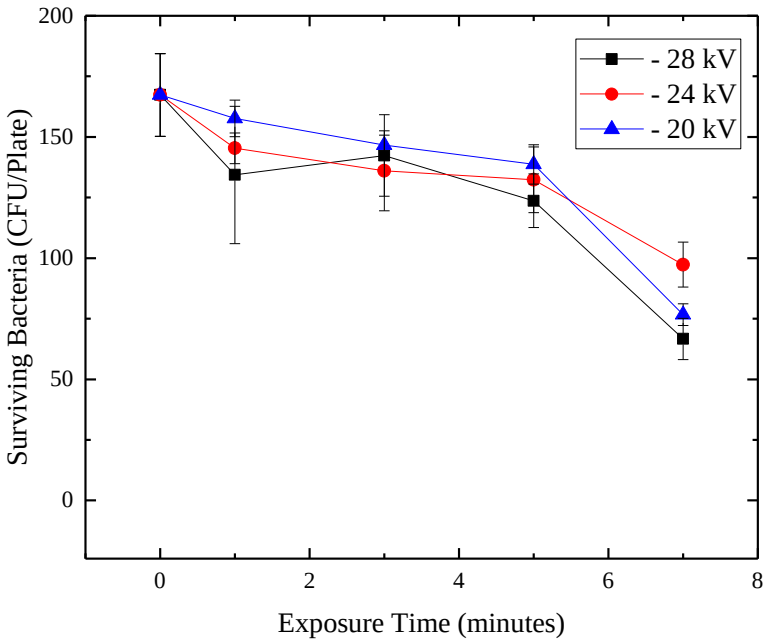

Figure 5.36. Surviving populations of *S. aureus* as a function of exposure time using negative, direct, transient plasma discharge treatment. All tests were conducted in triplicate, and each data point in this figure represents an average value. Error bars show the standard deviation. Solid lines are for visual guidance only.

The initial populations of *S. aureus* was in a range of 156–187 CFU/plate; a decrease in population was observed with an increase in treatment time. However, the inactivation effect on *S. aureus* was not as significant as in the case of *E. coli*. Even after 7 minutes of exposure to the direct, transient plasma discharges, the surviving bacterial population was still higher than 70 CFU/plate. Different breakdown voltages did not result in a difference in the inactivation effect.

The normalised population of *S. aureus* is presented in Figure 5.37 as a function of the delivered charge.

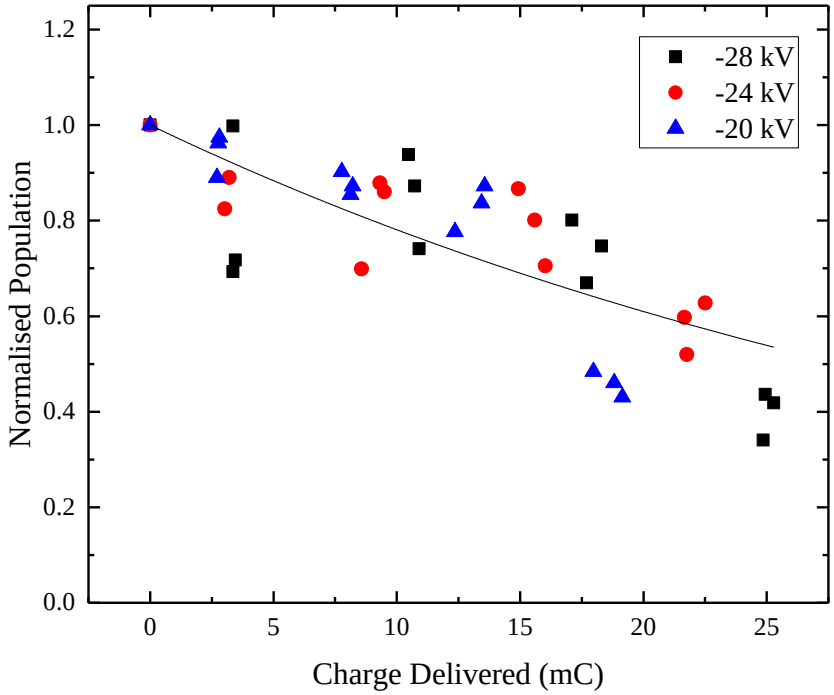

Figure 5.37. Normalised populations of *S. aureus* as a function of the delivered charge using negative, direct, transient plasma discharge. The solid line is an analytical fitting by equation (5.2). Each data point in this graph represents an individual test.

As shown in Figure 5.37, the normalised population of *S. aureus* was higher than in any other cases. After the exposure to the discharge with the highest delivered charge (~25 mC), the normalised population was still in the range of 0.34–0.43.

By applying the first-order kinetic fitting to the experimental of results, the rate of the inactivation process was found to be very low, $\lambda = 0.25 \cdot 10^{-1}$ mC^{-1}.

5.4.3 Summary of Bacterial inactivation by Impulsive Transient Plasma Discharge

The primary focus of this section of Chapter 5 was investigation of the inactivation capability of the transient, atmospheric plasma discharges. It was found that the impulsive transient plasma discharges produced a significant inactivation effect on the target bacterial samples on surface. Both the surface transient plasma discharge treatment and the direct transient plasma discharge treatment resulted in a noticeable decrease in bacterial population. The tendencies of the charge-dependent inactivation were observed.

In the case of the surface transient plasma discharges, the discharge developed across the sample/air interface. After exposure to the positive, surface, transient plasma discharges with a delivered charge of ~13.5 mC, complete inactivation of *E. coli* was observed (the normalised population was decreased to 0). The total charge of ~19.5 mC was required to achieve complete inactivation of *S. aureus*. When negative energisation was applied to the HV electrode, the complete inactivation of *E. coli* and 99% inactivation of *S. aureus* were achieved at the total delivered charge levels of 21 mC and 25 mC, respectively.

In the case of the direct transient plasma discharge treatment, more than 85% of the *S. aureus* population was inactivated after exposure to the positive, direct, transient plasma discharge treatment with the delivered charge of 21 mC. *E. coli* was also exposed to the positive, direct, transient plasma discharges: 96% inactivation was achieved at the maximum delivered charge of ~22 mC. When negative energisation was applied to the direct, transient plasma discharge system, the maximum delivered charge in *E. coli* tests was ~21 mC. The normalised population was in a range of 0.04–0.10, which means that 90% to 96% inactivation was achieved. In the case of *S. aureus*, the normalised population was decreased to 0.34–0.44; at a maximum delivered charge of ~25 mC, with only 56% to 66% of bacteria inactivated.

First-order kinetic fitting was used to fit the experimental datapoints. The inactivation rates were obtained using this fitting, and the results for all tests are listed in Table 5.2.

Table 5.2 Inactivation rate (mC^{-1}) for surface and direct transient plasma discharges.

Surface discharge			
Positive		Negative	
E. coli	*S. aureus*	*E. coli*	*S. aureus*
0.26 (0.23 – 0.30)	0.11 (0.10 –0.13)	0.19 (0.17–0.22)	$0.97 \cdot 10^{-1}$ ($0.88 \cdot 10^{-1}$ –0.11)
Direct discharge			
Positive		Negative	
E. coli	*S. aureus*	*E. coli*	*S. aureus*
0.13 (0.11 –0.14)	$0.57 \cdot 10^{-1}$ ($0.51 \cdot 10^{-1}$ – $0.63 \cdot 10^{-1}$)	$0.67 \cdot 10^{-1}$ ($0.57 \cdot 10^{-1}$ – $0.76 \cdot 10^{-1}$)	$0.25 \cdot 10^{-1}$ ($0.22 \cdot 10^{-1}$ – $0.28 \cdot 10^{-1}$)

Values in brackets indicate a 95% confidence interval.

The results obtained from these tests show that the inactivation capability of the direct transient plasma discharges is substantially lower than that of the surface transient plasma discharges. As listed in Table 5.2, the inactivation rates of the surface discharges are twice as high as the inactivation rates of the direct transient plasma discharges, for both types of bacteria and both polarities of energisation. As mentioned earlier, the direct transient plasma discharges propagate through the bulk of the agar sample, while the surface discharges propagate across the agar/air interface. Therefore, the surface discharges treat a larger surface area and demonstrate a substantially higher inactivation rate. However, the inactivation effect demonstrated by the direct transient plasma discharges is also noticeable.

This study also showed that *E. coli* has a higher sensitivity to the impulsive transient plasma discharges compared with *S. aureus*. The inactivation rates obtained for *E. coli* are twice as high as the inactivation rates for *S. aureus*. This higher sensitivity of *E. coli* to the transient plasma treatment is potentially caused by the difference in the cell structure of Gram-positive and Gram-negative bacteria. The thicker peptidoglycan layer of Gram-positive may help to protect these bacteria from the lethal damage caused by the transient plasma discharge treatment.

The difference in the breakdown voltage levels of the impulsive transient plasma discharges did not produce a noticeable difference in the inactivation results. However, it was found that the inactivation effect is a function of the total delivered charge.

Under the same experimental conditions (the same bacteria type, discharge polarity, and topology), the transient plasma discharge treatment with a higher delivered charge results in a higher degree of bacterial inactivation.

The inactivation capability of the impulsive transient plasma discharges was investigated. The experimental results will help in further study of the non-thermal plasma for decontamination applications, especially in the design and optimisation of the plasma treatment systems based on the transient discharges in atmospheric air.

5.5 Discussion and Conclusions

In this chapter, the decontamination capabilities of the steady-state corona discharges and the impulsive transient plasma discharges were investigated. An experimental study of the decontamination efficiency of the transient plasma discharges was completed, and the obtained results were presented and discussed. *E. coli* and *S. aureus* were used in the inactivation experiments as target microorganisms representing Gram-negative and Gram-positive bacteria, respectively.

It was shown that both steady-state corona discharges and impulsive transient plasma discharges produce a noticeable bio-decontamination effect, which is in line with the previously published results [32], [100]. The original experimental results also show that the degree of inactivation is charge-dependant: higher delivered charge always results in a higher degree of inactivation for the same type of discharges. Higher delivered charge is normally achieved from an increasing discharge current or exposure time. A similar result was obtained in [226]. In this research, Dobrynin *et. al* used DC corona discharges to inactivate *E. coli*, and they presented the surviving bacteria colonies number as a function of dose (charge per treated area, $\mu C/cm^2$). Their results showed that higher charge delivered to the sample could result in a more pronounced bio-decontamination effect: 1 log decrease in bacteria population was achieved by the plasma treatment with a dose of ~75 $\mu C/cm^2$ (total charge delivered during the treatment was ~2.5 mC), while plasma treatment with 300 $\mu C/cm^2$ (~10 mC total charge) resulted in more than 2-log reduction in bacterial population.

In the study of the steady-state corona discharges, the negative corona discharge was shown to provide a significant inactivation effect. In the case of the indirect corona discharge treatment, the inactivation rates were 0.575 mC^{-1} for *E. coli* and 0.264 mC^{-1} for *S. aureus*. In the case of the direct corona discharge treatment, the inactivation rates were even higher, 0.978 mC^{-1} for *E. coli* and 1.441 mC^{-1} for *S. aureus*. In the case of the negative direct corona discharge treatment, a minimum charge delivered to the bacterial sample resulted in a 0.99 reduction in the normalised population. In [226], a slightly higher charge (~7.3 mC) was required to achieve similar results by using negative corona discharges.

In addition, the corona discharge treatment used in this thesis demonstrated high bio-decontamination efficiency compared with other similar inactivation methods. 99% of *S. aureus* were inactivated by the negative direct corona discharge treatment with a duration of 1 minutes. In contrast, more than 20 hours are required to achieve 2-3 logs reduction in *S. aureus* population in the series of corona discharge treatment tests described in [236].

Ozone production during the discharge treatment has been investigated, and it was considered to be one of the most important factors that caused the difference in inactivation results for positive and negative corona discharges. The ozone concentration was much higher during the negative corona discharge treatment (13-30 ppm and 20–60 ppm in the case of indirect and direct discharges, respectively) than during the positive corona discharge treatment (1–2 ppm). Although a noticeable degree of inactivation was also achieved by the positive corona discharge treatment, faster and more intensive bio-decontamination effect was achieved by the negative corona discharge treatment with a higher ozone concentration. It confirms the dominating role of ozone in the bio-decontamination process by the corona discharge treatment. As reported in [237], air plasma treatment and ozone treatment with the same concentration resulted in a very similar reduction in bacterial population.

In the study of the impulsive transient plasma discharges, inactivation of *E. coli* and *S. aureus* was also achieved using different topologies and energisation modes. The results demonstrated that the different breakdown voltages do not produce different inactivation effects. Results showed that not only the charge delivered by the

discharge treatment, but also the energisation polarities and discharge topologies affect the inactivation results. The positive impulsive transient discharges resulted in slightly higher inactivation rates. More importantly, the surface transient plasma discharges produced a greater inactivation effect. This is because the surface discharges propagate through the sample/air interface; therefore, they act upon a larger sample area, which results in a higher inactivation rate.

Also, it was shown that Gram-negative bacteria are more sensitive to the transient plasma discharges than Gram-positive bacteria. The thicker peptidoglycan layer of Gram-positive bacteria may protects those microorganisms against the lethal damage caused by the transient plasma discharges. This has been confirmed by the results presented in [237]: 99% inactivation of *Pseudomonas aeruginosa* (Gram-negative) was achieved by 60 seconds of plasma treatment, while 80% inactivation of *S. aureus* (Gram-positive) was achieved by the same type of plasma treatment. A study [236] also reported that *E. coli* (Gram-negative) were more susceptible to the plasma germicidal effect than *S. aureus* (Gram-positive), as 3.5-log and (2.0-2.5)-log inactivation was achieved using the same plasma discharge treatment on *E. coli* and *S. aureus* respectively.

The ozone concentrations measured during the transient plasma treatment was 0 ppm. This indicates that other reactive oxygen species such as OH radicals and nitrogen reactive species contribute to the inactivation process. As reported in [68], [218] and [219], the concentration of H_2O_2 and NO_2^- in water solution increased after the plasma discharge treatment. The pH and conductivity of water solutions were also increased after the treatment. All these factors could lead to the bio-decontamination effect of the transient plasma discharge treatment.

Two types of discharges were investigated in this chapter, and the obtained decontamination results were presented and analysed. Several important factors which affect inactivation efficiency of the plasma discharges, such as energisation polarities, discharge topologies, and delivered charge were discussed. These results will help in further study of non-thermal plasma decontamination and the optimisation of this process.

CHAPTER 6

OH Radicals Produced by Atmospheric Non-Thermal Plasma Discharges

6.1 General Introduction

The oxidation capabilities of the non-thermal plasma discharges were evaluated in Chapter 4, and the decontamination capabilities of non-thermal plasma discharges were examined in Chapter 5. As mentioned previously, strong electric fields, UV emissions, and production of chemically reactive species by non-thermal plasma discharges are responsible for the oxidation and decontamination effects. Although the exact mechanisms of bio-decontamination of the transient plasma discharges still are not well understood, it is believed that the reactive chemical species are considered to be the main contributors to bacterial inactivation and chemical oxidation by air-based non-thermal plasma discharges [92], [142]. Optimisation of production of the reactive species by the non-thermal plasma discharges was identified as the main challenge related to the successful development of practical applications of the transient plasma discharges in environmental and medical fields [238].

It was demonstrated that the reactive oxygen species are the main contributors to the oxidation and decontamination capabilities of non-thermal plasma discharges [73], [107], [197]. This was established in Chapter 4 and Chapter 5: the negative corona discharges resulted in better decolorisation and decontamination effects with higher production of ozone. The appearance of ozone indicates the presence of the reactive oxygen species generated by plasma discharges. However, the role of each individual chemical species in the decontamination process was not determined.

It has been reported that hydroxyl radicals are detected in non-thermal atmospheric plasma discharges [239], [240]. OH radicals are highly reactive species, and these species can make a significant contribution to the oxidation and decontamination processes. In [241], OH radicals generated in humid air by dielectric barrier discharges are primarily responsible for the inactivation of *Geobacillus stearothermophilus* spores. Paper [144] suggested that OH radicals

produced by discharges in humid air quickly take part in chemical reactions and generate a significant amount of peroxides to inactivate *Bacillus atrophaeus* spores. In research publications such as [87] and [242], it was also reported that the OH radicals are the main reactive oxygen species that contribute to oxidation reaction and then inactivation of bacteria during atmospheric plasma discharges.

The OH radicals can be generated in multiple ways during non-thermal atmospheric plasma discharges, including direct electronic excitation of water molecules and dissociative recombination of excited water molecules [161], [162]:

$$H_2O + e^- \rightarrow OH + H + e^- \quad (6.1)$$

$$H_2O^+ + e^- \rightarrow OH + H \quad (6.2)$$

$$H_2O^+ + \ H_2O \rightarrow H^+(H_2O) + OH \quad (6.3)$$

Other mechanisms of hydroxyl radical formation in plasma treated liquid solutions are possible. For example, as discussed in [68], the formation of OH radicals involves the formation and subsequent dissociation of peroxynitrous acid.

As discussed in [243] and [244], ozone molecules can be decomposed in water through a chain reaction catalysed by hydroxyl radicals. Ozone reacts with OH radicals, resulting in the production of $\cdot O_2^-$. Then, an electron will be transferred to an ozone molecule to form $\cdot O_3^-$. $\cdot O_3^-$, in turn, reacts with water molecules to form OH radicals. Although the complex process of OH radical formation is still largely unexplored, further investigation on the reactions is not in the scope of this research.

Considering the non-thermal plasma discharges system used in this research (as described in Chapter 3), OH radicals can be produced in the air above the sample surface and then diffuse into the liquid (if their half-life is sufficient), or they can be produced directly in the liquid sample when discharges propagate to the liquid surface. It has been discussed in Chapter 2.3 that most of the OH radicals are generated at the air/liquid interface in the case of transient spark discharges.

Hydroxyl radicals have a short half-life (estimated half-life in nanoseconds [245]), and they also are highly reactive and typically have a low concentration in the liquid. Due to these characteristics, hydroxyl radicals may not be detected easily in optical emission plasma spectra. As reported in [246], OH radicals were not detected at 308.9 nm in the case of non-thermal plasma discharges until a much more intensive transient spark discharge in the atmospheric air was used. Multiple approaches have been used to detect OH radicals produced by plasma discharges, including laser-induced fluorescence techniques [239], light emission spectroscopy [247], electron paramagnetic resonance spectroscopy [248], and use of chemical probes [249]. A terephthalic (TA) acid-based method was proposed and used to detect OH radicals in [250] and [251]. TA as a highly selective OH scavenger would react only with OH radicals to form 2-hydroxyterephthalic acid (HTA). HTA provides fluorescence emission when excited with light at 310 nm. Measurement of concentration of OH radicals was based on the detection of the fluorescence signal emitted by HTA molecules after plasma treatment.

In this chapter, measurements of the concentration of OH radicals produced in the liquid by atmospheric non-thermal plasma discharges were conducted. To coordinate these measurement with the results of oxidation and decontamination studies reported in previous chapters, the steady-state corona discharges and the impulsive transient discharges were tested. The factors that may affect the OH radical production, such as discharge polarity, voltage, total charge delivered, air humidity, and discharge path are discussed. Through this research work, information for optimisation of OH production by plasma discharges was provided.

6.2 Methodology of OH Radical Detection

6.2.1 Terephthalic (TA) Acid and 2-Hydroxyterephthalic Acid (HTA) for OH Radical Detection

To investigate the production of hydroxyl radicals by non-thermal plasma discharges in atmospheric air, TA was selected as an OH scavenger in this series of experiments.

TA is a white solid in powder form, widely used in the industry process of making polyester. It is a low toxicity chemical which is hard to dissolve in water or alcohols. The formula of TA is $C_6H_4(CO_2H)_2$; the molecular weight is 166.13 g/mol, and its structure is shown in Figure 6.1.

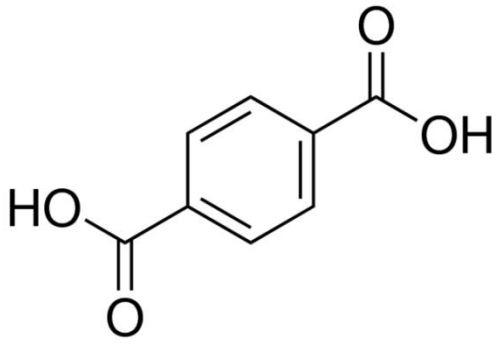

Figure 6.1. Molecular structure of terephthalic acid.

Several chemically active species can be produced by non-thermal atmospheric plasma discharges, including the reactive oxygen species (ROS) and reactive nitrogen species (RNS). Typical oxidation indicators would react with most of the ROS, not only with hydroxyl radicals. TA was selected because it specifically reacts with hydroxyl radicals only; it does not even react with ozone, which also is highly oxidative. This reaction transforms TA into 2-hydroxyterephtalic acid (HTA) through the addition of OH to its aromatic ring.

HTA (2-hydroxyterephthalic acid), $C_8H_6O_5$, is a chemical in powder or crystal form that typically has a white or yellow color. It has a molecular weight of 188.13 g/mol. One of the most important features of HTA is that it can give fluorescence under its excitation conditions. The fluorescence emission intensity is in proportion to the concentration of HTA under the excitation condition. The molecular structure of HTA is shown in Figure 6.2.

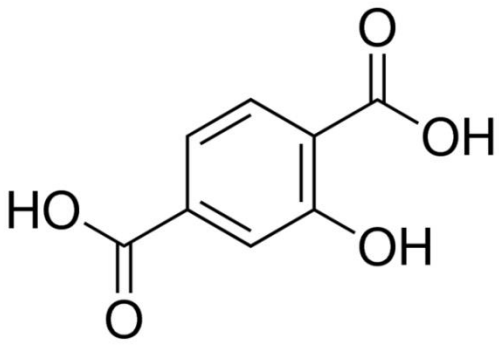

Figure 6.2. Molecular structure of 2-hydroxyterephthalic acid.

The excitation wavelength for HTA is ~315 nm, and the peak of its fluorescence emission is ~425 nm. The hydroxyl radicals generated by non-thermal plasma discharges will react with TA, and HTA will be the only product of this reaction. Therefore, the intensity of the fluorescence signal indicates the concentration of HTA, and using the yielding rate which can be obtained by calculation, the concentration of OH can be calculated. It has been reported that the OH yield from the oxidation of HTA by oxygen is 35% [249]–[251], and this rate can be used to calculate OH concentration in the conditions of this experimental work.

The general methodology of using TA and HTA to measure hydroxyl radical production by non-thermal plasma discharges is explained in Figure 6.3.

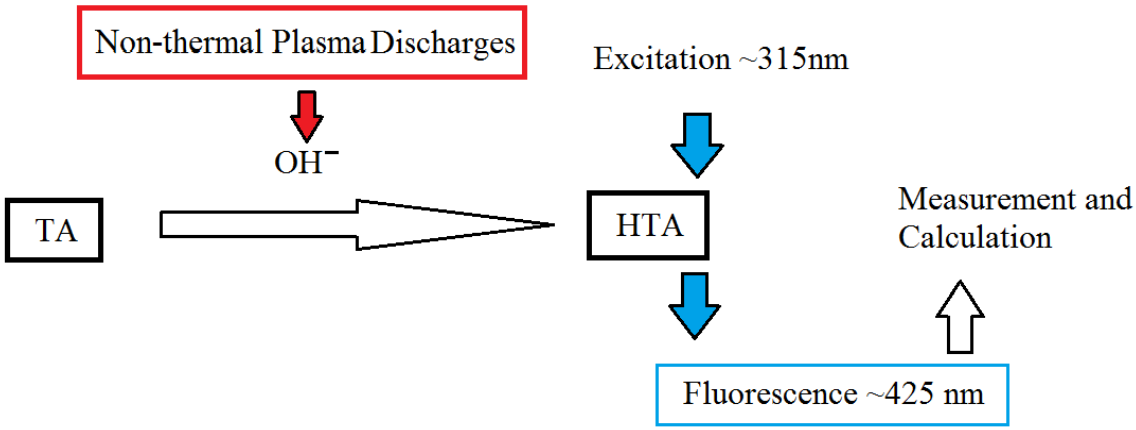

Figure 6.3. General schematic of OH radical measurements using TA and HTA.

The TA solution was prepared and then exposed to the non-thermal plasma discharges. After the treatment, the sample was placed into a spectrofluorophotometer in which 315 nm light was used as excitation light, and the fluorescence signal at 425 nm was measured.

6.2.2 Preparation of TA and HTA Samples

Terephthalic acid (TA) sample

The terephthalic acid powder, purchased from Acros Organics, has a high purity of 99+%. Because the TA poorly dissolves in water directly, NaOH water solution was prepared as the solvent for the liquid sample. First, 10.2 g of sodium hydroxide pellets (Sigma-Aldrich Ltd., purity>98%) was dissolved in 250 ml distilled water to make a NaOH solution with a concentration of 1 mole/L. Then, 5 ml of this solution was extracted and mixed with 95 ml of distilled water to make a 100 ml solution with NaOH concentration of 5 mM. Then, 34 mg of terephthalic powder was weighed on the digital analytical balance (Ohaus® Adventurer® balance AR 1530) and put into the NaOH solution to obtain the desired sample solution (2 mM TA and 5 mM NaOH). Figure 6.4 a, b, and c show the terephthalic acid, NaOH pellets, and sample solution, respectively.

Figure 6.4. (a)Terephthalic acid； (b) NaOH pellet； (c) 2 Mm TA, 5 mM NaOH sample solution.

The sample solution was held in a 250 ml bottle and kept in a cool, dark place. The pH of the sample solution was ~10.9, measured by the pH meter (Hanna Instruments PH 210). Then, 6 ml of TA solution was placed onto non-conductive (see Figure 6.5a) or conductive (see Figure 6.5b) platees and exposed to non-thermal plasma discharges for different time intervals. After exposure, samples were transferred into plastic cuvettes (see Figure 6.5c) and measured again for pH. More importantly, samples were placed into the spectrofluorophotometer, and the fluorescence signal was measured. Clean, plastic transfer pipettes (Thermo Scientific™ Sterilin™) were used to transfer the sample solution.

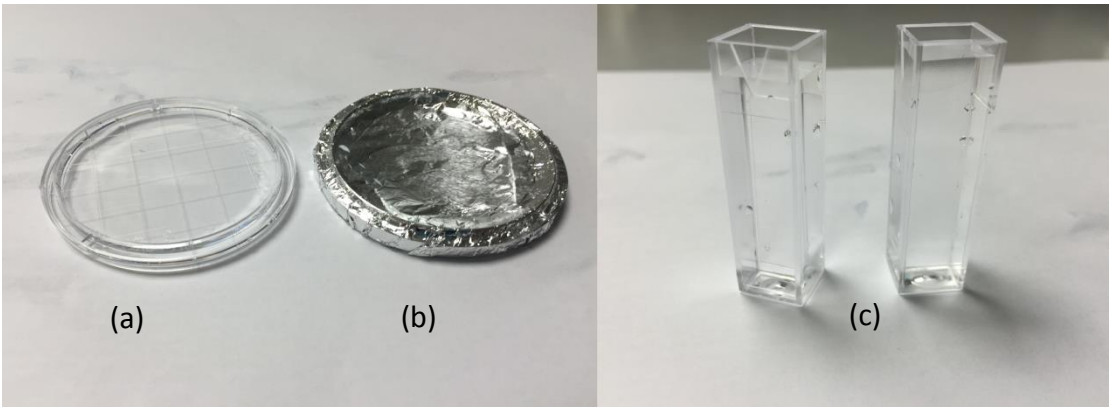

Figure 6.5. Terephthalic solution sample in (a) non-conductive plates, (b) conductive plates, and (c) in plastic cuvettes.

2-Hydroxyterephthalic acid (HTA) sample

In this research, HTA solution samples with different concentrations were used. HTA powder with purity ~97% was purchased from Sigma-Aldrich Ltd. (see Figure 6.6a). A total of 38 mg of this powder was weighed using the digital analytic balance (Ohaus® Adventurer® balance AR 1530) and dissolved into the prepared 5 mM NaOH solution to obtain an HTA solution with a concentration of 2 mM. This solution has a light yellow color. It was stored in a 250 ml bottle (see Figure 6.6b) and kept in a cool, dark place. After this step, 5 mM of the NaOH solution was used again to dilute the sample solution down to have samples with lower HTA concentration. In this way, all HTA samples were kept in the same NaOH concentration (5 mM) but with 11 different HTA concentrations: from 0.1 mM to 1.1 mM, increased by 0.1 mM. HTA

samples were transferred into plastic cuvettes (see Figure 6.6c) and placed into the spectrofluorophotometer (Shimadzu RF-5301PC) to have their fluorescence signals measured.

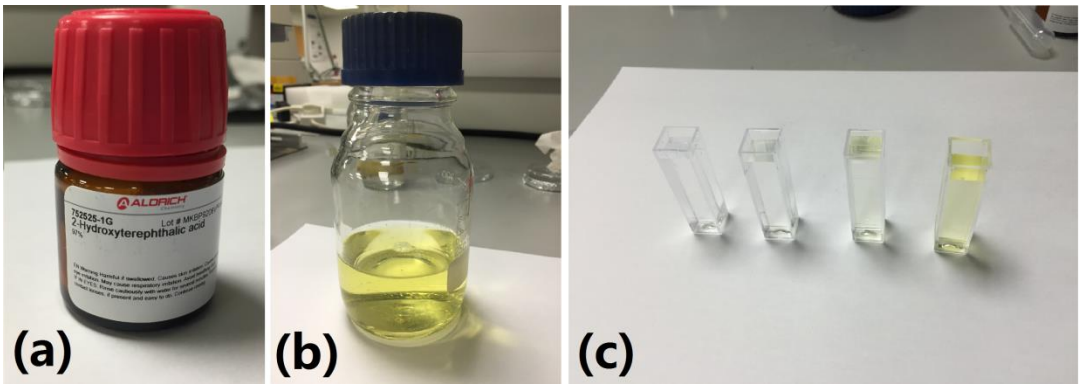

Figure 6.6. (a) 2-Hydroxyterephthalic Acid; (b) 2 mM HTA, 5Mm NaOH solution in 250 ml bottle; (c) HTA with different concentrations in plastic cuvettes.

6.2.3 Optical Measurement

TA solution samples which were exposed to non-thermal plasma discharges (or HTA sample solution) were transferred into plastic cuvettes and placed into a Shimadzu RF-5301PC spectrofluorophotometer. Fluorescence emission was measured using this spectrofluorophotometer, and spectrums were recorded.

Figure 6.7. Shimadzu RF-5301PC spectrofluorophotometer [252].

The spectrofluorophotometer (Shimadzu RF-5301PC) uses a 150 W xenon lamp, with ozone resolving type lamp housing, as the light source. The excitation wavelength

peak was set to 310 nm; the default slit width is 1.5/3.0 nm. The measurement scanning range was from 250 to 800 nm (the effective measurement range is from 220 nm to 900 nm). In this series of experiments, the expected fluorescence emission wavelength peak is at 425 nm. The measured intensity of the fluorescence signal was recorded in arbitrary unit (a.u.), and the measurement lower and upper limits are 0 a.u. and 1000 a.u.

First, the fluorescence emission signal from unexposed TA solution was measured. Its fluorescence spectrum was recorded and is shown in Figure 6.8.

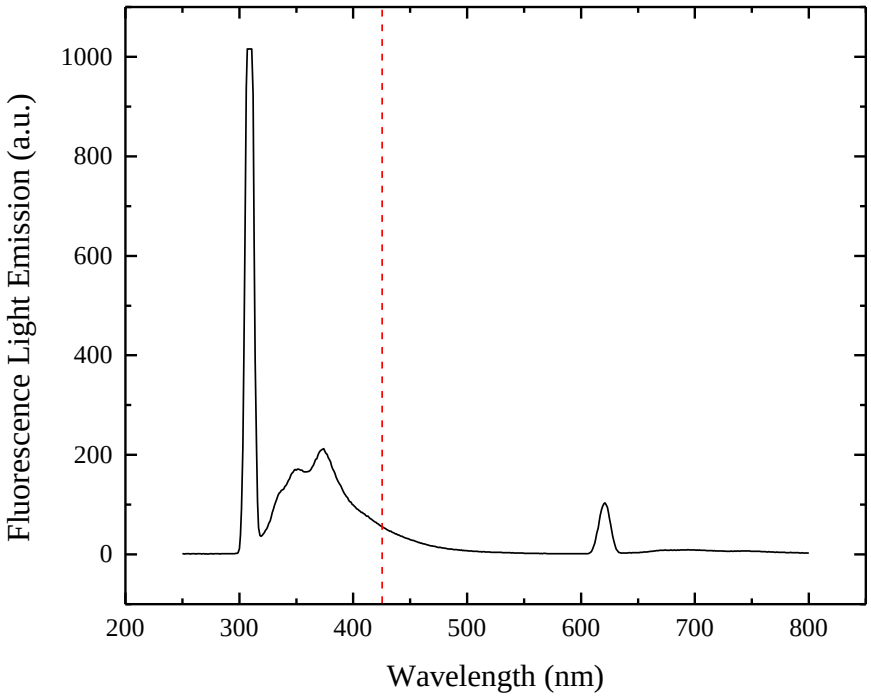

Figure 6.8. Fluorescence emission spectrum of unexposed TA sample solution. Red line indicates wavelength at 425 nm.

It can be seen clearly in this figure that no strong fluorescence signal was observed in the unexposed TA sample solution. This result is as expected, because HTA concentration in the unexposed TA sample solution is 0 mM. At 425 nm, a very low reading was recorded: 40-50 a.u. This number was then used as the baseline for fluorescence signal measurement of the exposed TA solution sample.

In the case of measuring the fluorescence signal from the TA solution which was exposed to non-thermal plasma discharges, the same procedure was used. The

fluorescence spectrum was recorded in a wavelength range from 350 nm to 600 nm. This is because the lamp (excitation at 310 nm) would bring some noise to the low wavelength range of the spectrum (< 350 nm), and less information is contained in the high wavelength range (> 600 nm). In the recorded spectrum, the major fluorescence peak at 425 nm was used for detection of the fluorescence signal level. An example of the spectrum is given in Figure 6.9, which shows the spectrum of TA solutions that have been exposed to 20 kV impulsive transient plasma discharges for 1, 3, 5, and 7 minutes.

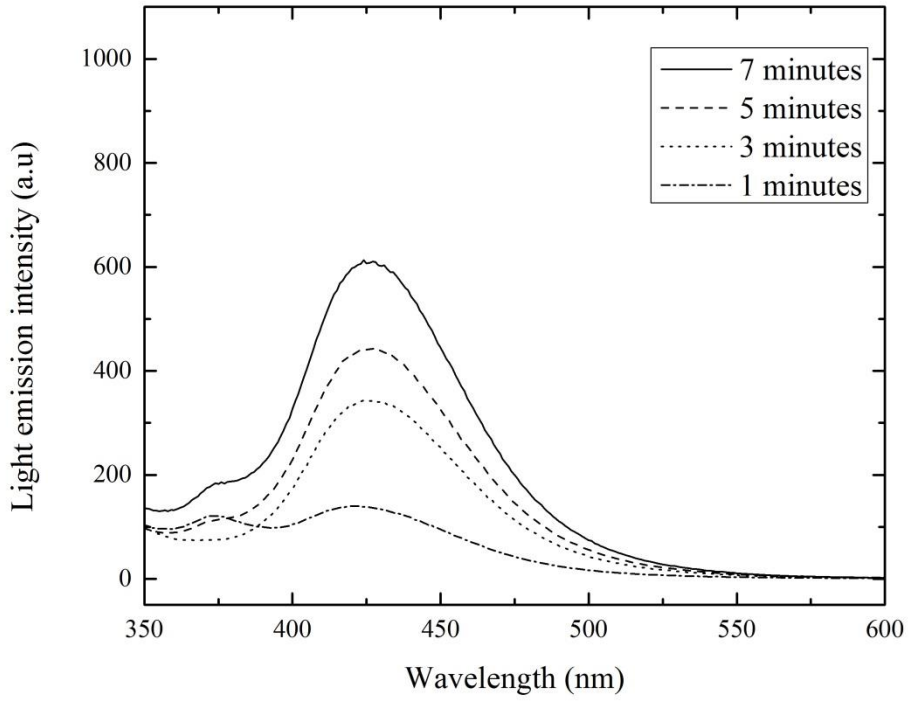

Figure 6.9. Fluorescence emission spectrum from the sample in dielectric plate holds sample after 20 kV positive discharge treatment for 1, 3, 5, and 7 minutes.

Several peaks can be observed in the spectrum in Figure 6.9. There is an increment in the peak of magnitude at 425 nm as the exposure time increases. The fluorescence peak intensity of each spectrum was recorded and compared, providing an indirect comparison of OH radical production for each energisation level. Analysis of the fluorescence related experiment will be presented as results in the next section.

6.2.4 Calculation of OH Concentration

As discussed in the previous section, the intensity of the fluorescence signal indirectly shows a tendency of OH radical production by non-thermal plasma discharges. High fluorescence signal intensity related to the high concentration of HTA in the sample solution as a result of high OH radical production. However, the amount of OH radical produced can also be calculated. It is necessary to quantify the amount of OH radicals produced by non-thermal plasma discharges. Based on the fluorescence emission intensity, a calculation method was developed.

First, a calibration curve was plotted. HTA sample solution with a concentration of 2 mM was diluted into 11 different HTA concentrations from 0.1 to 1.1 mM (concentration of NaOH was kept at 5 mM). Then, HTA samples were transferred into plastic cuvettes and their fluorescence signals were measured by spectrofluorophotometer using the same procedure as in the case of the exposed TA solution sample. Each spectrum was integrated from 425 nm to 600 nm, and this integral value was multiplied by a factor of two to recover an integration over the full range of axisymmetric fluorescence spectrum with a centre at 425 nm). This procedure allowed minimisation of noise in the low wavelength range from 250 to 400 nm. Each integral value was related to the corresponding HTA concentration. Thus, the calibration curve was plotted as shown in Figure 6.10.

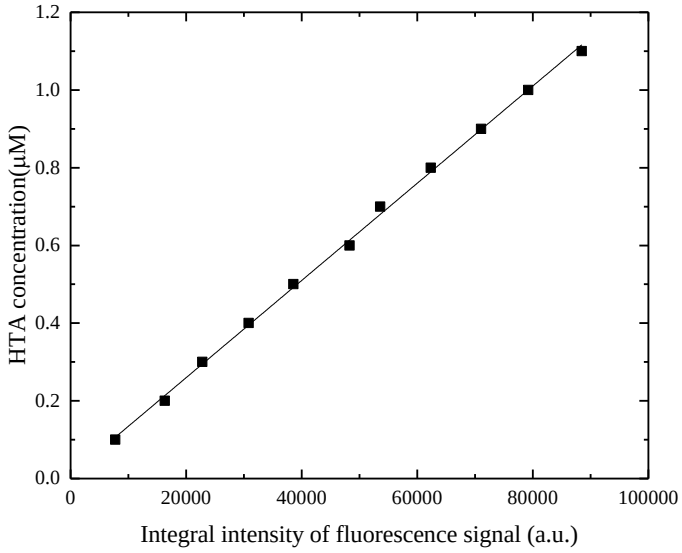

Figure 6.10. HTA concentration as a function of the integral intensity of fluorescence signal. Each point in this graph represents an individual test. The straight line as the calibration curve, shows the fitting by equation (6.4).

For the integral intensity of fluorescence signal from 0 to 10^5 a.u, the calibration curve can be fitted with a linear function as:

$$H = 0.0095 + 1.251 \cdot 10^{-5} \cdot Y \quad (6.4)$$

where H is the concentration of HTA
(μM)Y is the integral intensity of the fluorescence signal (a.u.)

If the integral intensity of the fluorescence signal is known, the concentration of HTA in the sample solution can be calculated. The valid range of concentration for this calculation of HTA is from 1 mM to 1 mM; this range corresponds to the integral intensity of the fluorescence signal range from 0 a.u. to 1000 a.u.
Once the concentration of HTA in the sample solution is obtained, this concentration can be used for the calculation of OH radical concentration. As mentioned in the previous section, TA reacts with OH radicals to produce HTA. In this reaction, formation of a single HTA molecule requires a single OH radical to be added to a TA molecule. Therefore, the ratio of 1:1 is held for every HTA molecule formed by a single OH radical. However, not all OH radicals are captured by TA molecules in the solution. Under the ambient conditions, oxygen is acting as a catalyst in this reaction, and the OH radical yielding rate is 35% as established in [249]–[251]. Therefore, the yielding rate of 35% should be considered when calculating the concentration of OH radicals.

To establish the efficiency of OH radical production by non-thermal plasma discharges, the total charge delivered was also obtained and presented along with the OH radical concentration. The charge delivered is calculated by taking the integral of the discharge current over exposure time. This procedure is similar to the procedure of calculating the total charge delivered in the indigo carmine decolorisation tests in Chapter 5.

6.3 OH Radical Produced by Steady-State Corona Discharges

In the previous chapters, the oxidation and decontamination capabilities of steady-state corona discharges have been obtained in a series of experiments. Ozone level was monitored during the plasma discharges. However, it is also important to investigate the production of hydroxyl radicals by corona discharges, as they may play a critical role in the bio-inactivation and oxidation effects.

It was reported that hydroxyl radicals can be produced by corona discharges over a liquid surface [8]. As hydroxyl radicals are one of the most important and highly oxidative chemical reactive species generated by the corona discharges, their production was investigated through a series of experiments.

To link the results of the oxidation and decontamination investigations presented in Chapter 4 and Chapter 5, the same steady-state corona discharge system was used for the testing discussed in this chapter. Both positive and negative discharges were tested, and the voltage level was kept at 30 kV. TA was used as the target sample and was treated in the test cell. Direct and indirect steady-state corona discharges (as described in Chapter 3) were used to treat the samples. Both bottled air and atmospheric air were used to provide the gas environment, and the pressure inside the test cell was kept at 0.2 bar gauge. The treatment time was selected as 1, 3, 5, and 7 minutes. The fluorescence emission was measured, and the results are presented in this chapter. The concentration of hydroxyl radicals was also calculated and presented as a function of the total charge delivered. The acidity of TA solutions was monitored by measuring the pH of plasma-treated samples.

6.3.1 Hydroxyl Radical Production by Indirect Steady-State Corona Discharges

The concentration of OH radicals in samples after exposure to the indirect corona discharges was obtained first. TA samples were placed in the test cell. The grounded

metallic mesh was located 25 mm above the sample to screen ions and charged particles.

a) Positive Energisation

The DC high-voltage power supply was switched to positive mode; positive corona discharges were generated to treat the TA sample. After the corona treatment, the fluorescence spectrum of the treated sample was measured using the spectrofluorophotometer. At the wavelength of 425 nm, the fluorescence light emission peak was observed. The intensity of this peak as a function of the exposure time is presented in Figure 6.11.

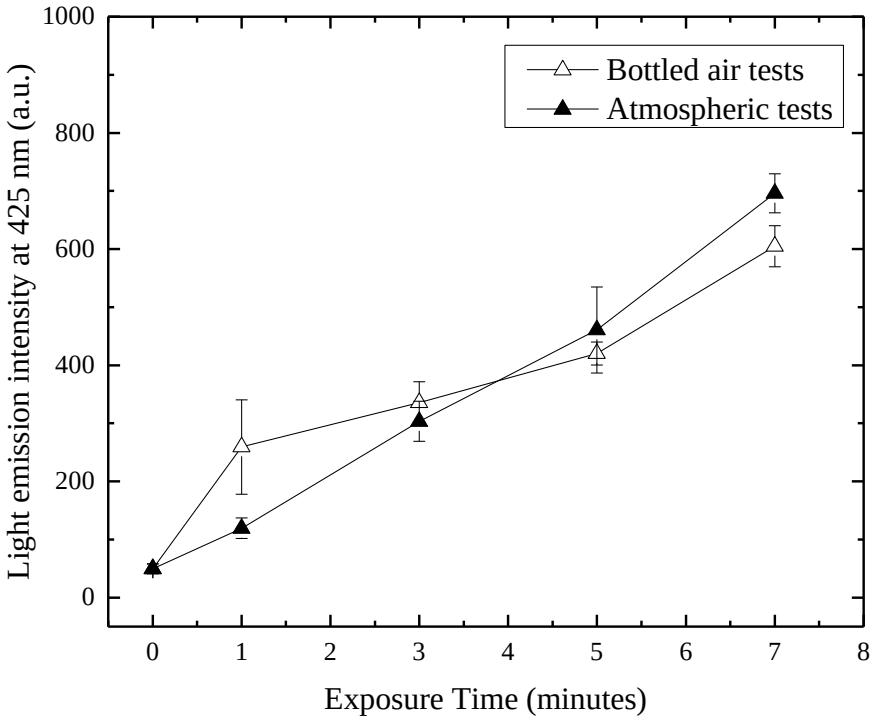

Figure 6.11. Fluorescence light intensity of samples treated with positive indirect steady-state corona discharges as a function of treatment time. Each point in this figure represents an average of three independent tests. The error bars show standard deviation values. Solid lines are for visual guidance only.

It can be seen from Figure 6.11 that the fluorescence light emission intensity of treated samples increases with an increase in the treatment time. Although there are slight differences, the light emission intensities from samples treated in the bottled air and in atmospheric air are similar. After 10 minutes of exposure to the positive indirect corona discharges, the light emission intensity at 425 nm was 570–650 a.u. for bottled air tests and 660–730 a.u. for atmospheric tests.

The light emission spectrum was used to convert the light emission intensity into OH radical concentration using the calibration equation (6.4). The concentration of OH radicals after exposure to positive indirect corona discharges is shown in Figure 6.12 as a function of total charge delivered.

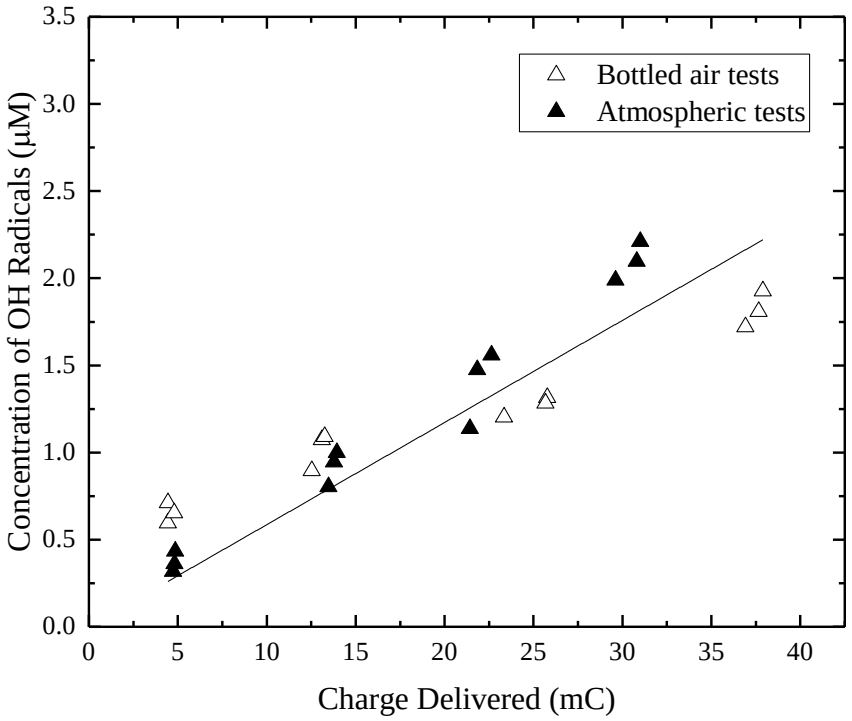

Figure 6.12. The concentration of OH radicals as a function of charge delivered after exposure to positive, indirect, steady-state corona discharges. Each point in this graph represents an individual test. The straight line shows the fitting by equation (6.5).

As shown in Figure 6.12, OH radicals were detected in the TA solution after exposure to positive indirect corona discharges. With longer exposure times, more charge was delivered, which resulted in a higher concentration of OH radicals. However, the concentration of OH radicals was low, less than 2.25 μM, as detected after the plasma

treatment in both dry and atmospheric air. A linear fit was applied using Origin Pro software; the fitting equation is the following:

$$C_{OH} = \gamma \cdot D \quad (6.5)$$

where C_{OH} is the concentration of OH radicals (μM)

D is the charge delivered by the discharge treatment (mC)

And γ is the production rate of OH radicals (μM/mC)

.

In the case of positive indirect corona discharge treatment, the production rate of OH radicals was found to be $0.59 \cdot 10^{-1}$ μM/mC.

b) Negative Energisation

In the case of the negative indirect corona discharges, the DC high-voltage power supply was switched to negative polarity. TA solutions were treated with negative corona discharges, and the fluorescence signals were measured using the spectrofluorophotometer. In these tests, highly intense fluorescence light emission was observed, and the intensity of these fluorescence signals exceeded the range of the spectrofluorophotometer. Therefore, a 20-fold dilution was made to ensure that the light emission intensity was within a measurable range. Then the fluorescence signals from the diluted samples were measured. The fluorescence light emission peak intensity at 425 nm as a function of exposed time is shown in Figure 6.13.

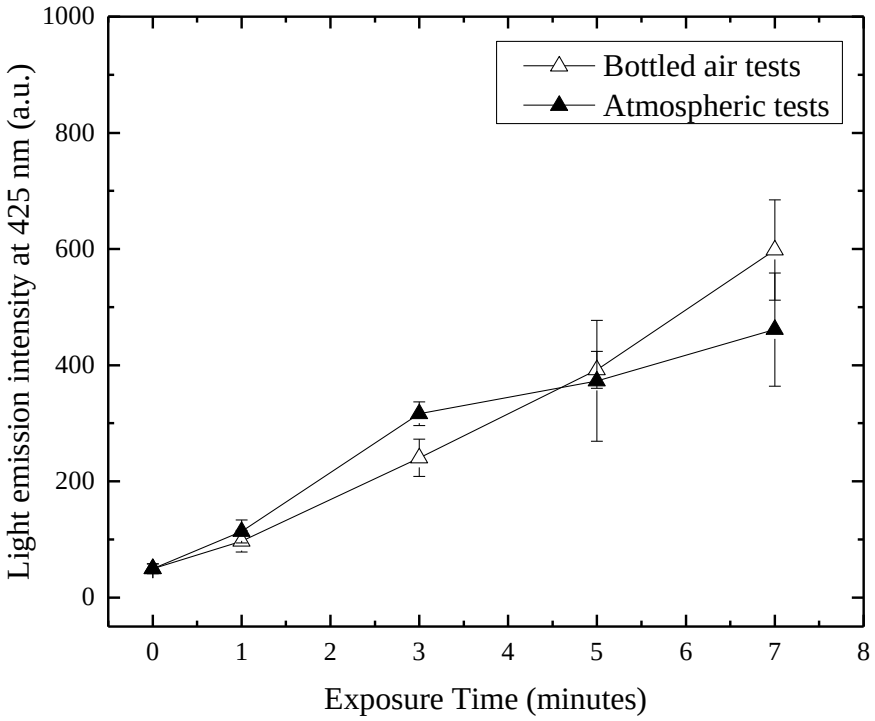

Figure 6.13. Fluorescence light intensity of 20-fold dilution of the samples treated with negative, indirect, steady-state corona discharges as a function of treatment time. Each point in this figure represents an average of three independent tests. Error bars show the standard deviation values. Solid lines are for visual guidance only.

As shown in Figure 6.13, the peak intensity of fluorescence light emission increases with the exposure time. No significant difference was seen between the intensity of fluorescence signals obtained in bottled air tests and in atmospheric air tests. By applying the calibration equation (6.4) and considering the dilution ratio, the concentration of OH radicals in the treated solution samples was calculated and presented in Figure 6.14 as a function of total charge delivered.

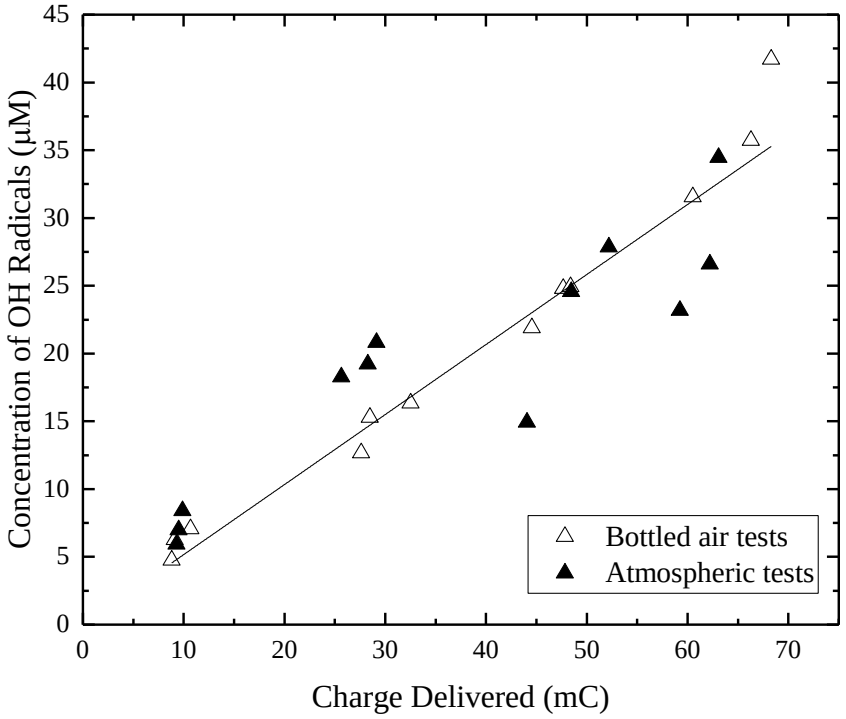

Figure 6.14. The concentration of OH radicals as a function of delivered charge after the exposure to negative indirect steady-state corona discharges. Each point in this graph represents an individual test. The straight line shows the fitting by equation (6.5).

It can be seen from Figure 6.14 that significantly higher concentrations of OH radicals were detected compared with the positive corona treatment tests. Although more charge was delivered during the negative discharge treatment, the OH radical production rate for the negative indirect corona discharges was still much higher than for the positive case. Linear fitting by equation (6.5) was applied to the results using Origin Pro software; the OH production rate was found to be $5.17 \cdot 10^{-1}$ μM/mC.

6.3.2 Measurement of Hydroxyl Radicals Produced by Direct Steady-State Corona Discharges

The concentration of OH radicals was also obtained in the case of the direct steady-state corona discharges. As in the case of the indirect corona discharges discussed in the previous section, samples of TA solution were treated with corona discharges and the intensity of the fluorescence light emission was measured. Using these measured intensities, the concentrations of the OH radicals were calculated.

a) Positive Energisation

TA solution samples were exposed to the positive direct corona discharges. After corona treatment, the fluorescence light emission was obtained. The peak intensity of this light emission is shown in Figure 6.5 as a function of exposure time.

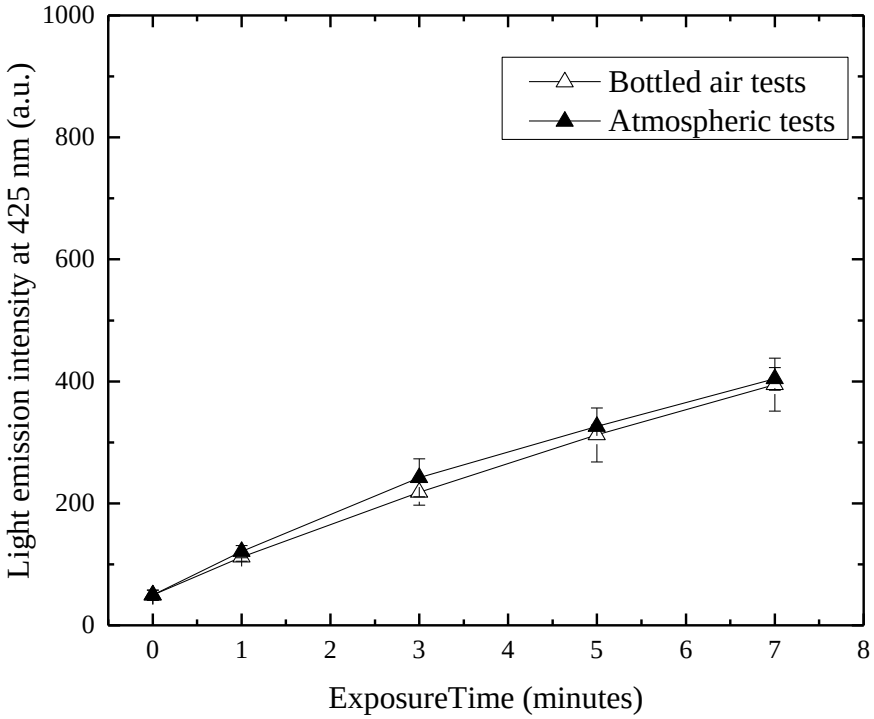

Figure 6.15. Fluorescence light intensity of samples treated with positive direct steady-state corona discharges as a function of the treatment time. Each point in this Figure represent an average of 3 independent tests, error bars show the standard deviation values. Solid lines are for visual guidance only.

As shown in Figure 6.15, the fluorescence light emission increases with an increase in the exposure time. The peak intensities of samples treated in bottled air and atmospheric air are very close; no significant difference was observed. However, the peak intensity of fluorescence light emission was low: less than 450 a.u., even after 7 minutes of exposure.

The OH radical concentration in the treated solution was calculated by equation (6.4). The concentration of OH radicals as a function of the total charge delivered is shown in Figure 6.16.

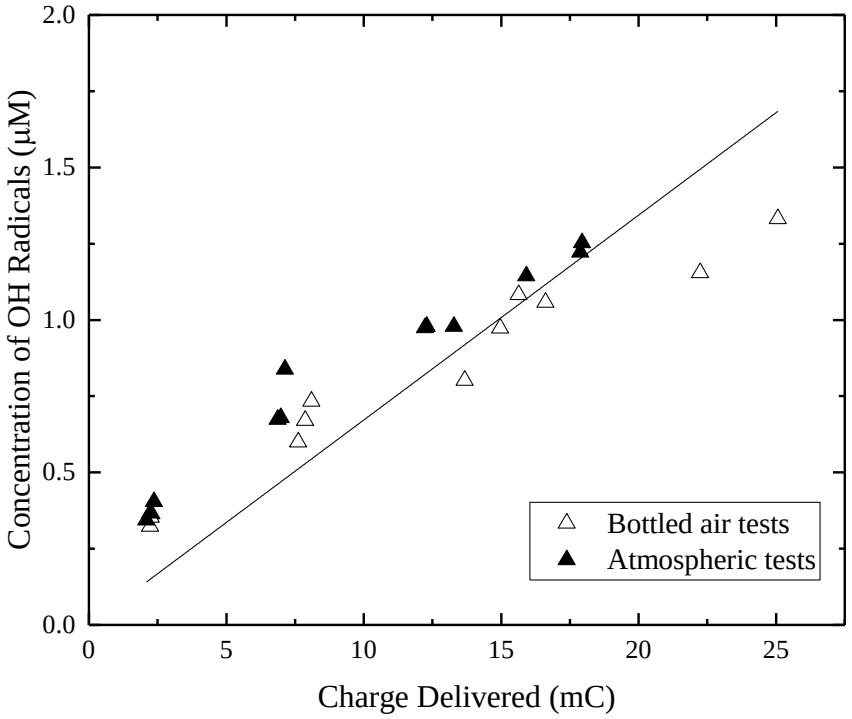

Figure 6.16. The concentration of OH radicals as a function of charge delivered after exposure to positive, direct, steady-state corona discharges. Each point in this graph represents an individual test. The straight line shows the fitting by equation (6.5).

As shown in Figure 6.16, the concentration of the OH radicals increases with an increase in the total charge delivered. The charge delivered, in this case, was lower than the indirect corona discharge treatment, and the concentration of OH radicals

was lower as well. After 7 minutes of exposure, less than 25 mC was delivered, and the concentration of OH radicals was lower than 1.4 μM. By applying the linear fitting equation, the rate of OH radical production γ was found to be $0.67 \cdot 10^{-1}$ μM/mC.

b) Negative Energisation

Negative direct corona discharges were used to treat the TA solutions, and the fluorescence light emission intensity was obtained. Similar to the negative indirect corona discharge case, the light emission intensity from the treated samples exceeded the measurement range of the spectrofluorophotometer. Therefore, a ten-fold dilution was made, and the fluorescence light emission intensity was measured. The peak of the fluorescence signal obtained in the diluted samples is presented in Figure 6.17 as a function of exposure time.

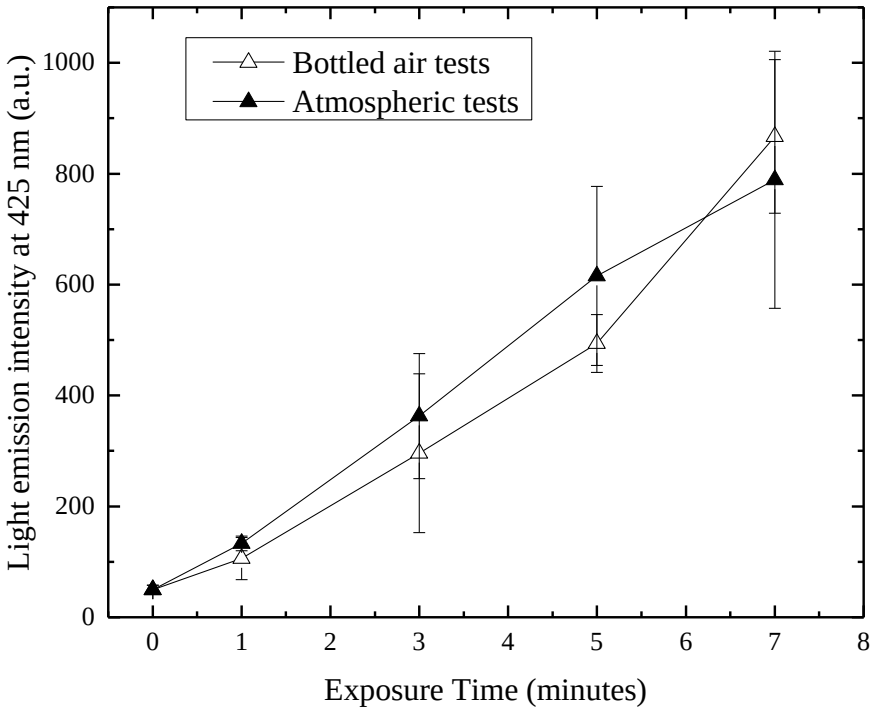

Figure 6.17. Fluorescence light intensity of the ten-fold dilution of the samples treated with negative, direct, steady-state corona discharges as a function of treatment time. Each point in this figure represents an average of three independent tests. Error bars show the standard deviation values. Solid lines are for visual guidance only.

The peak intensity of the fluorescence signal was higher than in the case of positive energisation. This intensity of the fluorescence signal in the diluted sample increased up to 1000 a.u. after exposure to the negative direct corona discharges. Again, similar intensity of the fluorescence signal was observed from samples exposed to the corona discharges in bottled air and in atmospheric air.

Next, the OH radical concentration in the original exposed samples was calculated. The OH concentration is presented in Figure 6.18 as a function of the total charge delivered.

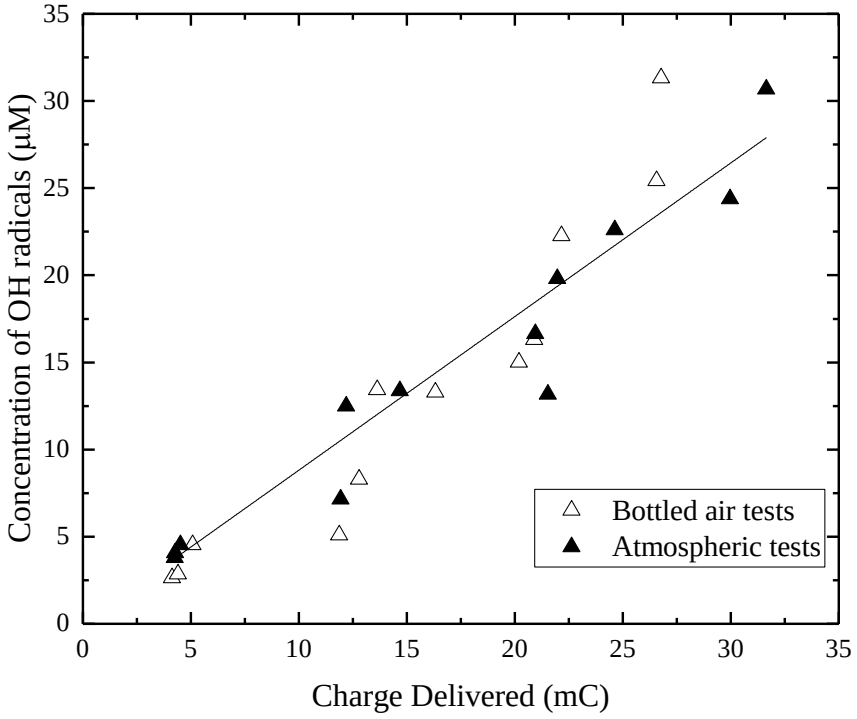

Figure 6.18. The concentration of OH radicals as a function of charge delivered after exposure to negative, direct, steady-state corona discharges. Each point in this graph represents an individual test. The straight line shows the fitting by equation (6.5).

High concentrations of OH radicals were obtained, as shown in Figure 6.18. The negative direct corona discharges delivered more charge than the positive discharges and resulted in a much higher concentration of OH radicals in the treated sample

solution. The linear fitting was again used to evaluate the production rate of OH radicals, and the rate was found to be $8.81 \cdot 10^{-1}$ μM/mC.

6.3.3 Change in Acidity of Treated Solutions

It was reported in the previous chapter that the acidity of the indigo carmine solution decreased after exposure to the steady-state corona discharges. This decrease is considered to be related to the decolorisation effect produced by the non-thermal plasma discharges. The pH of the TA solutions also was measured before and after exposure to corona discharges.

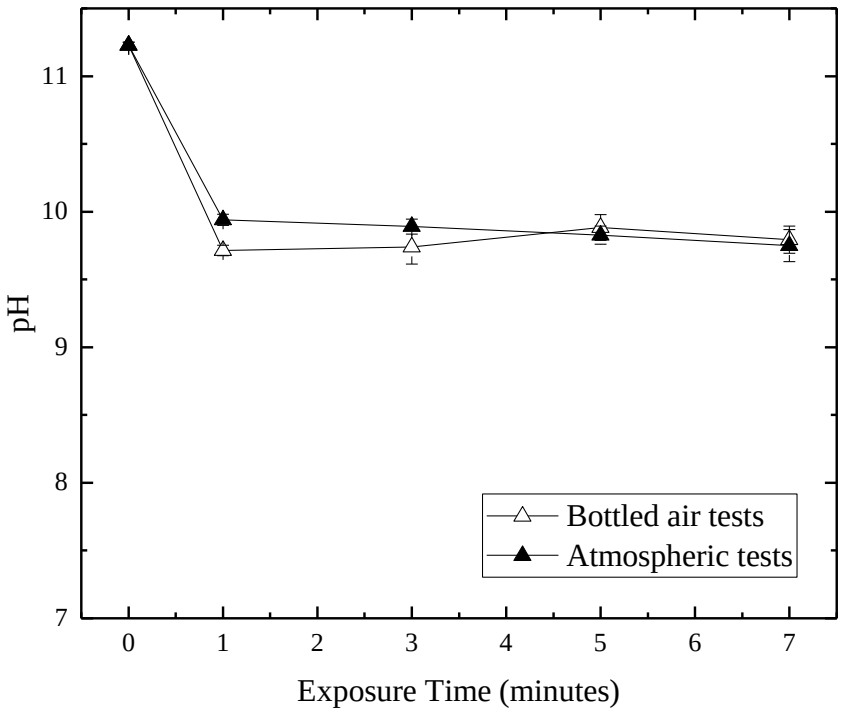

(a)

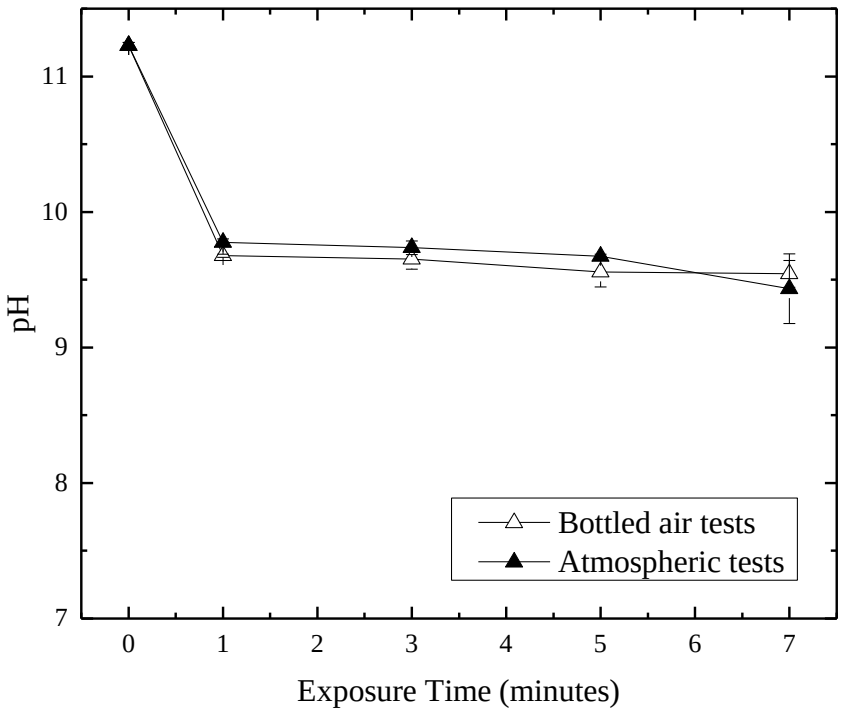

(b)

Figure 6.19. The pH of the TA solution sample after exposure to indirect steady-state corona discharges with (a) positive polarity and (b) negative polarity. Solid lines are for visual guidance only.

The initial pH of the TA solution sample was found to be ~11.2; pH of the treated solutions decreased to 9.5–10 after exposure to the steady-state corona discharges for 1 minute, regardless of corona discharge polarities. Generally, in the case of negative energisation, the pH of the TA solutions was found to be slightly lower than in the case of positive corona discharges. After longer exposure times, the pH of the TA solution sample did not show an obvious further decrease.

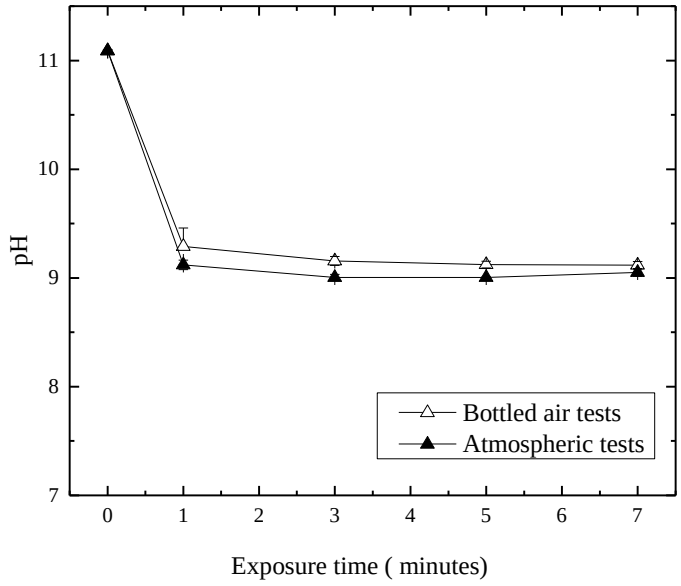

(a)

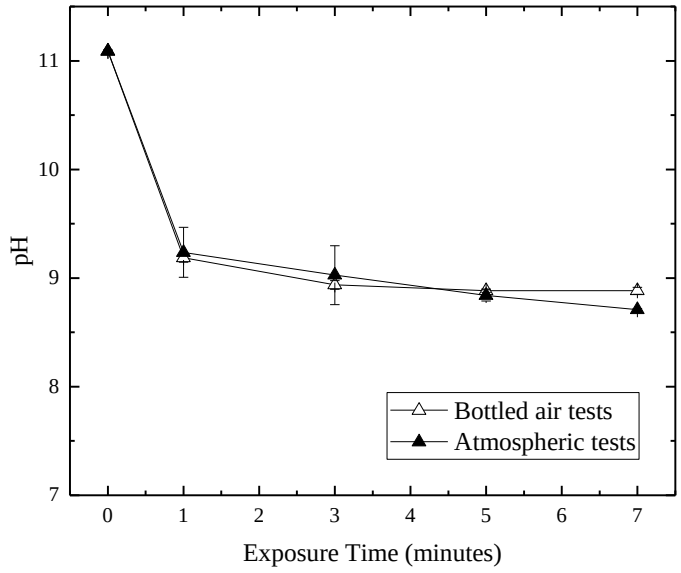

(b)

Figure 6.20. The pH of the TA solution sample after exposure to direct steady-state corona discharges with (a) positive polarity and (b) negative polarity. Solid lines are for visual guidance only.

The initial pH of the TA solution sample was ~11.1 in this group of tests. After exposure to positive direct corona discharges for 1 minute, the pH decreased to 9–9.5, and further decrease was not observed after a longer exposure. In the case of negative direct corona discharges treatment, the pH decrement was similar to that of the positive case. However, a slight further decrease was observed: pH decreased to ~8.9 after 7 minutes of exposure. The pH of solutions after direct corona treatment was slightly lower than the pH of solutions after indirect corona treatment.

6.3.4 Summary

In this section, the OH radical production in the TA solution treated with steady-state corona discharges was investigated. TA solution was used as an OH radical scavenger to trap OH radicals generated by corona discharges. Concentration of OH radicals was obtained using the fluorescence light emission signal from the treated samples. Both positive and negative polarities were used in generating steady-state corona discharges. TA samples were exposed to 30 kV corona discharges for 1, 3, 5, and 7 minutes in bottled air or atmospheric air. Two types of corona discharge treatment were tested in this series of experiments: direct and indirect corona discharge treatment. The metallic mesh was used in the case of the indirect treatment to screen ions and charged particles. For the direct treatment, a conductive sample plate was used; charged particles and ions were able to reach the sample surface, and the discharge current propagated through the sample.

The fluorescence emission signal was obtained from the samples after corona discharge treatment with different conditions. This means that OH radicals were produced by corona discharges with different polarities and in air humidity. It was also found that the humidity of air tested in these experiments (~12.5% RH for bottled air and ~40% RH for atmospheric air) did not result in a significant difference in OH production by corona discharges.

Negative corona discharge treatment resulted in a significantly higher OH production rate in both direct and indirect treatment tests. This is considered to be a result of high production of reactive chemical species that have an effect on the OH radical

production. It was found that the ozone level was much higher in the case of negative discharges (40 ppm and 20–60 ppm in the indirect and direct treatments) than in the case of positive discharges (~2 ppm)..

The concentration of OH radicals calculated in this research is considered to be consistent with the results obtained from oxidation and decontamination tests and presented in Chapter 4 and Chapter 5. For example, a higher degree of decontamination/oxidation was achieved using corona discharges with negative polarity. Similarly, a higher OH concentration was observed in the samples exposed to negative corona discharges as compared to positive corona discharges.

The production rate of OH radicals is found to be proportional to the total charge delivered by the discharges. Higher concentrations of OH radicals were obtained after exposure to the discharges which delivered a higher total charge. OH radical production rates were obtained and are presented in Table 6.1.

Table 6.1 OH production rate ($\cdot 10^{-1}$ μM/mC) for steady-state corona discharges.

Indirect		Direct	
Positive	Negative	Positive	Negative
0.59 (0.54 - 0.63)	5.17 (4.87 - 5.46)	0.67 (0.62 - 0.73)	8.81 (8.26 - 9.37)

Values in brackets indicate a 95% confidence interval.

As shown in Table 6.1, the direct corona discharges resulted in a higher rate of OH radical production. Negative indirect treatment did produce the highest amount of OH radicals (up to 43 μM after 7 minutes), but also more charge was delivered in this case. Therefore, the rate of production is lower than in the case of the direct negative treatment. In the case of direct treatment, charged particles and ions reach the liquid surface, and OH radicals are generated; in the case of indirect discharges, charged particles and ions are screened, and only neutral reactive species can contribute to OH radical generation.

Comparing the obtained results with the results reported by other research, it was found that the present treatment generates more OH radicals. In this study, the

negative indirect corona discharges produced OH radicals with rates up to $6.14 \cdot 10^{-10}$ mol/s, while a similar OH radical production rate of $(2–9) \cdot 10^{-10}$ mol/s was reported in [240] using 20 kHz DBD plasma jet .

Increase in acidity was also observed in the TA solutions after direct or indirect exposure to corona discharges. This result corresponds to results presented in Chapter 4 which showed a decrease of acidity in indigo carmine solution after corona discharge treatment.

6.4 OH Radical Production by Impulsive Transient Plasma Discharges

In Chapter 4 and Chapter 5, the oxidation and decontamination capabilities of the impulsive transient plasma discharges were investigated. The results showed that the indigo carmine solutions can be decolorised, and bacterial samples can be decontaminated by these discharges. Unlike the steady-state corona discharges, the ozone concentration produced by the transient plasma discharges was undetectably low. Therefore, OH radicals appear to be of high importance in this case. Thus, the measurement of OH concentrations and production rates are necessary to understand the oxidation and decontamination effects of the impulsive transient plasma discharges and to optimise atmospheric plasma systems for practical applications.

It was shown in [65] that OH radicals can be generated by transient plasma discharges across water surfaces under ambient atmospheric conditions. In the present section, the measurements of the concentration of OH radicals generated by impulsive transient plasma discharges were conducted. TA solution samples were placed onto conductive and non-conductive sample plates and treated with the direct transient plasma discharges and surface transient plasma discharges. Both positive and negative energisation mode and three different voltage levels: 20 kV, 24 kV, and 28 kV were tested. The conditions for this series of the experiment are the same as for the previous decolorisation and decontamination experiment. The fluorescence light emission of treated samples were measured using the spectrofluorimeter. Results were used to calculate the concentration of OH radicals. The pH of the solution was monitored as well.

6.4.1 Hydroxyl Radical Production by Surface Impulsive Transient Plasma Discharges

The TA sample was placed into the non-conductive sample plate (55 mm plastic contact plate) and treated with impulsive transient plasma discharges. As described in Chapter 3.3, in the case of the non-conductive sample plate, the transient plasma discharges propagated along the sample/air interface.

a) Positive Energisation

First, the positive energisation was used, and the TA solutions were treated by the positive transient plasma discharges. Fluorescence light emission was measured, and the peak intensity of the fluorescence signal at 425 nm was obtained. This peak intensity is presented in Figure 6.2 as a function of exposure time.

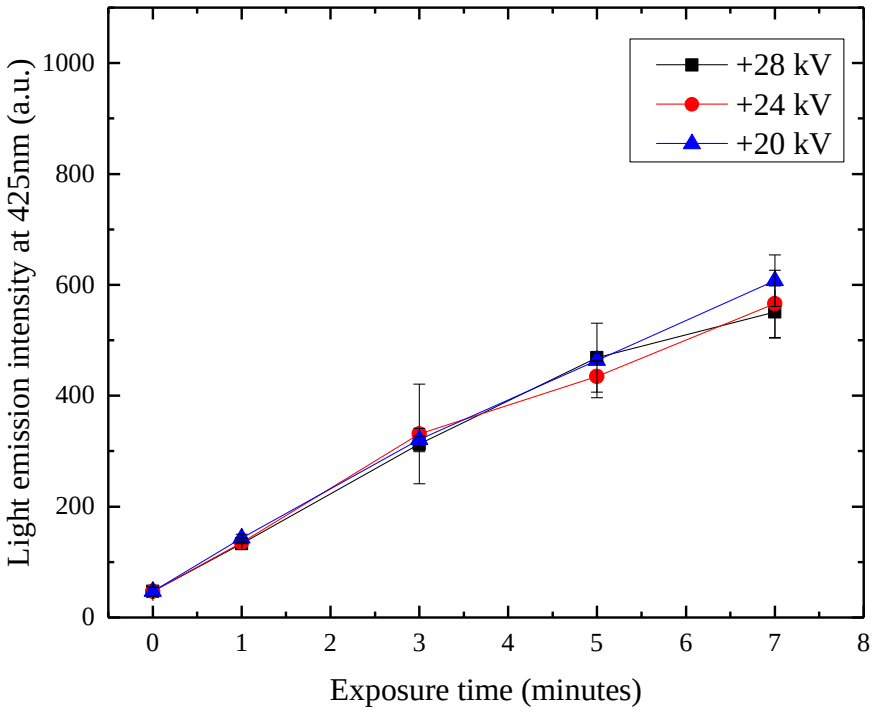

Figure 6.21. Fluorescence light intensity of the samples treated with the positive surface transient plasma discharges as a function of treatment time. Each point in this figure represents an average of three independent tests. Error bars show the standard deviation values. Solid lines are for visual guidance only.

As shown in Figure 6.21, the peak intensity of the fluorescence signal increased with the exposure time. Different voltage levels did not result in a noticeable difference in the fluorescence light emission. After the longest exposure of 7 minutes, the peak intensity increased to 500-650 a.u. The light emission intensity was then converted into the OH concentration, which is shown in Figure 6.22 as a function of the total charge delivered.

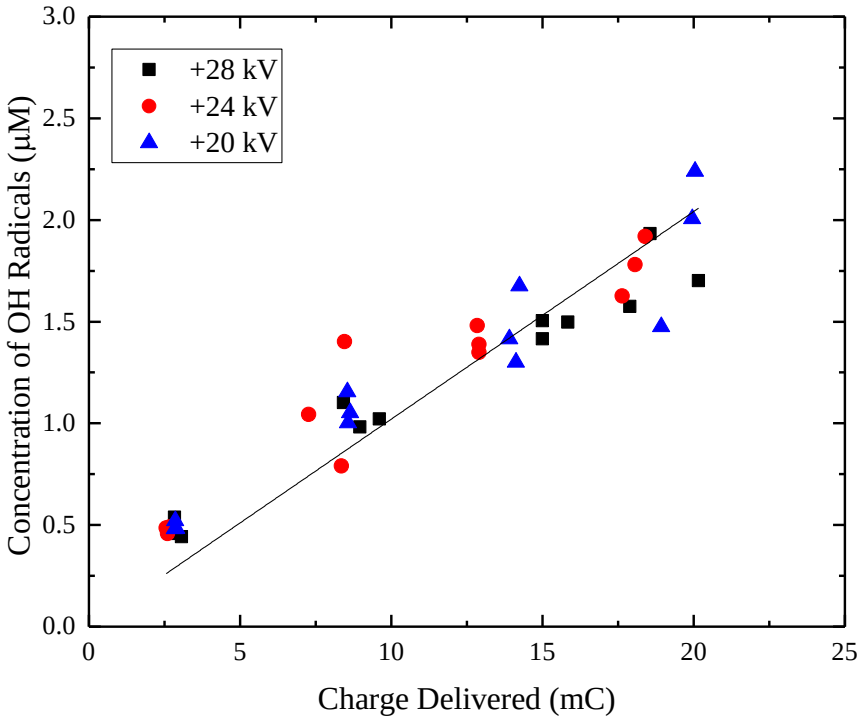

Figure 6.22. The concentration of OH radicals as a function of charge delivered after exposure to surface positive transient plasma discharges. Each point in this graph represents an individual test. The straight line shows the fitting by equation (6.5).

As shown in Figure 6.22, the total charge delivered during the treatment with positive surface transient plasma discharges was high. Up to 21 mC was delivered after 7 minutes of treatment, but the concentration of OH radicals was less than 2.2 µM. By applying the linear fitting as the solid line shown in Figure 6.22, the rate of OH production was found to be $1.02 \cdot 10^{-1}$ µM/mC.

b) Negative Energisation

Negative energisation was also used to generate the surface transient plasma discharges. The TA samples were treated with these negative transient discharges. The fluorescence light emission was detected from the treated solution samples, and the intensity of the fluorescence signal peak at 425 nm is shown in Figure 6.23 as a function of the exposure time.

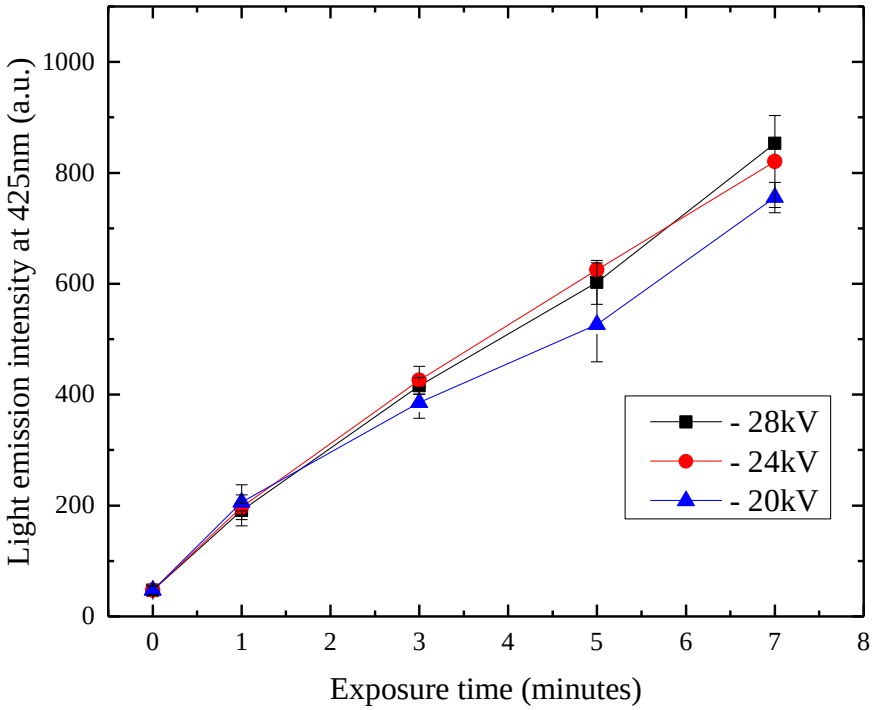

Figure 6.23. Fluorescence light intensity of samples treated with negative surface transient plasma discharges as a function of treatment time. Each point in this figure represents an average of three independent tests. Error bars show the standard deviation values. Solid lines are for visual guidance only.

The peak intensity was higher than for the case of positive energisation: 720–920 a.u. was observed after 7 minutes of treatment with negative surface transient plasma discharges. It was also observed that the voltage levels did not make a noticeable difference in the light emission intensity.

The concentration of OH radicals was calculated based on the light emission intensity. The results are shown in Figure 6.24 as a function of charge delivered.

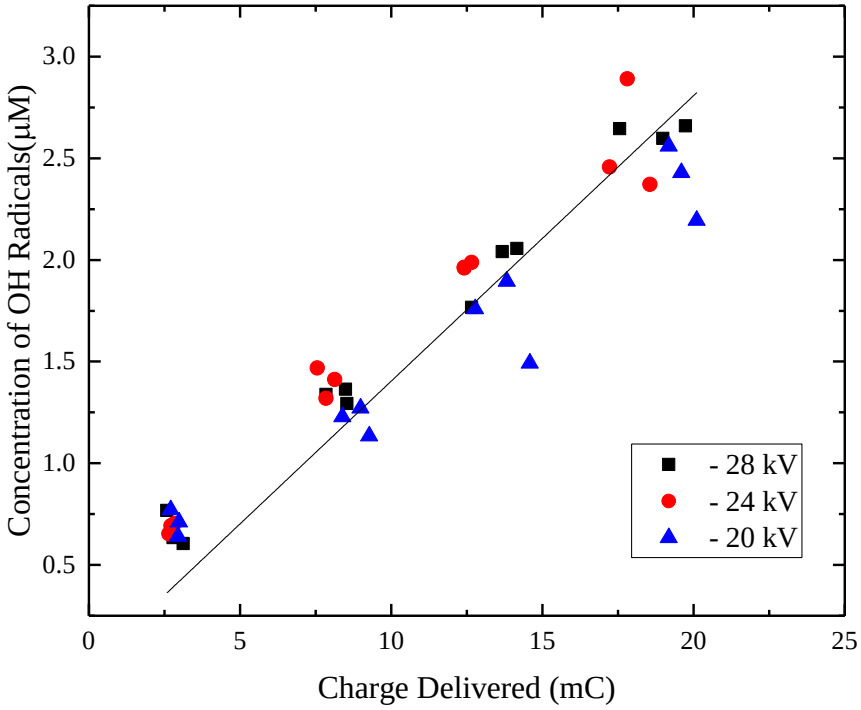

Figure 6.24. The concentration of OH radicals as a function of total charge delivered after exposure to negative surface transient plasma discharges. Each point in this graph represents an individual test. The straight line shows the fitting by equation (6.5).

As shown in Figure 6.24, the charge delivered by negative surface transient plasma discharges was similar to that of the previous positive energisation case, but the concentration of OH radicals was higher. This concentration was measured to be 2.2–2.9 μM in the sample treated by the negative surface transient plasma discharges for 7 minutes with 17–20 mC charge. Using linear equation (6.5) to fit the results, the solid line in Figure 6.24 represents this fitting. The rate of OH radical production, γ, was found to be $1.40 \cdot 10^{-1}$ μM/mC.

6.4.2 Hydroxyl Radical Production by Direct Impulsive Transient Plasma Discharges

The direct impulsive transient plasma discharge treatment also was used in this series of experiments. As mentioned in Chapter 3.3, the direct transient plasma discharges are generated when the conductive sample plates are used. The transient plasma does not propagate through the sample surface in this case of direct discharges, but the discharge current passes through the sample and reaches the grounded conductive sample plate. Oxidation and decontamination effects of the direct transient plasma discharges were obtained and were discussed in Chapters 4 and 5. Results are considered to be related to OH radicals produced during the discharges. In this section, measurement of OH radicals produced by direct transient plasma discharge treatment is presented.

a) Positive Energisation

The TA solution was treated by positive direct transient plasma discharges, and the fluorescence light emission was measured. As in the case of transient plasma discharges, the ozone level was undetectably low. The peak intensities of the fluorescence signals at 425 nm, recorded from the treated sample, are shown in Figure 6.25.

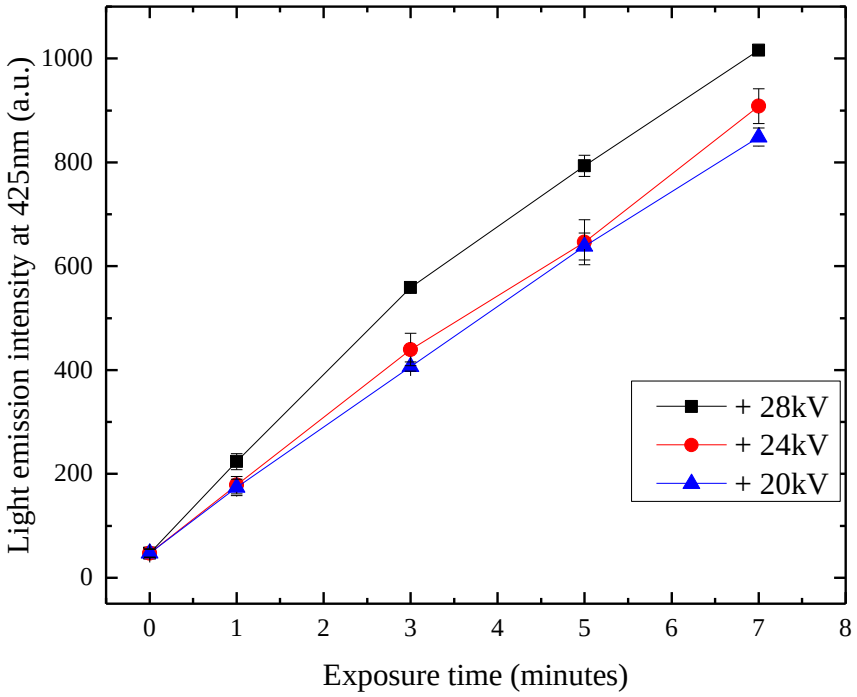

Figure 6.25. Fluorescence light intensity of samples treated with positive direct transient plasma discharges as a function of treatment time. Each point in this Figure represent an average of 3 independent tests, error bars show the standard deviation values. Solid lines are for visual guidance only.

Intensive fluorescence light emission was detected from the samples treated by the positive direct transient plasma discharges. After 7 minutes of exposure, the peak intensity of the fluorescence signal in the samples treated with 24 kV and 20 kV discharges was 830–930 a.u. The fluorescence signal in the samples treated with 28 kV discharges has a higher intensity, ~1000 a.u. after 7 minutes of treatment. This difference is primarily caused by the higher charge delivered in the 28 kV discharge case. The concentration of OH radicals in treated samples was calculated and is presented in Figure 6.26 as a function of the total charge delivered.

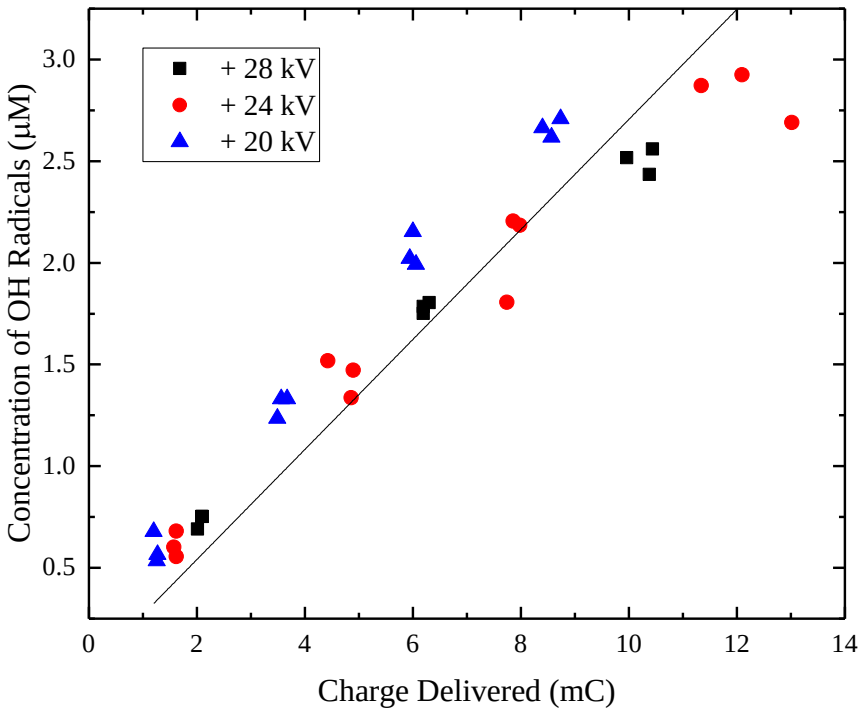

Figure 6.26. The concentration of OH radicals as a function of charge delivered after exposure to direct positive transient plasma discharges. Each point in this graph represents an individual test. The straight line shows the fitting by equation (6.5).

As can be seen from Figure 6.26, the charge delivered by direct transient plasma discharges was lower than the case of surface transient plasma discharges. However, the concentration of OH radicals was higher compared with that of samples treated by the positive surface transient plasma discharges. The linear equation (6.5) was used to fit the results, and the rate of OH radical production was found to be $2.71 \cdot 10^{-1}$ µM/mC.

b) Negative Energisation

The direct transient plasma discharges with negative polarity were used to treat the target TA solution sample, and fluorescence light emission was detected. The peak intensity of the fluorescence signal at 425 nm was obtained as a function of exposure time for different energisation levels and is shown in Figure 6.27.

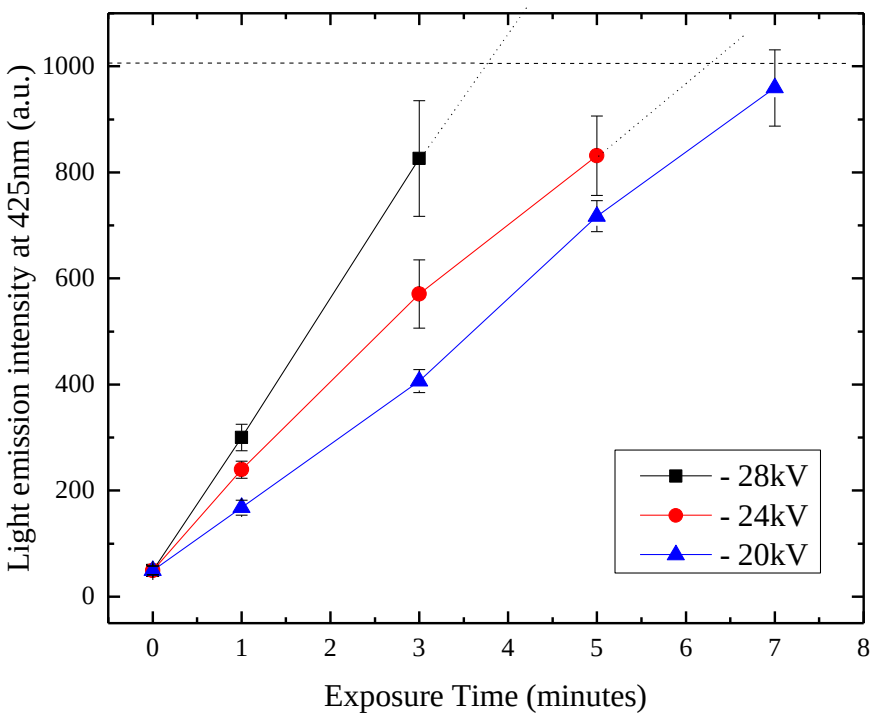

Figure 6.27. Fluorescence light intensity of samples treated with negative direct transient plasma discharges as a function of treatment time. Each point in this figure represents an average of three independent tests. Error bars show the standard deviation values. The horizontal dotted line shows the sensitivity limit of the spectrofluorophotometer. Solid lines are for visual guidance only.

The high-intensity fluorescence signals were obtained from the samples treated with negative direct transient plasma discharges. As shown in Figure 6.27, in the case of 20 kV discharges, the peak intensity of the fluorescence signal nearly reached the limit of the spectrofluorometer, 1015 (a.u.). The peak intensity of the fluorescence signals in samples treated with 24 kV discharges for 7 minutes exceeded this limit. For the

samples exposed to 28 kV discharges for 5 minutes, the peak intensity already exceeded the limit.

The light emission intensity was converted into OH radical concentration. The results are shown in Figure 6.28 as a function of charge delivered.

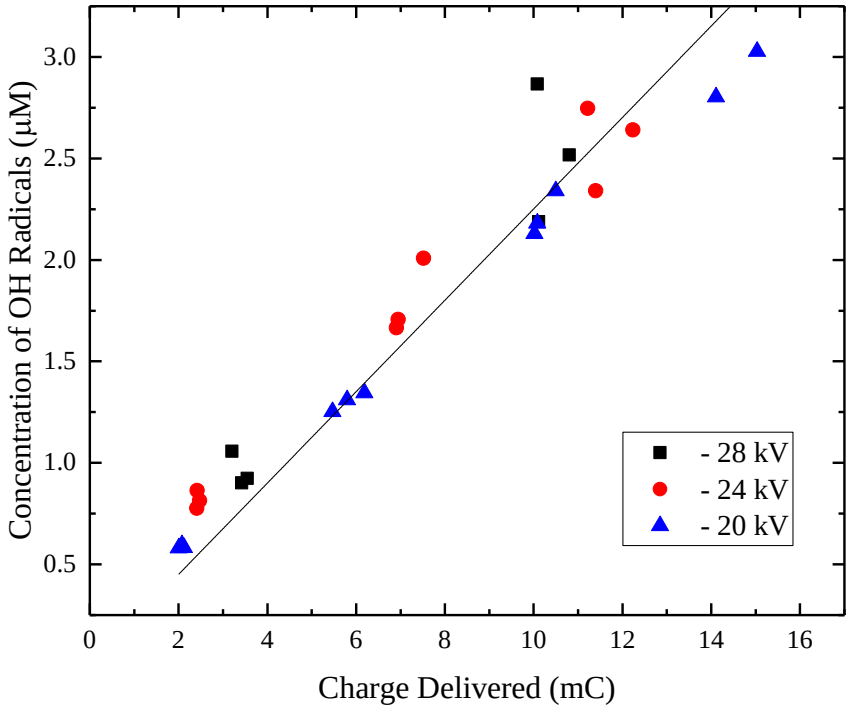

Figure 6.28. The concentration of OH radicals as a function of the total charge delivered after the exposure to direct negative transient plasma discharges. Each point in this graph represents an individual test. The straight line shows the fitting by equation (6.5).

The charge delivered by negative direct transient plasma discharges is slightly higher than that of the positive case, but still lower than for surface discharges. A similar tendency of increase in OH radical concentration was observed. The rate of OH radical production was found to be $2.25 \cdot 10^{-1}$ μM/mC by applying the linear fitting equation (6.5).

6.4.3 Change in Acidity of Plasma-Treated Solution Sample

As reported in Section 6.2.3, the acidity of the target solution decreases after treatment with the steady-state corona discharges. In this aspect of the research, the acidity of the plasma-treated samples was monitored. In the case of the surface transient plasma discharges, the pH of the solution demonstrated a slight decrease with an increase in exposure time. This dependence is shown in Figure 6.29.

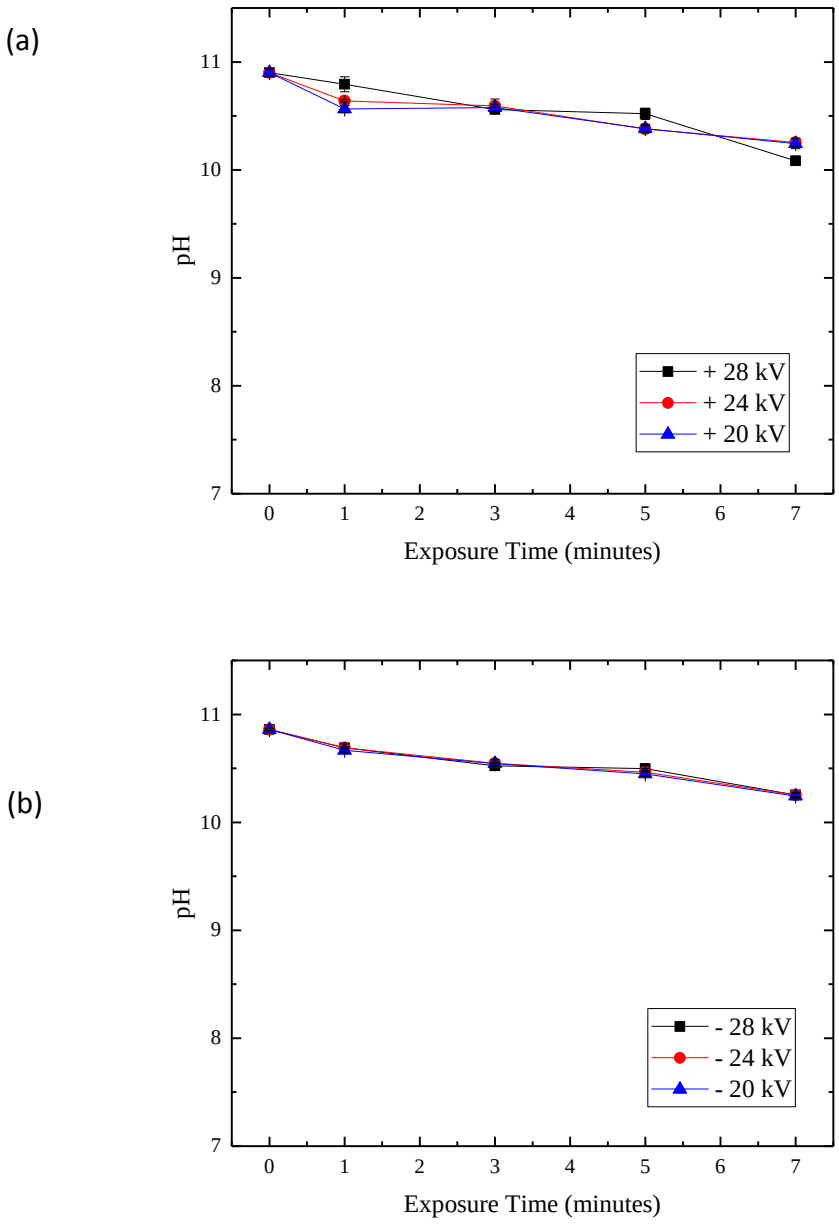

Figure 6.29. The pH of the TA solution sample as a function of treatment time after exposure to the surface impulsive transient plasma discharges with (a) positive polarity and (b) negative polarity. Solid lines are for visual guidance only.

As shown in Figure 6.29, the pH decreases with an increase in the treatment time for samples treated with the surface transient plasma discharges. This decrease is similar in both positive and negative energisation cases. The initial pH was 10.8–10.9, and it decreased to 10.2–10.3 after 7 minutes of exposure.

In the case of the direct transient plasma discharges, the pH values of the treated samples are shown in Figure 6.30. A slightly higher decrease in pH was observed in samples treated with direct transient plasma discharges. The initial pH was also 10.8–10.9, but it decreased to 9.2–9.6 after exposure to the positive direct transient plasma discharges. In the case of negative direct transient plasma discharges, the pH decreased to 9.4–9.9 after 7 minutes of exposure.

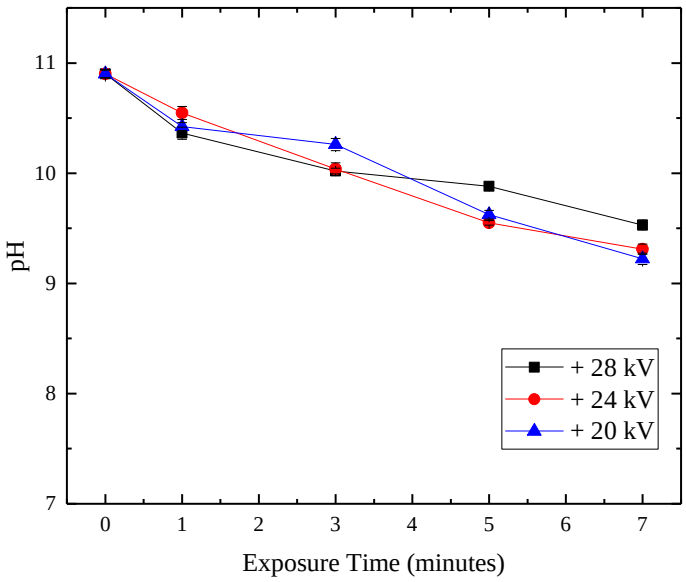

(a)

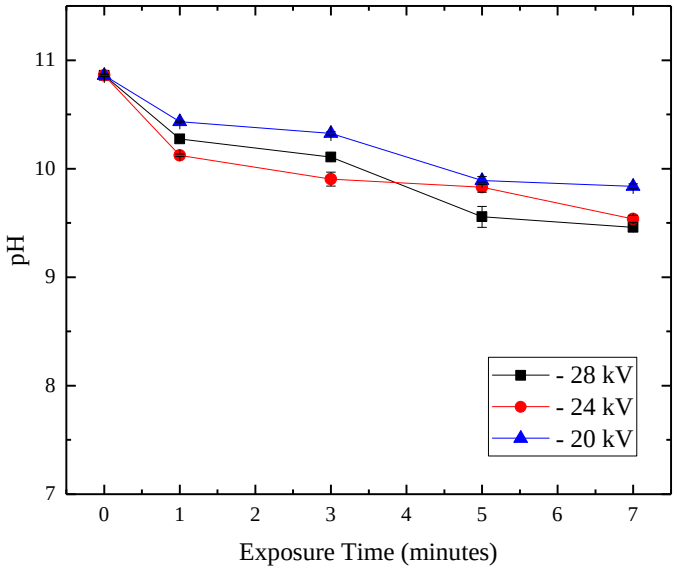

(b)

Figure 6.30. The pH of the TA solutions after exposure to the direct impulsive transient plasma discharges with (a) positive polarity and (b) negative polarity. Solid lines are for visual guidance only.

6.4.4 Impulsive Transient Plasma Discharge Treatment without Air Gap

a) Hydroxyl Radical Production by Impulsive Surface Transient Plasma Discharges

The direct and surface transient plasma discharge test results were discussed in Sections 6.4.1 and 6.4.2. The OH radicals produced in both cases were detected. To clarify the origin of the generation of OH radicals (whether generated in air or at the liquid sample surface), a special case was studied in this section. The stressed HV electrode was lowered to make contact with the surface of the liquid sample which was placed in the non-conductive sample plate. In this case, the transient plasma discharges would propagate along the sample/air interface only. TA solution samples

were treated with plasma discharges, and the intensity of fluorescence light emissions were measured. The breakdown voltage level, in this case, is ±18 kV. The peak fluorescence signal intensity at 425 nm is given in Figure 6.31 as a function of the exposure time.

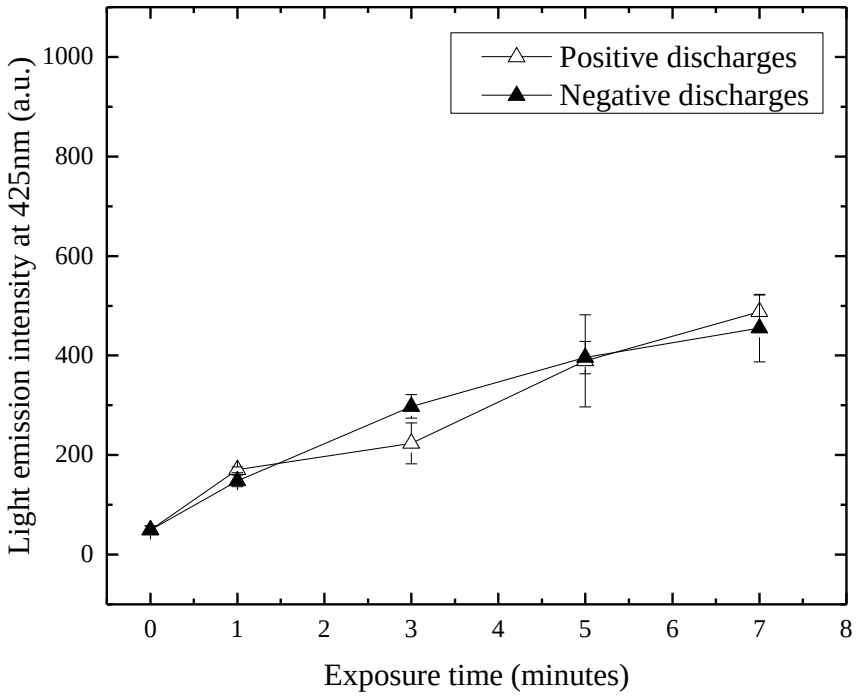

Figure 6.31. Fluorescence light intensity of samples treated with surface transient plasma discharges (without air gap) as a function of treatment time. Each point in this figure represents an average of three independent tests. Error bars show the standard deviation values. Solid lines are for visual guidance only.

As shown in Figure 6.31, the fluorescence light emission is detected from samples treated with the surface transient plasma discharges. First, it can be seen from this figure that there is no difference in the fluorescence emission intensities for samples exposed to the positive and negative surface transient plasma discharges. The intensity of the fluorescence emission, in this case, is much lower than in any other cases with the existence of air gap between the HV needle electrode and the liquid sample surface. For example, in the case of negative energisation, 7 minutes of exposure to surface transient plasma discharges resulted in a reduction of almost twice

the fluorescence emission intensity than negative surface transient plasma discharges for the same period of treatment time.

The concentration of OH radicals in the samples treated with the surface transient plasma discharges is shown in Figure 6.32 as a function of delivered charge.

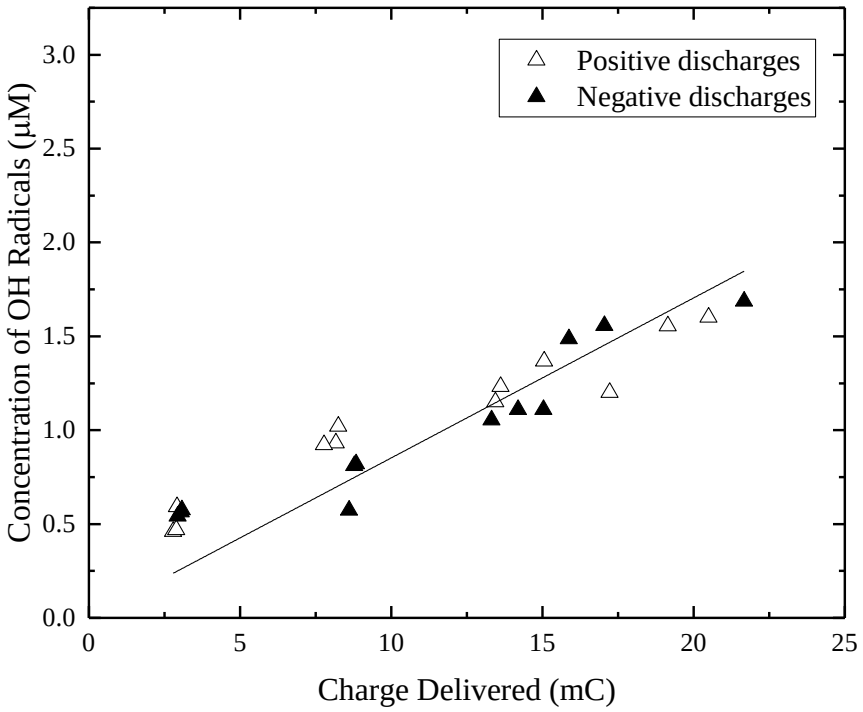

Figure 6.32. The concentration of OH radicals as a function of charge delivered after exposure to impulsive surface transient plasma discharges (without air gap). Each point in this graph represents an individual test. The straight line shows the fitting by equation (6.5).

As shown in Figure 6.32, the concentration of OH radicals produced by the surface transient plasma discharges without air gap is lower than the case of the surface transient plasma discharges with air gap. However, the surface transient plasma discharges produce a noticeable amount of OH radicals. The production rate, 0.085 μM/mC, is found to be the same for both positive and negative cases.

This result confirms that in the case of the surface discharge treatment, the reactive species which are responsible for production of OH radicals (including OH radical itself) are generated in both sections of the transient plasma discharge path: vertical propagation path through the air and horizontal propagation on path across the air/liquid interface.

b) Direct Transient Plasma Discharges without Air Gap

The direct transient plasma discharges were also used for sample treatment under the condition in which the needle electrode was in contact with liquid sample. Conductive sample plates were used in this case. The discharges were generated in the liquid itself, and the discharge current propagated through the bulk of the liquid samples only. Pulses with voltage levels at ± 30 kV were used to generate discharges in the liquid samples. After such treatment for a specific period of time (up to 7 minutes), the recorded fluorescence light emission signals were very low; no peak at 425 nm was observed. This means that the direct discharges without an air gap were inefficient for the generation of OH radicals in target liquid samples. A potential reason for this inefficiency is the relatively high conductivity of solutions (~400 μS/cm). The process of formation of the transient plasmas in such liquid samples stressed with the HV pulses used in the present tests is inefficient: most of the discharge current dissipated through Joule conduction without generating OH radicals.

This result indicates that in the case of the direct transient plasma discharges, the reactive species that are responsible for producing OH radicals (including OH radical itself) are mostly generated in air or at the air/liquid interface. Discharges through the bulk of the liquid do not make a detectable contribution to the production of OH radicals.

6.4.5 Summary

In this chapter, production of OH radicals in target liquid samples by impulsive transient plasma discharges was investigated. Specifically, a TA solution was used as the scavenger to detect OH radicals. Based on the intensity of fluorescence emission signals detected from samples exposed to the impulsive discharges, the concentration of OH radicals was calculated. Experimental work presented in this chapter includes the used of transient plasma discharges with different parameters: three different voltage levels were tested (20 kV, 24 kV, and 28 kV) in both positive and negative energisation modes.

Two different types of discharge treatments were used: surface discharge treatment (using non-conductive sample plate, discharges propagate vertically through air and then across air/liquid interface), and direct discharge treatment (discharges propagate vertically in air to the sample surface, and then the discharge current dissipates through the bulk of the liquid sample).

From the results, it was found that the concentration of OH radicals was proportional to the total charge delivered by the discharges, and this relation was almost linear. This defined the rate of OH production by the impulsive discharge treatment, and it enabled comparison of the efficiency of OH radical production for different cases.

Another important finding from these experiments is that the production of OH radicals does not depend on the voltage level when the same amount of charge is delivered to the sample. Again, this confirms that the total delivered charge defines the OH production rate.

Table 6.2. OH production rate ($\cdot 10^{-1}$ μM/mC) for surface and direct transient plasma discharges.

Surface		Direct	
Positive	Negative	Positive	Negative
1.02 (0.97 - 1.07)	1.40 (1.34 - 1.47)	2.71 (2.57 - 2.84)	2.25 (2.16 - 2.34)

Values in brackets indicate a 95% confidence interval.

Table 6.2 presents the OH production rates for surface and direct impulsive transient plasma discharges with positive and negative polarities. These results were obtained using Origin Pro with linear equation (6.5). In some specific cases, an even higher rate was achieved: for example, $3.24 \cdot 10^{-1}$ μM/mC for positive direct discharges, and $2.53 \cdot 10^{-1}$ μM/mC for negative direct discharges. It can be seen clearly from the table that direct discharges have a higher efficiency of generating OH radicals.

In the case of the HV needle electrode in contact with the sample surface, OH radicals could still be produced when a non-conductive sample plate was used. Discharges propagated along the liquid/air interface and generated OH radicals. The rate of production was found to be $0.85 \cdot 10^{-1}$ μM/mC (with a 95% confidence interval, $0.79 \cdot 10^{-1}$ – $0.91 \cdot 10^{-1}$). When a conductive sample plate was used, discharges were generated in the liquid, and no OH radicals were detected in the samples. The test results indicated that most of the reactive species which contributed to the production of OH radicals were generated in the air and at the air/liquid interface. The HV pulses used to generate discharges directly in the liquid were inefficient in the production of OH radicals.

The acidity of the solution was changed after the treatment with transient plasma discharges. This is consistent with the results of treating liquid samples with plasma in Chapter 4.

6.5 Discussion and Conclusions

It is recognised that OH radicals have the highest oxidation capability amongst all oxygen-based reactive species. The redox potential of OH radicals is ~2.7 V [254]. Thus, OH radicals produced by non-thermal plasma discharges play an important role in the oxidation of organic molecules and bacteria decontamination. It is important to investigate the OH production during non-thermal plasma discharges, and the information gained from this investigation will help in the optimisation of the cleaning and decontamination applications of non-thermal plasma discharge treatment.

This chapter discusses OH radical production by steady-state corona discharges and impulsive transient discharges that was investigated through a series of experiments. TA solution was used for OH radical scavengers and exposed to discharges. OH radicals produced by non-thermal plasma discharges reacted with TA to form HTA. Then, the fluorescence emission from HTA was measured, and the concentration of OH radicals was calculated. The fluorescence emission signal was observed in the samples exposed to corona discharges as well as impulsive transient discharges. This means that both types of discharges produced a detectable amount of OH radicals. In addition, the OH radical concentration in the exposed sample solution had a linear relation with the total charge delivered by non-thermal plasma discharge treatment. This is in line with the the results reported in [255]: as the discharge current increased from 15 mA to 50 mA, more charge was delivered to the sample solution with a pH of 10, the OH radical production rate was nearly three times as before.

In the case of steady-state corona discharges, a higher concentration of OH radicals was observed in samples after exposure to direct corona discharges as compared to samples treated by indirect corona discharges. Another important finding is that the corona discharges with negative polarity produced a higher amount of OH radicals. This is a result of the higher ozone concentration during negative corona discharges. The charge-dependent production rate of OH radicals was calculated for indirect and direct corona discharges with both positive and negative polarities. It is obvious that negative corona discharges with a higher ozone concentration resulted in a higher OH radical production. As reported in [153] and [159], the existence of ozone does increase the production rates of OH radicals.

After exposure to impulsive transient plasma discharges, OH radical concentration in the solution sample was measured. Results showed that the OH radical production is in proportion to the charge delivered. It also was confirmed that discharges in air as well as at the liquid/air interface produce reactive species that are responsible for OH radical generation. However, discharges directly in the liquid sample with pulses used in this research did not produce detectable OH radicals.

As reported in [153] and [159] and discussed in Chapter 2.4.2, ozone and other reactive oxygen species such as hydrogen peroxide could also have an effect on the OH radical production. However, in the present study, the ozone concentration during the transient plasma treatment was too low to be detected (less than 1 ppm) using available sensors. It is believed that in this series of transient plasma discharge tests, ozone did not make a significant contribution to the OH radical production.

Regardless of the charge delivered to the sample during the plasma treatment, the time-dependent efficiency of OH production was significant. For example, ~$0.8 \cdot 10^{-10}$ mol/s production rate was achieved in the negative direct transient plasma discharge treatment. This rate is higher than the efficiency of OH radical production by the underwater discharges reported in [250]. Other studies reported higher efficiencies, such as (2-9) $\cdot 10^{-10}$ mol/s, [240], and $1.67 \cdot 10^{-8}$ mol/s, [253]. However, continuous steady-state plasma treatment with higher frequency or higher voltage level was used in those experiments. The results presented in this chapter were obtained using the impulsive plasma discharges with a pulse repetition rate of 20 pps. Therefore, it can be stated that higher time-dependent efficiency of OH radical production can be achieved by increasing the pulse repetition rate and treatment time.

Comparing the results obtained using the steady-state corona discharges and impulsive transient plasma discharges, it may be concluded that the negative direct corona discharges resulted in a higher OH radical production rate $8.81 \cdot 10^{-1}$ μM/mC, These type of discharges also demonstrated a high time-dependent efficiency, 7.14 $\cdot 10^{-2}$ μM/s. This is primarily due to the high ozone concentrations produced by these discharges. The corona discharges demonstrated a lower OH production rate as compared with the impulsive transient plasma discharges when positive energisation mode was applied.

CHAPTER 7

TiO_2 as a Potential Catalyst for Improving the Efficiency of Non-Thermal Plasma Treatment

7.1 Introduction

In the previous chapters, the oxidation and bacterial inactivation capabilities of non-thermal plasma discharges were investigated. The obtained results provide valuable information for the optimisation of non-thermal plasma applications. As well as changing the discharge conditions, other methods can be used to improve the cleaning efficiency of the non-thermal plasma discharges. As reported in [256]–[260], catalysts can be used to enhance the performance of plasma systems: for example, to increase their energy efficiency. Also, by selecting a catalyst, production of unwanted by-products from the plasma cleaning process can be minimised. Toxic by-products such as CO can even be completely eliminated, and this makes the plasma-catalyst method even more attractive for practical applications.

TiO_2 is considered to be an efficient catalyst for plasma discharge processes. As reported in [261], [262], and [263], TiO_2 was used in the plasma treatment systems to help to remove different chemical pollutants. Multiple applications in which TiO_2 was employed as a plasma catalyst have been reported and include wastewater treatment, soil remediation [264], and cleaning of air streams [179].

TiO_2 is a photosensitive material; molecules of TiO_2 can be excited by UV light, as its band gap is 3.2 eV. Charged particles, UV photons, and strong electric fields generated by plasma discharges would act on the surface of TiO_2, electrons and holes-pairs can be generated, and chemically reactive species such as O_3 and H_2O_2 can be produced under the action of the non-thermal plasma discharges [265], [266]. Hence, the cleaning and decontamination effects of such discharges can be improved.

As suggested in [179], TiO_2 can be introduced into plasma systems in one of two ways: either a one-stage or a two-stage configuration. In the one-stage configuration, the catalyst is located in the discharge region and directly exposed to the active species (including ions, charged particles, and short-lived radicals), photons, and field

generated by the plasma discharges. In the two-stage configuration, the catalyst is located away from the discharge region and only exposed to long-lived chemical species that flow from the discharge region, such as O_3.

In this chapter, the use of TiO_2 as a catalyst is discussed, and the one-stage configuration of the plasma discharge system is described. This configuration was selected for excitation of TiO_2 with UV light, and generation of charged products by the plasma discharges to produce more reactive species and to improve the cleaning and inactivation ability of the plasma discharge treatment. The enhancement effect of the catalyst in the plasma discharge treatment system was investigated using two approaches. The oxidation capability of the discharges was obtained by measuring the decolorisation of indigo carmine, and the bio-decontamination capability of the plasma discharges was evaluated by the degree of bacterial inactivation, using *E. coli* and *S. aureus* as model bacteria. Although only preliminary experiments were performed, and further research is still needed, valuable information was obtained in the course of this study.

7.2 Methodology of Sample Preparation and Treatment

7.2.1 Sample Preparation

TiO_2 was used as a catalytic material in this series of tests. The oxidation capability of non-thermal plasma discharges in combination with the TiO_2 catalyst was investigated by measuring the degree of decolarisation of the indigo carmine water solution. The bio-decontamination efficiency of the non-thermal atmospheric plasma discharges in combination with TiO_2 was obtained using the same test microorganisms as previously, *E. coli* and *S. aureus*. However, the method of introduction of TiO_2 to the non-thermal discharge system is the first methodological issue which required attention. Based on the practical experience obtained during this project and information found in the literature, several approaches to introduce TiO_2 into the plasma discharge system were identified and tested. It was decided that TiO_2 porous film can potentially be used for effective interaction and enhancement of the chemical

effects of the atmospheric plasma discharges. In the case of the microbiological samples, it was decided to add TiO_2 fine particles (20 μm in diameter) to the agar nutritious media used to grow the microorganisms. The results of these tests in which chemical and biological samples with TiO_2 were exposed to the non-thermal discharges are described in this chapter.

A. Preparation of Porous TiO_2 Film

It is believed that the porous structure on nanometre-scale can change some chemical and physical properties of materials. The properties of porous TiO_2 film has been reported in many studies [267]–[269]. Compared with the bulk structure, the porous structure has a larger surface area which enhances the contact surface with the reactants and increases the absorption of photons. Synthesis of the porous TiO_2 films using nanometre size TiO_2 has been discussed in [270], [271], [272], and [273]. In this research, TiO_2 porous film was produced on the glass slides using TiO_2 powder. The following method was employed.

TiO_2 powder (5.56 g) with an average particle size of 20 μm (AEROXIDE® TiO_2 P 25, Evonik Industries [274]) was dissolved in 50 ml distilled water to make a solution with a concentration of 10% by weight. Then this solution was transferred into a petri dish and placed in an ultrasonic bath (U100 Ultrawave Limited, UK) for 15 minutes. After treatment in the ultrasonic bath, the slurry was spread evenly on a glass microscope slide. The size of the glass slide was 75×25 mm and thickness was 1–1.2 mm (Sail Brand 7101). The slurry was dried on the slides to form the first layer of the TiO_2 film.

The slurry was again dropped on the slides on top of the first layer of TiO_2 and then spread evenly to form the second layer. After the second layer dried, this step was repeated to form a third layer of TiO_2 on the slides. To stabilise the porous film, the glass slides with three layers of TiO_2 were put into the furnace (Carbolite® CTF 12/75) and baked for 30 minutes at 400℃. After cooling, the slides with the settled and dried TiO_2 porous films were ready to use and were stored in a dark, dry, and sterile place.

In the decolorisation tests in which the chemical activity of the plasma discharges was obtained, 1 ml of indigo carmine water solution was dropped on the slide with the TiO_2 porous film and treated by plasma discharges.

In the microbiological decontamination tests, 50 μL of PBS with a bacterial population of 10^3 CFU/ml was pipetted onto the slide with the TiO_2 porous film before and left to dry, then it was treated with atmospheric plasma discharges.

Figure 7.1 shows an original microscopic glass slide and another glass slide covered with a dry, three-layer TiO_2 porous film.

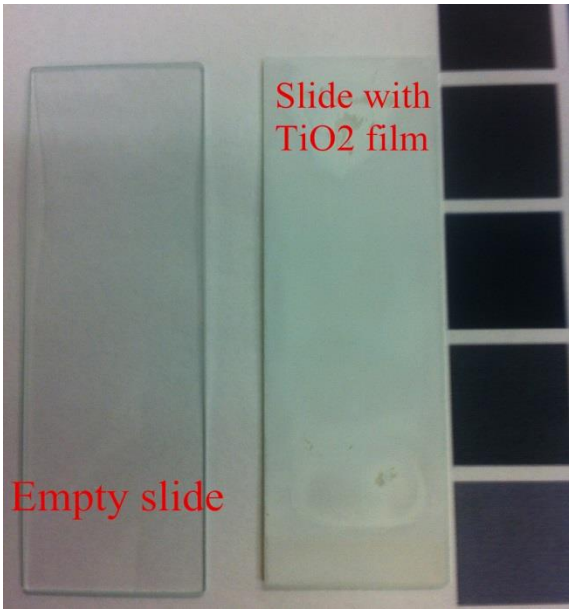

Figure 7.1. Blank glass slide and slide with TiO_2 porous film.

B. White Fabric with TiO_2

In another series of tests, a different approach to the preparation of samples with TiO_2 catalyst was used. A 10% TiO_2 solution was prepared as described in Section 7.2.1. Medical gauze was cut into pieces with a size of 20 mm × 10 mm, and then fully immersed into the TiO_2 solution. TiO_2 saturated fabric pieces were transferred into a petri dish, and stored in a dry, dark place until they were completely dry. After this process, the sample fabric was ready to use.

In the decolorisation tests, 1 ml of the indigo carmine solution was dropped onto the sample fabric and then treated by non-thermal plasma discharges.

C. TiO_2 Topped Agar

In this approach, TiO_2 fine particles were introduced directly into the top layer of agar. To prepare the samples, first, nutrient agar plates were made as described in Section 5.2.2.

TiO_2 water solution with particle concentrations of 1% (b/w) and 10% (b/w) was prepared and sterilised by autoclaving. This sterilised 5 ml TiO_2 solution was cooled to room temperature and then pipetted onto the top of each agar plate and spread as evenly as possible using an L-shape spreader and allow to dry. TiO_2 coated agar plates were seeded with bacteria and treated by non-thermal plasma discharges.

D. TiO_2 Mixed in Agar

Another approach to treatment of microbiological samples with TiO2 was through the introduction of TiO_2 particles into the bulk agar. In this case, 7 g of nutrient agar powder and 2.7 g of TiO_2 powder were dissolved in 250 ml distilled water. In this solution, the concentration of TiO_2 was 1% (b/w), and this sample maintained the required concentration of nutrient agar (28 g in 1 L of water as instructed by the manufacturer). This solution was then cooled in a water bath to 47 ℃. Then, 3.75 mg of TTC (2,3,5-Triphenyltetrazolium chloride from Sigma Aldrich, T8877) was added into this molten agar/TiO_2 mixture, mixed well, and poured into 55 ml plates covered with sterile aluminum foil.

Bacteria were seeded on these plates and treated in the plasma discharge system. Figure 7.2 shows a 55 mm diameter plate lined with aluminum foil and filled with agar/TiO_2 mixture.

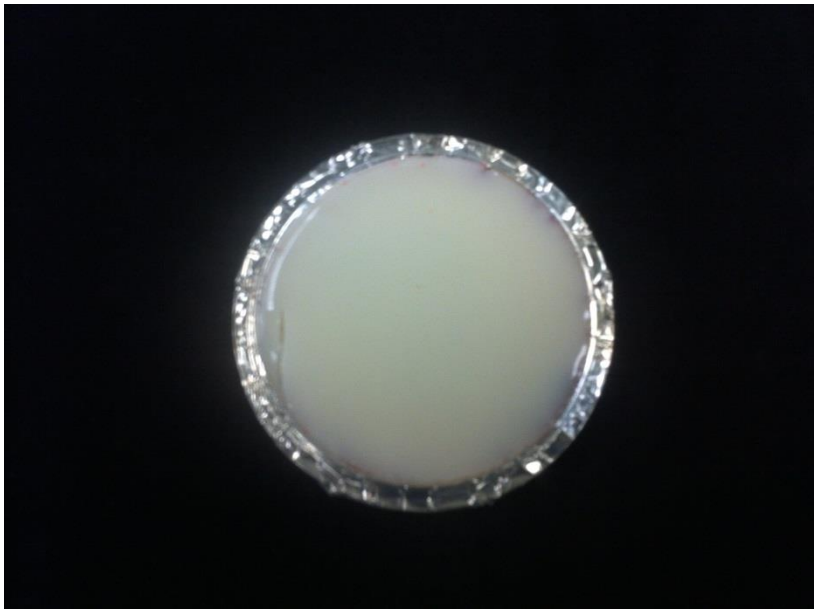

Figure 7.2. TiO_2/agar sample.

7.2.2 Discharge System for Preliminary Experiments

In this chapter, the negative steady-state corona discharges were used to decolorise indigo carmine solution samples and to inactivate test bacteria (*E. coli* and *S. aureus*). The corona discharge system used in this series of experiments is the same as described in Chapter 3.2. However, due to convenience and sample size, a different plasma treatment test cell was used. This test cell has the same size and dimensions as the test cell used in the transient plasma discharge tests described in Chapter 3.3. The main body of this test cell was made of Perspex cylinder with a diameter of 150 mm and height of 80 mm. Two PVC flanges cover the top and bottom of this cylinder. A metal plate with a 27 mm high rounded edge was located on the bottom flanges. The thickness of the plate was 10 mm, and the internal diameter was 100 mm. This plate was grounded through the earthed connection port on the bottom flange. Six gramophone needles (body diameter, 1.2 mm; tip radius, ~36 μm) were installed on the top flange through a screw into the metal bar. A DC high-voltage supply was connected to the needles through this bar. During the plasma discharge treatment, six needles were stressed with the same negative high voltage. The target sample was

placed on the metallic plate under the needle electrodes. This test cell is shown in Figure 7.3.

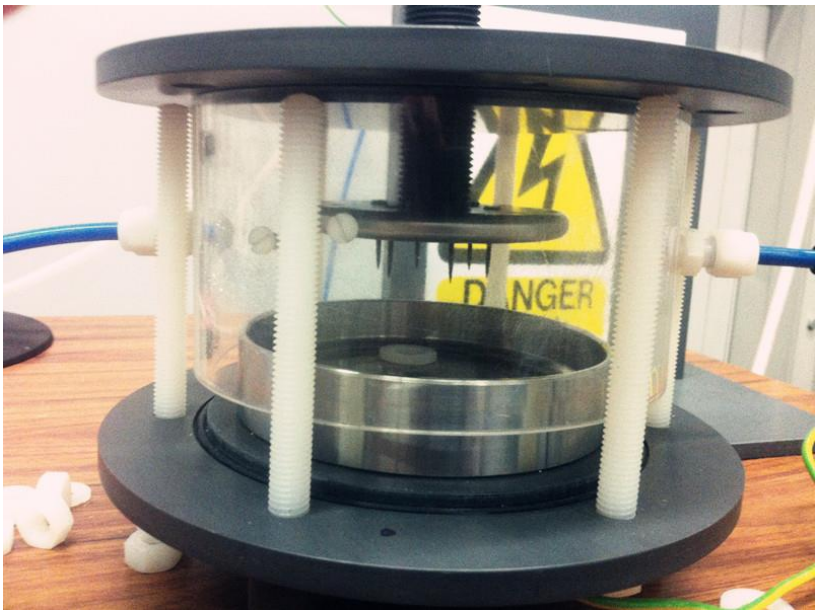

Figure 7.3. Six-needle plasma discharge test cell for the treatment of samples with TiO_2.

7.3 Experimental Procedures

7.3.1 Decolorisation of Indigo Carmine Solution

In the case of indigo carmine decolorisation tests, TiO_2 in the porous film form or on the fabric has direct contact with the dye solution. Different from the previous decolorisation study described in Chapter 4, in these tests some of the TiO_2 could be mixed with the indigo carmine solution, and could be impossible to provide readings in the transmittance measurement using the spectrophotometer. Also, it was not possible to separate these two substances. Thus, the degree of decolorisation should be determined in a different way rather than measuring the change in transmittance as in the previous chapter. A color analysis (Red-Green-Blue/RGB analysis) of pictures of the treated indigo carmine solution samples (on the top of TiO_2 porous films or TiO_2 saturated tissue) was used in the tests described in this chapter to evaluate the degree of decolorisation after the plasma treatment.

An example of RGB analysis is shown in Figure 7.4.

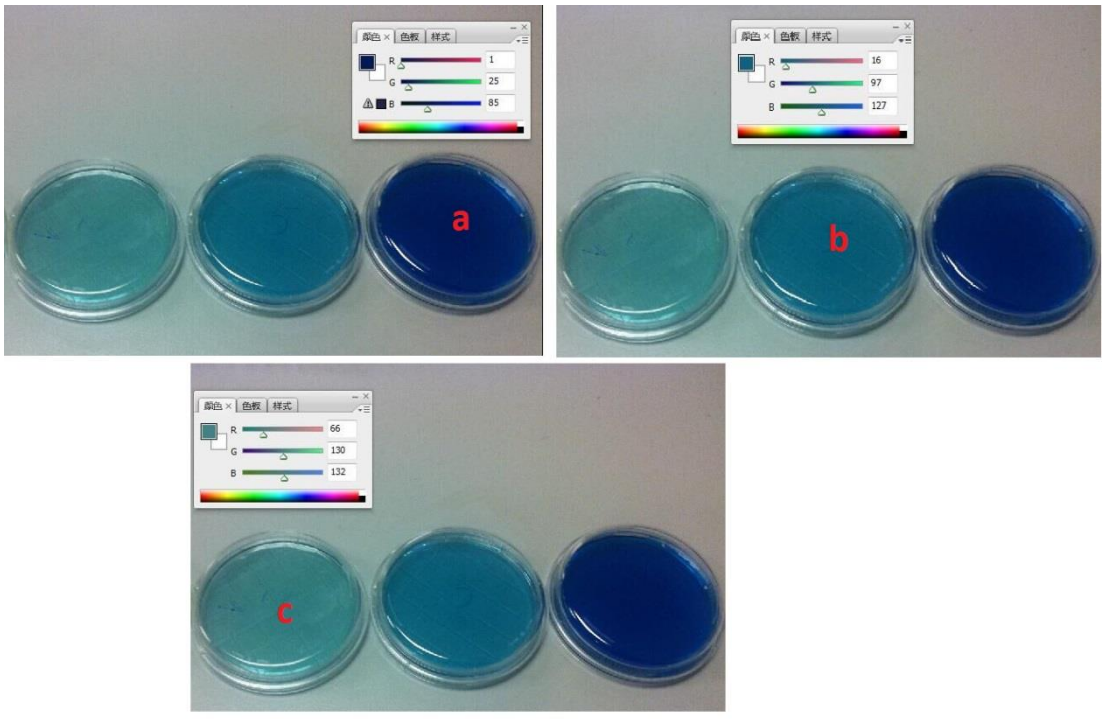

Figure 7.4. Blue tonal value of solutions with different concentrations of dye were obtained using RGB histogram (Adobe Photoshop CS3).

Sample “a” is the original indigo carmine solution; samples “b” and “c” are indigo carmine solution after treatment by indirect corona discharges for 5 minutes and 10 minutes. The concentration of indigo carmine in sample “a” is the highest; therefore, it has the darkest blue color. Sample “c” has the lowest indigo carmine concentration, so it has the lightest blue color. Blue tonal range values for samples a, b, and c were obtained using RGB histogram (Adobe Photoshop CS3). The tonality value is in the range of 0 to 255; lower tonal value indicates darker tonality of the object, while objects with lighter tonality have higher tonality values. As shown in Figure 7.4, the blue tonal value for samples a, b, and c are 85, 127, and 132, respectively. The blue value of the indigo carmine solution increased after decolorisation by plasma discharges. The increment was then used to quantify the level of decolorisation by plasma discharges.

The test procedure was as follows: 1 ml of dye solution was dropped on the glass slide with porous film (or on the fabric with TiO_2) and spread as uniformly as possible; a picture of the sample before plasma treatment was taken along with a color map (Photo A). Then, the sample was treated by negative corona discharges for a certain time period. After the discharge treatment, another photo (photo B) of the treated sample was taken with the color map under the same light conditions as picture A. Both photos, A and B, were analysed using Photoshop software, and the RGB values of each picture were recorded. Then the change in the blue value in the sample area was obtained using (7.1):

$$\Delta P = B_{sA} - B_{sB} \tag{7.1}$$

where ΔP is the change of blue value in the sample area;

B_{SA} is the average blue value of the sample area in photo A (after the discharge treatment); and

B_{SB} is the average blue value of the sample area in photo B (before the discharge treatment).

When taking the pictures of the samples before and after the discharge treatment, the light conditions were kept the same (as far as was reasonably practicable), and a color map was used for calibration. As mentioned before, a photo of the sample and the color map was taken at the same time, before and after the discharge treatment. The change in blue value in the chosen calibration area on the color map is:

$$\Delta C = B_{cA} - B_{cB} \quad (7.2)$$

where ΔC is the change of blue value in the color map caused by the light condition difference;

B_{cA} is the blue value in the calibration area in photo A (after the discharge treatment);

B_{cB} is the blue value in the calibration area in photo B (before the discharge treatment).

Therefore, the actual change in the blue value in the sample caused by the discharge treatment is:

$$\Delta B = \Delta P - \Delta C \quad (7.3)$$

where ΔB is the actual change in blue value caused by the discharge treatment

ΔP is the total change of blue value in sample area

ΔC is the change of blue value caused by the light condition difference

Therefore, the enhancement effect of TiO_2 on decolorisation caused by the plasma treatment can be obtained.

Figure 7.5 shows a picture of the sample (blue dye on the slide with the TiO_2 porous film) and a picture of the color map.

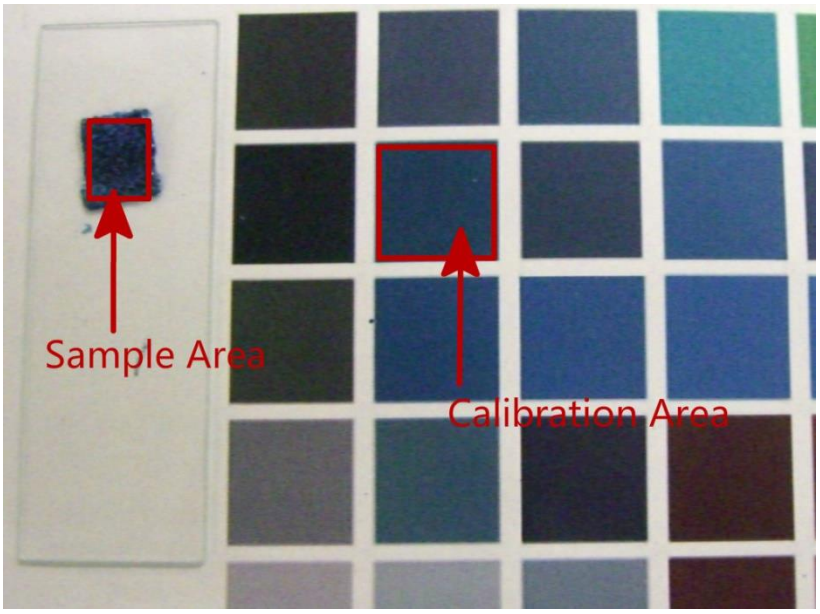

Figure 7.5. Picture of the treated blue dye sample and the color map; the sample and calibration areas are indicated by arrows.

By comparing the ΔB value of the sample treated by plasma discharges with TiO_2 and by plasma discharges only, the enhancement in the degree of decolorisation achieved using TiO_2 can be calculated with (7.4):

$$M = \Delta B_T - \Delta B_C \qquad (7.4)$$

where M is the enhancement degree of decolorisation using TiO_2

ΔB_T is the actual change in blue value caused by discharge treatment with TiO_2 as catalyst

ΔB_C is the actual change in blue value caused by discharge treatment without TiO_2 as catalyst.

7.3.2 Biological Decontamination Tests

The methodology used for the bacterial inactivation tests presented in this chapter is the same as that presented in Chapter 5.2. However, instead of using agar plates seeded with bacteria as the target samples for exposure to plasma discharges, four different approaches were employed in the present studies to establish the potential effect of TiO_2 on the plasma decontamination process.

(1) Biological inactivation tests with TiO_2 porous film

In these tests, instead of seeding bacteria on the agar, a bacterial sample of 50 µl was taken from the suspension with the bacterial population of 10^3 CFU/ml and spread over the glass slide with TiO_2 porous film. Then, this film was treated by the plasma discharges. After the treatment, the glass slide was placed onto the agar plate, and the side with bacteria was fully in contact with the agar and incubated. After 18–24 hours, bacterial colonies were counted.

(2) Biological inactivation tests with TiO_2 topped agar

A 50 µl bacterial suspensions with a population of 10^3 CFU/ml were spread evenly on the TiO_2 topped agar plate. Then, the sample was treated by plasma discharges. After the treatment, sample plates were incubated at 37℃ for 18–24 hours. Surviving bacterial colonies were counted.

(3) Biological inactivation tests with TiO_2 mixed with bacterial suspension

TiO_2 powder (1 g) was added to 99 ml distilled water to make a solution with a TiO_2 concentration of 1% (b/w). Then, this solution was used in the last step of bacterial suspension dilution (series dilution as discussed in Chapter 5.2.3) to have a bacterial suspension with 1% TiO_2. A total of 50 µL of this bacterial suspension was pipetted and spread onto the pure agar plates (no TiO_2 in agar). These samples were exposed to the negative corona discharges produced with a voltage of ~11 kV; average corona discharge current was ~100 µA. Air pressure inside the plasma treatment test cell was 0.2 bar gauge. The treated agar samples were then incubated at 37℃ for 18–24 hours, and the bacterial colonies were counted.

(4) Bacterial inactivation tests with TiO_2 mixed with the bulk agar

In these tests, the bulk agar was mixed with TiO_2 powder. Bacteria were seeded on these TiO_2 agar plates and exposed to the negative corona discharges for specific time intervals. Then, the treated samples were incubated at 37 ℃ for 18–24. As TTC was used in the preparation of agar, the bacterial colonies were in red instead of their original colors (yellowish for *E. coli* and *S. aureus*). After the incubation, bacterial colonies were counted and analysed.

7.4 Indigo Carmine Decolorisation Tests with TiO_2 as Catalyst

It has been reported in several research papers that the plasma discharges in combination with TiO_2 produce significant decomposition of organic molecules in water [275], [276], [277]. As mentioned earlier, TiO_2 can increase the production of the reactive chemical species during the plasma discharge treatment. Hence, it can increase the efficiency of the plasma-induced cleaning and decontamination.

In this section, the enhancement effect of TiO_2 as the catalyst is investigated. The experimental study was based on the decolorisation tests of the indigo carmine water solutions. Indigo carmine solution with a dye concentration of 0.25 g/L was used as a target sample and exposed to the plasma discharges with or without TiO_2. Then, the degree of the decolorisation was obtained and compared, and the enhancement effect of TiO_2 in the plasma treatment was evaluated.

7.4.1 Decolorisation Tests with TiO_2 Porous Film

First, the indigo carmine solution was spread evenly over the glass slide with the TiO_2 porous film. Then, it was treated by the negative corona discharges in the test cell. After the treatment, the degree of decolorisation was obtained and compared with the degree of decolorisation achieved in the discharge treated samples on glass slides without TiO_2. For both the blank slide and the slide with the TiO_2 film, the same

treatment conditions were applied. The treatment conditions that were used in the tests and presented in this chapter are listed in Table 7.1.

Table 7.1. Tested discharge treatment conditions.

Treatment conditions	Volume of dye solution (ml)	Negative Energisation Stress (kV)	Negative Discharge Current (μA)	Pressure inside test cell (bar-gauge)	Treatment Time (min)
Values	1, 2, 3	10, 11, 12, 13, 14	80-140	0.1, 0.2	0-10

The results of this study are summarised as follows: although in some groups of the tests, the decolorisation effect was observed, the enhancement in decolorisation using TiO_2 as catalysts was not achieved. For example, 3 ml indigo carmine solution was completely decolorised on both the blank slide and the slide with TiO_2 film after 10 minutes of treatment with -14 kV corona discharge, as shown in Figure 7.6.

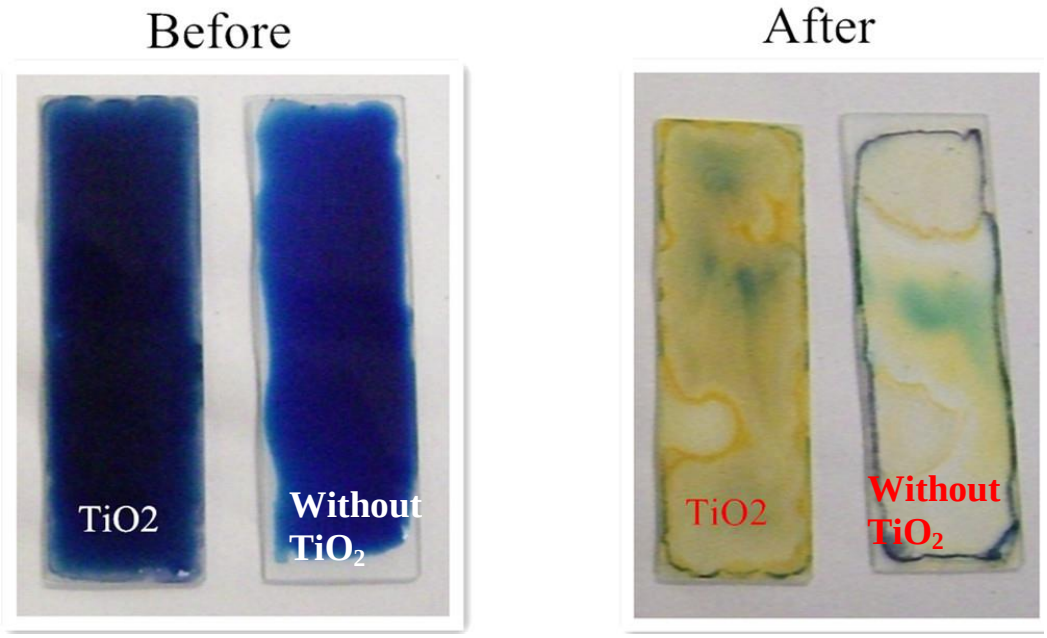

Figure 7.6. Complete decolorisation of indigo carmine by the plasma discharge treatment on glass slides with and without TiO_2 film.

With a shorter treatment time or less intensive discharge, a lower degree of decolorisation was achieved. Due to the influence of the evaporation and gas flow, the liquid solution was no longer uniformly spread over the entire slide; decolorisation was obvious in some areas, but not on the entire slide. It is difficult to quantify this decolorisation effect; the results from visual observation showed no enhancement from using TiO_2. An example is shown in Figure 7.7.

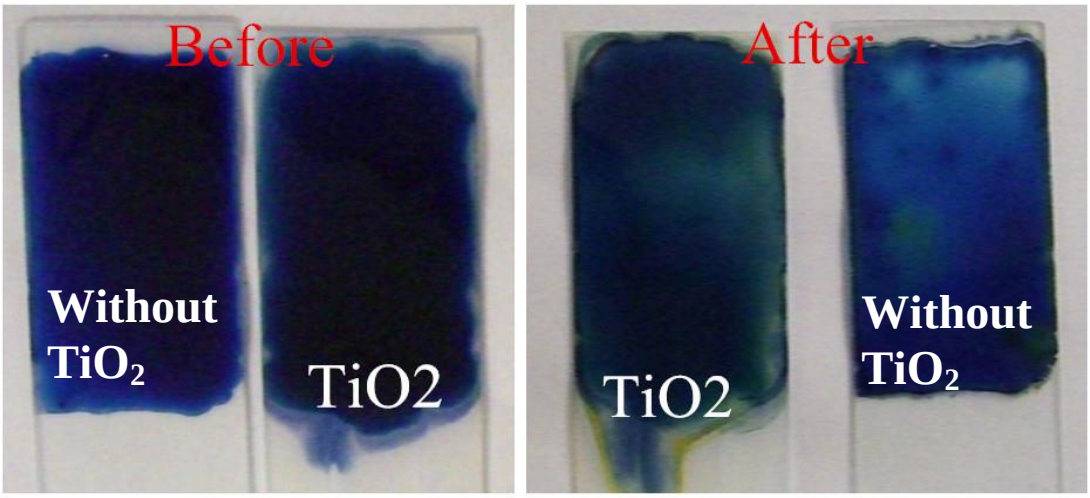

Figure 7.7. A solution of 2 ml indigo carmine on slides with and without TiO_2 and treated by -12 kV corona discharge for 7 minutes (test cell pressure at 0.2 bar gauge).

As shown in Figure 7.7, it is difficult to quantify the decolorisation effect with or without TiO_2 for the treated indigo carmine solution because the decolorisation enhancement in the case of using TiO_2 was not achieved. TiO_2 particles mixed with the liquid and became suspended. Therefore, the solution became visibly cloudy, and the transmittance measurements were not accurate in this situation.

In this approach, TiO_2 did not produce a quantifiable enhancement on the decolorisation effect of the plasma discharges. The liquid sample on top of TiO_2 possibly blocked charged and neutral chemically active particles, and light from discharges, so they were not able to excite electrons in TiO_2 and to increase bio-decontamination and chemical oxidation effects of plasma discharges. Moreover,

an accurate measurement method is needed instead of using optical transmittance for evaluation of the degree of decolorisation.

7.4.2 Decolorisation Tests with TiO_2 Fabric Samples

Another type of samples was tested in this study. White fabric (cut from medical gauze) with and without TiO_2 was used; 1 ml indigo carmine was dropped onto each fabric and exposed to the plasma discharges. After plasma discharge treatment, the degree of decolorisation of the samples with and without TiO_2 was obtained and compared. Decolorisation of indigo carmine was achieved on both fabrics after treatment by the negative corona discharges with voltage stress of -13 kV for 5 minutes (discharge current ~80 μA; measured ozone level was 25–45 ppm). It was observed that the fabrics with TiO_2 produce a higher degree of decolorisation. An example is presented in Figure 7.8.

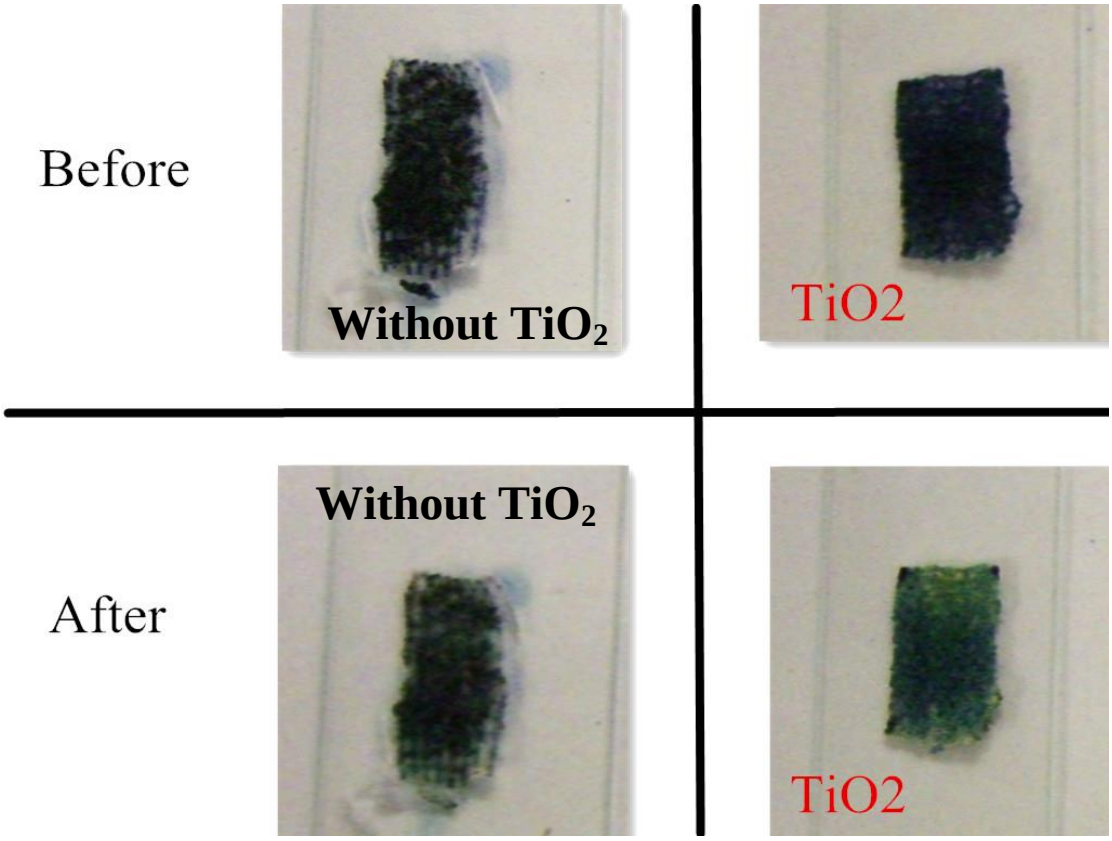

Figure 7.8. Fabric samples with and without TiO_2 treated by negative corona discharge with -13 kV for 5 minutes.

As can be seen from Figure 7.8, the sample with TiO_2 demonstrated a slightly higher degree of decolorisation. Each picture was analysed using the RGB color mapping method in Photoshop, and the actual change in blue value caused by the discharge treatment, ΔB, was calculated by Equations 7.1–7.3. The results are presented in Figure 7.9.

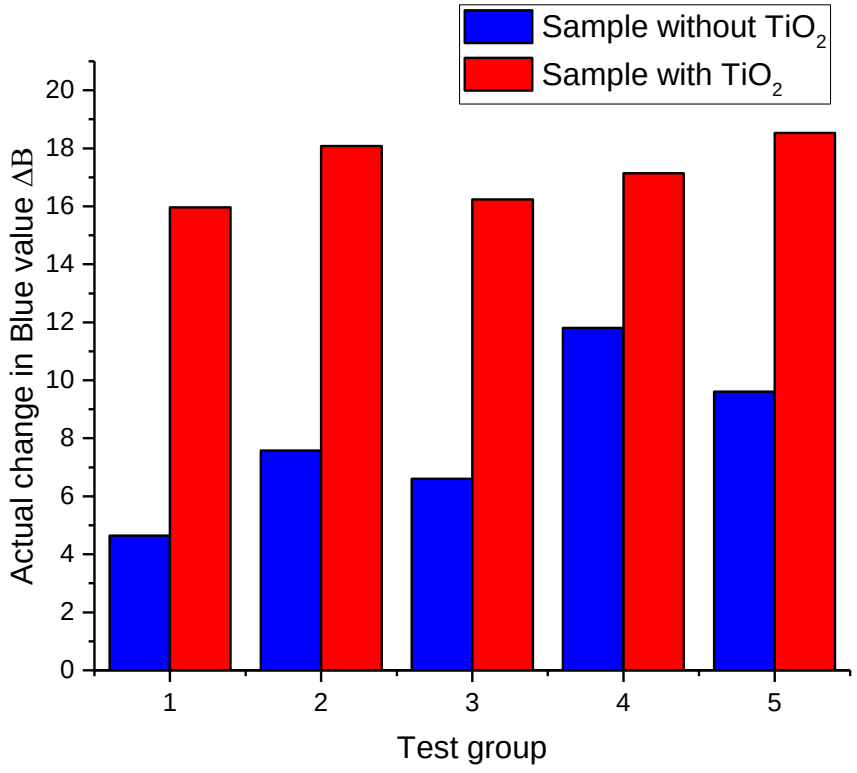

Figure 7.9. Change in the blue values caused by the plasma discharge treatment. Five independent tests (five test groups) were conducted.

Figure 7.9 shows that the change in blue color caused by the discharge treatment is higher in the case of the samples with TiO_2, which means a higher degree of decolorisation was achieved using TiO_2 as catalyst. By applying equation (7.4), the enhancement degree of decolorisation using TiO_2 was calculated. The average enhancement degree in this series of tests is $M = 9.14 \pm 2.32$. The average change in

blue value is 8.05 ±2.76 for samples without TiO_2 and 17.19 ± 1.11 for samples with TiO_2. To summarize, the decolorisation effect was doubled by using TiO_2.

7.4.3 Summary

In this section, preliminary investigation of using TiO_2 as a catalyst to decolorise indigo carmine samples was conducted. Two types of samples were investigated. By using TiO_2 porous film underneath indigo carmine solution, the enhancement decolorisation effect was not observed. The liquid layer of indigo carmine solution could potentially block ions and charged particles generated from non-thermal plasma discharges, and therefore TiO_2 was unable to increase the production of reactive species. Hence, the decolorisation effect was not improved.

In the tests with samples made of fabrics, the results using the sample with TiO_2 demonstrated an enhancement effect in decolorisation of indigo carmine. The change in blue value achieved with the use of TiO_2 was twice higher than in the case of the sample without TiO_2. Two possible reasons can explain this difference: 1) with dried TiO_2 on the fabric, the pores on the fabric were filled with TiO_2, and the area of the sample was increased in this way and a higher degree of decolorisation was achieved; 2) unlike in the case of the porous films, ions and charged particles were able to reach TiO_2 surface, so the number of reactive species produced by plasma was increased, which also can produce a higher decolorisation effect.

Although the enhancement effect was achieved in this series of preliminary tests, several methodological issues require attention. For example, the picture-based RGB value comparison is able to show the degree of decolorisation; however, the change in dye concentration cannot be obtained. Therefore, further investigation of potential effect of TiO_2 on plasma treatment efficiency is required.

7.5 Bacterial Decontamination Tests With TiO_2 as Catalysts

The bacterial inactivation effect of the non-thermal plasma discharges also may be improved using TiO_2 as catalysts. As mentioned before, the production of reactive species by non-thermal plasma discharges could possibly be increased due to the presence of TiO_2. In this section, bacterial decontamination ability of the negative corona discharge treatment with and without TiO_2 is examined. As in the preliminary decolorisation tests, four approaches were tested. In this section, each of the approaches is discussed, and the obtained results are presented. Two types of bacteria were used, *E. coli* and *S. aureus*, as representatives of Gram-negative and Gram-positive bacteria.

7.5.1 Bacteria on TiO_2 Porous Film

E. coli and *S. aureus* samples were prepared in the same way as Chapter 5.2 and diluted to 10^3 CFU/ml in PBS solution. Then, 50 µL of this bacterial suspension was spread evenly on the glass slide with and without TiO_2 porous film and treated by the negative corona discharges with voltage levels of -9 kV, -10 kV, -11 kV, and -12 kV. Atmospheric air was fed to the plasma treatment test cell, and the pressure inside the test cell was kept at 0.2 bar gauge. The treated glass slides were placed onto the agar, the side with bacteria was fully in contact with the agar. Samples were incubated at 37 ℃ for 18–24 hours. It was found that bacterial colonies formed in the slide-agar contact area were too difficult to count. Also, samples were easily contaminated during handling. Therefore, this approach was unsuitable for these tests.

7.5.2 Bacteria on TiO_2 Topped Agar

A 50 µL bacterial suspension with a population of 10^3 CFU/ml was spread on TiO_2 topped agar plates (topped with 10% or 1% TiO_2 solution) and exposed to the negative corona discharges (voltage levels of -9 kV, -10 kV, -11 kV, and -12 kV). Atmospheric air was fed to the test cell to keep the pressure at 0.2 bar gauge level.

Then the treated samples were incubated. It was found that bacterial colonies were unable to form correctly on agar with a TiO_2 layer on top. Therefore, this method was not used.

7.5.3 Bacterial Suspension Mixed with TiO_2

As mentioned in Section 7.3.2 (3), bacterial suspensions mixed with TiO_2 were spread on top of agar and treated by negative corona discharge with a voltage of -11 kV. The average corona discharge current was ~100 μA. The air pressure inside the test cell was 0.2 bar gauge. During the discharge treatment, the concentration of ozone was measured and found to be 15–35 ppm. The samples were treated for 30 seconds, 1 minute, and 3 minutes. The results are shown in Figure 7.10 and Figure 7.11.

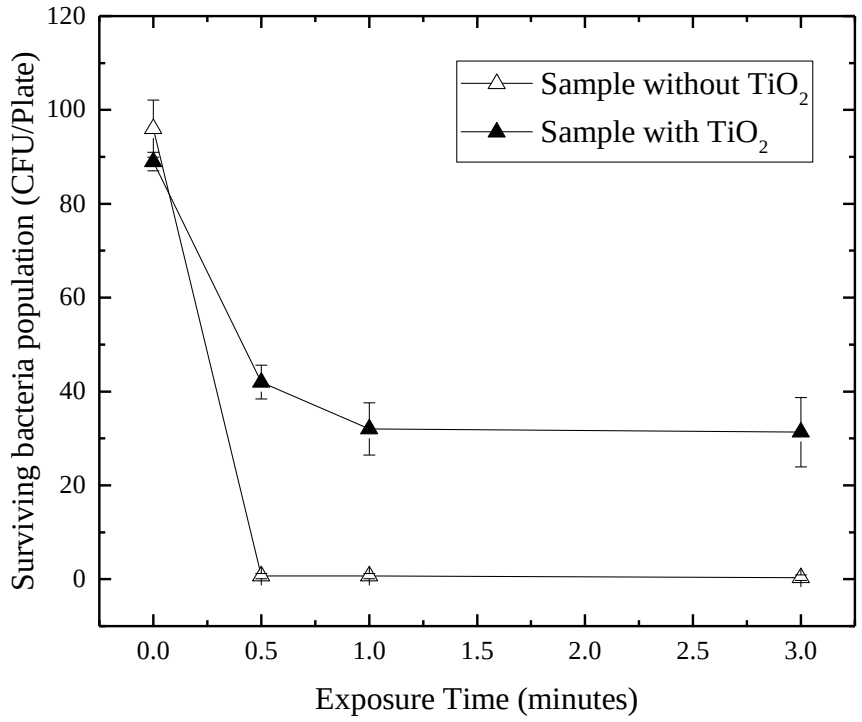

Figure 7.10. *E. coli* populations as a function of exposure time using negative corona discharge treatment with and without TiO_2 as the catalyst. Bacteria samples were prepared through bacteria suspension mixed with TiO_2. Each point in this figure represents an average of three independent tests. The error bars show standard deviation values. Solid lines are for visual guidance only.

The initial population of *E. coli* in these tests was 87–100 CFU/plate. After the treatment with negative corona discharges for 30 s without TiO_2, *E. col*i population on the agar plate was reduced to ~1 CFU/plate, which means that 99% of *E. coli* were inactivated. However, a lower degree of inactivation was achieved on the samples treated with TiO_2, with an average 31 CFU/plate observed after 3 minutes exposure. By adding TiO_2 to bacterial suspension and then treating these samples with plasma discharges, it was shown that no enhancement in inactivation of *E. coli* was achieved. On the contrary, the inactivation effect was weakened in the presence of TiO_2.

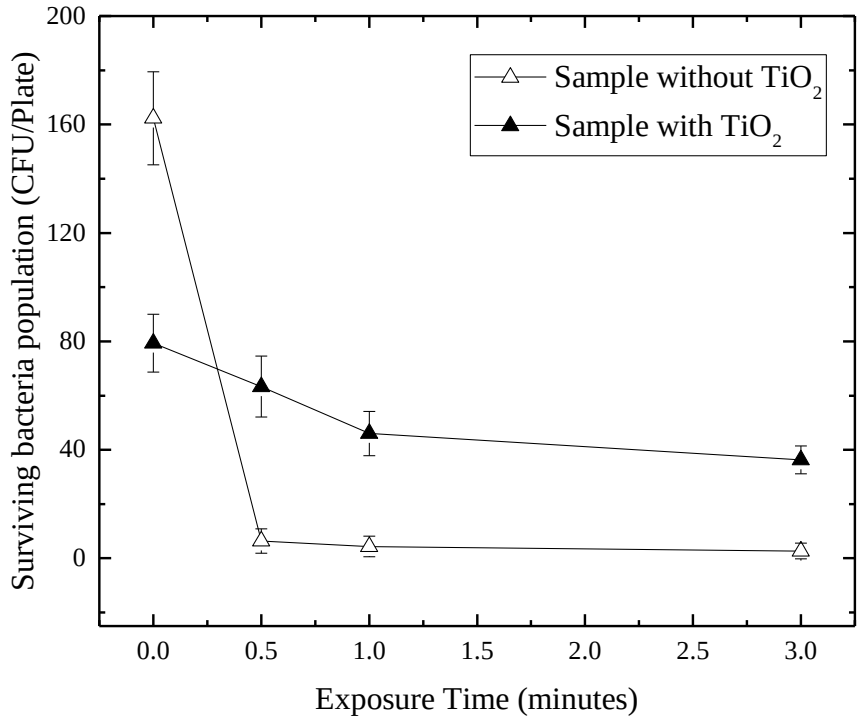

Figure 7.11. *S. aureus* populations as a function of exposure time using negative corona discharge treatment with and without TiO_2 as the catalyst. Bacteria samples were prepared through bacteria suspension mixed with TiO_2. Each point in this figure represents an average of three independent tests. The error bars show standard deviation values. Solid lines are for visual guidance only.

Figure 7.11 shows the populations of *S. aureus* treated with negative corona discharges with and without TiO_2. The initial population of *S. aureus* was 144–178 CFU/plate on the agar plate when bacterial suspensions without TiO_2 were used. This

number decreased to less than 10 CFU/plate after 30 seconds of the plasma discharge treatment. In the case of adding TiO_2 into the bacterial suspension, the initial population of *S. aureus* was much lower: ~80 CFU/plate. This population was also reduced after exposure to the plasma discharges. However, the reduction was much lower; the population of *S. aureus* was ~36 CFU/plate, even after treatment by the plasma discharges for 3 minutes.

Again, the enhancement effect of using TiO_2 was not observed in this method. The difference in the initial populations of microorganisms showed that TiO_2 had a negative effect on the *S. aureus* population and resulted in a 50% lower initial population.

7.5.4 Bacteria Seeded on Agar Mixed with Tio_2

In this section, TiO_2 was mixed with nutrient agar powder and distilled water (concentration of TiO_2 was 1% (b/w)), and sterilised to make a special type of agar. A total of 3.75 mg TTC was added to make the mixture, which was metabolized by the bacteria and made the bacterial colonies appear to be red. This allowed for easier enumeration against the white background of TiO_2-agar mixture, as shown in Figure 7.12.

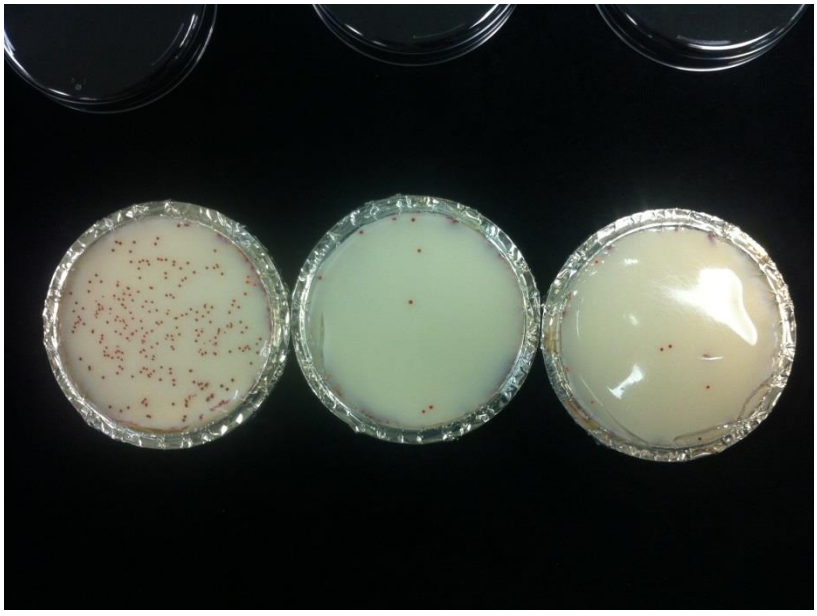

Figure 7.12. TiO_2 (1% (b/w)) mixed agar seeded with *S. aureus.*

These tests showed that the presence of TiO_2 does randomly influence the growth of bacteria on agar. This type of agar is also very easily dried during incubation. Therefore, it was concluded that 1% TiO_2 mixed agar was not suitable for this study.

Again, problems with the presence of TiO_2, at these concentrations appeared to have a negative impact on bacterial growth, making accurate experimental procedures difficult. This method was therefore not suitable.

7.5.5 Summary

In this section, the testing of four different methods is presented to examine the bacterial inactivation capability of the plasma discharges enhanced using TiO_2 as the catalyst. The enhancement effect brought by using TiO_2 in the plasma discharge treatment was not achieved in this series of experiments. Methods used in this study were proved not suitable for bacterial inactivation test, as the growth of bacteria were affected by TiO_2, and samples could be easily contaminated during handling.

Although no suitable method for testing of potential positive effects of TiO_2 on bio-decontamination efficiency of the plasma discharges was found, and the enhancement effect of TiO_2 was not achieved, valuable information still was obtained in this series of preliminary tests. For example, it was established that it would be beneficial to avoid direct contact between bacteria samples and TiO_2 particles. However, as mentioned in the decolorisation section of this chapter, TiO_2 particles should be in contact with electrons and ions generated by discharges to achieve increased production of chemically active species. Further investigation on the application of TiO_2 for enhancement of bio-decontamination effects of plasma discharges is required.

7.6 Discussion and Conclusions

In this chapter, several attempts were made to investigate the potential enhancement effect of using TiO_2 as the catalyst in the non-thermal plasma discharge treatment. Preliminary experiments were performed by decolorisation of indigo carmine dye and by inactivation of *E. coli* and *S. aureus*.

In the decolorisation tests, the indigo carmine solution was added on TiO_2 porous film and on TiO_2 added fabric; these samples were treated by the negative corona discharges. No significant enhancement effect was observed when the TiO_2 film was used. Alternatively, by analysing the blue value on the images of the treated and untreated samples, the enhancement effect was observed in the case of the treatment of indigo carmine solution placed on TiO_2-fabric samples. The increase in the blue value on the images of the sample with TiO_2 is twice that on images of the sample without TiO_2 after the plasma discharge treatment. However, the results obtained at this stage are insufficient to provide information for optimisation of the non-thermal plasma discharge treatment, and further studies are required.

Based on the results obtained in this study, the following conclusions can be made. First, the interaction between the plasma discharges and TiO_2 particles should be increased. When using the TiO_2 porous film, indigo carmine solution on the top of TiO_2 possibly blocks ions, charged particles, and even UV light produced by the plasma discharges. Hence, no enhancement was achieved. A suitable test configuration is needed to introduce TiO_2 particles to the plasma discharge system, such as that described in [278], where TiO_2 coated glass pellets were used in the air-liquid-solid system to enhance the decomposition of harmful chemical components by the plasma discharge treatment. TiO_2 in the form of porous film or powder could be mixed in the liquid samples and present difficulty for separation of the fine TiO_2 particles and liquid after plasma treatment. It is not possible to measure the optical transmittance of the samples accurately in this situation. Further improvements in the experimental system and methodology are required to overcome this issue. One possible approach is given in [279] and [280], where an electrochemical deposition method was used to make a TiO_2 thin film which cannot be mixed with the liquid solution.

Decolorisation of indigo carmine dye placed on TiO_2-fabric was evaluated by comparing the blue value on the pictures of the treated samples with the blue value obtained from the pictures of the untreated samples. Although the comparison showed an enhancement in the change of the blue color numbers achieved in the case of the TiO_2 samples, this method is not accurate enough to quantify the concentration of indigo carmine dye after the plasma treatment. In addition to measuring the optical transmittance, other methods could be used for evaluation of potential catalytic effects of TiO_2. For example, High-Performance Liquid Chromatography (HPLC) was used in [280] to measure the concentration of phenol in the liquid sample after the non-thermal plasma discharge treatment.

TiO_2 was also used to enhance the bacterial inactivation effect of the non-thermal plasma discharges. However, the results show that there was no conclusive outcome in this study. It was found that TiO_2 particles could interfere with the culture of bacterial samples. Also, it is difficult to introduce TiO_2 into the non-thermal plasma treatment system while keeping both bacteria sample and TiO_2 directly exposed to the plasma discharges. Using TiO_2 to enhance the bio-decontamination effect of atmospheric plasma discharge is a new topic, there are not too many published results in this area. However, many papers have reported that TiO_2 has enhanced the bio-decontamination effect of UV radiation. The advanced methodology could be used in the research of plasma/TiO_2 system. It was reported in [255] that TiO_2 film prepared through sol-gel method, chemical vapour deposition (CVP) and plasma enhanced chemical vapour deposition (PECVP) showed an enhanced bactericidal effect during exposure to UV radiation. The film they used in the study does not interfere the growth of bacteria. In another research [281], a plasma-spraying TiO_2 coating method was used, the material coated with TiO_2 was merged into fungus liquid and treated by UV radiation, fungus liquid was then withdrawn and used to culture fungus on agar. The TiO_2 film and coating reported in these study could be used in future research of TiO_2 in plasma discharge treatment. For example, coatings could be applied to grounded electrode (aluminum foil lined plate).

The experimental topology and methodology should be improved for future studies of potential catalytic effects of TiO_2 in combination with plasma discharges.

CHAPTER 8

Conclusions and Future Work

8.1 General

The atmospheric non-thermal plasma discharge is a novel, powerful technology for bio-decontamination, disinfection, and oxidation in cleaning operations. Although the oxidation and micro-biological decontamination effects of atmospheric non-thermal plasma discharges have been studied by many researchers, the mechanisms of these effects are not fully understood, and the efficacy of plasma treatment may vary depending on the discharge parameters. The current research presents an investigation of the oxidation and micro-biological decontamination efficacy of the DC steady-state corona discharges and transient plasma discharges. Different discharge topologies were used along with different discharge parameters including voltage levels, energisation polarities, and air humidity.

In the investigation of the oxidation efficacy of the atmospheric plasma discharges, a blue dye (indigo carmine) water solution with an initial dye concentration of 0.25 g/L was used as a chemical sensor. The dye solution was decolorised by the plasma discharge treatment, and changes in optical transmittance of the treated samples were measured and used to obtain the reduction in dye concentration. Thus, by comparing the reduction in dye concentrations caused by the different types of plasma discharges, their oxidation capability was obtained.

The micro-biological decontamination capability of the plasma discharges was investigated through a series of bacterial inactivation experiments. Gram-negative and Gram-positive bacteria, *E. coli* and *S. aureus*, were seeded on agar plates and treated by plasma discharges. Bacterial population was enumerated, and it was found that the plasma discharges reduced bacterial population. Thus, the decontamination capability of the plasma discharges was measured.

The concentration of hydroxyl radicals produced by the plasma discharges in water solution was measured using sample solutions made with 2 mM TA acid and 5 mM NaOH. Hydroxyl radicals produced by the plasma discharges reacted with TA and

formed HTA, which gives fluorescent signals at 425 nm. The fluorescence signals from the plasma-treated sample solution were obtained and used to calculate the concentration of OH radicals. The OH radical production rates by different types of plasma discharges were obtained, and these results were compared with the oxidation and bio-decontamination efficiencies of plasma discharge treatment.

In this study, an attempt was made to use a catalyst to enhance the oxidation and micro-biological decontamination effects of plasma discharges. TiO_2 was selected as a potential catalyst and used in the plasma discharge treatment tests. Several different approaches of introducing TiO_2 into the plasma system were identified, and indigo carmine decolorisation tests and bacterial inactivation tests were performed with and without TiO_2. Comparing the results, the enhancement effect of TiO_2 in each approach was evaluated, and the results were discussed.

This research confirmed the great potential of non-thermal atmospheric plasma discharges in cleaning and bio-decontamination. Methodologies and the obtained results with analysis are presented in this thesis. In this final chapter, conclusions obtained for each aspect of this study are presented, and directions for future work are also discussed.

8.2 Conclusions

8.2.1 Oxidation Capabilities of Non-Thermal Atmospheric Plasma Discharges

One of the main findings of this research was the establishment of the oxidation effects of the DC steady-state corona discharges and transient plasma discharges. The oxidation effects of the atmospheric non-thermal plasma discharges were studied using indigo carmine decolorisation under the action of the plasma treatment.

It was found that in the case of the steady-state corona discharges, the polarity of energisation affects the oxidation capability of the plasma discharges. In all tested electrode topologies, direct or indirect plasma treatment, it was established that higher

decrease in the dye (indigo carmine) concentration is achieved using the negative discharge treatment rather than the positive discharge treatment. This effect is more pronounced in the case of the direct plasma exposure; 10 minutes of negative corona discharge treatment resulted in a reduction of the dye concentration to 0.17–0.19 g/L, starting with the initial concentration of 0.25 g/L; while in the case of 10 minutes of positive discharge treatment, the final concentration was only 0.23 g/L. It was also established that the decolorisation process is a charge-dependent process. Although the total charge delivered to the dye samples was higher in the negative energisation case, the charge-dependent decolorisation rate (see Table 4.1) showed that the negative corona discharges produce a higher efficiency. It is suggested that this is due to a higher concentration of the reactive species produced by the negative corona discharges. For example, ozone concentration was much higher during the negative corona discharges rather than during the positive corona discharges. This confirms that chemically reactive species produced by atmospheric plasma discharges play an important role in the process of plasma-induced oxidation.

The oxidation capability of corona discharges is also influenced by the electrode topologies. It was established that higher decolorisation rates were achieved in samples directly exposed to the corona discharges as compared with indirect exposure. However, this difference is not only caused by the charged particles that can reach the sample surface in the case of direct exposure. The distance from the stressed HV electrode to the sample surface is shorter in this case, which makes it easier for short-lived chemical species to reach the sample surface. Therefore, the direct corona discharge treatment has higher oxidation efficiency. It was found that the decolorisation rate of indigo carmine caused by positive corona discharges is 3.22 C^{-1}, while the negative corona discharge treatment resulted in the decolorisation rate of 7.36 C^{-1}. In the case of indirect exposure, the achieved decolorisation rates were 2.79 C^{-1} and 4.35 C^{-1} with positive and negative polarity, respectively.

Also of note, it was found that the humidity of atmospheric air affected the oxidation efficiency of corona discharges to a lesser degree. The humidity of air used in this research was 12.5% and 40%, and it was found that this difference was insufficient to cause a significant change in decolorisation of the dye solution. In the confined test cell with liquid solution sample, this difference in humidity could be compensated by water vapor produced during the discharge.

In the case of the transient plasma discharges, the decrease in dye concentration was found to be a function of the total delivered charge. The polarity of energisation also had an influence on the oxidation capability, but this influence is different with the corona discharge case. In the case of surface discharges, the negative discharge treatment resulted in a slightly higher decolorisation rate (5.42 C^{-1} for positive and 5.77 C^{-1} for negative), while in the case of the direct transient plasma discharge, the positive discharge treatment resulted in a much higher decolorisation rate (7.59 C^{-1} for positive and 4.72 C^{-1} for negative). It was established that the breakdown voltage does not significantly affect the decolorisation effect: 20 kV, 24 kV, and 28 kV discharge treatment demonstrated similar charge-dependent decolorisation effects.

The reactive species are considered to be very important in the decolorisation of dye solution by the transient spark discharge treatment. Since the ozone concentration is undetectably low during all experiments with transient spark discharges, other reactive species such as OH radicals and NO_x species could be responsible for the decolorisation, especially NO, which has been reported to have a higher production rate by the positive discharges [221], [222]. In the case of the direct transient spark discharge treatment, the distance between the needle tip and the liquid surface is longer when the positive energisation mode is used to maintain the same breakdown voltage with the negative discharge. This could cause a difference in the production of NO and other nitrogen species; then, additional chemical reactions could be triggered and could result in a different decolorisation effect. Generally, the oxidation capability of the transient spark discharge treatment depends on delivered charge, polarity, and discharge topologies.

This research also confirmed the plasma-induced acidification effect. The decrease in pH was observed in the samples treated by plasma discharges, and it was found that the decrease in pH corresponds to the decolorisation effect.

8.2.2 Bio-Decontamination Capabilities of Non-Thermal Atmospheric Plasma Discharges

The bio-decontamination effect of both steady-corona discharge and transient spark discharge was found and investigated in the study. It was established that the plasma discharge treatment resulted in the inactivation of both *E. coli* (Gram-negative) and *S. aureus* (Gram-positive). It was found that for the same type of discharge treatment, the degree of inactivation is a function of the total delivered charge. The bio-decontamination efficiency was obtained and characterised by the charge-dependent inactivation rate.

In the case of steady-state corona discharge treatment, the different polarity of energisation resulted in a significant difference in the bio-decontamination effect. Using the negative direct corona discharge treatment, 99% or even complete inactivation was achieved with only ~5 mC delivered charge. The estimated inactivation rate of the negative direct corona discharges was 0.978 mC^{-1} and 1.441 mC^{-1} for *E. coli* and *S. aureus*, respectively. When the positive energisation mode was used, the inactivation rate was 0.029 mC^{-1} for *E. coli* and 0.037 mC^{-1} for *S. aureus*. High inactivation rate also was achieved using the negative indirect corona discharge treatment: 0.575 mC^{-1} and 0.264 mC^{-1} for *E. coli* and *S. aureus*, respectively. The inactivation rate was only 0.031 mC^{-1} and 0.023 mC^{-1} for *E. coli* and *S. aureus* in the case of positive indirect corona discharge treatment.

Ozone as a strong inactivation agent is produced by the corona discharges, and it is believed that ozone, amongst other chemical species, is responsible for oxidation and bio-decontamination effects. It was found that the ozone concentration was much lower in the case of positive corona discharges, ~2 ppm, as compared with 12–30 ppm produced by negative indirect discharge treatment and 20–60 ppm by negative direct discharge treatment.

Comparing these results of direct and indirect corona discharge treatment, it was established that indirect topology resulted in a slightly higher inactivation effect. However, the obtained difference in the case of direct and indirect treatment is not significant, which proved that neutral chemical species (ozone in this case) play the dominant role in inactivation instead of charged particles.

It was found that in the case of the transient spark discharge treatment, the decontamination effect also was affected by the polarities of the energisation modes. However, the positive transient spark discharges produced higher charge-dependent decontamination rates, especially in the case of the direct transient spark discharge treatment. The decontamination rate of the positive discharges is more than twice the decontamination rate produced by the negative discharges. As in the case of indigo carmine decolorisation tests, the ozone concentration was undetectably low in all tested transient discharge treatment cases; therefore, other reactive species such as OH radicals and NO are considered to play the important role in bacterial inactivation.

To establish the effect of the voltage on bio-decontamination capability of plasma discharges, different breakdown voltage levels were tested. However, it was found that the difference in the plasma-induced decontamination results was not very obvious. Alternatively, it was found that Gram-negative bacteria were more sensitive to the transient spark discharge treatment than Gram-positive bacteria. The thicker peptidoglycan layer of Gram-positive bacteria may help to protect them from the lethal damage from transient spark discharge treatment.

Higher decontamination rates were achieved using the surface discharge treatment. Surface discharges propagate through the sample/air interface. Therefore, these discharges treat a larger sample area. Major chemical reactions took place at the sample/air interface, and the bacteria were seeded on top of the agar. Therefore, surface discharges provided a higher inactivation rate.

In general, it was established that the steady-state corona discharges with negative polarity provide high decontamination rates, and both types of bacteria can be successfully inactivated in a very short time. The decontamination rates obtained in the case of steady-state corona discharges are much higher than the decontamination rates provided by the negative transient spark discharge treatment. It is believed that ozone with high concentration produced by negative corona discharges effectively participated in the bacterial inactivation process and resulted in such a high inactivation rate; while in the case of negative transient plasma discharges, ozone concentration is undetectably low.

When positive energisation mode was used, the transient spark discharge treatment provided a higher decontamination rate than positive corona discharge treatment. Unlike negative corona discharge, the positive corona discharge produces ozone with very low concentration (~2 ppm). Although this concentration of ozone is higher than in the case of transient plasma discharges, it is not enough to provide stronger bio-decontamination effects than positive transient plasma discharge. In this situation, OH radicals play an important role in plasma-induced bio-decontamination. As presented in Chapter 6, the positive transient plasma discharges provide a higher OH production rate than the positive corona discharges. Thus, a higher bio-decontamination rate was achieved by using positive transient plasma discharges rather than positive corona discharges.

In general, non-thermal plasma discharges provide a novel alternative approach for bio-decontamination. A comparison between Non-thermal plasma discharges and commonly used sterilization technologies are showed in Table 8.1.

Table 8.1 Comparison between non-thermal plasma and commonly used sterilisation technologies.

		Process	**Mechanisms**	**Material compatibility**	**Advantages**	**Disadvantages**
Non-Thermal Plasma Discharges	Steady-state corona discharges Impulsive transient plasma discharges	Straightforward exposure to plasma discharges, Ambient environment, Short treatment time (minutes)	Complex mechanism, plasma agents cause irreversible damage to the cell wall, membrane, DNA and its internal components	Compatible with most materials, including heat sensitive materials and liquids.	Straightforward process. Laboratory proved high efficacy. Environment-friendly. Applicable to a wide range of micro-organisms. Low temperature. No resistance of microorganisms reported.	Mechanism is not fully understood. Requires high voltage system. Further development is required for large scale treatment.
Commonly Used Sterilisation Technology	Ethylene Oxide	Complex process, Gas concentration (450 to 1200 mg/l); at 37 to 63 ℃; Relative humidity 40 to 80%; exposure time: 1 to 6 hours [286].	alkylation reaction with nucleic acid and functional proteins, causing denaturation [285]	Compatible with heat sensitive materials, incompatible with liquids.	Historically acceptable. High efficacy. Can be used for variety of material at low temperature.	Toxic and flammable gas. Long quarantined time (7-14 days). Complex process.

	Autoclaving	121 ℃ at ~100 kPa for tens of minutes with saturated steam [283].	Causing irreversible denaturation of enzymes and structural proteins [284].	Stainless steel glass and other materials. Incompatible with heat sensitive materials.	Most commonly used sterilization method. High efficacy. Simple and fast process. Low cost and non-toxic.	Require high temperature and pressure. Incompatible with heat sensitive materials such as most of plastics.
	Dry Heat	160 ℃ for 2 hours, or 170 ℃ for 1 hour. Dry environment [283]	Causing oxidation of cell constituents [284]			
	Electron Beam	Exposure to high energy electrons. Short treatment time (minutes)	Damage to DNA, indirect damage through generated radicals. [287]	Compatible with most materials.	Safe method with low oxidation damage, Compatible with most of the materials, fast process. [287]	Limited penetration, expensive equipment, Complexity of the system.
	Gamma Irradiation	Exposure to gamma radiation using the radioisotope Cobalt 60 as its energy source [288].	Breaking down DNA by high energy ionizing radiation , inhibiting cell division [289].	Compatible with most materials, incompatible with material such as PVC, plyacetals Polytetrafluoroethene [289].	Complete penetration. Non-thermal method. Bulk process. Widely used for many years.	Require radioactive source. Expensive system. Not compatible with some materials, causes degradation of polymers.
	UV	Exposure to UV lights (especially UV-C).	Damages the nucleic acids, disrupts DNA through UV photons [291].	Compatible with most materials, incompatible with polymers, may cause degradation of plastic materials.	Low cost. Simple process, widely applied in many areas such as water, air and food decontamination. [293].	Lack of penetration, Safety issues. Cause degradation of plastic material [290], [292].

8.2.3 OH Radical Production of Non-Thermal Atmospheric Plasma Discharges

Both steady-state corona discharge and transient spark discharge are proved to be able to produce OH radicals, and it was found that the OH radical production by plasma discharges is a charge-dependent process.

In the case of the steady-state corona treatment, negative discharges demonstrated a higher OH radical production rate for both indirect and direct topologies. This is in line with the results from the decolorisation tests which demonstrated a higher oxidation capability of the negative corona discharges. Ozone production by negative corona discharges is also higher than by positive corona discharges, which could partly contribute to a higher OH production.

Another important fact which was established in the present study is that the air humidity does not have a significant influence on the OH radical production. Most of the OH radicals were produced near the liquid/air interface or in the liquid sample. There might be some OH radicals produced in air and induced into the liquid sample, but due to the low production in the air and the short-lived feature of OH radicals, this part is negligible.

It was found that the charge-dependent rate of the indirect corona discharge treatment is 0.059 μM/mC for positive discharges and 0.517 μM/mC for negative discharges. In the case of direct corona discharge treatment, this rate is higher, 0.067 μM/mC for positive and 0.881 μM/mC for negative. In addition to the effect of ozone, charged particles produced by corona discharge and reaching the liquid sample surface during direct treatment could contribute to OH radical production.

In the case of transient spark discharges, the OH production efficiency is higher than corona discharge when the positive energisation mode is used: the production rates were 0.102 μM/mC for the surface discharge treatment and 0.271 μM/mC for the direct discharge treatment. In the case of positive transient plasma discharges, OH radicals are mostly generated at the sample/air interface or through the bulk of the liquid. In the case of corona discharges, OH radicals are mostly generated in air and

diffused into the liquid. Although positive corona discharges interact with water, this interaction is less intensive than in the case of transient plasma discharges. In addition, the HV stressed electrode in the case of positive transient plasma discharges is closer to the sample surface (distance ≤ 11.06 mm) than in the case of corona discharges (25 mm for direct treatment and 50 mm for indirect treatment) Thus, short-lived OH radicals or species that are responsible for OH radical generation can reach the liquid surface more easily in the case of transient plasma discharges. Hence, a higher charge-dependent inactivation rate was achieved by using positive transient plasma discharges rather than positive corona discharges.

When the negative energisation mode is used, the production rates were 0.14 μM/mC for the surface discharge treatment and 0.225 μM/mC for the direct discharge treatment, which are lower than for the negative corona discharge treatment. This difference is believed to be caused by different ozone concentrations. Negative corona discharge produces much higher ozone, hence it results in a higher OH production rate.

Compared with surface discharge topology, OH radical production rate was almost doubled by using the direct discharge treatment. This could be a result of reactions which produce OH radicals in the bulk of liquid via the O=NOOH pathway. Also, the direct transient plasma discharge treatment with positive energisation mode has a higher OH production rate than the negative energisation mode. This can be explained by higher concentration of NO_x produced in the positive energisation mode. These chemical species participate in the reaction in the bulk of liquid and produce more OH radicals.

According to the results obtained in this OH radical detection study, the OH radical production rates of steady-state corona discharges and transient spark discharges correspond to their oxidation and bio-decontamination effects. This provides strong evidence to prove the importance of OH radicals in plasma discharge related applications.

8.2.4 TiO_2 as Catalyst to Enhance the Plasma Discharge Treatment

TiO_2 is considered to be able to enhance the oxidation and bio-decontamination efficiency of the plasma discharge treatment. However, the results obtained in this experimental study demonstrated that an efficient way of introducing TiO_2 into the plasma discharge system is required.

In the dye decolorisation tests, the TiO_2 layer underneath the dye solution was not able to provide enhancement to the decolorisation effect produced by corona discharge. This is believed to be because the UV radiation, ions, and electrons generated by corona discharge were blocked by the liquid sample itself and were not able to contact the TiO_2. However, introduction of TiO_2 to the fabric resulted in an enhancement in the decolorisation effect produced by the plasma discharge treatment. Potentially, more reactive species were produced in this case due to the existence of TiO_2. Furthermore, dried TiO_2 covered the hole in the fabric sample, which enlarged the area of treatment.

The enhancement effect by using TiO_2 in corona discharge to inactivate bacteria was not achieved in this study. TiO_2 interfered with the growth of bacteria on the agar samples. Before making any conclusions on whether or not TiO_2 could enhance the bio-decontamination effect of plasma discharges, further study is needed.

8.3 Future Work

A comprehensive study of oxidation/bio-decontamination effects of non-thermal atmospheric plasma discharge was completed in this research project. However, multiple aspects still must be investigated to provide a better understanding of the mechanisms of plasma oxidation and bio-decontamination effects and for optimisation of plasma treatment efficiency in practical applications.

First, investigation of the reactive species generated by plasma discharge should be continued. In this research, ozone and OH radicals were measured during the discharge treatment. Ozone and OH radicals have very strong oxidation ability, and

they make a significant contribution to the oxidation and bio-decontamination processes of the non-thermal plasma discharge treatment. However, other reactive species generated by plasma discharges cannot be ruled out completely. For example, in the transient spark discharges which were studied in this research, nitrogen species produced by these discharges could have an effect on the oxidation and bio-decontamination capabilities. Also, those species could be involved in the reactions of generating OH radicals in liquid. Therefore, further investigation of their production is necessary, including detection and measurement of the reactive species generated by plasma discharge with different polarities and topologies.

Two types of bacteria were tested in this research: *E. coli* and *S. aureus*, representing Gram-negative and Gram-positive bacteria, respectively. It will be beneficial to use other types of bacteria in future inactivation tests. Different types of bacteria may have different sensitivities to the plasma discharge treatment, and this difference may be caused by the different cell structures. Further investigation on sensitivity of bacteria to plasma treatment can help in understanding the bio-decontamination mechanisms of plasma discharges.

The non-thermal atmospheric plasma discharges were acting primarily on the target sample surface in this research. The surface area and sample volume are small (55 mm diameter, 6 ml volume), the effect of plasma discharge may cover all of the sample surface. It will be important to investigate the effective area of the plasma discharge treatment. This can be done by applying plasma discharge treatment to samples with larger surface area. The effective depth of the plasma discharge treatment on samples also must be investigated.

In the present study, an attempt to use TiO_2 as catalyst was made; however, it did not show the desired enhancement effect. This is primarily due to lack of an efficient approach to introduce TiO_2 into the plasma system. However, this approach has merit, and further investigation with different topologies can potentially provide more confident results.

The synergetic effect between non-thermal plasma treatment and other decontamination technologies should also be investigated. As in [294], Gao *et. al.*. performed series of experiments on disruption of bacteria cell in waste activated sludge, they reported that higher efficiency could be achieved by using a combination

of DC corona discharge and pulsed electric field. It is highly possible that bio-decontamination and oxidation effect can also be increased by using a combination of plasma discharge and other technologies. Therefore, future research in this area is also needed.

In general, the non-thermal plasma discharge technology has great potential in many practical applications. It is a novel technology, and further investigation and development is required before it will meet wider industrial standards. To achieve a better understanding of the plasma oxidation and bio-decontamination mechanisms, and to optimise the energy efficiency of the plasma treatment, it will be important to continue to study the plasma chemical and biological effects.

REFERENCES

[1] V. Scholtz, J. Pazlarova, H. Souskova, J. Khun, and J. Julak, "Nonthermal plasma - A tool for decontamination and disinfection," *Biotechnol. Adv.*, vol. 33, no. 6, pp. 1108–1119, 2015.

[2] H. Kim, "Nonthermal plasma processing for air-pollution control : A historical review, current issues , and future prospects," *Plasma Process. Polym.*, vol. 1, pp. 91–110, 2004.

[3] D. Bayliss, "Understanding the inactivation mechanism of foodborne pathogens using cold atmospheric plasma," Ph.D Thesis, Loughborough University, 2012.

[4] S. Hati, S. Mandal, S. Vij, P. S. Minz, S. Basu, Y. Khetra, D. Yadav, and M. Dahiya, "Nonthermal plasma technology and its potential applications against foodborne microorganisms," *J. Food Process. Preserv.*, vol. 36, no. 6, pp. 518–524, 2012.

[5] A. Mizuno, "Industrial applications of atmospheric non-thermal plasma in environmental remediation," *Plasma Phys. Control. Fusion*, vol. 49, pp. A1–A15, 2007.

[6] B. Haertel, T. Von Woedtke, K. Weltmann, and U. Lindequist, "Non-thermal atmospheric-pressure plasma possible application in wound healing," *Biomol Ther*, vol. 22, no. 6, pp. 477–490, 2014.

[7] R. Ono and T. Oda, "Optical diagnosis of pulsed streamer discharge under atmospheric pressure," *Int. J. Plasma Environ. Sci. Technol.*, vol. 1, no. 2, pp. 123–129, 2007.

[8] W. F. L. M. Hoeben, E. M. van Veldhuizen, W. R. Rutgers, and G. M. W. Kroesen, "Gas phase corona discharges for oxidation of phenol in an aqueous solution," *J. Phys. D Appl. Phys.*, vol. 32, pp. L133–L137, 1999.

[9] Z. Buntat, I. R. Smith, and N. . A. . Razali, "Ozone generation by pulsed streamer discharge in air," *Appl. Phys. Res.*, vol. 1, no. 2, pp. 2–10, 2009.

[10] P. Lukes, M. Clupek, V. Babicky, V. Janda, and P. Sunka, "Generation of ozone by pulsed corona discharge over water surface in hybrid gas – liquid electrical discharge reactor," *J. Phys. D. Appl. Phys.*, vol. 38, pp. 409–416, 2005.

[11] R. Fitzpatrick, "Introduction," in *Plasma Physics: An Introduction*, CRC Press, pp. 1–12, 2014.

[12] A. Bogaerts, E. Neyts, R. Gijbels, and J. van der Mullen, "Gas discharge plasmas and their applications," *Spectrochim. Acta, Part B*, vol. 57, no. 4, pp. 609–658, 2002.

[13] U. Roland, F. Holzer, and F. D. Kopinke, "Improved oxidation of air pollutants in a non-thermal plasma," *Catal. Today*, vol. 73, no. 3–4, pp. 315–323, 2002.

[14] F. Pasquali, A. C. Stratakos, A. Koidis, A. Berardinelli, C. Cevoli, L. Ragni, R. Mancusi, G. Manfreda, and M. Trevisani, "Atmospheric cold plasma process for vegetable leaf decontamination: A feasibility study on radicchio (red chicory, Cichorium intybus L.)," *Food Control*, vol. 60, pp. 552–559, 2016.

[15] J. Harry, "Plasmas, an overview," in *Introduction to Plasma Technology: Science, Engineering and Applications*, Wiley VCH, pp. 1–14, 2010.

[16] A. Rutscher, "Characteristics of low-temperature plasmas under nonthermal conditions–a short summary," in *Low temperature plasmas: Fundamentals, Technologies and Techiniques*, ed. R. Hippler, H. Kersten, M. Schmidt, K. H. Schoenbach, Wiley, pp. 1–14, 2008.

[17] R. W. Smith, D. Wei, and D. Apelian, "Thermal plasma materaisl processing - applications and opportunities," *Plasma Chem. Plasma Process.*, vol. 9, no. 1, pp. 135–165, 1989.

[18] Y. Byun, M. Cho, S. Hwang, and J. Chung, "Thermal plasma gasification of municipal solid waste (MSW)," in *Gasification for Practical Applications*, 1st Edition, ed. Y. Yun, InTech, 2012 pp 183-210.

[19] P. Fauchais and A. Vardelle, "Thermal plasmas," *IEEE Trans. Plasma Sci.*, vol. 25, no. 6, pp. 1258–1280, 1997.

[20] A. N. Zavilopulo, F. F. Chipev, and O. B. Shpenik, "Ionization of nitrogen , oxygen, water, and carbon dioxide molecules by near-threshold electron impact," *Tech. Phys.*, vol. 50, no. 4, pp. 402–407, 2005.

[21] V. Nehra, A. Kumar, and H. K. Dwivedi, "Atmospheric non-thermal plasma sources," *Int. J. Eng.*, vol. 2, no. 1, pp. 53–68, 2008.

[22] M. Abdel-Salam, "4.3.4 streamer mechanism," in *High-Voltage Engineering: Theory and Practice, Second Edition*, M. A. Salam, CRC Press, pp.124-126, 2000.

[23] A. Fridman, A. Chirokov, and A. Gutsol, "Topical review: non-thermal atmospheric pressure discharges," *J. Phys. D*, vol. 38, pp. R1-R24, 2005.

[24] A. Luque, V. Ratushnaya, and U. Ebert, "Positive and negative streamers in ambient air: modeling evolution and velocities," *J. Phys. D Appl. Phys.*, vol. 41, pp. 1-18, 2008.

[25] T. M. P. Briels, J. Kos, G. J. J. Winands, E. M. van Veldhuizen, and U. Ebert, "Positive and negative streamers in ambient air: measuring diameter, velocity and dissipated energy," *J. Phys. D. Appl. Phys.*, vol. 41, pp.1- 20, 2008.

[26] W. X. Sima, Q.-J. Peng, Q. Yang, T. Yuan, and J. Shi, "Local electron mean energy profile of positive primary streamer discharge with pin-plate electrodes in oxygen—nitrogen mixtures," *Chinese Phys. B*, vol. 22, no. 1, pp. 1–9, 2013.

[27] M. Simek, "Optical diagnostics of streamer discharges in atmospheric gases," *J. Phys. D. Appl. Phys.*, vol. 47, pp. 1–31, 2014.

[28] A. Fridman and G. Fridman, “Chapter 4 Major plasma discharges and their applicability for plasma medicine,” in *Plasma medicine*, John Wiley & Sons Inc, pp. 165–268, 2012.

[29] A. Mizuno, J. S. Clements, and R. H. Davis, “A method for the removal of sulfur dioxide from exhaust gas utilizing pulsed streamer corona for electron energization,” *IEEE Trans. Ind. Appl.*, vol. I, no. 3, pp. 516–522, 1986.

[30] K. H. Hong, S. J. Oh, and S. H. Moon, “Degradation of pentachlorophenol by ozone generated by a pulsed power corona discharge,” *Water. Air. Soil Pollut.*, vol. 145, no. 1–4, pp. 187–203, 2003.

[31] A. Fridman, L. A. Kennedy, “Chapter 9： Non-equilibrium cold atmospheric pressure plasma: corona, dielectric barrier amd spark discharges,” in *Plasma Physics and Engineering:*, CRC Press, pp. 555–592, 2004.

[32] I. V Timoshkin, M. Maclean, M. P. Wilson, M. J. Given, S. J. Macgregor, T. Wang, and J. G. Anderson, “Bactericidal effect of corona discharges in atmospheric air,” *IEEE Trans. Plasma Sci*, vol. 40, no. 10, pp. 2322–2233, 2012.

[33] M. Goldman and A. Goldman, “Chapter 4: Corona discharges,” in *Gaseous Electronics, Volume 1*, M. N. Nirsh and H. J. Oskam, Eds. Academic Press, 1978, pp. 219–290.

[34] G. W. Trichel, “The mechanism of the negative point to plane corona near onset,” *Phys. Rev.*, vol. 54, no. 12, pp. 1078–1084, 1938.

[35] L. B. Loeb, “The mechanism of the trichel pulses of short time duration in air,” *Phys. Rev.*, vol. 86, pp. 256–257, 1952.

[36] L. B. Loeb, A. F. Kip, and G. G. Hudson, “Pulses in negative point-to-plane corona,” *Phys. Rev.*, vol. 60, pp. 714–722, 1941.

[37] K. Shang, X. Xue, and X. Wang, “Trichel pulse characteristics in negative dc corona discharge,” in *Asia-Pacific Power and Energy Engineering Conference, APPEEC*, pp. 1–4, 2011.

[38] C. L. Wadhwa, “Breakdown mechanism of gaseous, liquid and solid materials,” in *High Voltage Engineering*, New Age international Ltd., pp. 1–55, 2007.

[39] J. S. Chang, P. A. Lawless, and T. Yamamoto, “Corona discharge processes,” *IEEE Trans. Plasma Sci.*, vol. 19, no. 6, pp. 1152–1166, 1991.

[40] J. Chen and J. H. Davidson, “Ozone production in the negative dc corona: the dependence of discharge polarity,” *Plasma Chem. Plasma Process.*, vol. 23, no. 3, pp. 501–518, 2003.

[41] G. Dinelli, L. Covotano, and M. Rea, “Industrial experiments on pulse corona simultaneous removal of NOx,” in *Industry Applications Society Annual Meeting*, pp. 1620 – 1627, 1988.

[42] J. L. Brisset, B. Benstaali, D. Moussa, J. Fanmoe, and E. Njoyim-Tamungang, “Acidity control of plasma-chemical oxidation: applications to dye removal,

urban waste abatement and microbial inactivation," *Plasma Sources Sci. Technol.*, vol. 20, pp. 1–12, 2011.

[43] J. L. Brisset, D. Moussa, A. Doubla, E. Hnatiuc, B. Hnatiuc, G. Kamgang Youbi, J. M. Herry, M. Na ̈ıtali, and M. N. Bellon-Fontaine, "Chemical reactivity of discharges and temporal post-discharges in plasma treatment of aqueous media: examples of gliding discharge treated solutions," *Ind. Eng. Chem. Res.*, vol. 47, no. 16, pp. 5761–5781, 2008.

[44] R. Ono and T. Oda, "Measurement of hydroxyl radicals in pulsed corona discharge," *J. Electrostat.*, vol. 55, no. 3–4, pp. 333–342, 2002.

[45] S. Kanazawa, H. Tanaka, A. Kajiwara, T. Ohkubo, Y. Nomoto, M. Kocik, J. Mizeraczyk, and J. S. Chang, "LIF imaging of OH radicals in DC positive streamer coronas," *Thin Solid Films*, vol. 515, no. 9, pp. 4266–4271, 2007.

[46] L. F. Gaunt, C. B. Beggs, and G. E. Georghiou, "Bactericidal action of the reactive species produced by gas-discharge nonthermal plasma at atmospheric pressure: A review," *IEEE Trans. Plasma Sci.*, vol. 34, no. 4 II, pp. 1257–1269, 2006.

[47] F. Pontiga, H. P. Moreno, and A. Castellanos, "Corona discharge in owing synthetic air," in *Electrical Insulation and Dielectric Phenomena, 2008. CEIDP 2008. Annual Report Conference on*, 2008, pp. 618–621.

[48] M. Clupek and M. Simek, "Efficiency of ozone production by pulsed," *J. Phys. D. Appl. Phys.*, vol. 35, no. 11, pp. 1171–1175, 2002.

[49] J. Chen and J. H. Davidson, "Model of the nevative DC corona plasma comparison to the positive DC corona plasma," *Plasma Chem. Plasma Process.*, vol. 23, no. 1, pp. 83–102, 2003.

[50] J. Chen and J. H. Davidson, "Electron density and energy distributions in the positive dc corona: interpretation for corona-enhanced chemical reactions," *Plasma Chem. Plasma Process.*, vol. 22, no. 2, pp. 199–224, 2002.

[51] K. J. Boelter and J. H. Davidson, "Ozone generation by indoor, electrostatic air cleaners," *Aerosol Sci. Technol.*, vol. 27, no. 6, pp. 689–708, 1997.

[52] M. B. Awad and G. S. P. Castle, "Ozone generation in an electrostatic precipitator with a heated corona wire," *J. Air Pollut. Control Assoc.*, vol. 25, no. 4, pp. 369–374, 1975.

[53] J. J. Lowke and R. Morrow, "Theoretical analysis of removal of oxides of sulphur and nitrogen in pulsed operation of electrostatic precipitators," *IEEE Trans. Plasma Sci.*, vol. 23, no. 4, pp. 661–671, 1995.

[54] S. Masuda and H. Nakao, "Control of NOx by positive and negative pulsed corona discharges," *IEEE Trans. Ind. Appl.*, vol. 26, no. 2, pp. 374–383, 1990.

[55] S. V. Pancheshnyi, D. A. Lacoste, A. Bourdon, and C. O. Laux, "Ignition of propane-air mixtures by a repetitively pulsed nanosecond discharge," *IEEE Trans. Plasma Sci.*, vol. 34, no. 6, pp. 2478–2487, 2006.

[56] D. Pai, D. A. Lacoste, and C. O. Laux, “Images of nanosecond repetitively pulsed plasmas in preheated air at atmospheric pressure,” *IEEE Trans. Plasma Sci.*, vol. 36, no. 4 PART 1, pp. 974–975, 2008.

[57] J. L. Walsh, J. J. Shi, and M. G. Kong, “Submicrosecond pulsed atmospheric glow discharges sustained without dielectric barriers at kilohertz frequencies,” *Appl. Phys. Lett.*, vol. 89, no. 16, pp. 10–13, 2006.

[58] R. Hafez, S. Samson, and E. Marode, “A prevented spark reactor for pollution control. investigation of NOx removal,” in *12th ISPC (Minneapolis, MN)*, pp. 855–61, 1995.

[59] U. Kogelschatz, B. Eliasson, and W. Egli, “Dielectric-barrier discharges . principle and applications,” *J.Phys IV Fr.*, vol. 7, no. C4, pp.47-66, 1997.

[60] M. Meißer, “DBD system overview and structure of this work,” *Resonant Behaviour of Pulse Generators for efficient Drive of Optical Radiation Sources Based on Dielectric Barrier Discharges*. KIT Scientific Publishing, pp. 19-27, 2013.

[61] L. Zhang, D. Yang, W. Wang, S. Wang, H. Yuan, Z. Zhao, C. Sang, and L. Jia, “Needle-array to plate DBD plasma using sine AC and nanosecond pulse excitations for purpose of improving indoor air quality,” *Sci. Rep.*, vol. 6, no. April, p. 25242, 2016.

[62] M. Janda, Z. Machala, A. Niklová, and V. Martišovitš, “The streamer-to-spark transition in a transient spark: a dc-driven nanosecond-pulsed discharge in atmospheric air,” *Plasma Sources Sci. Technol.*, vol. 21, no. 4, pp.1-9, 2012.

[63] M. Janda, A. Niklová, V. Martišovitš and Z. Machala, “Transient spark–dc driven nanosecond pulsed discharge in atmospheric air,” *HAKONE XII. Trencianske Teplice, Slovakia, 12–17 September, 2010*.

[64] M. Janda, V. Martišovitš, and Z. Machala, “Transient spark: a dc-driven repetitively pulsed discharge and its control by electric circuit parameters,” *Plasma Sources Sci. Technol.*, vol. 20, no. 3, p. 35015, 2011.

[65] Z. Machala, M. Janda, K. Hensel, I. Jedlovský, L. Leštinská, V. Foltin, V. Martišovitš, and M. Morvová, “Emission spectroscopy of atmospheric pressure plasmas for bio-medical and environmental applications,” *J. Mol. Spectrosc.*, vol. 243, no. 2, pp. 194–201, 2007.

[66] M. Janda, Z. Machala, and C. O. Laux, “Optical and Electrical Study of Transient Spark Discharge in Air,” *Acta Phys. Univ. Comenianae*, vol. L–L1, no. 1 & 2, pp. 85–93, 2010.

[67] M. Janda, Z. Machala, G. D. Stancu, D. Pai, D. A. Lacoste, and C. O. Laux, “Transient spark in air at atmospheric pressure,” in *17th International Conference on Gas Discharges and Their Applications, 2008*, pp. 349–352.

[68] Z. Machala, B. Tarabova, K. Hensel, E. Spetlikova, L. Sikurova, and P. Lukes, “Formation of ROS and RNS in water electro-sprayed through transient spark

discharge in air and their bactericidal effects," *Plasma Process. Polym.*, vol. 10, no. 7, pp. 649–659, 2013.

[69] Z. Machala, I. Jedlovský, L. Chládeková, B. Pongrác, D. Giertl, M. Janda, L. Šikurová, and P. Polčic, "DC discharges in atmospheric air for bio-decontamination – spectroscopic methods for mechanism identification," *Eur. Phys. J. D*, vol. 54, no. 2, pp. 195–204, 2009.

[70] K. Hensel, K. Kučerová, B. Tarabová, M. Janda, Z. Machala, K. Sano, C. T. Mihai, M. Ciorpac, L. D. Gorgan, R. Jijie, V. Pohoata, and I. Topala, "Effects of air transient spark discharge and helium plasma jet on water, bacteria, cells, and biomolecules.," *Biointerphases*, vol. 10, no. 2, p. 029515, 2015.

[71] Y. Gorbanev, D. O'Connell, and V. Chechik, "Non-thermal plasma in contact with water: the origin of species," *Chem. - A Eur. J.*, vol. 22, no. 10, pp. 3496–3505, 2016.

[72] T. Takamatsu, K. Uehara, Y. Sasaki, H. Miyahara, Y. Matsumura, A. Iwasawa, N. Ito, T. Azuma, M. Kohno, and A. Okino, "Investigation of reactive species using various gas plasmas," *RSC Adv.*, vol. 4, no. 75, pp. 39901–39905, 2014.

[73] P. Lukes, E. Dolezalova, I. Sisrova, and M. Clupek, "Aqueous-phase chemistry and bactericidal effects from an air discharge plasma in contact with water: evidence for the formation of peroxynitrite through a pseudo-second-order post-discharge reaction of H_2O_2 and HNO_2," *Plasma Sources Sci. Technol.*, vol. 23, no. 1, pp. 1-15, 2014.

[74] S. Goldstein, J. Lind, and G. Merényi, "Chemistry of peroxynitrites as compared to peroxynitrates," *Chem. Rev.*, vol. 105, no. 6, pp. 2457–2470, 2005.

[75] M. J. Traylor, M. J. Pavlovich, S. Karim, P. Hait, Y. Sakiyama, D. S. Clark, and D. B. Graves, "Long-term antibacterial efficacy of air plasma-activated water," *J. Phys. D. Appl. Phys.*, vol. 44, no. 47, pp. 1- 4, 2011.

[76] D. B. Graves, "The emerging role of reactive oxygen and nitrogen species in redox biology and some implications for plasma applications to medicine and biology," *J. Phys. D. Appl. Phys.*, vol. 45, no. 45, pp. 1-42, 2012.

[77] J. Hoigne, H. Bader, W. R. Haag, and J. Staehelin, "Rate constants of reactions of ozone with organic and inorganic compounds in water-III. Inorganic compounds and radicals," *Water Res.*, vol. 19, no. 8, pp. 993–1004, 1985.

[78] M. Korachi, Z. Turan, K. Şentürk, F. Şahin, and N. Aslan, "An investigation into the biocidal effect of high voltage AC/DC atmospheric corona discharges on bacteria, yeasts, fungi and algae," *J. Electrostat.*, vol. 67, pp. 678–685, 2009.

[79] V. Scholtz, J. Julak, and V. Kriha, "The microbicidal effect of low-temperature plasma generated by corona discharge: Comparison of various microorganisms on an agar surface or in aqueous suspension," *Plasma Process. Polym.*, vol. 7, no. 3–4, pp. 237–243, 2010.

[80] C. Wonho, G. Bomi, D. bee Kim, and H. Jung, "Effects of atmospheric pressure plasma on microorganisms and human cells," presented at 39th *IEEE International Conference on Plasma Science,* Edinburgh, UK, 2012.

[81] I. E. Kieft, M. Kurdi, and E. Stoffels, "Reattachment and apoptosis after plasma-needle treatment of cultured cells," *IEEE Trans. Plasma Sci.*, vol. 34, no. 4 II, pp. 1331–1336, 2006.

[82] E. Stoffels, Y. Sakiyama, and D. B. Graves, "Cold atmospheric plasma : charged species and their interactions with cells and tissues," *IEEE Trans. Plasma Sci.*, vol. 36, no. 4, pp. 1441–1457, 2008.

[83] V. J. Thannickal and B. L. Fanburg, "Reactive oxygen species in cell signaling.," *Am. J. Physiol. Lung Cell. Mol. Physiol.*, vol. 279, no. 6, pp. L1005–28, 2000.

[84] S. Kalghatgi, C. Kelly, E. Cerchar, R. Sensenig, A. Brooks, A. Fridman, A. Morss-Clyne, J. Azizkhan-Clifford, and G. Friedman, "On the interaction of non-thermal atmospheric pressure plasma with tissues," *PPC2009 - 17th IEEE Int. Pulsed Power Conf.*, pp. 1133–1138, 2009.

[85] K. H. Schoenbach, S. Katsuki, R. H. Stark, E. S. Buescher, and S. J. Beebe, "Bioelectrics-new applications for pulsed power technology," *IEEE Trans. Plasma Sci.*, vol. 30, no. 1, pp. 293–300, 2002.

[86] Z. Machala, L. Chládeková, and M. Pelach, "Plasma agents in bio-decontamination by dc discharges in atmospheric air," *J. Phys. D. Appl. Phys.*, vol. 43, no. 22, pp. 1-7, 2010.

[87] E. Sysolyatina, A. Mukhachev, M. Yurova, M. Grushin, V. Karalnik, A. Petryakov, N. Trushkin, S. Ermolaeva, and Y. Akishev, "Role of the charged particles in bacteria inactivation by plasma of a positive and negative corona in ambient air," *Plasma Process. Polym.*, vol. 11, no. 4, pp. 315–334, 2014.

[88] A. Lin, N. Chernets, J. Han, Y. Alicea, D. Dobrynin, G. Fridman, T. A. Freeman, A. Fridman, and V. Miller, "Non-equilibrium dielectric barrier discharge treatment of mesenchymal stem cells : Charges and reactive oxygen species play the major role in cell death[a]," *Plasma Process. Polym.*, pp. 1117–1127, 2015.

[89] Y. Akishev, M. Grushin, V. Karalnik, N. Trushkin, V. Kholodenko, V. Chugunov, E. Kobzev, N. Zhirkova, I. Irkhina, and G. Kireev, "Atmospheric-pressure, nonthermal plasma sterilization of microorganisms in liquids and on surfaces," *Pure Appl. Chem.*, vol. 80, no. 9, pp. 1953–1969, 2008.

[90] M. Laroussi and M. Kong, "Chpater 9 Plasma-cell interaction: prokaryotes," in *Plasma Medicine*, Cambridge University Press, ed. M. Laroussi, pp. 216–226, 2012.

[91] M. R. Pervez, "Plasma based sterilization : overview and the stepwise inactivation process of microbial by non-thermal atmospheric pressure plasma jet," *IJET-IJENS*, vol. 14, no. 05, 2014.

[92] D. Dobrynin, G. Fridman, G. Friedman, and A. Fridman, “Physical and biological mechanisms of direct plasma interaction with living tissue,” *New J. Phys.*, vol. 11, pp. 115020–1–115020–26, 2009.

[93] S. Kalghatgi, C. M. Kelly, E. Cerchar, B. Torabi, O. Alekseev, A. Fridman, G. Friedman, and J. Azizkhan-Clifford, “Effects of non-thermal plasma on mammalian cells,” *PLoS One*, vol. 6, no. 1, pp. 1–12, 2011.

[94] X. Lu, T. Ye, Y. Cao, Z. Sun, Q. Xiong, Z. Tang, Z. Xiong, J. Hu, Z. Jiang, and Y. Pan, “The roles of the various plasma agents in the inactivation of bacteria,” *J. Appl. Phys.*, vol. 104, no. 5, pp. 053309.1-053309.5, 2008.

[95] M. Laroussi and F. Leipold, “Evaluation of the roles of reactive species, heat, and UV radiation in the inactivation of bacterial cells by air plasmas at atmospheric pressure,” *Int. J. Mass Spectrom.*, vol. 233, no. 1–3, pp. 81–86, 2004.

[96] X. Deng, J. Shi, and M. G. Kong, “Physical mechanisms of inactivation of Bacillus subtilis spores using cold atmospheric plasmas,” *IEEE Trans. Plasma Sci.*, vol. 34, no. 4 II, pp. 1310–1316, 2006.

[97] M. Laroussi, “Nonthermal decontamination of biological media by atmospheric-pressure plasmas: Review, analysis, and prospects,” *IEEE Trans. Plasma Sci.*, vol. 30, no. 4, pp. 1409–1415, 2002.

[98] M. Moisan, J. Barbeau, S. Moreau, J. Pelletier, M. Tabrizian, and L. Yahia, “Low-temperature sterilization using gas plasmas: A review of the experiments and an analysis of the inactivation mechanisms,” *Int. J. Pharm.*, vol. 226, no. 1–2, pp. 1–21, 2001.

[99] G. Macdonnell, “Sterilization and disinfection,” in *Encyclopedia of Microbiology*, 3rd edition, ed. M. Schaechter, San Diego: Academic Press, pp. 533–535, 2009.

[100] K. Sekimoto, R. Gonda, and M. Takayama, “Effects of ionic and neutral species on Esherichia coli (E . coli) inactivation in atmospheric pressure corona discharges,” in *ISPC 21*, 2015, pp. 3–6.

[101] R. A. Maslahati, E. Akhlaghi, S. Chelliapan, A. Kaboli, A. M. Roudi, H. Aslani, and S. B. Selvam, “Treatment of Landfill Leachate via Advanced Oxidation Process (AOPs) - A Review. Anita,” *Res. J. Pharm. Biol. Chem. Sci.*, vol. 6, no. 4, pp. 260–271, 2015.

[102] C. Barrera-Díaz, P. Cañizares, F. J. Fernández, R. Natividad, and M. A. Rodrigo, “Electrochemical advanced oxidation processes: An overview of the current applications to actual industrial effluents,” *J. Mex. Chem. Soc.*, vol. 58, no. 3, pp. 256–275, 2014.

[103] S. Perni, G. Shama, J. L. Hobman, P. A. Lund, C. . Kershaw, G. A. Hidalgo-arroyo, C. W. Penn, X. T. Deng, J. L. Walsh, and M. G. Kong, “Probing bactericidal mechanisms induced by cold atmospheric plasmas with Escherichia coli mutants.pdf,” *Appl. Phys. Lett.*, vol. 90, no. 7, pp. 1–13, 2007.

[104] H. W. Herrmann, I. Henins, J. Park, and G. S. Selwyn, “Decontamination of chemical and biological warfare (CBW) agents using an atmospheric pressure plasma jet (APPJ),” *Phys. Plasmas*, vol. 6, no. 5, pp. 2284–2289, 1999.

[105] N. N. Aye, B. Sun, X. M. Zhu, Z. Y. Gao, Y. J. Song, and M. Sato, “Inactivation of algae with multi-needle gas-liquid hybrid discharge reactor by introducing oxygen and air,” *Adv. Mater. Res.*, vol. 365, pp. 389–395, 2011.

[106] J. Shen, C. Cheng, Y. Zhao, D. Xiao, Y. Lan, H. Xie, J. Cheng, Y. Meng, J. Li, and P. K. Chu, “Inactivation of Bacillus subtilis spores upon exposure to a mixed oxygen/argon atmospheric-pressure plasma jet,” *Jpn. J. Appl. Phys.*, vol. 53, pp. 1–4, 2014.

[107] S. G. Joshi, M. Cooper, A. Yost, M. Paff, U. K. Ercan, G. Fridman, G. Friedman, A. Fridman, and A. D. Brooks, “Nonthermal dielectric-barrier discharge plasma-induced inactivation involves oxidative DNA damage and membrane lipid peroxidation in Escherichia coli,” *Antimicrob. Agents Chemother.*, vol. 55, no. 3, pp. 1053–1062, 2011.

[108] K. Yanallah, F. Pontiga, a Fernández-Rueda, and a Castellanos, “Experimental investigation and numerical modelling of positive corona discharge: ozone generation,” *J. Phys. D. Appl. Phys.*, vol. 42, no. 6, pp. 1-8, 2009.

[109] T. Ohmi, T. Isagawa, T. Imaoka, and I. Sugiyama, “Ozone decomposition in ultrapure water and continuous water system,” *J. Electrochem. Soc.*, vol. 139, no. 11, pp. 3336–3345, 1992.

[110] W. T. Broadwater, R. C. Hoehn, and P. H. King, “Sensitivity of three selected bacterial species to ozone,” *Appl. Microbiol.*, vol. 26, no. 3, pp. 391-393, 1973.

[111] L. James, A. K. Puniya, V. Mishra, and K. Singh, “Ozone: A potent disinfectant for application in food industry - An overview,” *J. Sci. Ind. Res. (India).*, vol. 61, no. 7, pp. 504–509, 2002.

[112] M. Sharma and J. B. Hudson, “Ozone gas is an effective and practical antibacterial agent,” *Apploed Epidemiol. Heal. care setting community*, vol. 36, no. 8, pp. 559–563, 2008.

[113] I. R. Komanapalli, B. H. S. Lau, “Ozone-induced damage of Escherichia coli K-12,” *Appl Micobiol Biotech* , vol. 46, pp. 610-614, pp. 610–614, 1996.

[114] B. Thanomsub, V. Anupunpisit, S. Chanphetch, T. Watcharachaipong, R. Poonkhum, and C. Srisukonth, “Effects of ozone treatment on cell growth and ultrastructural changes in bacteria.,” *J. Gen. Appl. Microbiol.*, vol. 48, no. 4, pp. 193–199, 2002.

[115] N. K. Hunt and B. J. Marĭas, “Inactivation of Escherichia coli with ozone: Chemical and inactivation kinetics,” *Water Res.*, vol. 33, no. 11, pp. 2633–2641, 1999.

[116] F. Leipold, “Inactivation of micro organisms by means of low temperature atmospheric pressure plasmas,” in *New Journal of Physics*, no. 16, pp. 2–4, 2007.

[117] V. Scholtz, J. Julák, V. Kríha, and J. Mosinger, “Decontamination effects of low-temperature plasma generated by corona discharge. Part I: an overview,” *Prague Med. Rep.*, vol. 108, no. 2, pp. 115–27, 2007.

[118] R. S. Sigmond, “Action of Corona Discharges on Bacteria and Spores,” *Czechoslov. J. Phys.*, vol. 49, no. 3, pp. 405–420, 1999.

[119] T. Takamatsu, K. Uehara, Y. Sasaki, M. Hidekazu, Y. Matsumura, A. Iwasawa, N. Ito, M. Kohno, T. Azuma, and A. Okino, “Microbial inactivation in the liquid phase induced by multigas plasma jet,” *PLoS One*, vol. 10, no. 7, pp. 1–9, 2015.

[120] X. Hao, A. M. Mattson, C. M. Edelblute, M. A. Malik, L. C. Heller, and J. F. Kolb, “Nitric oxide generation with an air operated non-thermal plasma jet and associated microbial inactivation mechanisms,” *Plasma Process. Polym.*, vol. 11, no. 11, pp. 1044–1056, 2014.

[121] S. J. Beebe, P. M. Fox, L. J. Rec, K. Somers, R. H. Stark, and K. H. Schoenbach, “Nanosecond pulsed electric field (nsPEF) effects on cells and tissues: Apoptosis induction and tumor growth inhibition,” *IEEE Trans. Plasma Sci.*, vol. 30, no. 1 II, pp. 286–292, 2002.

[122] V. O. Marquez, G. S. Mittal, and M. W. Griffiths, “Destruction and Inhibition of Bacterial Spores by High Voltage Pulsed Electric Field,” *J. Food Sci.*, vol. 62, no. 2, pp. 399–401, 1997.

[123] H. Hülsheger, J. Potel, and E. G. Niemann, “Electric field effects on bacteria and yeast cells.,” *Radiat. Environ. Biophys.*, vol. 22, no. 2, pp. 149–162, 1983.

[124] S. Katsuki, T. Majima, K. Nagata, and I. Lisitsyn, “Inactivation of Bacillus Stearothermophilus by Pulsed Electric Field,” *IEEE Trans. Plasma Sci*, vol. 28, no. 1, pp. 155–160, 2000.

[125] K. H. Schoenbach, B. Hargrave, R. P. Joshi, J. F. Kolb, R. Nuccitelli, C. Osgood, A. Pakhomov, M. Stacey, R. J. Swanson, J. A. White, S. Xiao, J. Zhang, S. J. Beebe, P. F. Blackmore, and E. S. Buescher, “Bioelectric effects of intense nanosecond pulses,” *IEEE Trans. Dielectr. Electr. Insul.*, vol. 14, no. 5, pp. 1088–1107, 2007.

[126] J. Kolb, W. Frey, J. A. White, R. O. Price, P. F. Blackmore, S. J. Beebe, R. P. Joshi, and K. H. Schoenbach, “Measurements of the transmembrane voltage in biological cells for nanosecond pulsed electric field exposures,” in *Digest of Technical Papers-IEEE International Pulsed Power Conference*, 2007, pp. 1286–1289.

[127] D. A. Mendis, M. Rosenberg, and F. Azam, “A note on the possible electrostatic disruption of bacteria,” *IEEE Trans. Plasma Sci.*, vol. 28, no. 4, pp. 1304–1306, 2000.

[128] K. H. Schoenbach, F. E. Peterkin, R. W. Alden, and S. J. Beebe, "The effect of pulsed electric fields on biological cells: experiments and applications," *IEEE Trans. Plasma Sci.*, vol. 25, no. 2, pp. 284–292, 1997.

[129] F. R. De Gruijl, H. J. Van Kranen, and L. H. F. Mullenders, "UV-induced DNA damage, repair, mutations and oncogenic pathways in skin cancer," *J. Photochem. Photobiol. B Biol.*, vol. 63, no. 1–3, pp. 19–27, 2001.

[130] P. Messerer and H. Halfmann, "Plasma sterilisation and surface modification of thermolabile materials," in *Proc. of the annual meeting of The Minerals, Metals & Materials Society*, 2005, pp. 205–215.

[131] M. Heise, W. Neff, O. Franken, P. Muranyi, and J. Wunderlich, "Sterilization of polymer foils with dielectric barrier discharges at atmospheric pressure," *Plasmas Polym.*, vol. 9, no. 1, pp. 23–33, 2004.

[132] M. Yamamoto, M. Nishioka, and M. Sadakata, "Sterilization by H_2O_2 droplets under corona discharge," *J. Electrostat.*, vol. 55, no. 2, pp. 173–187, 2002.

[133] I. A. Soloshenko, V. V. Tsiolko, V. A. Khomich, V. Y. Bazhenov, A. V. Ryabtsev, A. I. Schedrin, and I. L. Mikhno, "Features of sterilization using low-pressure DC-discharge hydrogen-peroxide plasma," *IEEE Trans. Plasma Sci.*, vol. 30, no. 4 I, pp. 1440–1444, 2002.

[134] M. Laroussi, "Sterilization of contaminated matter with an atmospheric pressure plasma," *IEEE Trans. Plasma Sci.*, vol. 24, no. 3, pp. 1188–1191, 1996.

[135] M. Moisan, J. Barbeau, M.-C. Crevier, J. Pelletier, N. Philip, and B. Saoudi, "Plasma sterilization. Methods and mechanisms," *Pure Appl. Chem.*, vol. 74, no. 3, pp. 349–358, 2002.

[136] N. Philip, B. Saoudi, M. C. Crevier, M. Moisan, J. Barbeau, and J. Pelletier, "The respective roles of UV photons and oxygen atoms in plasma sterilization at reduced gas pressure: The case of N_2-O_2 mixtures," *IEEE Trans. Plasma Sci.*, vol. 30, no. 4 I, pp. 1429–1436, 2002.

[137] E. Spetlikova, V. Janda, P. Lukes, and M. Clupek, "Role of UV Radiation , Solution Conductivity and Pulse Repetition Frequency in the Bactericidal Effects During Pulse Corona Discharges," in *WDS'10 Proceedings of Contributed Paper*, 2010, pp. 96–100.

[138] A. Norman, "The nuclear role in the ultraviolet inactivation of Neurospora Conidia," *J. Cell. Comp. Physiol.*, vol. 44, no. 1, pp. p. 1–10, 1954.

[139] R. Shrestha, U. M. Joshi, and D. P. Subedi, "Experimental study of ozone generation by atmospheric pressure dielectric barrier discharge," *Int. J. Res. Rev.*, vol. VIII, no. 4, pp. 24–29, 2015.

[140] B. Eliasson and U. Kogelschatz, "Nonequilibrium volume plasma chemical processing," *IEEE Trans. Plasma Sci.*, vol. 19, no. 6, pp. 1063–1077, 1991.

[141] L. Vaduganathan, B. A. Poonamallie, M. Nagalingam, and M. College, "Effects of temperature and flow rates of ozone generator on the DBD by

varying various electrical parameters," *Am. J. Appl. Sci.*, vol. 9, no. 9, pp. 1496–1502, 2012.

[142] G. Fridman, A. D. Brooks, M. Balasubramanian, A. Fridman, A. Gutsol, V. N. Vasilets, H. Ayan, and G. Friedman, "Comparison of direct and indirect effects of non-thermal atmospheric pressure plasma on bacteria," *Plasma Process. Polym.*, vol. 4, no. 4, pp. 370–375, 2007.

[143] D. Ziuzina, S. Patil, P. J. Cullen, K. M. Keener, and P. Bourke, "Atmospheric cold plasma inactivation of Escherichia coli in liquid media inside a sealed package," *J. Appl. Microbiol.*, vol. 114, no. 3, pp. 778–787, 2013.

[144] S. Patil, T. Moiseev, N. N. Misra, P. J. Cullen, J. P. Mosnier, K. M. Keener, and P. Bourke, "Influence of high voltage atmospheric cold plasma process parameters and role of relative humidity on inactivation of Bacillus atrophaeus spores inside a sealed package," *J. Hosp. Infect.*, vol. 88, no. 3, pp. 162–169, 2014.

[145] B. Yang, J. Chen, Q. Yu, M. Lin, A. Mustapha, and M. Chen, "Inactivation of Bacillus Spores using a low-temperature atmospheric plasma brush," *IEEE Trans. Plasma Sci.*, vol. 38, no. 7, pp. 1624–1631, 2010.

[146] T. Takamatsu, A. Kawate, T. Oshita, and H. Miyahara, "Investigation of reactive species in various gas plasmas treated liquid and sterilization effects," in *International Plasma Chemistry society conference 21*, 2014, pp. 4–7.

[147] K. Reineke, K. Langer, C. Hertwig, J. Ehlbeck, and O. Schlüter, "The impact of different process gas compositions on the inactivation effect of an atmospheric pressure plasma jet on Bacillus spores," *Innov. Food Sci. Emerg. Technol.*, vol. 30, pp. 112–118, 2015.

[148] F. Trompeter, W. J. Neff, O. Franken, M. Heise, M. Neiger, S. Liu, G. J. Pietsch, and A. B. Saveljew, "Reduction of Bacillus Subtilis and Aspergillus atmospheric gas discharges," *IEEE Trans. Plasma Sci.*, vol. 30, no. 4, pp. 1416–1423, 2002.

[149] M. Hähnel, T. Von Woedtke, and K. D. Weltmann, "Influence of the air humidity on the reduction of Bacillus spores in a defined environment at atmospheric pressure using a dielectric barrier surface discharge," *Plasma Process. Polym.*, vol. 7, no. 3–4, pp. 244–249, 2010.

[150] C. S. Li and Y. C. Wang, "Surface germicidal effects of ozone for microorganisms," American Industrial Hygiene Association *J. (Fairfax,. Va).*, vol. 64, no. 4, pp. 533–7, 2003.

[151] J. Chen and P. Wang, "Effect of relative humidity on electron distribution and ozone production by DC coronas in air," *IEEE Trans. Plasma Sci.*, vol. 33, no. 2 II, pp. 808–812, 2005.

[152] J. D. Skalný, J. Országh, Š. Matejčík, and N. J. Mason, "Ozone generation in positive and negative corona discharge fed by humid oxygen and carbon dioxide," *Phys. Scrip.*, vol. T131, p. 014012, 2008.

[153] G. Horváth, J. Országh, J. D. Skalný, N. J. Mason, and V. Chernyak, "Influence of humidity on ozone concentration in negative corona discharge fed by oxygen," in *International Workshop Ozotech*, 2007, pp. 40–43.

[154] J. E. Jones, J. Dupuy, G. O. S. Schreiber, and R. T. Waters, "Boundary conditions for the positive direct-current corona in a coaxial system," *J. Phys. D. Appl. Phys.*, vol. 21, no. 2, pp. 322–333, 1988.

[155] H. Ryzko, "Drift velocity of electrons and ions in dry and humid air and in water vapour," *Proc. Phys. Soc.*, vol. 85, no. 6, p. 1283, 1965.

[156] S. Sakata and T. Okada, "Effect of humidity on hydrated clusters-ion formation in a clean room corona discharge neutralizer," *J. Aerosol*, vol. 25, no. 5, pp. 879–893, 1994.

[157] J. T. Herron and D. S. Green, "Chemical kinetics database and predictive schemes for nonthermal humid air plasma chemistry. Part II. Neutral species reactions," *Plasma Chem. Plasma Process.*, vol. 21, no. 3, pp. 459–481, 2001.

[158] W. L. Morgan, M. Jacob, and E. R. Fisher, "Modeling the plasma chemistry of a pulsed corona discharge in dry and humid air," in *12th. Int. Symp. Plasma Chem.* Minneapolis, USA , 1995, pp. 741-746.

[159] A. S. Viner, P. A. Lawless, D. S. Ensor, and L. E. Sparks, "Ozone generation in dc-energized electrostatic precipitators," *IEEE Trans. Ind. Appl.*, vol. 28, no. 3, pp. 504–512, 1992.

[160] R. Dorai and M. J. Kushner, "A model for plasma modification of polypropylene using atmospheric pressure discharges," *J. Phys. D. Appl. Phys.*, vol. 36, no. 6, pp. 666–685, 2003.

[161] P. Bruggeman, F. Iza, P. Guns, D. Lauwers, M. G. Kong, Y. A. Gonzalvo, C. Leys, and D. C. Schram, "Electronic quenching of OH(A) by water in atmospheric pressure plasmas and its influence on the gas temperature determination by OH(A – X) emission," *Plasma Sources Sci. Technol.*, vol. 19, no. 1, pp. 1-7, 2010.

[162] H. Kim, K. C. Wright, I. Hwang, D. Lee, A. Rabinovich, A. Fridman, and Y. I. Cho, "Effects of H_2O_2 and low pH produced by gliding arc discharge on the inactivation of Escherichia Coli in water," *Plasma Med.*, vol. 1, no. 3–4, pp. 295–307, 2011.

[163] A. Fridman, "Elementary plasma-chemical reactions," in *plasma chemistry*. Cambridge University Press, 2008, pp. 12-63.

[164] R. Burlica, M. J. Kirkpatrick, and B. R. Locke, "Formation of reactive species in gliding arc discharges with liquid water," *J. Electrostat.*, vol. 64, no. 1, pp. 35–43, 2006.

[165] R. Burlica and B. R. Locke, "Pulsed plasma gliding-arc discharges with water spray," *IEEE Trans. Ind. Appl.*, vol. 44, no. 2, pp. 482–489, 2008.

[166] J. L. Brisset, J. Lelievre, A. Doubla, and J. Amouroux, “Interactions with aqueous solutions of the air corona products,” *Rev. Phys. Appliqué*, vol. 25, no. 6, pp. 535–543, 1990.

[167] S. Ikawa, K. Kitano, and S. Hamaguchi, “Effects of pH on bacterial inactivation in aqueous solutions due to low-temperature atmospheric pressure plasma application,” *Plasma Process. Polym.*, vol. 7, no. 1, pp. 33–42, 2010.

[168] J. Robertson, “High density plasma enhanced chemical vapor deposition of optical thin films,” *Eur. Phys. J. Appl. Phys.*, vol. 28, pp. 265–291, 2004.

[169] R. Burlica, M. J. Kirkpatrick, W. C. Finney, R. J. Clark, and B. R. Locke, “Organic dye removal from aqueous solution by glidarc discharges,” *J. Electrostat.*, vol. 62, pp. 309–321, 2004.

[170] N. Shainsky, D. Dobrynin, U. Ercan, S. G. Joshi, H. Ji, A. Brooks, G. Fridman, Y. Cho, A. Fridman, and G. Friedman, “Plasma acid: Water treated by dielectric barrier discharge,” *Plasma Process. Polym.*, vol. 9, pp. 1-6 , 2012.

[171] C. W. Chen, H. M. Lee, and M. B. Chang, “Influence of pH on inactivation of aquatic microorganism with a gas-liquid pulsed electrical discharge,” *J. Electrostat.*, vol. 67, no. 4, pp. 703–708, 2009.

[172] K. Oehmigen, M. Ha ̈hnel, Brandenburg.R, C. Wilke, K.-D. Weltmann, and T. Von Woedtke, “The role of acidification for antimicrobial activity of atmospheric pressure plasma in liquids,” *Plasma Process. Polym.*, vol. 7, no. 3–4, pp. 250–257, 2010.

[173] K. Satoh, S. J. MacGregor, J. G. Anderson, G. A. Woolsey, and R. A. Fouracre, “Pulsed-plasma disinfection of water containing Escherichia coli,” *Japanese J. Appl. Physics, Part 1 Regul. Pap. Short Notes Rev. Pap.*, vol. 46, no. 3 A, pp. 1137–1141, 2007.

[174] C. W. Chen, H. M. Lee, and M. B. Chang, “Inactivation of aquatic microorganisms by low-frequency AC discharges,” *IEEE Trans. Plasma Sci.*, vol. 36 PART 2, no. 1, pp. 215–219, 2008.

[175] M. Korachi and N. Aslan, “The effect of atmospheric pressure plasma corona discharge on pH, lipid content and DNA of bacterial cells,” *Plasma Sci. Technol.*, vol. 13, no. 1, pp. 99–105, 2011.

[176] M. A. Malik and S. A. Malik, “Catalyst enhanced oxidation of VOCs and methane in cold-plasma reactors,” *Platin. Met. Rev.*, vol. 43, no. 3, pp. 109–113, 1999.

[177] Y. Itoh, M. Ueda, H. Shinjoh, and K. Nakakita, “NOx Reduction under Oxidizing Conditions by Plasma-assisted Catalysis,” *R&D Rev. Toyota CRDL*, vol. 41, no. 2, pp. 49–62, 2006.

[178] B. Penetrante, “Exhaust aftertreatment using plasma-assisted catalysis,” in *Conference: Clean Fuels* 2000, San Diego, CA. February 7-9, 2000, pp. 1-5.

[179] J. C. Whitehead, “Plasma catalysis: A solution for environmental problems,” *Pure Appl. Chem.*, vol. 82, no. 6, pp. 1329–1336, 2010.

[180] H. L. Chen, H. M. Lee, S. H. Chen, M. B. Chang, S. J. Yu, and S. N. Li, "Removal of volatile organic compounds by single-stage and two-stage plasma catalysis systems: A review of the performance enhancement mechanisms, current status, and suitable applications," *Environ. Sci. Technol.*, vol. 43, no. 7, pp. 2216–2227, 2009.

[181] J. C. Whitehead, "Plasma–catalysis: the known knowns, the known unknowns and the unknown unknowns," *J. Phys. D. Appl. Phys.*, vol. 49, no. 24, p. 243001, 2016.

[182] X. Tu and J. C. Whitehead, "Plasma-catalytic dry reforming of methane in an atmospheric dielectric barrier discharge: Understanding the synergistic effect at low temperature," *Appl. Catal. B Environ.*, vol. 125, pp. 439–448, 2012.

[183] C. Chen, P. Lei, H. Ji, W. Ma, J. Zhao, H. Hidaka, and N. Serpone, "Photocatalysis by titanium dioxide and polyoxometalate/TiO2 cocatalysts. intermediates and mechanistic study," *Environ. Sci. Technol.*, vol. 38, no. 1, pp. 329–337, 2004.

[184] A. E. Wallis, J. C. Whitehead, and K. Zhang, "Plasma-assisted catalysis for the destruction of CFC-12 in atmospheric pressure gas streams using TiO2," *Catal. Letters*, vol. 113, no. 1–2, pp. 29–33, 2007.

[185] H. Wang, Y. Yang, J. Wei, L. Le, Y. Liu, C. Pan, P. Fang, R. Xiong, and J. Shi, "Effective photocatalytic properties of N doped titanium dioxide nanotube arrays prepared by anodization," *React. Kinet. Mech. Catal.*, vol. 106, no. 2, pp. 341–353, 2012.

[186] A. M. Harling, V. Demidyuk, S. J. Fischer, and J. C. Whitehead, "Plasma-catalysis destruction of aromatics for environmental clean-up: Effect of temperature and configuration," *Appl. Catal. B Environ.*, vol. 82, no. 3–4, pp. 180–189, 2008.

[187] S. J. Macgregor, J. M. Koutsoubis, and S. M. Turnbull, "The design and operation of a compact high-voltage, high pulse repetition frequency trigger generator," *Meas. Sci. Technol.*, vol. 9, no. 11, pp. 1899–1905, 1998.

[188] A. D. Yost and S. G. Joshi, "Atmospheric nonthermal plasma-treated PBS inactivates Escherichia coli by oxidative DNA damage," *PLoS One*, vol. 10, no. 10, pp. 1–20, 2015.

[189] B. Jiang, J. Zheng, Q. Liu, and M. Wu, "Degradation of azo dye using non-thermal plasma advanced oxidation process in a circulatory airtight reactor system," *Chem. Eng. J.*, vol. 204–205, pp. 32–39, 2012.

[190] B. Jiang, J. Zheng, S. Qiu, M. Wu, Q. Zhang, Z. Yan, and Q. Xue, "Review on electrical discharge plasma technology for wastewater remediation," *Chem. Eng. J.*, vol. 236, pp. 348–368, 2014.

[191] R. B. Zhang, Y. Wu, J. Li, G. F. Li, T. F. Li, and Z. G. Zhou, "Water treatment by the bipolar pulsed dielectric barrier discharge (DBD) in water-air mixture," *J. Adv. Oxidation Tech*, vol. 7, no. 2. pp. 172–177, 2004.

[192] Sonia Muradia, “Study of low-voltage pulsed plasma discharges inside water using a bubble-generating porous ceramic electrode for wastewater treatment,” ph.D thesis, Shizuoka University, 2013.

[193] R. Zhang, C. Zhang, X. Cheng, L. Wang, Y. Wu, and Z. Guan, “Kinetics of decolorization of azo dye by bipolar pulsed barrier discharge in a three-phase discharge plasma reactor,” *J. Hazard. Mater.*, vol. 142, no. 1–2, pp. 105–110, 2007.

[194] Y. Ma, J. Chen, B. Yang, and Q. Yu, “Degradation of high concentration methanol in aqueous solution by dielectric barrier discharge,” *IEEE Trans. Plasma Sci.*, vol. 41, no. 7, pp. 1716–1724, 2013.

[195] Y. Z. Wen, H. J. Liu, W. P. Liu, and X. zhen Jiang, “Degradation of organic contaminants in water by pulsed corona discharge,” *Plasma Chem. Plasma Process.*, vol. 5, no. 2, pp. 137–146, 2005.

[196] M. Sato, S. Member, T. Tokutake, T. Ohshima, and A. T. Sugiarto, “Aqueous phenol decomposition by pulsed discharges on the water surface,” IEEE Trans. Plasma Sci., vol. 44, no. 5, pp. 1397–1402, 2008.

[197] K. Shimizu, N. Masamura, and M. Blajan, “Water purification by using microplasma treatment,” *J. Phys. Conf. Ser.*, vol. 441, no. 1, p. 012005, 2013.

[198] A. J. Kettle, B. M. Clark, and C. C. Winterbourn, “Superoxide converts indigo carmine to isatin sulfonic acid: Implications for the hypothesis that neutrophils produce ozone,” *J. Biol. Chem.*, vol. 279, no. 18, pp. 18521–18525, 2004.

[199] T. Miwa, Y. Y. Maruo, K. Akaoka, T. Kunioka, and J. Nakamura, “Development of colorimetric ozone detection papers with high ultraviolet resistance using ultraviolet absorbers,” *J. Air Waste Manag. Assoc.*, vol. 59, no. 7, pp. 801–808, 2009.

[200] Y. Y. Maruo, “Colorimetric ozone sensing paper and ozone monitoring,” in *Ozone and Ozone Depletion*, R. Sethi, S. Manchanda, and V. Sethi, Eds. Nova Science Publishers, Inc, 2013, pp. 141–155.

[201] M. Selma and K. Takashima, “Decolorization of indigo carmine dye by spark discharge in water,” *Int. J. Plasma Environ. Sci. Technol.*, vol. 2, no. 1, pp. 56–64, 2008.

[202] A. P. Fartode and D. V Parwate, “UV photolytic decolorization study of synthetic waste water containing indigo carmine dye in presence of H_2O_2,” vol. 3, no. 3, pp. 22–31, 2014.

[203] S. Ammar, R. Abdelhedi, C. Flox, C. Arias, and E. Brillas, “Electrochemical degradation of the dye indigo carmine at boron-doped diamond anode for wastewaters remediation,” *Environ. Chem. Lett.*, vol. 4, no. 4, pp. 229–233, 2006.

[204] D. Li, D. Yakushiji, S. Kanazawa, T. Ohkubo, and Y. Nomoto, “Decomposition of toluene by streamer corona discharge with catalyst,” *J. Electrostat.*, vol. 55, no. 3–4, pp. 311–319, 2002.

[205] I. Panorel, L. Kaijanen, I. Kornev, S. Preis, M. Louhi-Kultanen, and H. Siren, “Pulsed corona discharge oxidation of aqueous lignin: decomposition and aldehydes formation,” *Environ. Technol.*, vol. 35, no. 2, pp. 171–176, 2014.

[206] W. Xu, M.-W. Li, G.-H. Xu, and Y.-L. Tian, “Decomposition of CO_2 using dc corona discharge at atmospheric pressure,” *Jpn. J. Appl. Phys.*, vol. 43, no. 12, pp. 8310–8311, 2004.

[207] L. Zhengchao, P. Xunxi, D. Wenbo, and H. Huiqi, “Decomposition of CF3Cl by corona discharge,” *J. Enviromental Sci.*, vol. 9, no. 1, pp. 95–99, 1997.

[208] K. Satoh, T. Matsuzawa, and H. Itoh, “Decomposition of benzene in a corona discharge at atmospheric pressure,” *Thin Solid Films*, vol. 516, no. 13, pp. 4423–4429, 2008.

[209] J. Jarrige and P. Vervisch, “Decomposition of three volatile organic compounds by nanosecond pulsed corona discharge: Study of by-product formation and influence of high voltage pulse parameters,” *J. Appl. Phys.*, vol. 99, no. 11, pp. 113303.1- 113303-10, 2006.

[210] M. Elsawah, H. H. A. Ghafar, N. N. Morgan, S. Hassaballa, A. Samir, F. F. Elakshar, and A. A. Garamoon, “Corona discharge with electrospraying system for phenol removal from water,” *IEEE Trans. Plasma Sci.*, vol. 40, no. 1, pp. 29–34, 2012.

[211] T. Zhu, J. Li, Y. Jin, Y. Liang, and G. Ma, “Decomposition of benzene by non-thermal plasma processing: Photocatalyst and ozone effect,” *Int. J. Environ. Sci. Technol.*, vol. 5, no. 3, pp. 375–384, 2008.

[212] J. Van Durme, J. Dewulf, W. Sysmans, C. Leys, and H. Van Langenhove, “Efficient toluene abatement in indoor air by a plasma catalytic hybrid system,” *Appl. Catal. B Environ.*, vol. 74, no. 1–2, pp. 161–169, 2007.

[213] J. Leli, N. Dubreuil, J. Brisset, J. Leli, N. Dubreuil, J. Brisset, E. Processes, and D. C. Corona, “Electrolysis processes in d . c . corona discharges in humid air,” *J.PHYS III Fr.*, vol. 5, pp. 447–457, 1995.

[214] T. Sugai, K. Ogasawara, T. N. Son, A. Tokuchi, W. Jiang, and Y. Minamitani, “Investigation for development of high efficiency water treatment system using pulsed streamer discharge,” *2013 19th IEEE Pulsed Power Conf.*, pp. 1–5, 2013.

[215] T. Miichi, T. Fujimoto, and T. Takeda, “Decomposition of persistent organic compounds in water using pulsed discharge on water,” *Electrical Engineering in Japan*, vol. 186, no. 1, pp. 853–859, 2014.

[216] H. Akiyama, “Streamer discharges in liquids and their applications,” *IEEE Trans. Dielectr. Electr. Insul.*, vol. 7, no. 5, pp. 646–653, 2000.

[217] Z. Machala, M. Morvová, E. Marode, and I. Morva, “Removal of cyclohexanone in transition electric discharges at atmospheric pressure,” *J. Phys. D. Appl. Phys.*, vol. 33, pp. 3198–3213, 2000.

[218] B. Tarabová, K. Tarabová, K. Hensel, L. Šikurová, and Z. Machala, "Chemical and bactericidal effects induced in water treated by air transient spark," in *14th International symposium on high pressure low temperature plasma chemistry (HAKONE XIV), Zinnowitz, Germany.* 2014, pp1-6.

[219] K. Kučerová and K. Hensel, "Biological and chemical effect of dc transient spark discharge on Escherichia Coli," in *WDS'15*, 2015, pp. 192–198.

[220] A. T. Sugiarto, T. Ohshima, and M. Sato, "Advanced oxidation processes using pulsed streamer corona discharge in water," *Thin Solid Films*, vol. 407, no. 1–2, pp. 174–178, 2002.

[221] S. Yonemori and R. Ono, "Effect of discharge polarity on the propagation of atmospheric-pressure helium plasma jets and the densities of OH , NO , and O radicals," *Biointerphases*, vol. 10, no. 2, pp. 1–7, 2015.

[222] G. J. Pietsch and C. Humpert, "Discharge mechanism and ozone generation by surface discharges depending on polarity," in *Proceedings of International Symposium on High Pressure, Low Temperature Plasma Chemistry*, 2002, July 21 - 25, 2002 at Pühajärve, Estonia, pp. 1–5.

[223] T. Yano, N. Shimomura, I. Uchiyama, F. Fukawa, K. Teranishi and H. Akiyama. "Decolorization of indigo carmine solution using nanosecond pulsed power." *IEEE Transactions on Dielectrics and Electrical Insulation*, vol. 16, no. 4, pp 1081-1087, 2009.

[224] T. Kobayashi, T. Sugai, T. Handa, Y. Minamitani and T. Nose. "The effect of spraying of water droplets and location of water droplets on the water treatment by pulsed discharge in air." *IEEE Transactions on Plasma Science*, vol. 38, no. 10, pp 2675-2680, 2010.

[225] J. Ehlbeck, U. Schnabel, and M. Polak, "Low temperature atmospheric pressure plasma sources for microbial decontamination," *J. Phys. D: Appl. Phys*, vol. 44, pp. 453–459, 2011.

[226] D. Dobrynin, G. Friedman, A. Fridman, and A. Starikovskiy, "Inactivation of bacteria using dc corona discharge: Role of ions and humidity," *New J. Phys.*, vol. 13, pp. 1-14, 2011.

[227] H. Feng, P. Sun, Y. Chai, G. Tong, J. Zhang, W. Zhu, and J. Fang, "The interaction of a direct-current cold atmospheric-pressure air plasma with bacteria," *IEEE Trans. Plasma Sci.*, vol. 37, no. 1, pp. 121–127, 2009.

[228] Y. Li, "Production of vitamin B12 in recombinant Escherichia coli: An important step for heterologous production of structurally complex small molecules," *Biotechnol. J.*, vol. 9, no. 12, pp. 1478–1479, 2014.

[229] Y. L. Ji, W. Y. Jang, C. J. Hovde, "A brief overview of Escherichia coli O157:H7 and its plasmid O157", *J. Microbiol. Biotechnol.* vol. 20, no. 1, pp. 5–14, 2010.

[230] T. Foster, "Staphylococcus," in *Medical Microbiology*, 4th Edition, ed. Baron S. ,The University of Texas, Medical Branch at Galveston, 1996.

[231] M. M. Dinges, P. M. Orwin, P. M. Schlievert, M. M. Dinges, and P. M. Orwin, "Exotoxins of Staphylococcus aureus exotoxins of Staphylococcus aureus," *Clin. Microbiol. Rev.*, vol. 13, no. 1, pp. 16–34, 2000.

[232] E. Scallan, R. M. Hoekstra, F. J. Angulo, R. V. Tauxe, M. A. Widdowson, S. L. Roy, J. L. Jones, and P. M. Griffin, "Foodborne illness acquired in the United States-Major pathogens," *Emerg. Infect. Dis.*, vol. 17, no. 1, pp. 7–15, 2011.

[233] J. Kadariya, T. C. Smith, and D. Thapaliya, "*Staphylococcus aureus* and staphylococcal food-borne disease: an ongoing challenge in public health.," *Biomed Res. Int.*, vol. 2014, pp. 1–9, 2014.

[234] F. Lowy, "Antimicrobial resistance: the example of *Staphylococcus aureus*," *J. Clin. Invest.*, vol. 111, no. 9, pp. 1265–1273, 2003.

[235] A. Peschel, R. W. Jack, M. Otto, L. V Collins, P. Staubitz, G. Nicholson, H. Kalbacher, W. F. Nieuwenhuizen, G. Jung, A. Tarkowski, K. P. van Kessel, and J. a van Strijp, "Staphylococcus aureus resistance to human defensins and evasion of neutrophil killing via the novel virulence factor MprF is based on modification of membrane lipids with l-lysine.," *J. Exp. Med.*, vol. 193, no. 9, pp. 1067–1076, 2001.

[236] C. Mok, T. Lee, and P. Puligundla. "Afterglow corona discharge air plasma (ACDAP) for inactivation of common food-borne pathogens." *Food Research International*, vol. 69, pp 418-423, 2015.

[237] O. Lunov, V. Zablotskii, O. Churpita, A. Jäger, L. Polívka, E. Syková, N. Terebova, A. Kulikov, Š. Kubinová and A. Dejneka, "Towards the understanding of non-thermal air plasma action: effects on bacteria and fibroblasts." *RSC Advances*, vol. 6, no. 30, pp.25286-25292, 2016.

[238] S. Samukawa, M. Hori, S. Rauf, K. Tachibana, P. Bruggeman, G. Kroesen, J. C. Whitehead, A. B. Murphy, A. F. Gutsol, S. Starikovskaia, U. Kortshagen, J. P. Boeuf, T. J. Sommerer, M. J. Kushner, U. Czarnetzki, and N. Mason, "The 2012 Plasma Roadmap," *J. Phys. D Appl. Phys. J. Phys. D Appl. Phys*, vol. 45, no. 45, pp. 253001–253001, 2012.

[239] S. Kanazawa, H. Kawano, S. Watanabe, T. Furuki, S. Akamine, R. Ichiki, T. Ohkubo, M. Kocik, and J. Mizeraczyk, "Observation of OH radicals produced by pulsed discharges on the surface of a liquid," *Plasma Sources Sci. Technol.*, vol. 20, no. 3, p. 034010, Jun. 2011.

[240] S. Kanazawa, T. Furuki, T. Nakaji, S. Akamine, and R. Ichiki, "Measurement of OH radicals in aqueous solution produced by atmospheric-pressure LF plasma jet," in *Ecological Society of America Conf., USA*, 2012.

[241] H. Eto, Y. Ono, A. Ogino, and M. Nagatsu, "Low-temperature sterilization of wrapped materials using flexible sheet-type dielectric barrier discharge," *Appl. Phys. Lett.*, vol. 93, no. 22, 2008.

[242] J. Guo, K. Huang, and J. Wang, "Bactericidal effect of various non-thermal plasma agents and the influence of experimental conditions in microbial inactivation: A review," *Food Control*, vol. 50, pp. 482–490, 2015.

[243] B. G. Ershov and P. A. Morozov, “The kinetics of ozone decomposition in water, the influence of pH and temperature,” *Russ. J. Phys. Chem. A*, vol. 83, no. 8, pp. 1295–1299, 2009.

[244] J. Staehelin and J. Hoigne, “Decomposition of ozone in water in the presence of organic solutes acting as promoters and inhibitors of radical chain reactions,” *Environ. Sci. Technol.*, vol. 19, no. 12, pp. 1206–1213, 1985.

[245] I. E. Dreosti, *Trace Elements, Micronutrients, and Free Radicals*. Springer Science & Business Media, 1991.

[246] M. Sun and L. J. Cai, “Diagnosis of OH radicals in air negative pulsed discharge with nozzle-cylinder electrode by optical emission spectroscopy,” *IEEE Trans. Plasma Sci.*, vol. 40, no. 5 part 2, pp. 1395–1398, 2012.

[247] Y. Ikeda, A. Moon, and M. Kaneko, “Development of microwave-enhanced spark-induced breakdown spectroscopy,” *Appl. Opt.*, vol. 49, no. 13, pp. C95–C100, 2010.

[248] H. Tresp, M. U. Hammer, J. Winter, K.-D. Weltmann, and S. Reuter, “Quantitative detection of plasma-generated radicals in liquids by electron paramagnetic resonance spectroscopy,” *J. Phys. D. Appl. Phys.*, vol. 46, no. 43, p. 435401, 2013.

[249] S. E. Page, W. A. Arnold, and K. McNeill, “Terephthalate as a probe for photochemically generated hydroxyl radical.,” *J. Environ. Monit.*, vol. 12, no. 9, pp. 1658–1665, 2010.

[250] S. Kanazawa, T. Furuki, T. Nakaji, S. Akamine, and R. Ichiki, “Application of chemical dosimetry to hydroxyl radical measurement during underwater discharge,” *J. Phys. Conf. Ser.*, vol. 418, pp. 5-12, Mar. 2013.

[251] T. Mason, J. P. Lorimer, and Y. Zhao, “Dosimetry in sonochemistry: the use of aqueous terephthalic ion as a fluorescence monitor,” *Ultrason. Sonochem.*, vol. 1, no. 2, pp. 2–6, 1994.

[252] http://www.ssi.shimadzu.com/products/productgroup.cfm?subcatlink=spectrofluoro

[253] M. Sahni and B. R. Locke, “Quantification of hydroxyl radicals produced in aqueous phase pulsed electrical discharge reactors,” *Ind. Eng. Chem. Res.*, vol. 45, no. 17, pp. 5819–5825, 2006.

[254] D. M. Stanbury, “Reduction potentials involving inorganic free radicals in aqueous solution,” *Advances in Inorganic Chemistry*, vol. 33, no. C. pp. 69–138, 1989.

[255] P. Hajkova, P. Spatenka, J. Horsky, I. Horska and A. Kolouch. "Photocatalytic effect of TiO2 films on viruses and bacteria."*Plasma Processes and Polymers*, vol. 4, no. S1, pp S397-S401, 2007.

[256] S. Futamura, A. Zhang, H. Einaga, and H. Kabashima, “Involvement of catalyst materials in nonthermal plasma chemical processing of hazardous air pollutants,” *Catal. Today*, vol. 72, no. 3–4, pp. 259–265, 2002.

[257] T. Hammer, T. Kappes, and M. Baldauf, “Plasma catalytic hybrid processes: Gas discharge initiation and plasma activation of catalytic processes,” *Catal. Today*, vol. 89, no. 1–2, pp. 5–14, 2004.

[258] S. Futamura, H. Einaga, H. Kabashima, and L. Y. Hwan, “Synergistic effect of silent discharge plasma and catalysts on benzene decomposition,” *Catal. Today*, vol. 89, no. 1–2, pp. 89–95, 2004.

[259] S. Delagrange, L. Pinard, and J. M. Tatibouët, “Combination of a non-thermal plasma and a catalyst for toluene removal from air: Manganese based oxide catalysts,” *Appl. Catal. B Environ.*, vol. 68, no. 3–4, pp. 92–98, 2006.

[260] A. Vandenbroucke, R. Morent, N. De Geyter, M. T. N. Dinh, J. Giraudon, J. Lamonier, and C. Leys, “Plasma-catalytic Decomposition of TCE,” *Int. J. Plas. Envir Sci. & Technol.* vol. 4, no. 2, pp. 135–138, 2010.

[261] X. L. Hao, M. H. Zhou, and L. C. Lei, “Non-thermal plasma-induced photocatalytic degradation of 4-chlorophenol in water,” *J. Hazard. Mater.*, vol. 141, no. 3, pp. 475–482, 2007.

[262] P. Lukes, M. Clupek, P. Sunka, F. Peterka, T. Sano, N. Negishi, S. Matsuzawa, and K. Takeuchi, “Degradation of phenol by underwater pulsed corona discharge in combination with TiO_2 photocatalysis,” *Res. Chem. Intermed.*, vol. 31, no. 4, pp. 285–294, 2005.

[263] K. Marouf-Khelifa, F. Abdelmalek, A. Khelifa, and A. Addou, “TiO_2-assisted degradation of a perfluorinated surfactant in aqueous solutions treated by gliding arc discharge,” *Chemosphere*, vol. 70, no. 11, pp. 1995–2001, 2008.

[264] T. C. Wang, N. Lu, J. Li, and Y. Wu, “Plasma-TiO_2 catalytic method for high-efficiency remediation of p-nitrophenol contaminated soil in pulsed discharge,” *Environ. Sci. Technol.*, vol. 45, no. 21, pp. 9301–9307, 2011.

[265] C. Gu and C. Shannon, “Investigation of the photocatalytic activity of TiO2-polyoxometalate systems for the oxidation of methanol,” *J. Mol. Catal. A Chem.*, vol. 262, no. 1–2, pp. 185–189, 2007.

[266] M. Castellote and N. Bengtsson, “Chapter 2 Principles of TiO_2 Photocatalysis,” in *Applications of Titanium Dioxide Photocatalysis to Construction Materials*, ed. Ohama, Yoshihiko, Van Gemert, Dionys, Springer, 2011, pp. 5–10.

[267] P. Innocenzi and L. Malfatti, “Mesoporous thin films: properties and applications.,” *Chem. Soc. Rev.*, vol. 42, no. 9, pp. 4198–216, 2013.

[268] W. Li, Z. Wu, J. Wang, A. a Elzatahry, and D. Zhao, “A Perspective on Mesoporous TiO_2 Materials,” *Chem. Mater.*, vol. 26, pp. 287–298, 2014.

[269] A. Mills, M. Sheik, C. O’Rourke, and M. McFarlane, “Adsorption and photocatalysed destruction of cationic and anionic dyes on mesoporous titania films: Reactions at the air-solid interface,” *Appl. Catal. B Environ.*, vol. 89, no. 1–2, pp. 189–195, 2009.

[270] A. Mills, A. Lepre, N. Elliott, S. Bhopal, I. P. Parkin, and S. A. O’Neill, “Characterisation of the photocatalyst Pilkington Activ™: A reference film

photocatalyst?," *J. Photochem. Photobiol. A Chem.*, vol. 160, no. 3, pp. 213–224, 2003.

[271] X. Yang, H. Fu, A. Yu, and X. Jiang, "Large-surface mesoporous TiO_2 nanoparticles: Synthesis, growth and photocatalytic performance," *J. Colloid Interface Sci.*, vol. 387, no. 1, pp. 74–83, 2012.

[272] W. Chen, X. Sun, Q. Cai, D. Weng, and H. Li, "Facile synthesis of thick ordered mesoporous TiO2 film for dye-sensitized solar cell use," *Electrochem. commun.*, vol. 9, no. 3, pp. 382–385, 2007.

[273] D. Feng, W. Luo, J. Zhang, M. Xu, R. Zhang, H. Wu, Y. Lv, A. M. Asiri, S. B. Khan, M. M. Rahman, G. Zheng, and D. Zhao, "Multi-layered mesoporous TiO_2 thin films with large pores and highly crystalline frameworks for efficient photoelectrochemical conversion," *J. Mater. Chem. A*, vol. 1, no. 5, pp. 1591–1599, 2013.

[274] Evonik Industry, "AEROXIDE®, AERODISP® and AEROPERL® Titanium Dioxide as Photocatalyst Technical Information 1243," 2015.

[275] D. He, Y. Sun, L. Xin, and J. Feng, "Aqueous tetracycline degradation by non-thermal plasma combined with nano-TiO2," *Chem. Eng. J.*, vol. 258, pp. 18–25, 2014.

[276] J. Li, Z. Zhou, H. Wang, G. Li, and Y. Wu, "Research on decoloration of dye wastewater by combination of pulsed discharge plasma and TiO_2 nanoparticles," *Desalination*, vol. 212, no. 1–3, pp. 123–128, 2007.

[277] H. Wang, J. Chu, H. Ou, R. Zhao, and J. Han, "Analysis of TiO2 photocatalysis in a pulsed discharge system for phenol degradation," *J. Electrostat.*, vol. 67, no. 6, pp. 886–889, 2009.

[278] Y. Zhang, R. Zhang, W. Ma, X. Zhang, L. Wang, and Z. Guan, "Purification of water by bipolar pulsed discharge plasma combined with TiO_2 catalysis," *J. Phys. Conf. Ser.*, vol. 418, p. 012125, 2013.

[279] L. Lei, Y. Su, M. Zhou, X. Zhang, and X. Chen, "Fabrication of multi-non-metal-doped TiO2 nanotubes by anodization in mixed acid electrolyte," *Mater. Res. Bull.*, vol. 42, no. 12, pp. 2230–2236, 2007.

[280] Y. Zhang, Q. Xin, Y. Cong, Q. Wang, and B. Jiang, "Application of TiO_2 nanotubes with pulsed plasma for phenol degradation," *Chem. Eng. J.*, vol. 215–216, pp. 261–268, 2013.

[281] Y. Takahashi, Y. Shibata, M. Maeda, Y. Miyano, K. Murai and A. Ohmori. "Plasma-spraying synthesis of high-performance photocatalytic TiO2 coatings." In *IOP Conference Series: Materials Science and Engineering*, vol. 61, no. 1, p. 012039. IOP Publishing, 2014.

[283] Jyotsna Rao, "Section 3 Microbiology-Key Points to Remember" in *QRS for BDS II Year,* 2nd ed. Elsevier Health Sciences, US, pp 353-355. 2014.

[284] World Health Organization , "5.8 Methods of sterilization" in *The International Pharmacopoeia - Fifth Edition*, 2015

[285] G. Mendez, T. R. Brandão and C. L. Silva, "Ethylene oxide sterilization of medical devices: A review", *Am. J. Infect Control. Vol. 25, issue. 9,* pp 574-581, 2007.

[286] W. A. Rutala, D. J. Weber, and the Healthcare Infection Control Practices Advisory Committee (HICPAC), "Guideline for Disinfection and Sterilization in Healthcare Facilities", Centers for Disease Control and Prevention, University of North Carolina, 2008.

[287] M. Silindir, A. Y. Özer, "Sterilization Methods and the Comparison of E-Beam Sterilization with Gamma Radiation Sterilization", *FABAD J. Pharm. Sci., vol. 34,* pp 43–53, 2009.

[288] T. Rodon, E. Poppe, A. Fabbro, T. Baltus, "The effect of common sterilization techniques on the mechanical properties of DuPont Performance Polymers Special Control (SC) and Premium Control (PC) grades", Du Pont de Nemours Intl. USA, pp1-26, 2010

[289] K. A. da Silva Aquino, "9 Sterilization by Gamma Irradiation" in *Gamma Radiation,* Ed. F. Adrovic, In Tech, pp 171-206, 2012

[290] G. Dvorak, "Disinfection 101", Center for Food Security and Public Health, Iowa State University, pp 1-20, 2008

[291] A. Sharma, "An Ultraviolet-Sterilization Protocol for Microtitre Plates", *J. Exp. Micro. and Immu.vol. 16,* pp 144-147, 2012

[292] MD. I. A. ANSARI and A. K. DATTA. "an overview of sterilization methods for packaging materials used in aseptic packaging systems", *Trans. IChemE., vol 81, Part C,* pp 57-65, 2003.

[293] G. Katara, N. Hemvani, S. Chitnis, V. Chitnis, and DS. Chitnis, "Surface disinfection by exposure to germicidal UV light", *Indi. J. Med. Micobial, vol. 26. issure. 3,* pp 241-242, 2008.

[294] Y. Gao, Y. Deng, and Y. Men, "Disruption of microbial cell within waste activated sludge by DC corona assisted pulsed electric field", *IEEE Trans. Plasma Sci., vol. 44, no. 11,* pp. 2682–2691, 2016.

APPENDIX: PUBLISHED PAPERS

Steady-State Corona Discharges in Atmospheric Air for Cleaning and Decontamination

Sirui Li, Igor V. Timoshkin, *Member, IEEE*, Michelle Maclean, Scott J. MacGregor, *Member, IEEE*, Mark P. Wilson, *Member, IEEE*, Martin J. Given, *Senior Member, IEEE*, John G. Anderson, and Tao Wang

***Abstract*— It is shown that high-voltage corona discharges in atmospheric air have significant potential for bacterial inactivation. Neutral reactive oxygen and nitrogen species and ions generated by the corona discharges act upon the target liquid or solid surfaces and produce chemical or biological effects. The concentration of ions and reactive species including ozone generated by these discharges defines the efficiency of the corona treatment. In this paper, the chemical (oxidation) effect of direct corona discharges (where ions act upon the target surface) and indirect corona discharges (where ions are screened by a grounded metallic mesh) in atmospheric air is studied by measuring the degree of decolorization of a blue dye dissolved in water. The biological effects of the direct and indirect discharges are studied by observing the degree of bacterial inactivation of gram-negative and gram-positive microorganisms, *Escherichia coli* and *Staphylococcus aureus*, seeded on agar plates. The relationship between the ozone concentration and biological efficiency of the corona treatment is evaluated. The obtained results can be used for optimization of cleaning and inactivation treatment processes based on the use of nonthermal plasma produced under dc energization conditions.**

***Index Terms*— Bactericidal effects, corona discharges.**

I. Introduction

CORONA discharges in air are produced by highly divergent electric fields, which result in ionization of gas molecules in the vicinity of a high-voltage electrode. Oxygen is an electronegative gas, and in the case of negative corona discharge, electrons generated in the ionization zone can form negative ions (mainly super oxide anions), which travel toward the anode. Formation and removal of negative space charge in the transport zone of the discharge results in the formation of transient current impulses (Trichel impulses).

In the case of positive corona discharges, space charge effects may result in the formation of flashing discharges, large current impulses that are associated with the formation and development of positive streamers and have significantly higher magnitude as compared with Trichel impulses generated at the same negative voltage.

Depending upon the energization level and gas parameters, steady-state corona discharges can also be generated. Negative ions are the main charge carriers in the case of negative corona discharges; positively charged clusters and positive ions are the main charge carriers that reach the earthed electrode in the case of positive corona discharges [1]. Corona discharges in air produce a complex mixture of ions, charged clusters, and neutral chemical species. Although the chemical composition of nonthermal plasma discharges in air is not yet fully understood, it is known that such discharges generate super oxide anions, hydroxyl and hydro-peroxyl radicals, hydrogen peroxide, nitrogen oxide species, and reactive oxygen species (ROS) including ozone and other chemical species.

Biological effects of corona discharges were studied and reported in [2]–[5]. Chemically active species generated by corona discharges are able to induce oxidation damage to biomolecules and cause alteration in the functioning of biological membranes [6]. Ozone is the main oxygen species produced by nonthermal plasma discharges in air. Ozone has a high oxidation potential and can play a leading role in the bactericidal effects of corona discharges [7]–[9]. However, other ROS and reactive nitrogen species (RNS) generated by corona discharges are capable of producing a significant bactericidal effect.

In this paper, two types of corona discharges are used to investigate their chemical (oxidation) and biological (inactivation) capability: direct and indirect discharges. Biological samples used in this paper are bacterial seeded agar plates, and the samples used to study the oxidation capability are samples of blue dye (indigo carmine solution). In the case of direct corona discharges the samples are located directly under the corona generating electrode. The plates are covered with sterile aluminum foil (which acted as a ground electrode) and filled with agar or indigo carmine solution. In this case all kinds of chemical species, charged and neutral, are able to reach the bacterial samples on the agar surfaces or liquid solution surface. In the case of indirect corona treatment, a metallic mesh is used as a grounded electrode. In this case, the bacterial-seeded agar plates or plates with indigo carmine solution are located behind this mesh. Thus, only electrically neutral species are able to pass through the mesh to interact with the samples. UV light generated by corona discharges is able to reach the samples in both, direct and indirect cases. The corona generating electrode is stressed with positive and negative dc voltages, and steady-state positive corona discharges and negative discharges are produced. The bacteria used in this paper are *Staphylococcus aureus* (*S. aureus*) and *Escherichia coli* (*E. coli*).

Manuscript received December 21, 2012; revised March 27, 2013 and April 7, 2013; accepted May 11, 2013. Date of publication June 18, 2013; date of current version October 7, 2013.

The authors are with the Department of Electronic and Electrical Engineering, University of Strathclyde, Glasgow G1 1XW, U.K. (e-mail: s.li@strath.ac.uk; igor.timoshkin@strath.ac.uk; michelle.maclean@strath.ac.uk; s.macgregor@strath.ac.uk; m.wilson@eee.strath.ac.uk; m.given@eee.strath.ac.uk; j.g.anderson@strath.ac.uk; t.wang@eee.strath.ac.uk).

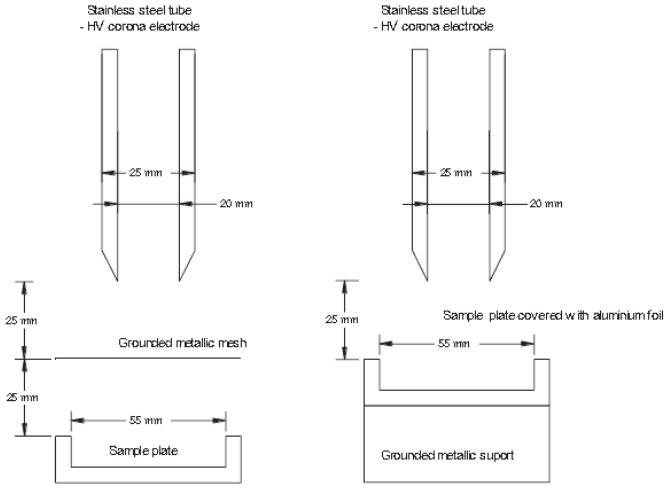

Fig. 1. Diagrams of (left) indirect and (right) direct corona discharge treatment cells.

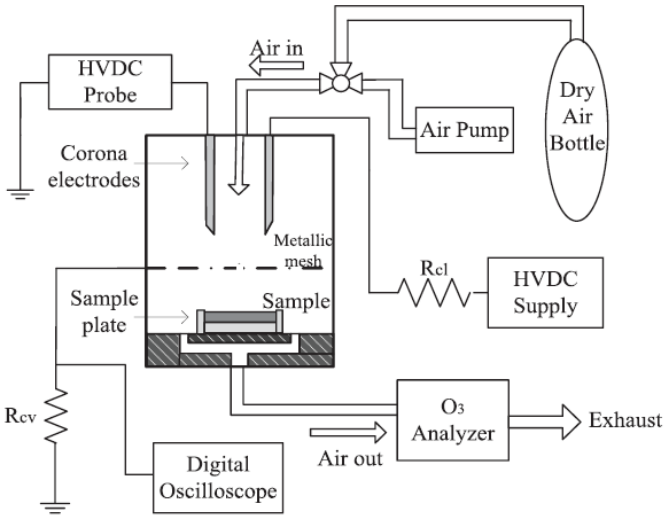

Fig. 2. Schematic diagram of the plasma treatment system configured for indirect treatment.

These are chosen as test bacteria as they are significant pathogens and represent a gram-positive and a gram-negative bacterial species, respectively. The chemical oxidation effect of corona discharges is studied by measuring the degree of decolorization of indigo carmine water solution using a spectrophotometer. Ozone concentration and current waveforms are monitored in the present tests to establish potential correlation between the electrical parameters of corona discharges, the concentration of ROS produced by these discharges and their chemical and bactericidal capability.

II. Description of the Experimental System

Two different plasma treatment test cells are used in the experiments, indirect and direct treatment cells. The cross sections of both treatment cells are shown in Fig. 1.

In both cases, the main bodies of the test cells are made of a Perspex cylinder with an inside diameter of 79 mm. Two polyvinyl chloride (PVC) flanges cover the top and bottom of this cylinder. A stainless-steel tube with a sharp edge (20-mm internal diameter; 25-mm external diameter) is located inside the cylinder and connected to the high-voltage terminal at the top of the cell. This stainless-steel tube acted as a corona discharge electrode. In the case of direct treatment tests sample plates covered with aluminum foil are placed on a metallic support stand inside the test cell that provides electrical contact between the foil and the grounded electrode. This grounded electrode provided a return path for corona current in this system. Thus, the foil is kept at earth potential and the indigo carmine solution or agar seeded with bacteria, which is placed on top of this aluminum foil, is subjected to the direct action of corona discharges. The distance between the edge of the corona electrode and the biological or chemical sample surface is 25 mm. These samples (bacterial seeded agar or indigo carmine solution) are contained in 55-mm diameter plastic plates covered with aluminum foil as discussed above. In the case of indirect treatment, a grounded metallic mesh is located 25 mm down from the sharp edge of the corona electrode. For this type of treatment the chemical and microbiological samples are also contained in 55-mm diameter plastic plates (but not covered with foil) and are placed at the bottom area of this test cell, behind the grounded mesh. The distance between the sample and the metallic mesh is also 25 mm. The PVC flanges are equipped with gas ports to ensure air flow through the test cell during experiments. A schematic diagram of the indirect corona discharge treatment system is shown in Fig. 2, in the case of direct treatment the system is the same except the test cell which is as shown in Fig. 1.

The plasma treatment test cells are energized using a high-voltage dc power supply, which is connected to the test cell through a current-limiting resistor (R_{cl} = 28 MΩ). A high-voltage dc probe (TesTech) is attached to the tubular corona electrode, and the applied voltage is monitored using a digital multimeter (ISOTECH 705). To monitor transient and dc corona currents, a 1-kΩ current viewing resistor R_{cv} is used. The shunt is connected to the mesh in the case of indirect treatment, or the conductive sample holder in the case of direct treatment. The voltage drop across this shunt is monitored using a Tektronix TDS 2024 digital oscilloscope (bandwidth 200 MHz, sampling rate 2 G samples/s). A 50-Ω BNC cable is used to connect the oscilloscope and the resistive shunt.

Two types of air are used in the decolorization tests: ambient atmospheric air and compressed air. In bacterial inactivation, only compressed air (~1.5% relative humidity) is used. Ambient atmospheric air (~40% relative humidity) is delivered to the test cell using an air compressor (FIAC FX95). This compressor is connected to the top inlet gas port of the test cell through a gas distribution board that allowed a constant flow rate and pressure to be maintained. Air pressure in the test cell is kept at 0.2-atm gauge for both dry air and atmospheric air tests. An ozone analyzer (IN-2000 LOCON, INUSA Inc.) is connected to the gas outlet port of the test cell to monitor ozone concentration during the experiments.

The magnitude of voltage applied to the test cell to generate corona discharge is 30 ± 0.2 kV; both polarities, positive

TABLE I
CORONA DISCHARGE CURRENTS

Treatment	Type of Gas	+30 kV	−30 kV
Indirect	Atmospheric air	(80–90) μA	−(120–140) μA
Indirect	Compressed air	(68–80) μA	−(138–152) μA
Direct	Atmospheric air	(30–40) μA	−(70–90) μA
Direct	Compressed air	(33–50) μA	−(70–100) μA

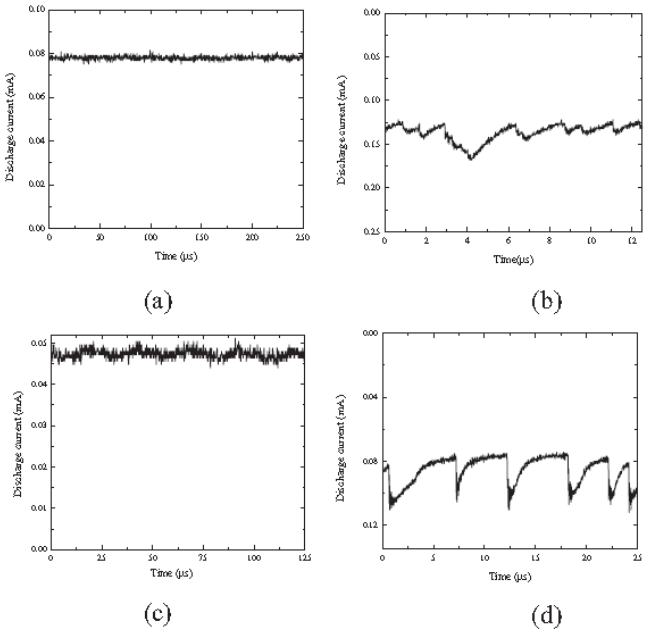

Fig. 3. Corona current waveforms: (a) +30 kV (indirect). (b) −30 kV (indirect); (c) +30 kV (direct); and (d) −30 kV (direct).

and negative are used. The discharge currents of positive and negative corona discharges for indirect and direct treatments are listed in Table I and typical current waveforms for these corona discharges are shown in Fig. 3.

Observed variations in the corona discharge current can be a result of the stochastic nature of the discharges and potential slight changes in humidity inside the test cell during treatment of the samples.

The electric field inside the direct and indirect treatment test cells is simulated using ELECTRO electrostatic field simulation software (INTEGRATED Engineering Software, Canada) and the results of this analysis are shown in Fig. 4. The vertical walls of the sample plates are at 12 and 67 mm, the field between these two points across the sample–air interface (0.05 mm above the sample surface) is calculated. The bacterial seeded agar is modeled as a medium with relative permittivity of 51 [10] and indigo carmine water solution is modeled as medium with relative permittivity of 80.

Inside the direct treatment test cell, the strength of the electric field across the sample surface–air interface is significantly higher as compared with the same interface in the indirect treatment test cell. This is due to the screening effect of the metallic mesh and the longer distance between the sample surface and the edge of the high-voltage electrode. These

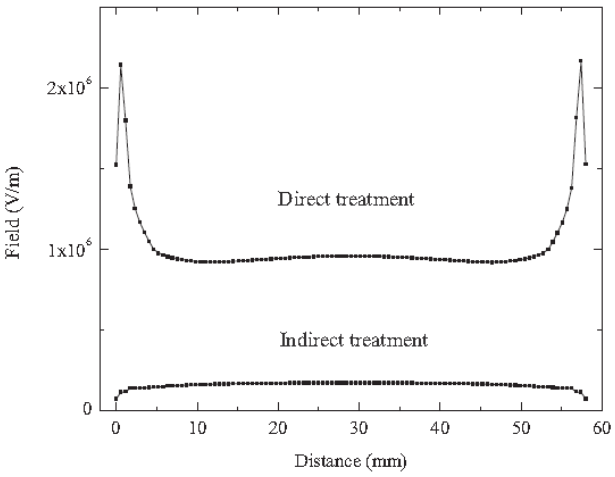

Fig. 4. Electric field magnitude across the interface between the sample surface and air in the case of direct and indirect treatment. Solid points: agar surface. Solid lines: water surface.

simulation results show that there is practically no difference in the field magnitude across indigo carmine solution and agar surfaces and that during indirect treatment the potential field effects will be minimal.

III. OXIDATION OF BLUE DYE SOLUTION

Indigo carmine dye ($C_{16}H_8N_2Na_2O_8S_2$) is used for evaluation of the oxidation capability of corona discharges. An oxidation effect is achieved due to ozone, superoxides, and other ROS produced by the corona discharges in air. Reactions with ROS can convert indigo carmine to isatin-5-sulfonic acid; therefore, a sample of blue indigo carmine solution can be decolorized, and its optical transmittance will be changed [11], [12]. A UV-visible spectrophotometer (Biomate, Thermo-Spectronics Europe) is used to measure the change in transmittance of corona treated samples. A pH meter (Hanna Instruments PH 210) with a miniature probe (Sentek) is used to measure pH values of dye samples before and after corona treatment.

A. Optical Properties of Untreated Dye Solution

Chemical samples (indigo carmine solutions) are prepared by dissolving 50 mg of dye in 200 ml of distilled water. The concentration of indigo carmine dye is 0.25 g/L, and the initial pH value of this solution is 5.0–5.2. The transmittance of the untreated blue dye solutions is measured, and compared with that of pure distilled water this differential spectrum is shown in Fig. 4.

The transmittance of the indigo carmine solutions in the range 500–600 nm is zero, indicating a strong absorbance of light in this wavelength region.

B. Decolorization by Indirect Corona Discharges

Samples of indigo carmine solution are exposed to indirect corona discharges. Treatment time intervals are 2, 5, and 10 min. The difference in transmittance between the treated and untreated samples is measured. Positive corona discharges

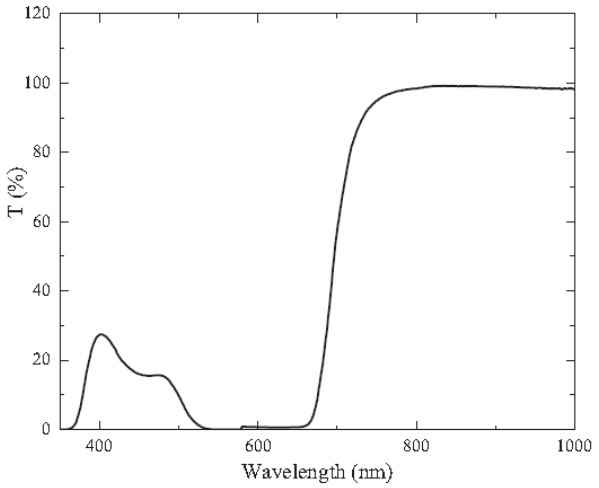

Fig. 5. Differential transmittance of the untreated indigo carmine solution and pure water.

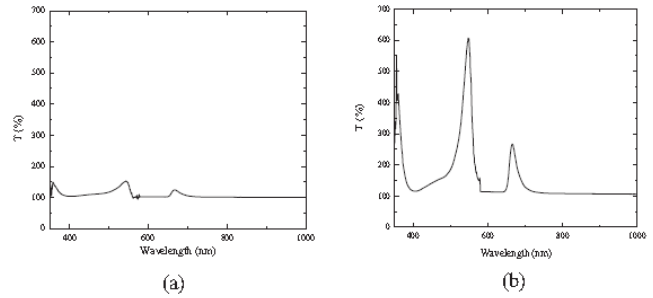

Fig. 6. Relative change in transmittance induced by positive indirect corona discharges: (a) 2- and (b) 10-min treatment time.

resulted in an increase in the transmittance, T, of indigo carmine solutions; this change in transmittance for 2- and 10-min intervals of indirect treatment is shown in Fig. 6.

Ozone concentration is monitored during these tests. Ozone concentrations generated by this type of corona discharge are in the range 1–2 ppm (for both types of air, compressed and atmospheric). A change in pH of dye solution is registered after indirect corona action: the pH decreased to 4.5–4.7 after 10-min exposure.

A peak in relative transmittance at 550 nm is selected as an indicator of the oxidation capability of corona discharges. Using the Beer–Lambert law, the concentration of indigo carmine in unexposed and exposed solutions is calculated, and the results are shown in Fig. 7(a). Significantly higher concentrations of ozone are observed in the case of negative indirect corona discharges, up to 40 ppm in both dry air and atmospheric air. The pH value of treated dye solutions decreased to 3.8–4.1 after 10-min exposure. The decolorization effect is more pronounced in this case, and the change in concentration of indigo carmine in solution as a function of exposure time is shown in Fig. 7(b). Each point on these graph represents an average value over three individual tests, vertical bars show the corresponding standard deviation. Specific energies, J/m^2, are also shown in Fig. 7 for dry and atmospheric air. These energies are calculated by dividing the total energy

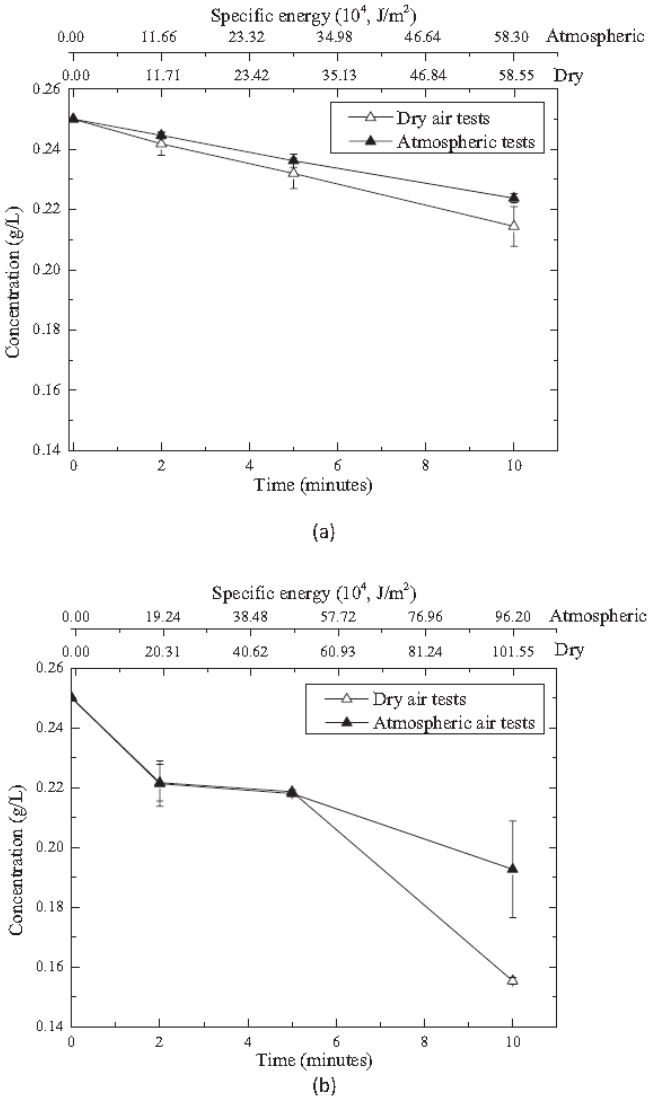

Fig. 7. Concentration of indigo carmine as a function of exposure time and specific energy. (a) Positive indirect corona discharges and (b) negative indirect corona discharges.

(current of corona discharge multiplied by exposure time and by voltage) by the surface area of the sample plate. Although in the case of indirect treatment the majority of charged particles are not able to reach the sample surface, these specific energies can be used for efficiency comparison in the case of direct and indirect processes.

C. Decolorization by Direct Corona Discharges

Indigo carmine solution of the same concentration is exposed to direct corona discharges. Treatment time intervals are the same as in the case of indirect corona treatment (2, 5, and 10 min). For positive direct corona treatment, the ozone concentrations in both dry air and atmospheric air are in the range of 1–2 ppm, and the pH values of the sample solution decreased to 4.6–4.9 after 10-min exposure. In the case of negative direct corona treatment, the ozone concentrations are 40–80 ppm. The pH value for this type of treatment is lower

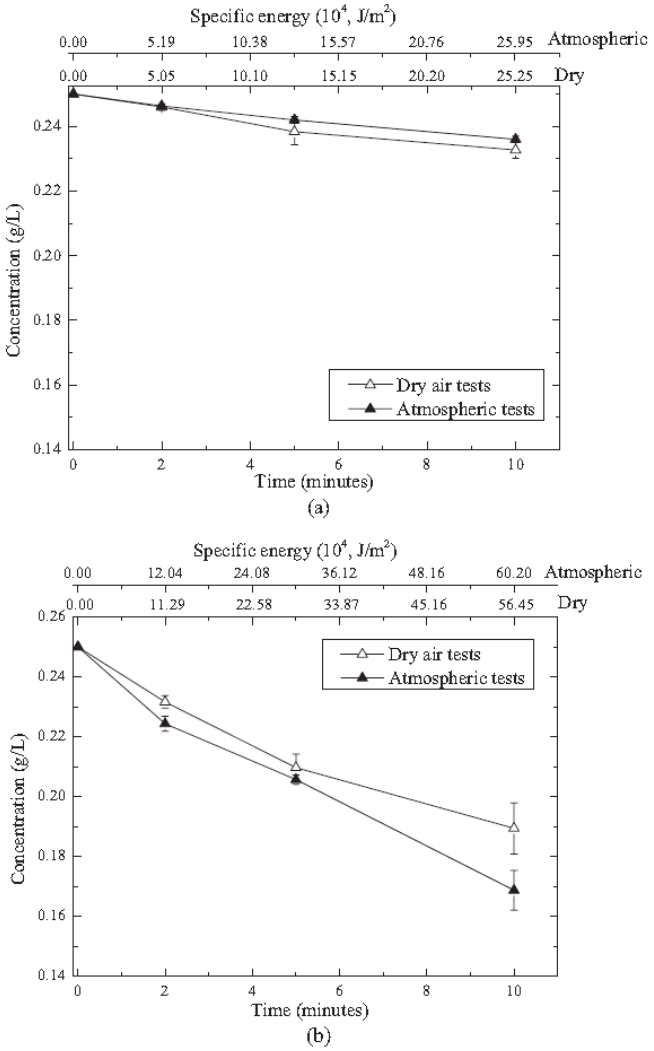

Fig. 8. Concentration of indigo carmine as a function of exposure time and specific energy. (a) Positive direct corona discharges and (b) negative direct corona discharges.

as compared with the positive direct treatment; this value decreased to 3.9–4.0 after 10-min exposure. The change in the concentration of indigo carmine solution after direct corona discharge treatment is shown in Fig. 8.

IV. Bacterial Inactivation by Corona Discharges

Two types of bacteria, *E. coli* (gram-negative) and *S. aureus* (gram-positive) are used in the biological tests to evaluate the inactivation efficiency of direct and indirect discharges of both polarities. Bacteria are grown in 100 ml of nutrient broth at 37 °C for 18 h under rotary conditions (120 rpm), then diluted in phosphate buffered saline to a population density of 10^3 colony forming units (CFUs) per milliliter. For indirect exposure tests, 100 μl of this is plated onto the agar-filled 55-mm diameter plastic sample plates, giving a starting population of approximately 100–200 CFU/plate. For direct exposure tests, 100 μl of bacterial sample is plated onto agar surfaces held in foil-covered 55-mm diameter sample plates. The starting population is the same as in the case of direct

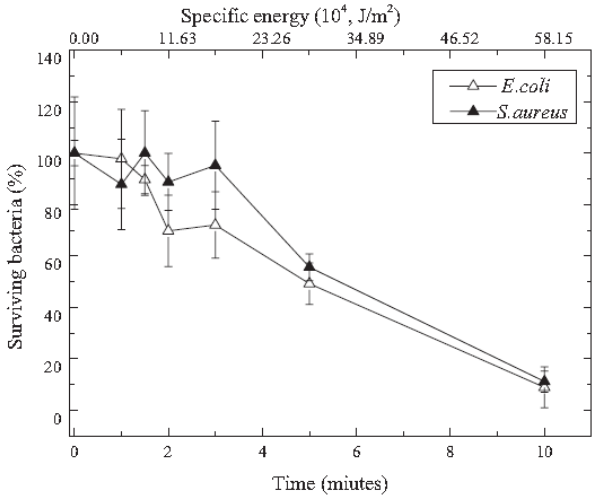

Fig. 9. Surviving fractions of *E. coli* and *S. aureus* after exposure to positive indirect corona discharges. Horizontal scales: exposure time and specific energy.

exposure tests. During corona treatment each bacterial seeded plate is located in the corresponding corona treatment test cell. Dry air is fed into these test cells to keep gas pressure inside at 0.2-atm gauge. Bacterial samples are exposed to direct and indirect corona discharges for different time intervals: 1, 1.5, 2, 3, 5, and 10 min. Corona treatment samples are then incubated at 37 °C for 24 h and then enumerated.

A. Inactivation Effect of Positive Indirect Corona Discharges

In the case of positive energization (+30 kV) the observed ozone concentration is ~2 ppm. Inactivation rates achieved for both types of bacteria in these indirect corona tests are shown in Fig. 9. Each point on this graph represents an average value over three individual inactivation tests, vertical bars show the corresponding standard deviation. The top horizontal scale in Fig. 9 shows the specific energy, J/m^2. The maximum specific energy in the case of positive energization is $58.15 \cdot 10^4$ J/m^2 (10-min exposure time). This energy produces a noticeable bactericidal effect, ~91% for *E. coli* and ~89% for *S. aureus*, although in the case of indirect treatment the majority of the charged particles do not reach the agar surface.

B. Inactivation Effect of Negative Indirect Corona Discharges

In the case of negative energization (−30 kV) the observed ozone concentration is significantly higher, 12–30 ppm. The bactericidal effect in this case is also stronger, and inactivation rates for both types of bacteria exposed to negative indirect corona discharges are shown in Fig. 10. Almost complete inactivation of *E. coli* (~99%) is achieved after 1 min of treatment. The population of *S. aureus* is also reduced significantly, by ~93%, by 1 min of indirect corona treatment.

As in the case of positive energization, each point on Fig. 10 represents an average value over three individual inactivation tests, vertical bars show the corresponding standard deviation. The top horizontal scale in Fig. 10 shows the specific energy as in the case of Fig. 9. The maximum specific energy in the

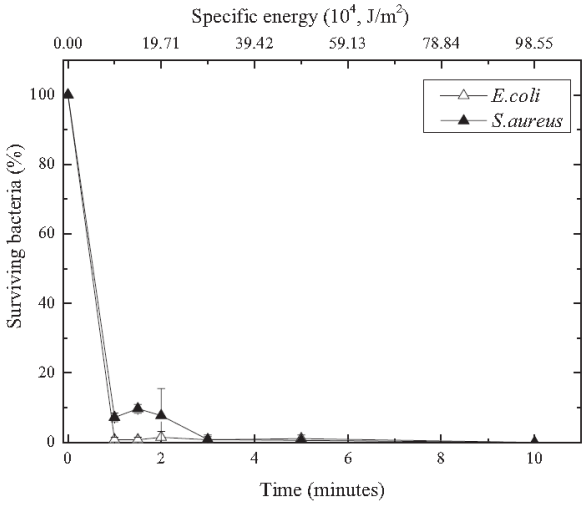

Fig. 10. Surviving fractions of *E. coli* and *S. aureus* after exposure to negative indirect corona discharges.

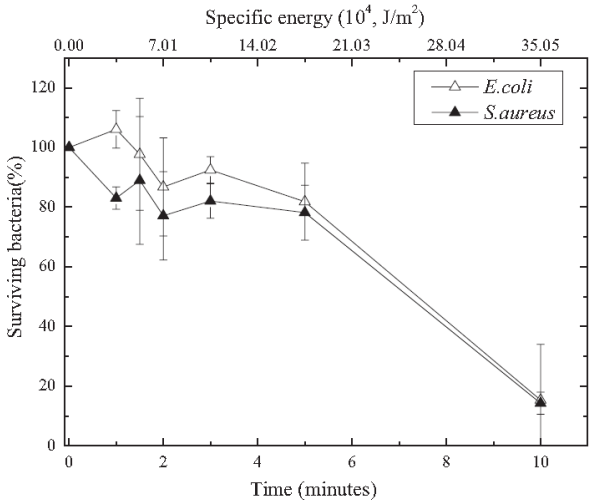

Fig. 11. Surviving fractions of *E. coli* and *S. aureus* after exposure to positive direct corona discharges. Horizontal scales: exposure time and specific energy.

case of negative energization (achieved for 10-min exposure time) is $98.55 \cdot 10^4$ J/m^2. This energy produces a significant bactericidal effect, ~99.9 % for both types of microorganisms. However, in the case of negative energization a smaller specific energy of $\sim 10 \cdot 10^4$ J/m^2 also resulted in a strong bactericidal effect: ~93% inactivation of *S. aureus* and ~99% inactivation of *E. coli*.

C. Inactivation Effect of Positive Direct Corona Discharges

In the case of positive direct corona treatment, the observed ozone concentrations are similar as in the case of positive indirect corona discharges, 1–2 ppm. However the specific energies in this case are lower as compared with indirect discharges: the maximum specific energy in the case of direct positive corona treatment is $\sim 35 \cdot 10^4$ J/m^2.

The bactericidal effect produced by positive direct corona discharges is also similar to the effect produced by positive indirect corona treatment, with the population of both bacterial species reduced by ~85% during 10-min exposure. Inactivation curves for *E. coli* and *S. aureus* in the case of direct positive corona discharges are shown in Fig. 11. In the case of direct discharges, the specific energy is calculated in the same way as in the case of the indirect discharges, however in this case the charges are able to reach the target surface. The specific energy that resulted in ~85% inactivation of both bacterial species in the case of positive direct energization is $\sim 35 \cdot 10^4$ J/m^2 (10-min exposure time, Fig. 11).

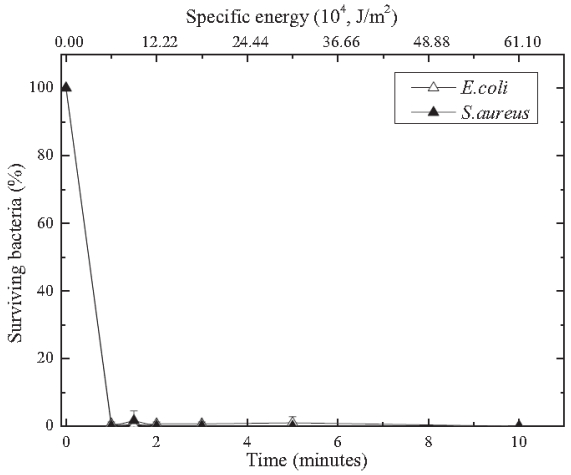

Fig. 12. Surviving fractions of *E. coli* and *S. aureus* after exposure to negative direct corona discharges.

D. Inactivation Effect of Negative Direct Corona Discharges

Negative direct corona discharges produced significantly higher ozone concentrations (20–60 ppm) and a more pronounced bactericidal effect: all microorganisms are killed after 1-min exposure. Inactivation results for negative direct discharges are shown in Fig. 12. The specific energy required to achieve almost 100% inactivation in this case is $\sim 6.1 \cdot 10^4$ J/m^2. This energy is slightly lower than the specific energy resulted in similar bactericidal effect in the case of indirect negative treatment (Fig. 10).

V. Conclusion

Bactericidal and chemical (oxidation) effects of direct and indirect corona discharges in atmospheric air were studied in this paper. It was shown that both types of corona treatment can produce notable oxidation and inactivation effects. The degree of decolorization of blue indigo carmine dye solution was used as an indicator of the oxidation capability of corona discharges. It was shown that in the case of positive energization, the decolorization effect of direct and indirect corona treatment was similar (~8% reduction in the concentration of the blue dye) for both types of air, atmospheric and dry air. In the case of negative indirect treatment the decolorization effect was stronger (27–36% reduction in the concentration of the blue dye). This increase in oxidation capability can be explained by higher energies, higher currents and higher ozone concentrations in the case of negative energization

(a few tens of ppm as compared with just a few ppm for positive energization).

For investigation of the bactericidal effects, two bacterial species were used, *E. coli* and *S. aureus*. As in the case of chemical tests, the inactivation effect of direct and indirect corona treatment was approximately the same for positive energization. For example, for 1- and 2-min exposures the degree of inactivation of both bacterial species was in the range 0–20%, Figs. 9 and 11. In addition, the same levels of ozone concentration were observed for these two types of treatment, ~2 ppm. However, in the case of negative energization, indirect exposure to corona discharge produced a significantly higher inactivation effect, with both bacterial species completely inactivated after 5-min exposure time. The ozone levels in this case were up to 40 ppm. Higher ozone concentrations were observed in the case of direct negative treatment: 20–60 ppm. In the case of negative direct treatment all microorganisms were killed after 1 min of treatment.

The specific energies that were used in the case of direct and indirect treatment were higher than the specific energies used in [7], [13] but lower than in [14]. For example, direct positive corona treatment with a specific energy of ~25 kJ/m^2 resulted in 99.97% inactivation of *E. coli* seeded on agar surfaces in aluminum plates [7]; indirect positive corona treatment with a specific energy of ~165 kJ/m^2 resulted in 99.9% inactivation of *E. coli* [13]. In these tests, the current was kept at a constant value of 100 μA, and the estimated applied voltage was ~11 kV. In this paper, the specific energy required to achieve ~85 % inactivation of *E. coli* in the case of positive direct treatment was ~350 kJ/m^2 and the specific energy required to achieve 99.9% inactivation of *E. coli* in the case of negative direct treatment was ~61 kJ/m^2. However, the doses (current of corona discharge multiplied by exposure time, C/m^2) used in this paper were similar or lower then doses reported in [7], [13]. For example, the doses required for inactivation of *E. coli* in the case of negative direct treatment was ~2 C/m^2 (current paper) and ~2.25 C/m^2 [7]. In the tests described in [14], *E. coli* or *S. aureus* in water samples were treated using direct corona discharges generated using positive dc voltage of 20 kV, the energy per plate required to inactivate both microorganisms was ~216 kJ/plate. In this paper, the energy per plate used to inactivate *E. coli* or *S. aureus* with direct discharges was significantly lower, ~0.86 kJ/plate in the case of positive discharges and ~0.15 kJ/plate in the case of negative discharges. The higher inactivation energy per plate reported in [14] can be potentially explained by a restricted corona treatment area (a single point corona electrode was used), and by the use of water samples inoculated with microorganisms rather than bacterial seeded agar plates as in this paper. These results demonstrated that energy consumption of the corona discharge treatment can be optimized, however this optimization is beyond the scope of this paper.

It was shown that the chemical and biological effects had a potential correlation with specific energies of corona treatment and ozone produced by corona discharges. Although the exact mechanism of the chemical (oxidation) and bactericidal effects of corona discharges require further investigation and analysis, as different ROS and RNS make their contribution to these effects, ozone can potentially be used as an indicator of the production of ROS and the bactericidal and oxidation efficiency of corona discharges.

References

[1] A. Fridman, A. Chirokov, and A. Gutsol, "Non-thermal atmospheric pressure discharges," *J. Phys. D, Appl. Phys.*, vol. 38, no. 2, pp. R1–R24, 2005.

[2] I. Timoshkin, M. Maclean, M. Wilson, M. Given, S. MacGregor, T. Wang, and J. Anderson, "Bactericidal effect of corona discharges in atmospheric air," *IEEE Trans. Plasma Sci.*, vol. 40, no. 10, pp. 2322–2333, Oct. 2012.

[3] Z. Machala, L. Chladekova, and M. Pelach, "Plasma agents in bio-decontamination by dc discharges in atmospheric air," *J. Phys. D, Appl. Phys.*, vol. 43, no. 22, pp. 222001-1–222001-7, 2010.

[4] D. Dobrynin, G. Friedman, A. Fridman, and A. Starikovskiy, "Inactivation of bacteria using dc corona discharge: Role of ions and humidity," *New J. Phys.*, vol. 13, pp. 103033-1–103033-13, Oct. 2011.

[5] V. Scholtz, J. Julák, V. Kíha, and J. Mosinger, "Decontamination effects of low-temperature plasma generated by corona discharge part 1: An overview," *Prague Med. Rep.*, vol. 108, no. 2, pp. 115–127, 2007.

[6] L. Gaunt, C. Beggs, and G. Georghiou, "Bactericidal action of the reactive species produced by gas-discharge nonthermal plasma at atmospheric pressure: A review," *IEEE Trans. Plasma Sci.*, vol. 34, no. 4, pp. 1257–1269, Aug. 2006.

[7] N. Vaze, M. Gallagher, S. Park, G. Fridman, V. Vasilets, A. Gutsol, S. Anandan, G. Friedman, and A. Fridman, "Inactivation of bacteria in flight by direct exposure to nonthermal plasma," *IEEE Trans. Plasma Sci.*, vol. 38, no. 11, pp. 3234–3240, Nov. 2010.

[8] I. Komanapalli and B. Lau, "Ozone-induced damage of Escherichia coli K-12," *Appl. Microbiol. Biotechnol.*, vol. 46, nos. 5–6, pp. 610–614, 1996.

[9] N. Hunt and B. Mariñas, "Inactivation of Escherichia coli with ozone: Chemical and inactivation kinetics," *Water Res.*, vol. 33, no. 11, pp. 2633–2641, 1999.

[10] R. Zajíek, L. Oppl, and J. Vrba, "Broadband measurement of complex permittivity using reflection method and coaxial probes," *Radioengineering*, vol. 17, no. 1, pp. 14–19, 2008.

[11] S. Ammar, R. Abdelhedi, C. Flox, C. Arias, and E. Brillas, "Electrochemical degradation of the dye indigo carmine at boron-doped diamond anode for wastewaters remediation," *Environ. Chem. Lett.*, vol. 4, pp. 229–233, Apr. 2006.

[12] T. Kobayashi, T. Sugai, T. Handa, Y. Minamitani, and T. Nose, "The effect of spraying of water droplets and location of water droplets on the water treatment by pulsed discharge in air," *IEEE Trans. Plasma Sci.*, vol. 38, no. 10, pp. 1031–1034, Oct. 2010.

[13] D. Dobrynin, A. Fridman, G. Friedman, and A. Starikovskiy, "Bacteria inactivation effect of ions generated by dc corona discharge," in *Proc. 18th Int. Conf. Gas Discharges Their Appl.*, 2010, pp. 432–435.

[14] M. Korachi, C. Gurol, and N. Aslan, "Atmospheric plasma discharge sterilization effects on whole cell fatty acid profiles of Escherichia coli and staphylococcus aureus," *J. Electrostat.*, vol. 68, pp. 508–512, Jul. 2010.

Sirui Li was born in Yunnan, China, in 1988. He received the B.Eng. (Hons.) and M.Sc. degrees in electronic and electrical engineering from the University of Strathclyde, Glasgow, U.K., in 2010 and 2011, respectively. He is currently pursuing the Ph.D. degree with the University of Strathclyde, on nonthermal plasma discharge for air treatment and surface decontamination.

Igor V. Timoshkin (M'07) received the Degree in physics from Moscow State University, Moscow, Russia, in 1992, and the Diploma and Ph.D. degrees from the Imperial College of Science, Technology and Medicine, London, U.K., in 2001.

He was a Researcher with Moscow State Agro-Engineering University, Moscow, and then at the Institute for High Temperatures of the Russian Academy of Sciences before moving to ICSTM in 1997. He joined the Department of Electronic and Electrical Engineering, University of Strathclyde, Glasgow, U.K., in 2001, as an Academic Visitor, where he became a Senior Lecturer in 2011. His current research interests include properties of solid and liquid dielectric materials, electronics of plasma discharges in condensed media, practical applications of electrohydraulic and high-power ultrasound pulses, biodielectrics, and effects of electromagnetic fields on biological objects.

Michelle Maclean was born on Isle of Lewis, Scotland, in 1980. She received the B.Sc. (Hons.) degree in microbiology and immunology and the Ph.D. degree in electronic and electrical engineering from the University of Strathclyde, Glasgow, U.K., in 2002 and 2006, respectively.

She is currently a Research Fellow with the Robertson Trust Laboratory for Electronic Sterilization Technologies, University of Strathclyde, and her interdisciplinary research work involves the development and application of novel electro-technologies for biological decontamination and sterilization applications in clinical and public health environments.

Dr. Maclean is a member of the Society for General Microbiology and the American Society of Microbiology.

Scott J. MacGregor (M'95) received the B.Sc. and Ph.D. degrees from the University of Strathclyde, Glasgow, U.K., in 1982 and 1986, respectively.

He is currently with the University of Strathclyde, where he became a Pulsed-Power Research Fellow in 1986, a Lecturer in pulsed-power technology in 1989, a Senior Lecturer in 1994, and a Reader and a Professor of high-voltage engineering in 1999 and 2001, respectively. He has been the Dean of Engineering with the University of Strathclyde since January 2010. His current research interests include high-voltage pulse generation, high-frequency diagnostics, high-power repetitive switching, high-speed switching, electronic methods for food pasteurization and sterilization, generation of high-power ultrasound (HPU), plasma channel drilling, pulsed-plasma cleaning of pipes, and stimulation of oil wells with HPU.

Mark P. Wilson (M'10) was born in Stranraer, Scotland, in 1982. He received the B.Eng. (Hons.), M.Phil., and Ph.D. degrees in electronic and electrical engineering from the University of Strathclyde, Glasgow, U.K., in 2004, 2007, and 2011, respectively.

He is currently a Teaching Associate with the University of Strathclyde, where he continues to investigate surface flashover of solids immersed in insulating oil.

Dr. Wilson is a member of the IEEE Nuclear and Plasma Sciences Society, from which he received the Graduate Scholarship Award in 2011, the IEEE Dielectrics and Electrical Insulation Society, and the IET.

Martin J. Given (M'99–SM'11) received the Degree in physics from the University of Sussex, Sussex, U.K., in 1981, and the Ph.D. degree in electronic and electrical engineering from the University of Strathclyde, Glasgow, U.K, in 1996.

He is currently a Senior Lecturer with the Department of Electronic and Electrical Engineering, University of Strathclyde. His current research interests include ageing processes and condition monitoring in solid and liquid insulation systems, high-speed switching, and pulse power applications.

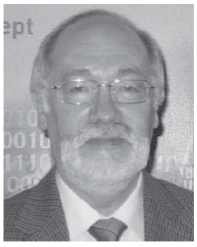

John G. Anderson was born in Glasgow, U.K., on September 2, 1942. He received the B.Sc. degree in applied microbiology and the Ph.D. degree in fungal physiology from the University of Strathclyde, Glasgow, in 1968 and 1971, respectively.

He has been with the Department of Bioscience and Biotechnology, University of Strathclyde, since 1971, where he became a Professor of microbiology and the Head of Department. He is currently an Emeritus Professor with the University of Strathclyde. His current research interests include various aspects of food, biomedical and environmental microbiology with interdisciplinary collaboration on the application of electro-technologies for electronic pasteurization and sterilization.

Tao Wang received the B.Eng. and M.Sc degrees from Northeast China Dianli University, Dianli, China, in 1993 and 1996, respectively, and the Ph.D. degree from the University of Strathclyde, Glasgow, U.K., in 2005.

He joined Newland Entech as a Research Fellow, developing a high-efficiency industrial ozone generator. He joined the Department of Electronic and Electrical Engineering, University of Strathclyde, as a Lecturer in 2010. His current research interests include nonthermal gas discharges and their applications in gas synthesis, water disinfection, and advanced oxidation process in water.

Fluorescence Detection of Hydroxyl Radicals in Water Produced by Atmospheric Pulsed Discharges

S. Li[1], I. V. Timoshkin[1], M. Maclean[1,2], S. J. MacGregor[1], M. P. Wilson[1], M. J. Given[1], T. Wang[1] and J. G. Anderson[1]

[1] Department of Electronic and Electrical Engineering, University of Strathclyde, Glasgow, G1 1XW, UK

[2] Department of Biomedical Engineering, University of Strathclyde, Glasgow, G4 0NW, UK

ABSTRACT

It has been proven that hydroxyl (OH) radicals can be generated by streamer discharges across water surfaces under ambient atmospheric conditions. Hydroxyl radicals have the highest oxidation capability amongst all oxygen-based reactive species, thus OH play an important role in oxidation of organic molecules and the bactericidal effects of plasma discharges. In this study, generation of hydroxyl radicals in water by pulsed streamer discharges was investigated. Terephthalic acid was used as a chemical probe as this acid is converted into 2-hydroxyterephthalic acid (HTA) by chemical reaction with OH radicals. The concentration of OH radicals was quantified by measuring the fluorescence light intensity generated by HTA molecules in water solutions. Both positive and negative pulsed discharges with different voltage levels were tested. Two different types of sample holder – non-conductive plastic dishes, and dishes lined with conductive aluminum foil – were used in order to investigate the effect of the discharge propagation path on the efficiency of OH production. The efficiency of OH production was measured as a function of: the distance between the needle electrode and the water surface; the magnitude and polarity of HV energization; and the total delivered charge. The obtained results will help in optimization of non-thermal plasma systems for chemical and biological decontamination.

Index Terms — **Streamer discharges, OH radicals, Fluorescence.**

1 INTRODUCTION

OVER recent years, strong interest in the microbiological and chemical actions of non-thermal plasmas has resulted in the development of a number of potential practical (environmental and medical) applications of such plasma discharges. Atmospheric-pressure plasma discharges including plasma jets, plasma bullets, and transient and steady-state corona discharges in ambient air, produce strong biological and chemical oxidation effects [1, 2], which provide a basis for chemical, environmental and medical plasma-based technologies. It has been proven that low-temperature atmospheric plasmas (including corona discharges in air) generate charged particles and reactive oxygen and nitrogen species, including ground-state oxygen, superoxide, singlet oxygen, ozone, hydrogen peroxide, hydroxyl radicals, nitric oxide, and nitrogen dioxide. These reactive species, together with UV photons and strong electric fields, lead to the bactericidal and oxidative action of such non-thermal plasmas. It has also been shown that, in the case of air-based non-thermal plasmas, the reactive chemical species are the main contributor to the process of bacterial inactivation, [3, 4]. However, despite significant efforts to investigate the bio-decontamination effects of atmospheric non-thermal plasmas, further understanding of the production of the reactive species has been identified as one of the main challenges related to the successful use of such plasmas in environmental and medical applications, [5]. It has been demonstrated that in the case of non-thermal atmospheric air plasmas, or plasmas in which oxygen is used as a component of the gaseous environment, reactive oxygen species may have a dominant effect in the inactivation processes. For example, a correlation between ozone generation and the bactericidal efficacy of atmospheric corona discharges is discussed in [6]. Ozone was used as an indicator of the generation of reactive oxygen species, and the role of each individual species was not determined. There is a strong indication that hydroxyl radicals produced by non-thermal plasma discharges make a significant contribution to the biological damage. In [7], the authors argue that OH radicals, produced in humid air by a dielectric barrier discharge through direct chemical reactions with water molecules, play the main role in the inactivation of *Geobacillus stearothermophilus* spores. Paper [8] states that, in the case of non-thermal plasma in air with a high relative humidity (the authors used air with a relative humidity up to 70%), OH radicals quickly take part in chemical reactions (their half-period life in biological cells is 1 ns), and generate significant

Manuscript received on 16 December 2014, in final form 19 May 2015, accepted 19 May 2015.

amount of peroxides which make a contribution to the inactivation of *Bacillus atrophaeus* spores. The authors of [9] investigated the efficiency of producing OH radicals in air by pulsed discharges, and found that the efficiency of the generation of hydroxyl radicals in atmospheric air depends on its humidity, and has a maximum at ~55% rh.

Their short lifetime and relatively low concentrations mean that OH radicals may not be detected in optical emission plasma spectra, and the authors of [9] reported that they were not able to observe the OH emission line at 308.9 nm. However, in the case of more intensive transient spark discharges in atmospheric air, the OH emission line at 308.9 nm was clearly detected, which indicates that such non-thermal plasma discharges are capable of generating a significant concentration of OH radicals in gaseous medium [10]. As indicated in [11], the concentration of OH radicals in non-thermal plasma can be 10^{13}-10^{15} cm^{-3}.

In [11], OH radicals have been identified as one of the main reactive oxygen species produced by transient corona discharges in air. The authors describe OH radicals as extremely reactive and able to trigger oxidation reactions in the lipid layer of bio-membrane. The review paper [12] also indicates that in numerous studies OH radicals are considered the main contributor to the bactericidal effects of non-thermal atmospheric plasmas. Therefore, it can be stated that in the case when plasmas are developed in humid atmospheric air, or in contact with water or water-based surfaces, OH radicals make a significant contribution to the biological and chemical [30] effects of plasma. However, the exact role and mechanism of the hydroxyl radicals in plasma action, OH production rates, and their migration capabilities in water or water-based solutions, are not fully known.

The present paper is focused on investigating the generation of OH radicals in water-based solutions by transient atmospheric plasma (streamer) discharges. It is important to understand the role of the high voltage wave-forms (their polarity, duration, voltage and current magnitudes) and test cell topologies, in the efficiency of the production of OH radicals, in order to optimize the parameters of transient plasmas required for different practical applications.

The hydroxyl radical can be formed through different mechanisms, including direct electronic excitation of water molecules and dissociative recombination of exited water molecules, [13-15]:

$$\begin{aligned} &H_2O + e^- \rightarrow OH + H + e^- \\ &H_2O^+ + e^- \rightarrow OH + H \\ &H_2O^+ + H_2O \rightarrow H^+(H_2O) + OH \end{aligned} \qquad (1)$$

Other mechanisms of formation of the hydroxyl radical in plasma-treated water solutions can involve formation and subsequent dissociation of peroxynitrous acid and/or peroxynitrite, as discussed in [31]. Peroxynitrous acid and peroxynitrite can be formed in an acidic environment through reaction between nitrite, hydrogen peroxide and H^+ ions; decomposition of this acid and its conjugate (peroxynitrite) base then results in formation of OH and NO_2 radicals [31]. As indicated in [2] and [31], these complex processes of formation of OH radicals through chemical reactions involving nitrites, nitrates, hydrogen peroxide and ozone are not fully understood and further investigations are needed: for example, direct measurements of the main chemical species generated by plasma discharges (hydrogen peroxide and others) could be importart for further understanding of these plasma-induced chemical processes in water-based solutions.

Therefore, OH radicals may be produced by plasma in air above the sample surface, and these radicals may diffuse into the liquid sample (if their half-life will be sufficient for such processes) [16]. Diffused OH radicals will then react with water molecules, resulting in production of hydrogen peroxide, which will be involved in the chemical reactions discussed above. Alternatively, OH radicals can be produced directly in the liquid in the case of contact between plasma and a water/water-based solution surface, according to the chemical reactions in equation (1).

Due to a short half-life time and the highly reactive nature of hydroxyl radicals, it is difficult to detect plasma-produced OH species in aqueous solutions. OH radicals can quickly form H_2O_2 or other products by recombination or oxidation reactions. In order to detect and to measure the concentration of OH radicals, different approaches have been used, including laser-induced fluorescence techniques [16], light emission spectroscopy [17], electron paramagnetic resonance spectroscopy [32] and use of chemical probes [18].

A method which is based on using terephthalic acid (TA) as a chemical probe was suggested in [19, 20]. TA acid reacts specifically with OH radicals, transforming into 2-hydroxylterephtalic acid (HTA) through addition of OH to its aromatic ring. When excited with light of ~ 310 nm wavelength, HTA molecules generate a strong fluorescent signal with a peak at 425 nm which can be readily detected and measured. The intensity of this fluorescence signal is directly related to the HTA concentration in the tested liquid. Therefore, the concentration of OH radicals in this liquid can be quantified if the HTA concentration is known. The use of TA as a chemical probe is an efficient way to detect plasma-generated OH radicals, as terephthalic acid is a highly selective and sensitive OH scavenger, [18]: OH radicals can react with TA molecules before they form other products; other reactive oxygen species, even those with a high oxidative potential such as ozone, will not react with TA.

In the present study, HV impulses of both polarities, and with different peak voltages, were used to produce transient plasma (spark) discharges. Transient atmospheric plasma discharges have been selected for this study due to their high bio-inactivation capability: it has been shown in [10] that such transient sparks demonstrate a higher bactericidal efficiency as compared with corona discharges. In the present paper, the efficiency of OH production in water-based solutions by the transient plasma discharges was obtained as a function of peak voltage level, polarity, total delivered charge, and discharge propagation path.

2 EXPERIMENTAL SYSTEM

2.1 TREATMENT CELL AND ENERGIZATION SYSTEM

An 80 mm high Perspex cylinder with a diameter of 150 mm and two nylon flanges was used as the test cell body. The high voltage (HV) electrode, a gramophone needle with a body diameter of 1.2 mm and a tip radius of ~36 μm, was fixed in the upper nylon flange, which could be screwed in or out of the test cell, thus providing the ability to change the distance between the electrode and the sample surface. A grounded electrode (aluminum plate with a thickness of 10 mm, external diameter of 120 mm) was placed at the bottom of the test cell. Plastic dishes with an internal diameter of 55 mm were used to hold liquid samples on top of the grounded electrode. The HV electrode was stressed with positive and negative HV impulses, and was located above the surface of water-based solutions. The distance between the HV electrode and the liquid surface was varied from ~11 mm till 0 mm (the electrode was in contact with the surface of the liquid sample). Two different types of liquid container were used in this work: non-conductive plastic dishes and plastic dishes lined with a grounded aluminum foil (conductive dishes). During the tests, both the conductive and non-conductive sample holders were filled with 6 ml TA water-based solution. These topologies were used in order to compare the efficiency of OH production in two different cases. An air pump (VP 1HV, KNF Neuberger Ltd) was used to gently flush the test cell with ambient laboratory air with a relative humidity of ~ 40%. Ozone concentration during plasma treatment was monitored by an ozone analyzer IN-2000 LOCON, IN USA Inc.

Transient plasma impulses were generated by energization of a HV electrode with HV impulses produced by a pulsed power generator (Samtech Ltd, Scotland). This pulsed power supply, based on a high voltage autotransformer, is capable of delivering voltage impulses with a magnitude up to 30 kV, and a rate of rise of ~$(3\text{-}5)\cdot 10^2$ kV/ms, [21]. The pulse repetition rate used in the present work was 20 pulses per second. A high voltage probe (Tektronix P6015A, with bandwidth of 75 MHz) was used to monitor the high voltage wave-forms. The transient current in the discharge circuit was measured using a Pearson current monitor, model 6585 with a bandwidth of 250 MHz. Both high voltage and current waveforms were recorded using a Tektronix TDS 2024 digitizing oscilloscope (200 MHz bandwidth, 2 GSamples/sec sampling rate). The HV and current probes were connected to the oscilloscope using 50 Ω BNC cables. Schematic diagram of the test cell is shown in Figure 1a.

The cross-sections of the plastic dishes and the HV electrode used for generation of the transient plasma discharges and treatment of liquids are shown in Figures 1b and 1c. In the first case (Figure 1b), non-conductive plastic dishes were filled with liquid samples and were placed on a grounded metal plate. In this topology, discharges propagate from the HV needle electrode down to the surface of the liquid sample, then discharges continue to develop across the liquid/air interface towards the border of the plastic dish, and finally they reach the grounded plate.

(a)

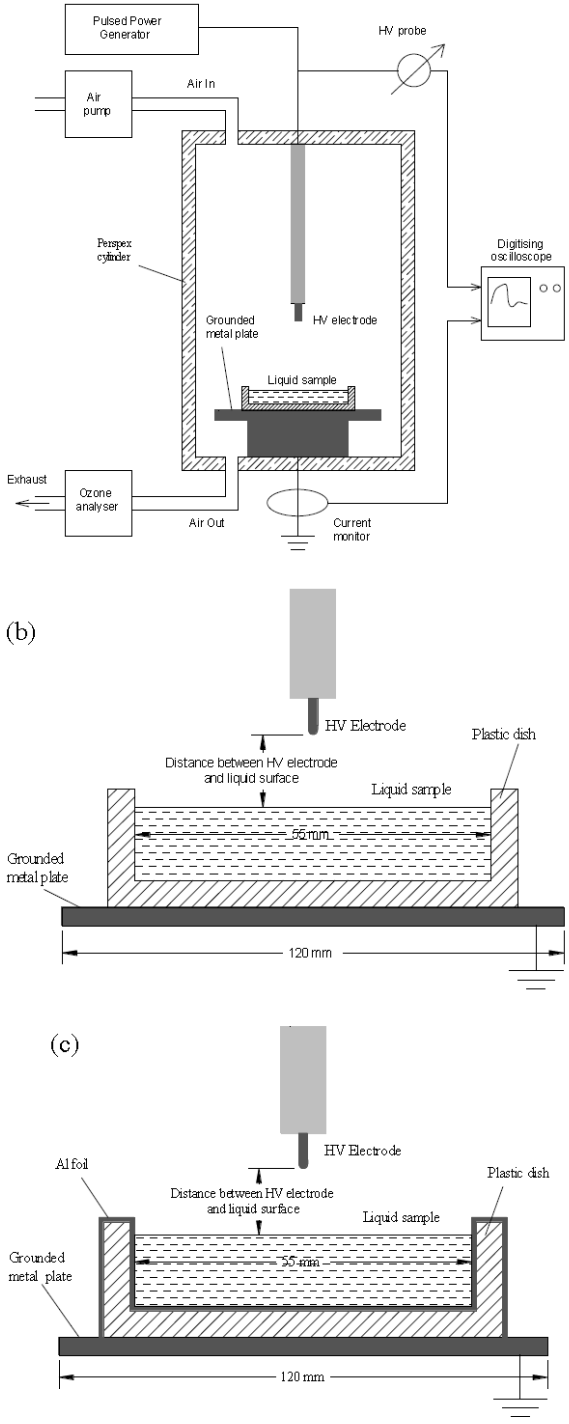

Figure 1. Cross-section of the treatment cells; (a) Schematic diagram of the experimental set-up; (b) plastic dish filled with the liquid sample (non-conductive dish); (c) plastic dish lined with aluminium foil and filled with the liquid sample (conductive dish).

In the second case (Figure 1c), water-based solutions were placed in plastic dishes lined with a grounded aluminum foil (which acted as conductive dishes). As in the previous topology, the HV electrode was located directly above the center of the plate. In the case of the conductive dishes (Figure 1c), the discharges propagate straight down to the liquid surface, then the ionic current flows through the liquid sample towards the

aluminum foil, which is grounded by direct contact with the grounded metallic support plate. In the case of the non-conductive dishes, when the HV electrode was in contact with the liquid surface discharges were generated at the air/liquid interface, these discharges propagated along this interface and the border of the dish towards the grounded plate. Alternatively, in the case of the conductive dishes, when the HV electrode was in contact with the liquid, all discharge activity and ionic conduction took place in the liquid, and no visible discharges across the liquid/air interface were observed.

2.2 CURRENT AND VOLTAGE WAVE-FORMS

One of the main parameters in this set-up which influences the high voltage and current waveforms is the distance between the HV needle tip and the surface of the liquid sample. The impulsive breakdown voltage varies with this distance. Table 1 shows the obtained breakdown voltages for different distances and topological configurations.

Table 1. Breakdown voltage for different distances between the HV needle electrode and liquid surface in the two types of sample holder.

Voltage, (kV)	Non-conductive plastic dish, (mm)	Conductive (Al-foil lined) dish, (mm)
+20	0.53	4.98
+24	5.06	7.73
+28	7.25	11.06
-20	0.68	1.72
-24	1.37	3.32
-28	3.65	6.03

As Table 1 shows, the breakdown distance using the non-conductive dish is much shorter than the distance using the foil-lined conductive dish, under the same breakdown voltage level. Tests with zero gap between the HV electrode and the sample surface (the HV electrode was in contact with the liquid) were also conducted for both types of sample holder.

Figure 3 shows typical voltage and current waveforms for the conductive and non-conductive dishes, with the HV electrode energized with ±24 kV. As shown in Figures 3a and 3b, multiple peaks were observed in the voltage and current waveforms in the case of the non-conductive dish. This indicates multiple transient streamers (flashes) before the main voltage collapse, i.e. the development of a transient spark which can be referred to as a complete breakdown in the gap between the HV and ground electrodes. For this type of sample holder the breakdown path includes the vertical path through air between the HV needle tip and the liquid surface, and the path across the air/liquid interface.

Figure 3 shows typical voltage and current waveforms for the conductive and non-conductive dishes, with the HV electrode energized with ± 24 kV. As shown in Figures 3a and 3b, multiple peaks were observed in the voltage and current waveforms in the case of the non-conductive dish. This indicates multiple transient streamers (flashes) before the main voltage collapse, i.e. the development of a transient spark which can be referred to as a complete breakdown in the gap between the HV and ground electrodes. For this type of sample holder the breakdown path includes the vertical path through air between the HV needle tip and the liquid surface, and the path across the air/liquid interface.

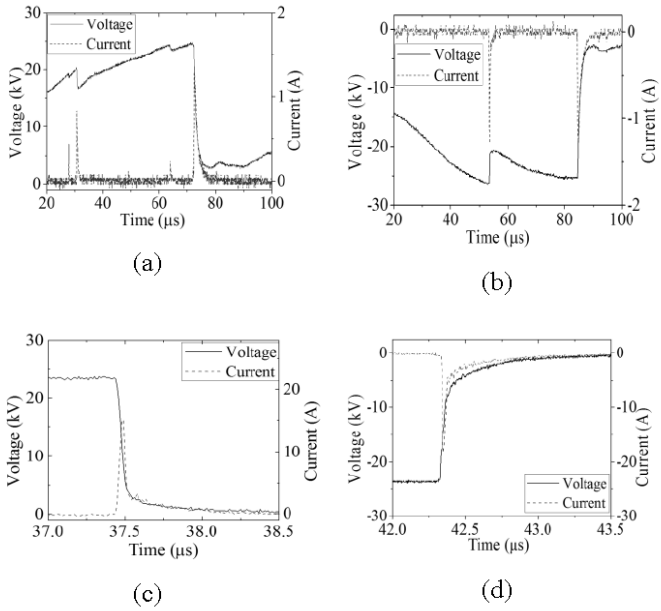

Figure 3. Voltage and current waveforms: (a) +24 kV non-conductive plastic dish; (b) - 24 kV non-conductive plastic dish; (c), +24 kV conductive foil-lined dish; (d), -24 kV conductive foil-lined dish.

As can be seen from Figure 3, the peak discharge current in the case of non-conductive dishes is ~1.36 A, (breakdown voltage +24.6 kV), the duration of the current impulse is ~10 μs. This peak current is much lower compared with the discharge current in the case of the conductive foil-lined dish, ~16.16 A (breakdown voltage +23.8 kV), however in this case the current pulse is much shorter, ~1 μs. Moreover, only a single main voltage collapse was observed in the case of the conductive sample dishes (no pre-breakdown transient events), which indicates only a single breakdown path/event between the high-voltage needle and the liquid surface. Also, it was observed that the peak current increases with increasing applied voltage.

However, taking into consideration all these factors (appearance of multiple current peaks, different duration of current impulses in different topologies) it was decided to investigate the efficiency of OH production as a function of the total charge delivered during each high-voltage impulse, rather than the peak magnitude of individual current pulses. The total delivered charge was calculated by integration of the current waveforms. The results of this analysis (OH production as a function of the total charge in different topologies) are presented in Section 3.5.

3 FLUORESCENT LIGHT EMISSION

Terephthalic acid, $C_6H_4(COOH)_2$, (Sigma-Aldrich Ltd., 99+% purity) was used in the current work for detection of OH radicals in water. As discussed in Section I, this acid reacts specifically with OH radicals to produce 2-hydroxyterephthalic acid, $C_8H_6O_5$. Other reactive oxygen species such as ozone or hydrogen peroxide don't directly react with TA acid, [16, 18].

While TA molecules don't produce fluorescent light, molecules of HTA generates strong fluorescent light emission with a peak at 425 nm when excited with UV-A light and their concentration can be obtained by measuring the intensity of the fluorescence light signal. After that, using a calibration curve (fluorescent light emission as a function of HTA concentration) and the conversion rate of OH radicals into HTA acid, the concentration of OH radicals can be calculated. In the present work, water based solutions with 2 mM concentration of TA acid were treated with transient plasma discharges (similar TA concentration was used in [19]). Water based TA solutions were prepared by dissolving 66 mg of TA acid in a 200 ml, 5 mM NaOH (distilled) water solution. Then 6 ml of TA solution was placed into non-conductive or conductive dishes for treatment.

After the plasma treatment, the solution was transferred into plastic cuvettes and the fluorescent light emission was measured using a spectrofluorophotometer Shimadzu RF-5301PC. The excitation wavelength was 310 nm and the peak of the fluorescence signal was detected at 425 nm. Also, the pH of plasma treated TA solutions was measured using a pH meter (Hanna Instruments PH 210).

3.1 UNTREATED TA SOLUTION

To confirm that TA acid does not produce fluorescent light, an untreated TA solution was examined. As expected, no pronounced fluorescence light emission at 425 nm was detected in the case of untreated samples. Low readings of 40-50 a.u. at this wavelength were used as a baseline (control) to compare with signals obtained from plasma treated samples.

3.2. TA SOLUTION TREATED IN NON-CONDUCTIVE DISHES

6 ml of a water based, 2 mM, TA solution was transferred into a non-conductive dish and placed in the centre of the treatment chamber on the grounded metallic surface, directly under the HV needle electrode and treated for 1, 3, 5 and 7 minutes. The needle electrode was stressed with HV impulses of both polarities, with peak voltages of 20 kV, 24 kV and 28 kV. The liquid samples were then transferred into cuvettes and the fluorescence light emission spectra were recorded.

Figure 4 summaries the results of the fluorescent light peak measurements for different voltage levels and different polarity of the HV impulses. There is an almost linear increase in the magnitude of the fluorescent signal with an increase in the duration of treatment. This tendency was observed for both polarities. However, there is no major difference in the fluorescent light signal intensity for different voltage levels.

A potential reason for this effect is the difference in the distance between the HV needle and the sample surface: higher voltages produce more intensive plasma discharges, however the distance between the needle and the surface is longer and the active species travel a longer distance before they reach the liquid sample. It is expected that, due to reaction processes in the air above the liquid surface, not all particles are able to reach the liquid. Conversely, for lower voltages, this distance is shorter, and a higher number of active particles produced by the plasma discharges can reach the liquid surface. Thus, these two factors may compensate each other, resulting in a similar intensity of the fluorescent signals for different voltages at the same treatment time. The same factors are potentially responsible for the higher fluorescence signal from samples treated with negative impulses as compared with positive impulses (Figure 4). In the case of HV impulses with negative polarity, the distance between the HV needle and the surface of the water sample is shorter as compared with the case of positive impulses (at the same level of breakdown voltage), Table 1. Thus, more chemically-active species will be produced in liquid samples in the case of shorter distances between the HV electrode and the liquid surface.

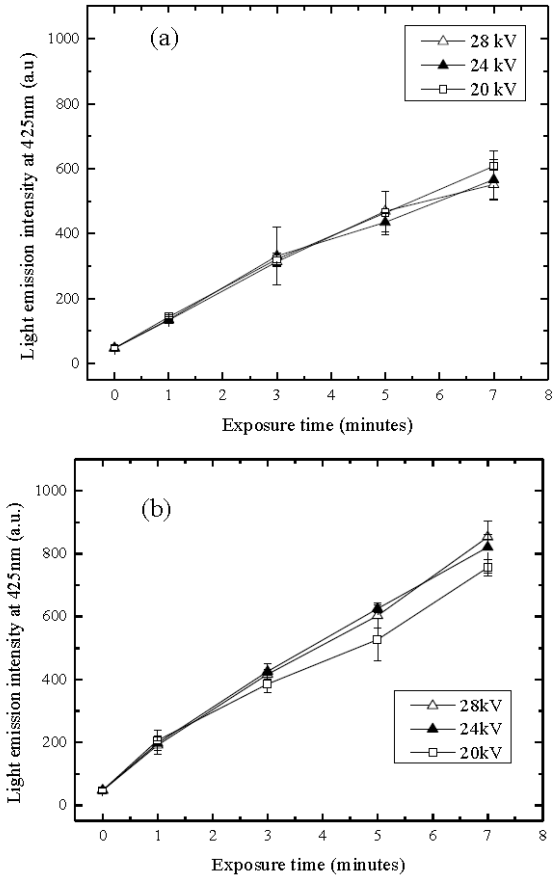

Figure 4. Fluorescence light intensity of samples treated with impulsive discharges in non-conductive dishes as a function of treatment time and voltage levels. (a) positive discharges; (b) negative discharges.

The acidity of the plasma treated TA solution sample was examined. The pH of TA solutions treated in non-conductive dishes with both positive and negative transient plasma discharges, reduced from ~10.9 (untreated liquid) to ~10.3 (7 min plasma treatment). The high pH of the original untreated samples is explained by the addition of NaOH to the solutions, as TA acid is poorly soluble in water. No major difference in acidity levels for positive and negative energization was observed. A similar decrease in the pH of water treated with plasma was reported in [14-16], and this increase in acidity of plasma-treated samples may be explained by the production of

H^+ ions. One mechanism of production of these ions is dissociation of water molecules, (Eq. (1)). Other routes of production of H^+ ions may include dissolution and dissociation in water solutions of nitrogen oxides produced by plasma with formation of nitrites and nitrates together with H^+ ions, [2], [31]:

$$NO_2 + NO_2 + H_2O \rightarrow NO_2^- + NO_3^- + 2H^+ \quad (2)$$
$$NO + NO_2 + H_2O \rightarrow 2NO_2^- + 2H^+$$

In [31], it is shown that low-acidity liquids (buffer solution) treated with plasma discharges demonstrated higher concentration of nitrites, lower concentration of hydrogen peroxide and significantly lower decrease in pH, as compared with water. This result is correlated with the relatively small reduction in the pH value of plasma-treated TA solutions obtained in the present paper.

3.3. TA SOLUTION TREATED IN CONDUCTIVE DISHES

In order to investigate the efficiency of OH production by plasma discharges in the case when the discharge current passes through the sample directly, conductive foil-covered dishes were used.

6 ml samples of 2 mM TA solution were placed in the conductive dishes and located in the centre of the test cell, beneath the HV electrode (Figure 1c). The needle was stressed with the same HV impulses as used with the plastic dishes. Visual observation confirmed that bright transient plasma discharges propagate vertically and hit the sample surface: as in the case of conductive dishes, no streamers across the air/liquid interface were observed. After treatment with HV impulses, the samples were transferred into cuvettes and fluorescence light emission was measured.

Figure 5 shows the peak magnitude of the light fluorescence as a function of the treatment time, polarity, and peak voltage of the HV impulses. Figure 5 demonstrates that the peak fluorescent light intensity is an almost linear function of the treatment time for both polarities. However, there is a clear indication that the plasma discharges generated with higher voltages produce fluorescent light with a higher intensity. This tendency is especially noticeable in the case of negative energization of the HV electrode. Also, due to the high intensity of fluorescent light emitted by TA solutions treated for 5 and 7 min with -28 kV discharges, and those treated for 7 min with -24 kV discharges, it was not possible to measure the peak magnitude due to saturation of the fluorescent signal.

The pH of the plasma treated TA solutions in conductive dishes reduces with an increase in the duration of plasma treatment, however this decrease is more pronounced than that observed when treated in non-conductive dishes: pH of the samples treated with conductive dishes decreases from 10.9 (prior to the plasma treatment) to 9.8-9.2 (7 min plasma treatment). This is further confirmation that direct discharges in the case of the foil-lined conductive dishes resulted in a higher concentration of reactive species delivered into the water.

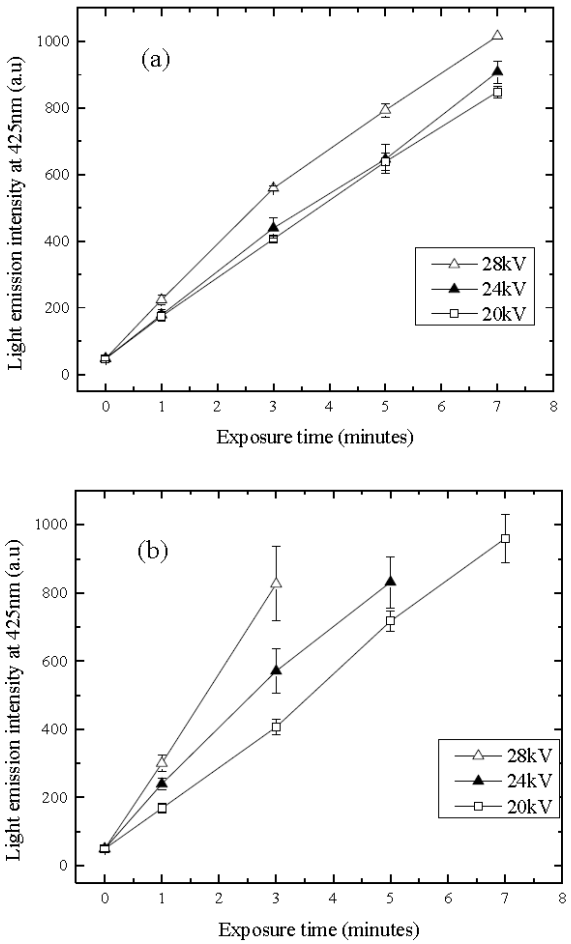

Figure 5. Fluorescent light intensity of TA solutions treated with impulsive plasma in conductive foil-covered dishes. Magnitude of the fluorescent light as function of treatment time for (a), positive energization; (b), negative energization.

It can be noted that in the case of conductive dishes, the intensity of the fluorescence signals is stronger than in the case of the non-conductive dishes. Also, in the former case, a more pronounced separation between fluorescence light emission curves for different energization voltages is observed. This separation can potentially be explained by the difference in the distances between the HV electrode and the liquid surface for positive and negative impulses at the same voltage level. As can be seen from Table 1, negative impulses require substantially lower distances as compared with positive impulses, in order to achieve the same breakdown voltage. Moreover, in the case of non-conductive dishes, the relative difference in the total length of the discharge path (in air and across the air/liquid interface) for the lowest and highest voltages is ~10%, while the relative difference in the discharge path for the lowest and highest voltages in the case of conductive dishes (which is only the vertical path through air) is substantially larger, ~70%. Thus, it may be argued that, in this case, production of OH radicals is more sensitive to changing distance between the HV electrode and the surface of the liquid, resulting in larger separation between the fluorescence curves for different energization voltages. However, further investigation is required to establish

the exact reason for this effect, which may involve measurements of other reactive chemical species produced in water-based solutions by transient plasma discharges.

3.4. HV ELECTRODE IN CONTACT WITH THE SAMPLE

It is known that plasma discharges which are generated directly in water can produce highly reactive species including OH radicals, [22-24]. In order to compare the efficiency of OH radical production by the plasma transient discharges generated above water and in the case when the high tension electrode is in direct contact with the liquid surface, the needle HV electrode was lowered down until it was in contact with the treated liquid. In this case, there is no air gap and the HV electrode was energized with ±18 kV voltage impulses, using non-conductive dishes (plasma discharges propagate across air/liquid interface only).

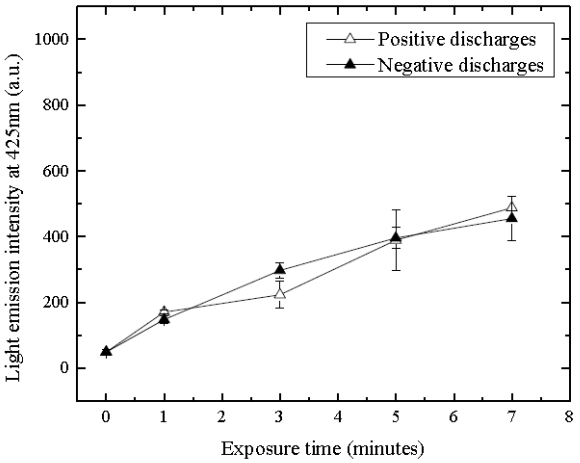

Figure 6. Fluorescence light intensity as a function of treatment time in the case of direct contact of the high tension electrode with the TA solution surface. ±18kV, non-conductive dish.

Figure 6 shows the peak fluorescent light emission as a function of treatment time for the non-conductive dishes. It can be seen that the intensity of the fluorescent signal is lower than in the case of discharges with the air gap between the sample surface and the HV electrode. For negative energization, the magnitude of the peak fluorescent signal after 7 min plasma treatment is almost twice lower than that for the air gap topology used in Section 3.2, for the same treatment time. Also, in the case of the direct contact of the high tension electrode and the liquid surface, no difference in the intensity of the fluorescent light was observed for positive and negative energization.

These results confirm that the reactive species responsible for the production of OH radicals (and OH radicals themselves) are generated in both sections of the transient plasma path: the vertical path section (propagation through air) and the horizontal path section (across the air/liquid interface in the case of non-conductive dishes, Figure 1c).

However, in the case of the conductive dishes, the discharge current propagates to the ground directly through air (if there is an air gap between the HV electrode and the liquid surface) and the bulk of the liquid, Figure 1c. When the HV electrode was in contact with the surface of liquid samples in conductive dishes, the discharge was generated in the liquid itself, and the discharge current propagated through the bulk of the liquid sample only. In these tests ± 30 kV voltage impulses were used to generate discharges in the liquid. This voltage level is close to the maximum energization voltage used in the tests with air gaps between the HV electrode and the surface of the liquid samples. It was found that, in the case when the electrode was in contact with the liquid sample, fluorescent light emission was very low, (no significant emission peak at 425 nm was resolved). Thus, direct discharges in liquid (no air gap between the HV electrode and the liquid surface) generated by the waveform used in the present study are not efficient for production of OH radicals in water based solutions. A potential reason for this is the relatively high conductivity of the tested solutions (~ 400 μS/cm), which means that the process of formation of plasma streamers in the liquid samples stressed with the HV impulses used in the present tests (Section 2.1) is inefficient, and most of the discharge current dissipates through Joule conduction, without generation of OH radicals.

Thus, these results demonstrate that the transient plasma discharges which propagate through air and across the air/liquid interface are more efficient in production of OH radicals, as compared with the discharges which are generated directly in the liquid when the HV electrode is in contact with the liquid surface.

3.5 CONCENTRATION OF OH RADICALS

The intensities of fluorescent light emission obtained in Sections 3.2 and 3.3 have been used for evaluation of the concentration of OH radicals produced in water based solutions by the transient plasma discharges.

As discussed above, the fluorescent light peak at 425 nm indicates the presence and concentration of HTA acid, which can be related to the concentration of OH radicals. A calibration curve which links the fluorescence peak magnitude and HTA concentration has been obtained using solutions with known concentrations of HTA. It is known that the OH yield from oxidation of HTA by oxygen is 35%, [18-20]. The concentration of OH radicals in the plasma treated samples was obtained using the fluorescent light intensity the calibration curve, and the yield factor.

The obtained concentrations of OH radicals for all tested voltages and topologies are shown in Figure 7. These OH concentrations are plotted as functions of the total delivered charge in each treatment case. The total charge was calculated by integration of the current waveforms for each individual case. It is shown that the concentration of OH radicals in the TA solutions increases linearly with the delivered charge and does not depend on voltage for the voltage levels tested in the present study. In the case of the direct contact of the high tension electrode with the liquid surface, the concentration of OH radicals is low: for example, based on the fluorescence light emission intensity produced by the TA solutions treated in plastic dishes, the concentration of OH radicals is less than 0.1 μM, even after 7 min treatment time. The concentration of OH radicals observed in the samples treated in non-conductive

dishes is slightly higher, 0.5-0.6 μM after 7 min plasma treatment.

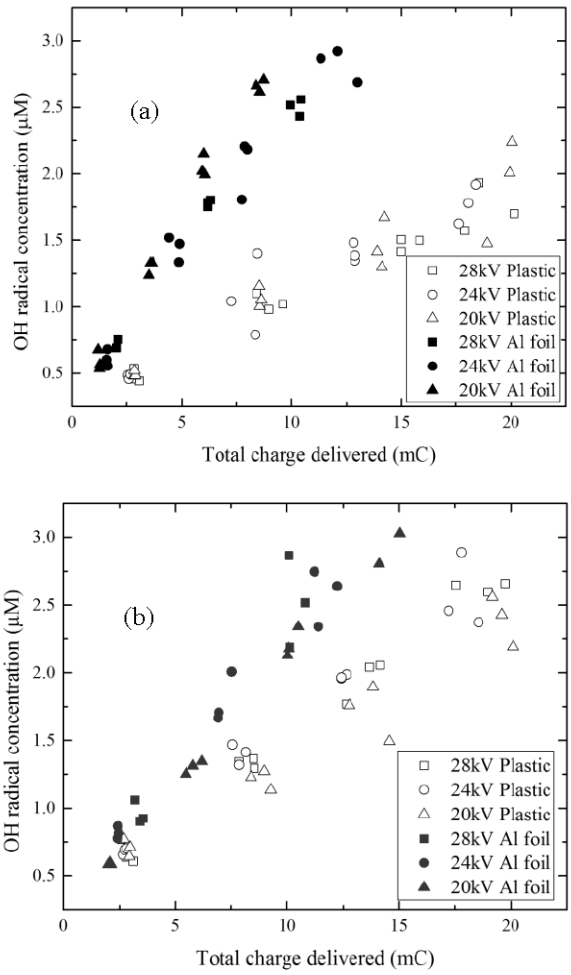

Figure 7. OH concentration as a function of total charge delivered by transient plasma discharges. (a), positive energization, non-conductive (plastic) and conductive (Al foil lined) dishes; (b), negative energization, non-conductive and conductive dishes.

4 CONCLUSIONS

OH radicals have the highest oxidation capability amongst all oxygen-based reactive species with redox potential of 2.7 V, [25]. Thus, these radicals can play an important role in chemical oxidation of organic molecules and in biological decontamination. Non-thermal plasmas are actively studied in order to establish their capability of generation of reactive oxygen and nitrogen species and their use in practical environmental and medical applications. Therefore, it is important to characterise production of the strongest oxidant (hydroxyl radicals) in water based solutions by non-thermal transient plasma discharges. Information on the concentration of OH radicals and their rate of production will help in optimization of practical cleaning and decontamination processes based on non-thermal transient plasma discharges. In the present work, production of hydroxyl radicals in TA water based solutions by the transient plasma discharges has been investigated. The concentration of plasma generated OH radicals was obtained by measuring the intensity of fluorescent light emitted by HTA acid, which is formed in water-based solution of terephthalic acid, as TA acid reacts specifically with OH radicals. The dependency of the concentration of the plasma generated OH radicals on discharge driving voltage, its polarity, and total delivered charge and treatment time was obtained.

Different discharge energization voltage levels were used in the present study to generate transient plasmas (± 20, ± 24 and ± 28 kV) and two types of dishes (sample holders) were used to treat TA water based samples: non-conductive plastic dishes located on the grounded metallic holder, and conductive aluminum foil-covered dishes, also located on the grounded metallic support within the treatment test cell. In the first case the plasma discharges propagate vertically through air and then across air/liquid interface. In the second case, the discharges propagate only vertically and then the discharge current dissipates through the bulk of the liquid sample. A higher efficiency of OH radical production was observed in the latter case: for the conductive sample holders, the obtained specific production efficiency was 0.324 μM/mC for positive impulses, and 0.253 μM/mC for negative impulses. In the case of the non-conductivve dishes, the specific production efficiency was lower: 0.125 μM/mC for positive impulses and 0.171 μM/mC for negative impulses.

Indirect chemical processes with involvement of other reactive oxygen species such as ozone and hydrogen peroxide could also have an effect on OH radical production. For example, ozone molecules can be decomposed in water through a chain reaction catalyzed by hydroxyl radicals. Ozone reacts with OH radicals resulting in production of $\cdot O_2^-$, then an electron will be transferred to ozone molecule to form $\cdot O_3^-$. $\cdot O_3^-$ which in turn react with water molecules to form OH radicals [26, 27]. However, in the current work, the ozone concentration generated in the test cell was minimal, less than 1 ppm, and it is believed that ozone based reactions did not make a significant contribution to the production of OH radicals in the present tests.

Another important finding of this paper includes the fact that the rate of OH production depends almost linearly on the total delivered charge. The concentration of the plasma produced OH radicals practically does not depend on the magnitude of HV impulses used to generate the transient discharges at the same delivered charge. Thus, it confirms that the total charge delivered by the plasma discharges defines the production rate of reactive species and plays an important role in the advanced oxygen processes.

A comparison of the concentrations of OH radicals generated by the transient plasma discharges in non-conductive and conductive dishes reveals that, in the case of the conductive dish, plasma discharges produce more OH radicals. Also, it has been shown that in the case when the high tension electrode is in touch with a surface of the treated liquid, the efficiency of OH production is low. In the present study, the maximum OH production efficiency of $1.39 \cdot 10^{-8}$ μM/s was achieved using negative energization of the HV electrode. This figure is higher than the production rate of OH reported in [19] for underwater discharges. In [28] and [29], steady-state plasma was used to generate OH radicals in water. The production rates

reported in these papers are slightly higher than the rate of OH production achieved in the present paper, $(1\text{-}4.7)\cdot10^{-8}$ M/s [28], and $1.67\cdot10^{-8}$ M/s [29]. However, these figures were obtained using continuous steady-state plasma treatment. In the current work, impulsive treatment was used (with a pulse repetition rate of 20 pulses per second), and it is therefore expected that with an increase in pulse repetition rate and/or treatment time, significantly higher OH production rates can be achieved. The results obtained in the present paper will help in optimization of OH production in liquids by transient plasma discharges.

ACKNOWLEDGEMENTS

The authors would like to thank the Department of Biomedical Engineering at the University of Strathclyde for access to their fluorescence spectrophotometer.

REFERENCES

[1] S. Li, I. Timoshkin, M. Maclean, M. Wilson, M. Given, S. MacGregor, T. Wang and J. Anderson, "Steady-State Corona Discharges in Atmospheric Air for Cleaning and Decontamination", IEEE Trans. Plasma Sci., Vol. 41, pp. 2871 - 2878, 2013.

[2] P. Lukes, E. Dolezalova, I. Sisrova and M. Clupek, "Aqueous-phase chemistry and bactericidal effects from an air discharge plasma in contact with water: evidence for the formation of peroxynitrite through a pseudo-second-order post-discharge reaction of H_2O_2 and HNO_2", Plasma Sources Sci. Technol., Vol. 23, 015019, 15pp, 2014.

[3] D. Dobrynin, G. Fridman, G. Friedman and A. Fridman, "Physical and biological mechanisms of direct plasma interaction with living tissue", New J. Phys. Vol. 11, 11502, 2009.

[4] G. Fridman, A. D. Brooks, B. Manjula, A. Fridman, A. Gutsol, V. N. Vasilets, H. Ayan and G. Friedman, "Comparison of direct and indirect effects of non-thermal atmospheric pressure plasma on bacteria", Plasma Process. Polym., Vol. 4, pp. 370–375, 2007.

[5] S.Samukawa, M. Hori, S. Rauf, K. Tachibana, P. Bruggeman, G. Kroesen, J. Whitehead, A. Murphy, A. Gutsol, S. Starikovskaia, U. Kortshagen, J.-P. Boeuf, T. Sommerer, M. Kushner, U. Czarnetzki and N. Mason, "The 2012 Plasma Roadmap", J. Phys. D: Appl. Phys., Vol. 45, 253001 (37pp), 2012.

[6] I. V. Timoshkin, M. Maclean, M. P. Wilson, M. J. Given, S. J. MacGregor, T. Wang and J. G. Anderson, "Bactericidal effect of corona discharges in atmospheric air". IEEE Trans. Plasma Science, Vol. 40, No. 10, pp. 2322-2333, 2012.

[7] H. Eto, Y. Ono, A. Ogino and M. Nagatsua, "Low-temperature sterilization of wrapped materials using flexible sheet-type dielectric barrier discharge", Appl. Phys. Letters, Vol. 93, 221502, 2008.

[8] S. Patil, T. Moiseev, N.N. Misra, P.J. Cullen, J.P. Mosnier, K.M. Keener and P. Bourke "Influence of high voltage atmospheric cold plasma process parameters and role of relative humidity on inactivation of Bacillus atrophaeus spores inside a sealed package", J. Hospital Infection, Vol. 88, pp.162-169, 2014.

[9] M. Sun and L. Cai, "Diagnosis of OH radicals in air negative pulsed discharges with nozzle-cylinder electrode by optical emission spectroscopy", IEEE Trans. Plasma Sci., Vol. 40, No. 5, pp.1395-1398, 2012.

[10] Z. Machala, I. Jedlovsky, L. Chladekova, B. Pongrac, D. Giertl, M. Janda, L. Sikurova, P. Polcic, "DC discharges in atmospheric air for bio-decontamination – spectroscopic methods for mechanism identification", Eur. Phys. J. D, Vol. 54, pp. 195-204, 2009.

[11] E. Sysolyatina, A. Mukhachev, M. Yurova, M. Grushin, V. Karalnik, A. Petryakov, N. Trushkin, S. Ermolaeva and Y. Akishev, "Role of the Charged Particles in Bacteria Inactivation by Plasma of a Positive and Negative Corona in Ambient Air", Plasma Process. Polym., Vol. 11 No. 4, pp. 315-334, 2014.

[12] J. Guo, K. Huang and J. Wang, "Bactericidal effect of various non-thermal plasma agents and the influence of experimental conditions in microbial inactivation: A review", Food Control, Vol. 50, pp. 482-490, 2014.

[13] P. Bruggeman, F. Iza, P. Guns, D. Lauwers, M. G. Kong, Y. A. Gonzalvo, C. Leys and D. C. Schram, "Electronic quenching of OH(A) by water in atmospheric pressure plasmas and its influence on the gas temperature determination by OH(A-X) emission" Plasma Sources Sci. Technol. Vol. 19, 015016, 7pp, 2010.

[14] H. Kim, K. Wright, I. Hwang, D. Lee, A. Rabinovich, A. Fridman, Y. Cho, "Effect of H_2O_2 and low pH produced by gliding arc discharge on the inactivation of Escherichia Coli in water", Plasma medicine, Vol. 1(3-4), pp. 295-307, 2011.

[15] A. Fridman, *Plasma Chemistry*, Cambridge University Press, 2008.

[16] S. Kanazawa, H. Kawano, S. Watanabe, T. Furuki, S. Akamine, R. Ichiki, T. Ohkubo, M. Kocik and J. Mizeraczyk, "Observation of OH radicals produced by pulsed discharges on the surface of a liquid", Plasma Sources Sci. Technology, Vol. 20, 034010(8pp), 2011.

[17] Y. Ikeda, A. Moon and M. Kaneko, "Development of microwave-enhanced spark-induced breakdown spectroscopy", Appl. optics, Vol. 49, n.13, pp. 95-100, 2010.

[18] S. Page, W. Arnold and K. Mcneill, "Terephthalate as a probe for photochemically generated hydroxyl radical", J. Environ. Monit., Vol. 12, pp. 1658-1665, 2010.

[19] S. Kanazawa, T. Furuki, T. Nakaji, S. Akamine and R. Ichiki, "Application of chemical dosimetry to hydroxyl radical measurement during underwater discharge", ICAES-2012, J. Phys.: Conf. Series 418(2013)012102 DOI:10.1088/1742-6596/418/1/012102.

[20] T. Mason, J. Lorimer, D. Bates and Y. Zhao, "Dosimetry in sonochemistry: the use of aqueous terephthalic ion as a fluorescence monitor", Ultrasonic Sonochemistry, Vol. 1, no.2, pp.s91 – s95, 1994.

[21] S. J. MacGregor, J. M. Koutsoubis and S. M. Turnbull, "The design and operation of a compact high-voltage, high pulse repetition frequency trigger generator", Meas. Sci. Technol., Vol. 9, pp. 1899–1905, 1998.

[22] B. Sun, M. Sato and J. S. Clements, "Optical study of active species produced by a pulsed streamer corona discharge in water" J. Electrostat., Vol. 39, pp. 189–202, 1997.

[23] P. Sunka, V. Babicky, M. Clupek, P. Lukes, M. Simek, J. Schmidt and M. Cernak, "Generation of chemically active species by electrical discharges in water" Plasma Sources Sci. Technol., Vol. 8, pp. 258-265, 1999.

[24] M. Sato, T. Ohgiyama and J. S. Clements, "Formation of chemical species and their effects on microorganisms using a pulsed high voltage discharge in water" IEEE Trans. Ind. Appl., Vol. 32, pp. 106–12, 1996.

[25] D. M. Stanbury, "Reduction potentials involving inorganic free radicals in aqueous solution", Adv. Inorg. Checm, Vol. 33, pp. 69-138, 1989.

[26] B. G. Ershov and P. A. Morozov, "The kinetics of ozone decomposition in water, the influence of pH and temperature", Russian J. Phys. Chem. A, Vol. 83, No. 8, pp. 1295-1299, 2009.

[27] J. Staehelin and J. Hoigne, "Decomposition of ozone in water in the presence of organic solutes acting as promoters and inhibitors of radical chain reactions", Environ. Sci. Technol., Vol. 19, n.12, pp. 1206–1213, 1985.

[28] S. Kanazawa, T. Furuki, T. Nakaji, S. Akamine and R. Ichiki, "Measurement of OH Radicals in Aqueous Solution Produced by Atmospheric-pressure LF Plasma Jet", Ecological Society of America Conf. 2012, http://www.electrostatics.org/images/ESA2012_N3.pdf

[29] M. Sahni and B. R. Locke, "Quantification of Hydroxyl Radicals Produced in Aqueous Phase Pulsed Electrical Discharge Reactors," Ind. Eng. Chem. Res., Vol. 45, pp.5819-5825, 2006.

[30] Y. Zhao, T. Wang, S. MacGregor, M. Wilson, M. Given and I. Timoshkin, "Investigation of plasma-induced methylene blue degradation using dielectric barrier discharge", Int'l. Conf. Gas Discharges and Their Applications, Orleans, France, pp. 566-569, 2014.

[31] Z. Machala, B. Tarabova, K. Hensel, E. Spetlikova, L. Sikurova and P. Lukes, "Formation of ROS and RNS in water Electro-sprayed through Transient Spark Discharge in Air and their Bactericidal effect", Plasma Process. Polym., Vol. 10, pp.649-659, 2013.

[32] H. Tresp, M.U. Hammer, J. Winter, K-D. Weltmann and S. Reuter, "Quantitative detection of plasma-generated radicals in liquids by electron paramagnetic resonance spectroscopy", J. Phys. D: Appl. Phys., Vol. 46, 8 pp. 435401-09, 2013

Sirui Li was born in Yunnan, China, in 1988. He received the B.Eng. (with honours) and M.Sc. degrees in electronic and electrical engineering from the University of Strathclyde, Glasgow, U.K., in 2010 and 2011. He is currently a Ph.D. student at the University of Strathclyde, majoring in non-thermal plasma discharge for air treatment and surface decontamination.

Igor V. Timoshkin (M'07-SM'14) received a degree in physics from the Moscow State University (Russia) in 1992, and the Diploma and the Ph.D. degree from the Imperial College of Science, Technology and Medicine, (London, UK) in 2001. After graduation from MSU he worked as a Researcher at Moscow State Agro-Engineering University, and then at the Institute for High Temperatures of Russian Academy of Sciences before moving to ICSTM in 1997. He joined the Department of Electronic and Electrical Engineering of the University of Strathclyde (Glasgow, UK) in 2001 as an Academic Visitor, where he became a Senior Lecturer in 2011. His research interests include properties of solid and liquid dielectric materials, electronics of plasma discharges in condensed media, practical applications of electro-hydraulic and high-power ultrasound pulses, bio-dielectrics and effects of electromagnetic fields on biological objects.

Michelle Maclean was born on the Isle of Lewis, Scotland, in 1980. She received the B.Sc. (1st class honors) degree in microbiology and immunology in 2002, and the Ph.D. degree in electronic and electrical engineering in 2006, both from the University of Strathclyde, Glasgow, U.K. She is presently working as a Lecturer at the University of Strathclyde, and her interdisciplinary research work involves the development and application of novel electro-technologies for biological decontamination and sterilization applications in clinical and public health environments. She is a member of The Society for General Microbiology and The American Society of Microbiology.

Scott J. MacGregor (M'95-SM14) received the B.Sc. and Ph.D. degrees from the University of Strathclyde, Glasgow, U.K., in 1982 and 1986, respectively. He is currently with the University of Strathclyde, where he became a Pulsed-Power Research Fellow in 1986, a Lecturer in pulsed-power technology in 1989, a Senior Lecturer in 1994, and a Reader and a Professor of high-voltage engineering in 1999 and 2001, respectively. He has been Dean of Engineering at the University of Strathclyde since January 2010. His research interests include high-voltage pulse generation, high-frequency diagnostics, high-power repetitive switching, high-speed switching, electronic methods for food pasteurization and sterilization, generation of high-power ultrasound (HPU), plasma channel drilling, pulsed-plasma cleaning of pipes, and stimulation of oil wells with HPU.

Mark P. Wilson (M'10) was born in Stranraer, Scotland, in 1982. He received the B.Eng. (with honours), M.Phil., and Ph.D. degrees in electronic and electrical engineering from the University of Strathclyde, Glasgow, U.K., in 2004, 2007, and 2011, respectively. He is presently working as a Teaching Associate at the University of Strathclyde, where he continues to investigate surface flashover of solids immersed in insulating oil. Mark is a member of the IEEE Nuclear and Plasma Sciences Society, from whom he received a Graduate Scholarship Award in 2011, the IEEE Dielectrics and Electrical Insulation Society, and the IET.

Martin J. Given (M'99-SM'11) is currently a Senior Lecturer in the Department of Electronic and Electrical Engineering at the University of Strathclyde. He received a degree in physics from the University of Sussex in 1981 and a Ph.D. in electronic and electrical engineering from the University of Strathclyde in 1996. His research interests include, ageing processes and condition monitoring in solid and liquid insulation systems, high speed switching and pulse power applications.

Tao Wang received the B.Eng. and M.Sc. degrees from Northeast China Dianli University (China) in 1993 and 1996, respectively, and the Ph.D. degree from the University of Strathclyde (Glasgow, UK) in 2005. He then joined the Newland Entech as a research fellow developing high efficiency industrial ozone generator. He joined the department of Electronic and Electrical Engineering of University of Strathclyde as a lecturer in 2010. His research interests include non-thermal gas discharges and their applications in gas synthesis, water disinfection and advanced oxidation process in water

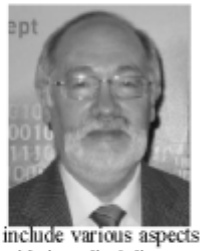

John Anderson was born in Glasgow, U.K., on 2 September 1942. He received the B.Sc. degree in applied microbiology in 1968, and the Ph.D. degree in fungal physiology in 1971, both from the University of Strathclyde, Glasgow. Since 1971, he has been with the Department of Bioscience and Biotechnology, University of Strathclyde, where he became a Professor of Microbiology and Head of the Department. He is currently an Emeritus Professor at the University of Strathclyde. His research interests include various aspects of food, biomedical and environmental microbiology with interdisciplinary collaboration on the application of electro-technologies for electronic pasteurization and sterilization.

Oxidation and Biodecontamination Effects of Impulsive Discharges in Atmospheric Air

Sirui Li, Igor V. Timoshkin, *Senior Member, IEEE*, Michelle Maclean, Scott J. MacGregor, *Senior Member, IEEE*, Mark P. Wilson, *Member, IEEE*, Martin J. Given, *Senior Member, IEEE*, Tao Wang, and John G. Anderson

***Abstract*— Chemical oxidation and the bactericidal capabilities of nonthermal plasma discharges can be used in different practical applications, such as biodecontamination, sterilisation of medical equipment, waste water treatment, syn-gas treatment, and others. In this paper, the oxidation and biodecontamination effects of impulsive plasma discharge, which propagate across a liquid sample/air interface (surface discharges), and through the bulk of a liquid sample (direct discharges), have been investigated. The oxidizing capability was analyzed by measuring the degree of decolorization of indigo carmine dye in water solutions. Gram-negative and gram-positive bacterias, *E. coli* and *S. aureus*, respectively, were used as model microorganisms in the investigation of the biocidal effects of plasma discharges. Surface and direct plasma discharges were generated by high-voltage impulses of both polarities, with the magnitudes of 20, 24, and 28 kV, and the chemical oxidation and biodecontamination capabilities of such discharges have been obtained and analyzed. It has been established that the defining factor in the chemical and biological effects of plasma discharges is the normalized delivered charge (dose). The results obtained in this paper show that surface discharges have greater biodecontamination capability as compared with direct transient plasma discharges. Also, it was shown that the decontamination rate of *E. coli* is more than double than that of *S. aureus*.**

***Index Terms*— Biodecontamination, nonthermal plasma discharges, OH-radicals, oxidation.**

I. Introduction

NONTHERMAL plasma discharges have attracted the attention of researchers and engineers who are working on the development of novel methods for oxidation and biodecontamination. It has been shown that atmospheric-pressure plasma discharges produce significant oxidation and bactericidal effects [1]. As a result, multiple practical applications are now being developed, including nonthermal plasma discharges for gas treatment, water purification, biodecontamination, and wound treatment [2], [3]. However, the exact mechanisms of the chemical and microbiological effects of transient atmospheric plasma (TAP) discharges are still not fully understood. There are several factors which make a significant contribution to these processes: production of chemically active oxygen and nitrogen species, emission of UV light, and generation of a strong electric field. TAP discharges produce multiple chemically active species, including OH radicals, ozone, hydrogen peroxide, singlet oxygen, nitric dioxide, peroxynitrites, and others [4]–[7]. OH radicals have the highest redox potential of 2.7 V, amongst all oxygen-based reactive species [8], while the redox potential of superoxide anions is 2.42 V, ozone is 2.07 V, and hydrogen peroxide is 1.78 V [9]. In [10] and [11], it was shown that OH radicals have higher reaction rates than other species, including ozone: OH radicals are able to react with organic compounds significantly (10^6–10^{12} times) faster than ozone. Therefore, chemical species with high oxidizing capability play an important role in the chemical and microbiological activity of plasma discharges [12]–[14]. For example, it was suggested in [15] that OH radicals together with ozone produced by an underwater air plasma jet play a major role in the decomposition of methylene blue dye in water solution. Possible mechanisms of OH production at the plasma–water interface are discussed in [9] and [16]; amongst, these mechanisms are the disassociation of water molecules by energetic electrons and dissociative attachment of electrons to water molecules. Plasma discharges in water can produce other reactive oxygen species (ROS) with high redox potential, such as superoxide anions, ozone, and hydrogen peroxide [16], [17].

Different types of TAP discharges can result in different rates of production of these chemically active species and, thus, can result in a different degree of chemical or microbiological activity. For further development of practical applications of TAP discharges, it is important to establish the optimal discharge topologies, and therefore, it is necessary to investigate the oxidation and microbiological efficacy of different types of discharges and their dependence on different discharge parameters, such as the magnitude and polarity of the applied voltage, the charge delivered during the plasma treatment, and the discharge propagation path.

In this paper, the chemical and biological effects of pulsed discharges in atmospheric air, which propagate across the interface between the sample under test (water-based dye solution and water-based agar seeded with microorganisms) and air, or through the bulk of the sample under test, have been studied. This approach allowed the comparison of the biodecontamination and oxidation efficacy of surface and direct plasma discharges. The oxidation capability of TAP discharges was investigated using a water-based solution of blue dye (indigo carmine), and the degree of decolorization of

Manuscript received December 23, 2015; revised April 15, 2016; accepted June 6, 2016. Date of publication June 24, 2016; date of current version October 7, 2016.

The authors are with the Department of Electronic and Electrical Engineering, University of Strathclyde, Glasgow G1 1XW, U.K. (e-mail: s.li@strath.ac.uk; igor.timoshkin@strath.ac.uk; michelle.maclean@strath.ac.uk; scott.macgregor@strath.ac.uk; mark.p.wilson@strath.ac.uk; m.given@strath.ac.uk; tao.wang@strath.ac.uk; j.g.anderson@strath.ac.uk).

Color versions of one or more of the figures in this paper are available online at http://ieeexplore.ieee.org.

Digital Object Identifier 10.1109/TPS.2016.2581317

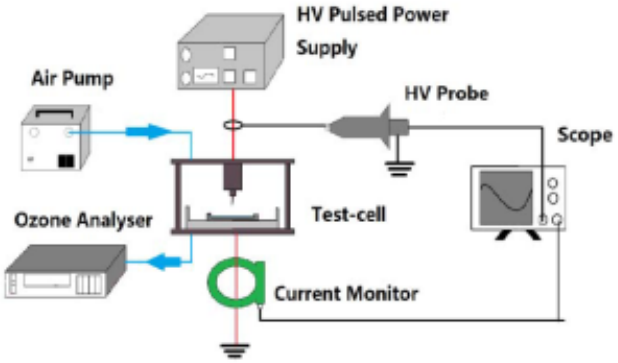

Fig. 1. Diagram of the experimental system used for decolorization and microbiological inactivation.

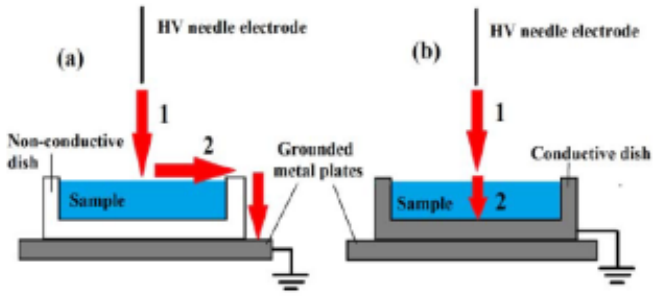

Fig. 2. Cross-sectional diagram of the sample dish held within the test cell (not to scale). (a) Nonconductive plastic dish. (b) Plastic dish lined with aluminum foil (conductive dish). Arrows: paths followed by the generated transient discharges. (a) vertical path through the air toward the sample surface and interfacial path in the case of nonconductive sample holder. (b) Path through the bulk of liquid sample in the case of the conductive sample holder.

this dye was obtained for different voltages, specific charges, and for different discharge propagation paths. Also, the bioinactivation capability of the TAP discharges was investigated using the gram-negative and gram-positive microorganisms, *E. coli* and *S. aureus*, respectively. The results obtained in this paper confirm that TAP discharges produce significant oxidation and biodecontamination effects, which will aid in further development and optimization of atmospheric plasma treatment systems for practical applications, including the use of such plasma discharges in environmental and medical technologies.

II. Experimental System

The main aim of this paper was to investigate the production of OH radicals in water-based solutions, and the chemical oxidation and microbiological decontamination capabilities of two types of TAP discharges: surface discharges which propagate along the sample/air interface and direct discharges which propagate through the bulk of the sample. To conduct this paper, a dedicated experimental system was designed and developed. This system includes a pulsed-power supply to generate transient plasma discharges, different test cells to hold water solutions and microbiological samples, diagnostic devices to monitor high-voltage (HV) and current waveforms, an air pump with a gas distribution board, and an ozone analyzer.

A diagram of this experimental system is shown in Fig. 1. A TG-01 trigger generator (Samtech Ltd, Scotland) was used as a pulsed-power source, and the output of the pulse generator was connected to the HV needle electrode located inside the test cell. The trigger generator was capable of producing positive and negative HV impulses with a peak magnitude of 30 kV and a rise time of ~60 μs [18]. The pulse repetition rate used in this paper was 20 pulses per second (pps).

The transient voltage waveforms associated with the discharges generated were monitored by a Tektronix P6015A HV probe (1000:1 division ratio, 75-MHz bandwidth). The discharge current was monitored by a Pearson 6585 current monitor (250-MHz bandwidth). The HV probe and the current monitor were connected to the high-impedance inputs of a Tektronix TDS 2024 digitizing oscilloscope (200-MHz bandwidth and 2-GSamples/s sampling rate). A 50-Ω coaxial cable was used to connect the Pearson monitor and the oscilloscope, and this cable was terminated by a 50-Ω resistive load.

A test cell, designed to house water-based dye solution and microbiological agar samples, was made of a Perspex cylinder (80 mm high) with an outer diameter of 150 mm. The ends of the cylinder were covered by two Polyvinyl chloride (PVC) flanges. Inside this cylinder, a gramophone needle with a tip radius of ~36 μm was placed in a vertical holder fixed on the upper PVC flange, forming the HV electrode. The grounded electrode (an aluminum plate) was located on the lower PVC flange, inside the Perspex cylinder.

Liquid and microbiological (agar) samples were placed in two different types of sample holder, as shown in Fig. 2. These sample holders were located on the grounded aluminum plate inside the Perspex container and subjected to HV discharges. Transparent, nonconductive, plastic plates (55 mm diameter) were used for the generation of interfacial discharges [Fig. 2(a)]; the same plates were lined with an aluminum foil [Fig. 2(b)] and used to generate discharges through the bulk of liquid samples. The volume of each liquid sample was 6 mL; therefore, the depth of liquid in the sample holders was only ~2.4 mm. Agar samples were ~2.5 mm thick.

When the nonconductive plastic dish was used, Fig. 2(a), the discharge initiated at the tip of the needle HV electrode propagates vertically down toward the surface of the sample (path 1). The discharge continues its development across the sample/air interface toward the edge of the sample holder (path 2), before reaching the grounded metallic plate. In the case of conductive sample holders, Fig. 2(b), the transient discharge produced at the tip of the HV needle propagates vertically down toward the sample surface (path 1), and the ionic current closes the circuit by flowing through the bulk of the sample toward the grounded aluminum foil. Therefore, in the case of the nonconductive dish, a shorter path length is required to achieve the same breakdown voltage as in the case of the conductive sample holder, where the surface of the sample acts as a virtual ground.

During the tests, an air pump (VP 1HV, KNF Neuberger Ltd.) was used to supply a gentle air flow (flow rate was 5 L/min) through the test cell, and the gas leaving the test cell was sent to an ozone analyzer. The air delivered to

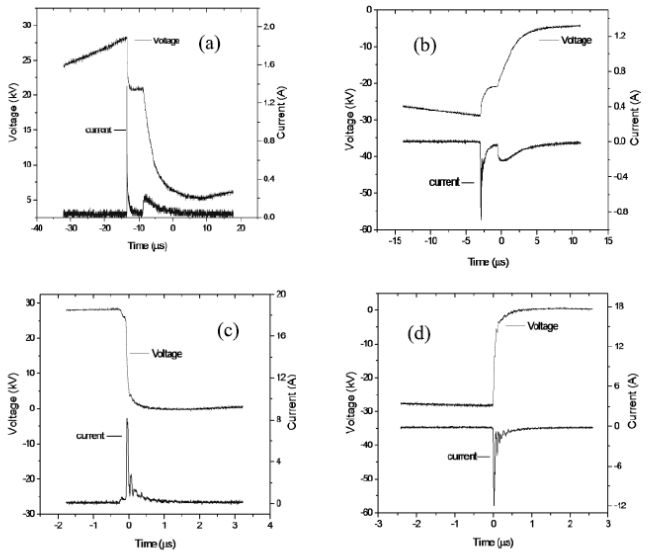

Fig. 3. Voltage and current waveforms for two different sample holders. (a) +28-kV nonconductive dish. (b) −28-kV nonconductive dish. (c) +28-kV foil-lined conductive dish. (d) −28-kV foil-lined conductive dish.

the test cell was laboratory air at ambient temperature and humidity (~20 °C and ~40% relative humidity).

The pH of the liquid and the agar samples was measured before and after plasma treatment, using a pH meter (Hanna Instruments PH 210) for the liquid samples, and using pH indicator strips (Johnson Universal pH 1-14) for the agar samples. The conductivity of the liquid samples was measured using a conductivity meter (Hanna Instruments HI 933000), the conductivity of the agar samples was measured in the test cell with two parallel electrodes using an AVOmeter model 8 Mk7.

The presence of transient discharges in the test cell was detected by the collapse of the voltage waveform. The maximum voltage before the voltage collapse is called the breakdown voltage in this paper. Fig. 3 shows the voltage and current waveforms in the cases of nonconductive and conductive sample holders for water solution samples (similar waveforms were obtained for agar samples). It can be seen that in the case of nonconductive dishes [Fig. 3(a) and (b)], a double voltage collapse and two current peaks were observed for both polarities. This is indicative of the two-stage discharge propagation process discussed earlier: vertical transient discharges propagating toward the sample surface [path 1 in Fig. 2(a)], and surface discharges [path 2 in Fig. 2(a)]. However, in the case of the conductive sample holder, only single voltage collapse event and a single current impulse were observed [Fig. 3(c) and (d)]. These processes correspond to the direct vertical discharge propagation path shown in Fig. 2(b), the current then dissipating via ionic conduction through the bulk of the sample.

The waveforms shown in Fig. 3 are similar to transeint spark discharge waveforms [19], [20]. A transient spark discharge is characterized by the development of an initial streamer and its transformation into a transient spark, which manifests

TABLE I

DISTANCES FROM THE TIP OF THE HV NEEDLE ELECTRODE TO THE SAMPLE SURFACE AND CORRESPONDING BREAKDOWN VOLTAGES

Breakdown voltage, kV	Non-conductive sample holder, mm		Conductive sample holder, mm	
	Positive	Negative	Positive	Negative
+20	0.5	0.7	4.9	1.7
+24	5.1	1.4	7.7	3.3
+28	7.3	3.7	11.1	6.0

itself via the appearance of a high-current impulse. In the case of transient sparks, the nonequilibrium plasma has a gas temperature in the range of 500–1500 K [19], [20]. Thus, transient spark discharges differ from typical spark discharges in which significantly hotter plasma can be close to its local thermodynamic equilibrium. The plasma of transient spark discharges is highly reactive, such discharges producing OH radicals, ozone, excited ions, and atomic radicals and molecules [20], with application in chemical oxidation [21], and biodecontamination treatment [22].

The distance between the needle electrode and the sample surface was adjustable, and was used to obtain three different breakdown voltages: 20, 24, and 30 kV. The distance between the HV needle electrode and the sample surface and corresponding breakdown voltages is shown in Table I.

As shown in Table I, the distance from the HV needle electrode to the sample surface to achieve the same breakdown voltage is much shorter for the nonconductive sample holders as compared with the conductive sample holders. This is due to the longer total discharge path in the case of the nonconductive sample holders as compared with the conductive dishes. Also, Table I shows that a shorter distance from the negatively energized HV electrode to the sample surface is required in order to achieve the same breakdown voltage as for positive impulses. This reduction in the distance is required to compensate for the higher breakdown voltage of atmospheric air in the case of a negatively energized sharp HV electrode, which is due to the electronegativity of air.

III. OXIDATION CAPABILITY OF TRANSIENT DISCHARGES

The oxidation capability of the impulsive atmospheric discharges generated was studied using indigo carmine dye ($C_{16}H_8N_2Na_2O_8S_2$, Sigma Aldrich Ltd) as a chemical probe. Samples of aqueous indigo carmine solution were treated in nonconductive and conductive sample holders, and their optical transmittance was measured. The chemical species produced by the transient discharges can react with the dye and can convert indigo carmine molecules into isatin-5-sulfonic acid, resulting in the decolorization effect. The difference in the optical transmittances of the treated and untreated samples allows a reduction in the dye concentration to be obtained. This reduction is an indicator of the chemical oxidation capability of the transient discharges, as the change in transmittance is a result of disintegration of chromogenic bonds in indigo carmine dye [23]. The optical transmittance of the dye solutions was obtained using a UV-visible

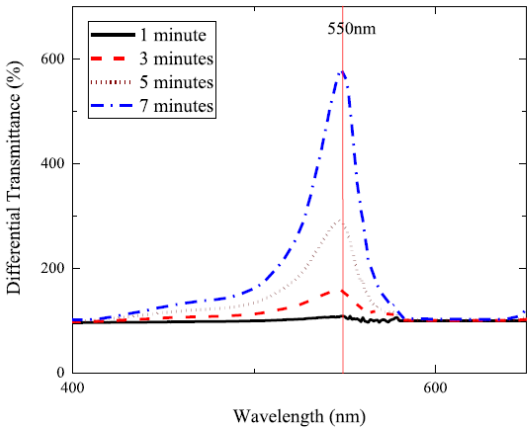

Fig. 4. Differential optical transmittance of indigo carmine aqueous solutions treated with surface discharges at +28 kV and untreated (control) solutions.

spectrophotometer (Biomate, Thermo-Spectronics Europe). Section III-A presents the results of the investigation into the oxidation effects of the surface transient discharges, which propagate along the sample/air interface (samples were treated in the nonconductive sample holders), and Section III-B presents the oxidation results obtained in the case of the direct discharges (treatment in the conductive sample holders).

A. Oxidation Capability of the Surface Transient Discharges

An indigo carmine aqueous solution with a dye concentration of 0.25 g/L was prepared using distilled water. A 5-mL sample of this solution was transferred to the nonconductive sample holder using a pipette. The sample holder was placed on the top of the metallic grounded plate inside the Perspex container and exposed to plasma discharges for four different treatment times (1, 3, 5, and 7 min) and for impulses of both polarities, all at 20 pps. During the treatment, the Perspex container was flushed with ambient air, which then passed through the ozone analyzer. The ozone levels in all tests were lower than 1 ppm. After each exposure, the optical transmittance of the sample was measured along with that of an unexposed control sample. The differential transmittance, T, at 550 nm was calculated using

$$T = \frac{T_b}{T_a} \cdot 100\% \qquad (1)$$

where T_a is the transmittance of the unexposed sample and T_b is the transmittance of treated sample. Examples of the differential transmittance spectra for the dye samples treated for different time intervals are shown in Fig. 4.

Using the differential optical transmittance and the Beer–Lambert law, the concentration of indigo carmine in water was obtained. The results of this analysis are shown in Fig. 5; this graph represents a normalised concentration of the dye in water as a function of the total charge delivered during the plasma treatment, normalised by the surface area of the sample holder.

The normalised charge (dose) was selected in this paper to represent the oxidation capability of the transient plasma

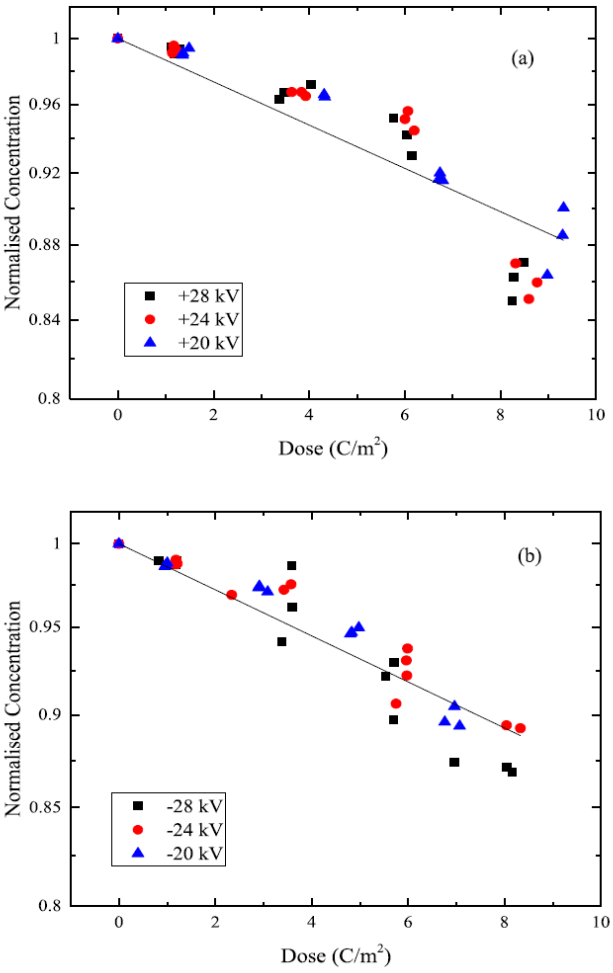

Fig. 5. Concentration of indigo carmine as a function of the dose after treatment with (a) positive surface discharges and (b) negative surface discharges. Solid lines, fitting by (3) (a) $\mu = 0.013$ m^2/C and (b) $\mu = 0.014$ m^2/C.

discharges. In this paper, the water-dye solutions and the agar samples were treated with direct positive and negative plasma discharges in air. Therefore, the liquid and agar samples were subjected to the action of both charged and neutral chemial species generated by the transient plasma discharges. Such direct exposure is considered to be more efficient for biodecontamination as compared with exposure of biosamples to the plasma afterglow by locating these samples outside the direct discharge zone [24]. It is known that the charged particles produced by the plasma discharges are responsible for the generation of chemically active neutral species and direct chemical oxidation [13], [25].

Generation of charged particles (electrons, ions, and clusters) in the discharge leads to the appearance of electric current in the circuit. The electrons and the ions are involved in the formation of neutral chemical species; therefore, it can be assumed that the current is a parameter which provides information not only on the presence of charged particles, but also correlating with the total amount of newly developed chemical species. The charged, chemically active

species include nitrites, nitrates, and oxygen anions which are negatively charged; positively charged species include protons, oxygen ions, and positively charged NO_x species. The neutral activated species include both ROS and reactive nitrogen species (RNS). Amongst, the neutral ROS are singlet oxygen, ozone, hydrogen peroxide, and hydroxyl radicals; neutral RNS include nitric oxide and nitrogen dioxide. A detailed description of the chemical processes involved in the formation of neutral and charged species can be found in [24] and [25].

It was established in [27] that in the case of corona discharges in ambient air, the electrical parameters that control the sample's treatment area and the flux of neutral activated species are the voltage, the current, and the exposure time. Moreover, it was found that in the case of fixed electrical parameters, the pH of water treated with corona discharges generated by an HV electrode located above the water surface in air is a linear function of the exposure time [27].

The results obtained in this paper, Fig. 5, demonstrate that the variation in voltage does not significantly affect the bioinactivation and oxidation processes. Also, in this paper, the distance between the HV electrode and the sample surface was variable; therefore, different proportions of energy may be dissipated in the plasma above the sample. Therefore, it is reasonable to introduce the total normalised charge (dose) as a parameter which can be used for the description of the kinetics of the plasma treatment process. It is expected that the dose-dependent kinetic relationships will depend upon the disharge regime. The total charge in the present tests was calculated by integration of the experimentally obtained current waveforms, and the dose was obtained by dividing the total charge by the surface area of the sample plate. This normalisation was done for both cases, surface and direct discharges. Although in the case of direct discharge treatment, the actual cross section of plasma interaction with the sample surface is smaller than in the case of surface discharges, and this normalisation procedure helps to compare the efficacy of both types of plasma discharge in the present experimental conditions.

The normalized dose-dependent concentration, $K(D)$, was obtained by

$$K(D) = C(D)/C_0 \tag{2}$$

where $C(D)$ is the actual concentration of the dye in water (mg/L), C_0 is the initial concentration of the dye (250 mg/L in this paper), and D is the dose (C/m^2).

It is known from the literature that time of plasma exposure can be used as an independent parameter for the descripton of the decolorisation kinetics and a time-dependent (pseudo) first-order kinetic process was used in the analysis of the plasma decolorization rates of different water-soluble dyes subjected to pulsed dielectric barrier discharges [28], spark discharges [29], and glow discharges [30]. However, in the case of transient plasma regimes, it is important to consider not only time but also the total delivered charge. The area-normalized charge was therefore selected as an independent parameter for the kinetic analysis in this paper.

Fig. 5 shows the normalized concentration of the dye as a function of the dose for positive and negative discharges (for all tested voltages). It was found that the concentration of indigo carmine in water reduces with an increase in the dose. The dye concentration is a function of the dose only and does not depend on the breakdown voltage. The change in the normalized concentration of the dye is relatively small, ~15%, and it is problematic to establish the exact functional behavior of $K(D)$: for example, several different functions can be used to fit the experimental data in Fig. 5. To provide a quantitative comparison of the oxidation capability of the discharges, an exponential fitting function (3) was used, and this approach is consistent with the description of the decolorization kinetic processes provided in [28], [30]

$$K(D) = \exp(-\mu D) \tag{3}$$

where μ is the dose-dependence of the decolorization process (m^2/C). Values for μ have been obtained using the fitting procedure in Origin Pro 8 graphing software package, and found to be 0.013 and 0.014 m^2/C for the positive and negative discharges, respectively. The analytical fitting lines were plotted using the obtained values of μ, and these analytical lines are shown in Fig. 5. Note that the normalized concentration axes in Figs. 5 and 6 are logarithmic. Thus, this analysis shows that the oxidation capability of surface discharges is similar for both positive and negative polarities.

B. Oxidation Capability of Direct Discharges

The oxidation effects of direct transient discharges that propagate through the bulk of the sample were investigated. As with the surface discharges, a 6-mL sample of indigo carmine aqueous solution was placed into a conductive sample holder which was located on the top of the grounded aluminum electrode. The samples were again treated with impulsive discharges, under the same experimental conditions described in Section III-A. The differential transmittance of the treated and control samples obtained at 550 nm was used for the calculation of the dye concentration. The results of this analysis are shown in Fig. 6, which represents the normalised dye concentration obtained by (2) as a function of the dose, D, for direct positive and negative discharges.

The electrical conductivity and the pH of the water-dye solutions were measured before and after plasma treatment. For both types of treatment, surface discharge and direct discharge treatment, an increase in the electrical conductivity of the solutions was observed. However, this increase was not significant, the initial conductivity being ~0.11 mS/m, and the largest change observed being for negative direct streamer discharge treatment, where the conductivity increased to ~0.15 mS/m. In all treatment cases, a decrease in pH of the water-dye solutions was observed, the pH decreasing from ~5.5 to a minimum value of ~3.5 for surface discharge treatment, and to 3.5–4 for direct discharge treatment. A decrease in pH of water-dye solutions after plasma treatment was also observed in [16].

As in the case of surface discharges, the dye concentration is a dose-dependent parameter only, and this concentration

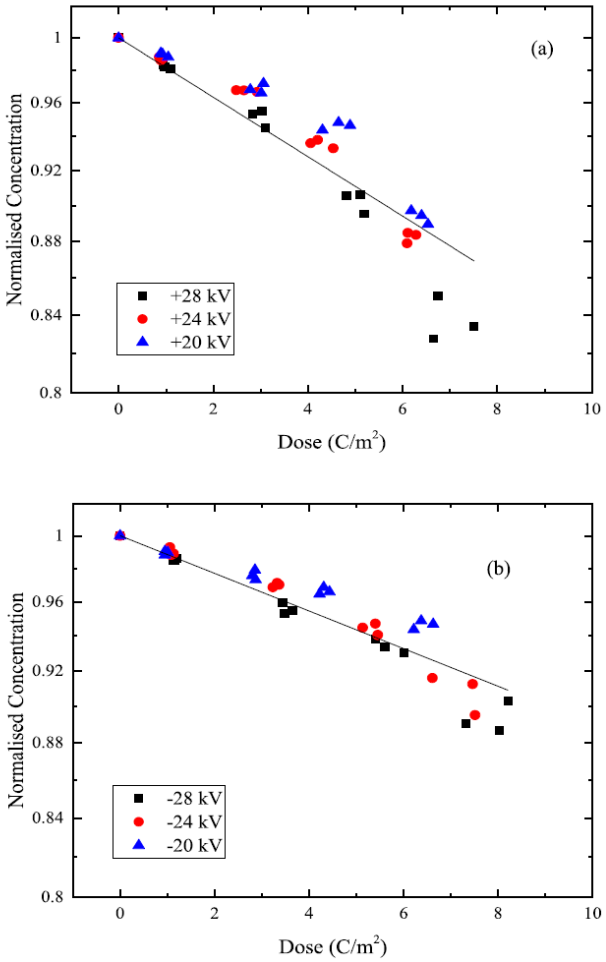

Fig. 6. Concentration of indigo carmine as a function of the dose after treatment with (a) positive direct discharges and (b) negative direct discharges. Solid lines, fitting by (3) (a) $\mu = 0.019$ m^2/C and (b) $\mu = 0.012$ m^2/C.

decreases with an increase in the dose. The decolorization process can be described by function (3). Values of μ have been obtained using the fitting procedure in Origin Pro 8 graphing software package, and found to be 0.019 and 0.012 m^2/C for the positive and negative discharges, respectively. Thus, the positive direct discharges resulted in a higher decolorization rate as compared with the negative discharges, also this rate is higher than the decolorization rate achieved by the surface discharges.

IV. Biodecontamination Effects of Transient Discharges

This section is focused on investigation of the biodecontamination effects of the atmospheric plasma discharges, which propagate across the sample/air interface and through the bulk of the samples. Again, two different sample holders (nonconductive and conductive) were used to produce the surface and direct discharges. These sample holders were filled with nutrient agar and microorganisms were seeded onto this water-based agar. The agar-filled biocontaminated plates were located in the test cell under the HV needle electrode and treated with impulsive discharges of both polarities. The breakdown voltages, the treatment time intervals, and the pulse repetition rate used in this paper were the same as in Section III. Two types of bacteria were selected for the biodecontamination study: gram-negative *E. coli* and gram-positive *S. aureus*. These microorganisms were grown in 100-mL nutrient broth and incubated under rotary conditions (120 r/min) at 37 °C for 18 h. Bacterial cultures were then centrifuged ($3939 \times g$ for 10 min) and cells resuspended and serially diluted in phosphate buffered saline to make bacteria suspensions with a population density of 10^3 colony forming units (CFU)/mL. Agar was prepared in nonconductive and conductive sample holders, 100 μL of bacteria suspension was evenly spread on the agar surface using an L-shaped spreader, providing a seeding population on the agar surface of 100–200 CFU/plate. After exposure to the positive or negative discharges for 1, 3, 5, and 7 min (20-pps pulse repetition rate), the exposed samples were incubated at 37 °C for 24 h and then enumerated.

A. Inactivation by Surface Transeint Discharges

Microbiological samples were exposed to the positive and negative discharges in the nonconductive sample holders, which ensure their interfacial propagation path across the agar/air interface. Following enumeration of the surviving bacteria, inactivation curves were plotted: the normalized population, $S(D)$, is presented as a function of the dose, D.

The dose-dependent population of microorganisms was obtained using (4) for each test

$$S(D) = P(D)/P_0 \tag{4}$$

where $P(D)$ is the actual surviving bacterial population, P_0 is the initial population of bacteria, and D is the dose (C/m^2).

The normalized population as a function of the dose can be fitted with a pseudofirst-order kinetic function (5) for all tested voltages and for both types of microorganisms

$$S(D) = \exp(-\lambda D) \tag{5}$$

where λ is the dose-dependence of the inactivation process (m^2/C).

Fig. 7 shows the normalized surviving fraction, $S(D)$, of *E. coli* and *S. aureus* treated by surface discharges as a function of the dose. As the normalized population in this figure is shown in a semilog scale, the vertical lines labeled nondetected indicate doses at which no CFU was detected in the majority of sample dishes after the treatment. The fitting procedure was implemented in Origin Pro 8 graphing software and the analytical fitting lines are shown in Fig. 7. Values of λ were found to be 0.648 and 0.281 m^2/C for *E. coli* and *S. aureus*, respectively. These inactivation rates confirm that *E. coli* is substantially more sensitive to the plasma treatment than *S. aureus*.

Fig. 8 shows the normalized population, $S(D)$, of *E. coli* and *S. aureus* as a function of the dose in the case of negative surface-discharge treatment. As in the case of positive surface-discharge treatment (Fig. 7), Fig. 8 shows that inactivation by negative surface discharges depends only on the dose, and is

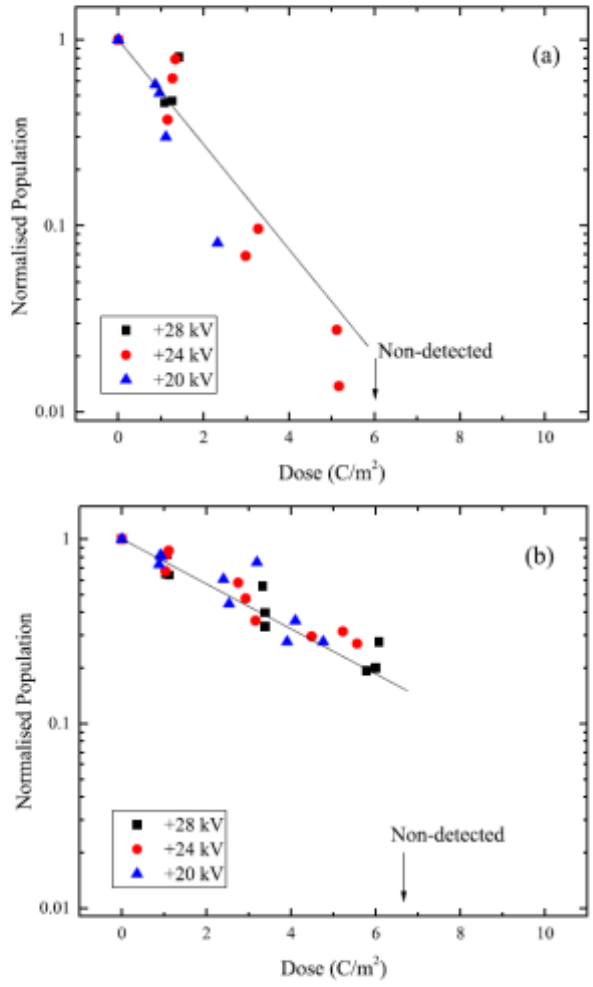

Fig. 7. Normalized surviving population of (a) *E. coli* and (b) *S. aureus*, after exposure to positive surface discharges. Solid lines, fitting by (5) (a) $\lambda = 0.648$ m^2/C and (b) $\lambda = 0.281$ m^2/C.

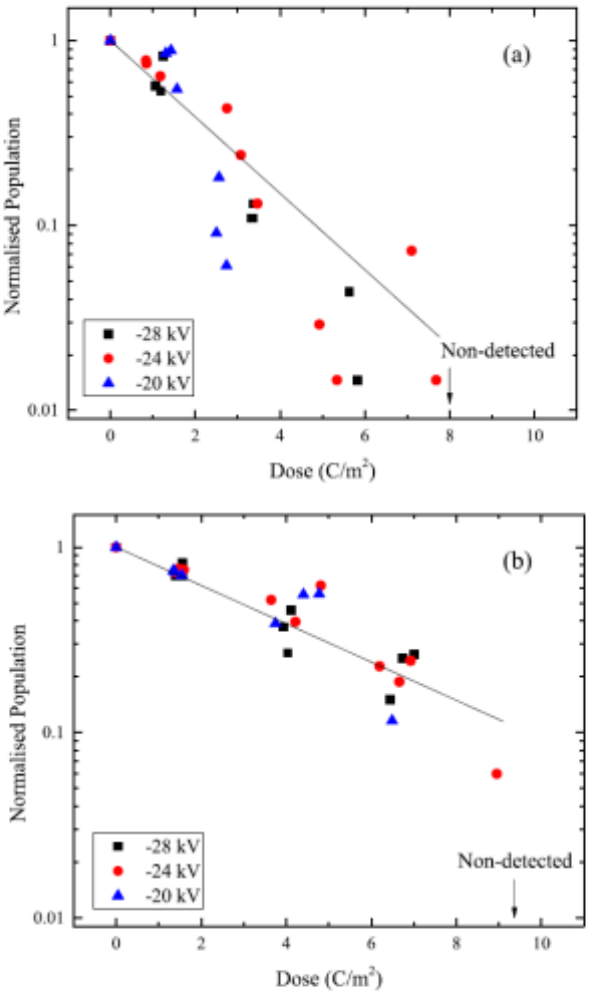

Fig. 8. Normalized surviving population of (a) *E. coli* and (b) *S. aureus*, after exposure to negative surface discharges. Solid lines, fitting by (5) (a) $\lambda = 0.476$ m^2/C and (b) $\lambda = 0.238$ m^2/C.

almost independent of the breakdown voltage. The experimental data in Fig. 8 were fitted with the exponential function (5), and this fitting confirms that the inactivation process can be described by a pseudofirst-order kinetic. The fitting procedure was implemented using Origin Pro 8 graphing software and the rates of inactivation, λ, were found to be 0.476 m^2/C for *E. coli* and 0.238 m^2/C for *S. aureus*. Again, these results confirm that *E. coli* is more sensitive to the plasma discharge treatment than *S. aureus*.

B. Inactivation by Direct Transient Discharges

The inactivation kinetics of *E. coli* and *S. aureus* were also studied using direct transient discharges: discharges which propagate through the bulk of the agar sample. To provide such a discharge path, aluminum foil lined sample holders were used. The results of this paper allow for a comparison between the inactivation capabilities of surface and direct transient discharges to be made.

Microorganisms were seeded onto agar which was placed on the conductive sample holders and exposed to the transient discharges generated by the same voltages as in Section IV-A. In the case of the direct discharges, the cross-sectional contact area between the direct plasma channel and surface of the sample is (visually) small. However, the activated species produced by the transient plasma on and above the agar surface can move across the surface of the agar and reach the periphery of the plate, and in the present tests, the effects of the discharge on the bacteria were observed at the edges of the sample holders. After the direct discharge treatment, enumeration of the surviving microorganisms was conducted.

Fig. 9 shows the normalized population of *E. coli* and *S. aureus* as a function of the dose, $S(D)$, after exposure to positive direct discharges. The experimental inactivation data presented in Fig. 9 were fitted with the pseudofirst-order kinetic function (5). As in the case of the surface discharges, *S. aureus* demonstrated a higher degree of resistance to the plasma treatment; the rate of inactivation of *E. coli* (0.311 m^2/C) is more than double the rate of inactivation of *S. aureus* (0.140 m^2/C).

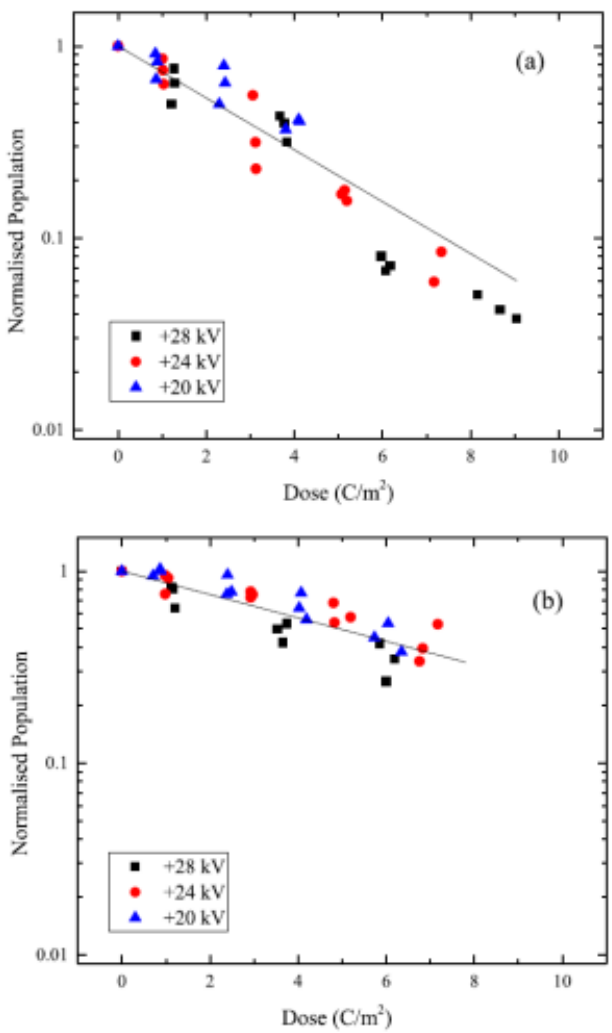

Fig. 9. Normalized surviving population of (a) *E. coli* and (b) *S. aureus*, after exposure to positive direct discharges. Solid lines, fitting by (5) (a) $\lambda = 0.311$ m^2/C and (b) $\lambda = 0.140$ m^2/C.

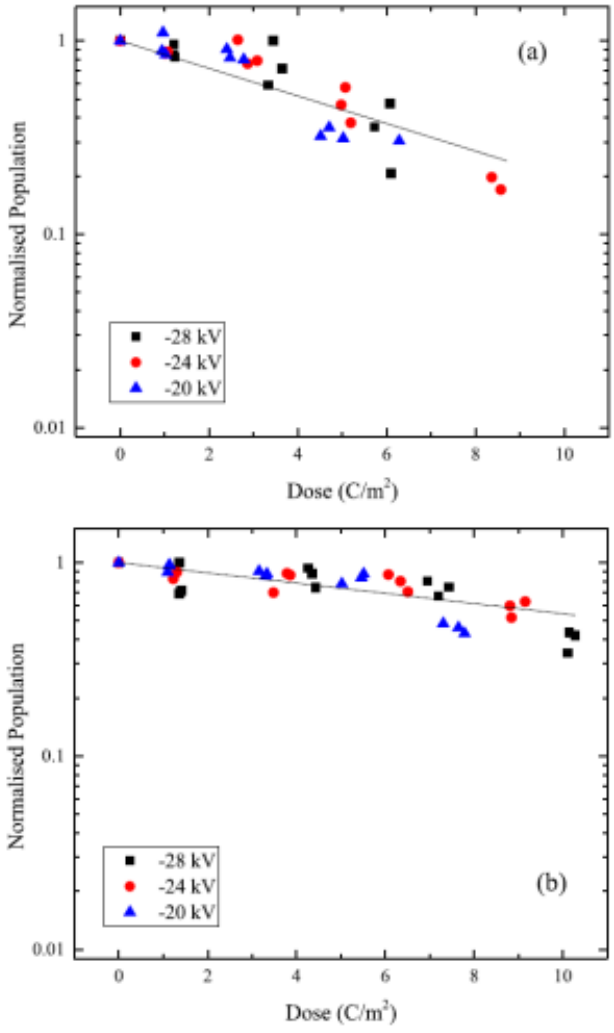

Fig. 10. Normalized surviving population of (a) *E. coli* and (b) *S. aureus*, after exposure to negative direct transient discharges. Solid lines, fitting by (5) (a) $\lambda = 0.164$ m^2/C and (b) $\lambda = 0.061$ m^2/C.

The results of the inactivation tests using negative direct discharges are shown in Fig. 10. This figure shows a normalized surviving population as a function of the dose, $S(D)$, and the experimental data were fitted with the pseudofirst-order kinetic equation (5). The fitting procedure was implemented in Origin Pro 8 graphing software, and the inactivation rates for both microorganisms were obtained: again, the rate of inactivation of *E. coli* (0.16 m^2/C) was found to be more than two-fold higher than the rate of inactivation of *S. aureus* (0.06 m^2/C).

It can be seen that the negative direct transient discharges demonstrated lower inactivation capability for both microorganisms as compared with the positive direct discharges.

V. Discussion and Conclusion

The main objective of this paper was to investigate the oxidation and decontamination effects of surface and direct impulsive atmospheric discharges. This paper helps to answer the important question: which type of transient plasma discharge (TAP) is more efficient for chemical oxidation and microbiological decontamination? The results of this paper can be used in further optimization of the energization parameters of the impulsive discharges and of the topologies of plasma treatment reactors for different practical applications, as is now discussed. It has been confirmed in this paper that impulsive transient discharges produce significant oxidation and decontamination effects, which is in line with previously published results [22], [31], [32]. Transient discharges of both polarities, with different peak voltage levels, were able to reduce the concentration of the dye in water and to inactivate microorganisms on agar surfaces. It has been shown that although both surface and direct transient discharges resulted in chemical oxidation and microbiological decontamination, there was a noticeable difference in the rates of these processes for these two types of discharge.

Table II summarizes the decolorization rates obtained in this paper: it can be seen that in the case of surface transient discharges, the difference in the decolorization rates for positive and negative energization is less than 10%. However, positive

TABLE II

DECOLORIZATION RATE (m^2/C) FOR SURFACE AND DIRECT DISCHARGES

Surface discharge		Direct discharge	
pos	neg	pos	neg
0.013 (0.012 - 0.014)	0.014 (0.013 - 0.015)	0.019 (0.018 - 0.20)	0.012 (0.011 - 0.013)

"Pos" for positive energisation, "neg" for negative energisation
Values in brackets indicate a 95% confidence interval.

TABLE III

INACTIVATION RATE (m^2/C) FOR SURFACE AND DIRECT DISCHARGES

Surface discharge				Direct discharge			
E.coli		*S.aureus*		*E.coli*		*S.aureus*	
pos	neg	pos	neg	pos	neg	pos	neg
0.648 (0.565 – 0.731)	0.476 (0.416 –0.536)	0.281 (0.256 –0.306)	0.238 (0.216 –0.260)	0.311 (0.280 –0.342)	0.164 (0.141 –0.187)	0.140 (0.125 –0.155)	0.061 (0.053 –0.069)

"Pos" for positive energisation, "neg" for negative energisation
Values in brackets indicate a 95% confidence interval.

direct discharges resulted in a higher decolorization efficacy as compared with negative direct discharges: the difference between these two decolorization rates is ~37%.

The maximum energy efficiency of the decolorization of the indigo carmine dye obtained in this paper is ~5 μmol/kJ for positive direct discharges. This value is higher than the efficiency of decolorization of the indigo carmine dye achieved in [33], which is 3.7 μmol/kJ for the dye concentration of 0.05 g/L. This concentration is five-fold lower than the concentration used in this paper, 0.25 g/L. It was also shown that the efficiency of decolorization of the indigo carmine dye increases with an increase in the initial concentration of the dye in water [33]. The initial concentrations tested in [33] were in the range between 0.01 and 0.05 g/L. However, no experimental data are provided for higher concentrations.

The biological inactivation capability of impulsive discharges has been also investigated in this paper. *E. coli* and *S. aureus* were used as model gram-negative and gram-positive microorganisms, respectively. The inactivation results demonstrated the strong bactericidal effects produced by both surface and direct discharges. In the decontamination tests, all surviving CFUs on the whole plate surface were counted in order to obtain the inactivation rate. Therefore, this quantitative approach does not take into account nonuniformities in decontamination on the plate surface, and for example, the most significant decontamination effect on the agar surface was obtained directly under the HV needle; however, a decontamination effect was also observed at the edges of the plate surface. Table III summarizes the inactivation rates obtained in this paper.

It was established that the inactivation capability of direct discharges is substantially lower than that of surface discharges: the inactivation rates associated with direct discharges are ~two-fold lower than the inactivation rates of surface dischares, for both microorganisms, and for both polarities. In the case of the nonconductive sample holders, the surface discharges treat a larger surface area as compared with the direct discharges (treatment in the conductive sample holders). As microorganisms were seeded onto agar surfaces, the treatment with surface discharges resulted in a higher degree of inactivation for the same dose as compared with the direct transient discharges. Thus, the surface discharges demonstrated substantially higher biodecontamination rates. However, even in the case of direct discharges, transient plasma results in a notable reduction of the bacterial population on the agar surfaces. As in the case of dye solutions, the electrical conductivity and the pH of agar were measured before and after plasma treatment. It was found that, as in the case of dye solutions, the conductivity of agar increased. However, this increase was not negligible, the maximum change being observed for negative surface treatment: the electrical conductivity of agar before plasma treatment was ~1.1 mS/m, and the conductivity after such plasma treatment increased up to ~1.5 mS/m.

Using pH-sensitive strips, it was found that there was a change in pH of the agar beneath the HV needle electrode. The radius of the spot of the agar surface which differed from the initial pH value was ~3 mm. However, no change in pH was observed outside this localized spot on the agar surface (a pH value was ~7). This change in pH on the agar surface beneath the point HV electrode depends on the polarity of the HV impulses. For positive impulses, an increase in pH was registered (up to ~8 based on analysis of the color of the strip). For negative impulses, a decrease in pH was registered, down to ~5 based on analysis of the color of the strips. This increase in pH on the agar surface may be a result of the chemical action of cations produced by positive discharges—this suggestion is supported by the results obtained in [27], where it was found that the cations produced by positive corona discharges in air above the water surface resulted in an increase in the pH of water. Therefore, the observed difference in pH tendencies may help to explain the higher inactivation and decolorization rates for positive direct discharges obtained in this paper. However, further investigation into pH variations due to transient plasma discharges of both polarities is needed to provide more detailed information on the role of pH changes in plasma-induced inactivation and biodecontamination processes.

The higher decontamination efficiency for positive transient spark discharges was reported in [22], where *S. typhimurium* in water was treated with transient spark discharges, and it was found that positive transient sparks provided higher decontamination efficiency as compared with negative transient sparks. However, in the case of chemical oxidation capability, it was reported that the removal efficiency of cyclohexanone by the transient plasma spark discharges was ~50% for both polarities of transient spark discharges [19]. Further investigation is required to enable a more-detailed analysis of the biodecontamination and chemical oxidation efficacies of TAP discharges.

Also, it was found that *E. coli* has a higher sensitivity to both types of plasma discharge than *S. aureus*: the inactivation rates obtained for *E. coli* are more than two-fold higher than the inactivation rates for *S. aureus*. This result can potentially be

explained by the structural difference between gram-negative and gram-positive bacteria: the thicker peptidoglycan layer of gram-positive bacteria may help to protect their cells from the lethal damage caused by transient discharges.

The results obtained in this paper will help in the further understanding of the oxidation effects and microbiological inactivation capability of impulsive atmospheric discharges. These results may be used in potential design and optimization of plasma treatment systems based on transient discharges in atmospheric air.

REFERENCES

[1] L. A. Rosocha, "Nonthermal plasma applications to the environment: Gaseous electronics and power conditioning," *IEEE Trans. Plasma Sci.*, vol. 33, no. 1, pp. 129–137, Feb. 2005.

[2] A. Mizuno, "Industrial applications of atmospheric non-thermal plasma in environmental remediation," *Plasma Phys. Control. Fusion*, vol. 49, no. 5A, pp. A1–A15, 2007.

[3] B. Haertel, T. von Woedtke, K.-D. Weltmann, and U. Lindequist, "Non-thermal atmospheric-pressure plasma possible application in wound healing," *Biomolecules Therapeutics*, vol. 22, no. 6, pp. 477–490, 2014.

[4] R. Ono and T. Oda, "Optical diagnosis of pulsed streamer discharge under atmospheric pressure," *Int. J. Plasma Environ. Sci. Technol.*, vol. 1, no. 2, pp. 123–129, 2007.

[5] W. F. L. M. Hoeben, E. M. van Veldhuizen, W. R. Rutgers, and G. M. W. Kroesen, "Gas phase corona discharges for oxidation of phenol in an aqueous solution," *J. Phys. D, Appl. Phys.*, vol. 32, no. 24, pp. L133–L137, 1999.

[6] Z. Buntat, I. R. Smith, and N. A. M. Razali, "Ozone generation by pulsed streamer discharge in air," *Appl. Phys. Res.*, vol. 1, no. 2, pp. 2–10, 2009.

[7] P. Lukes, M. Clupek, V. Babicky, V. Janda, and P. Sunka, "Generation of ozone by pulsed corona discharge over water surface in hybrid gas–liquid electrical discharge reactor," *J. Phys. D, Appl. Phys.*, vol. 38, no. 3, pp. 409–416, 2005.

[8] D. M. Stanbury, "Reduction potentials involving inorganic free radicals in aqueous solution," *Adv. Inorganic Chem.*, vol. 33, pp. 69–138, 1989.

[9] M. A. Malik, A. Ghaffar, and S. A. Malik, "Water purification by electrical discharges," *Plasma Sour. Sci. Technol.*, vol. 10, no. 1, pp. 82–91, Feb. 2001.

[10] A. T. Sugiarto, S. Ito, T. Ohshima, M. Sato, and J. D. Skalny, "Oxidative decoloration of dyes by pulsed discharge plasma in water," *J. Electrostatics*, vol. 58, pp. 135–145, May 2003.

[11] X. Domènech, W. F. Jardim, and M. I. Litter, "Procesos avanzados de oxidación para la eliminación de contaminantes," in *Eliminación de Contaminantes por Fotocatálisis Heterogénea*, (in Spanish) M. A. Blesa, Ed. Argentina por Gráfica: Impreso en La Plata, 2001, pp. 3–26.

[12] D. Dobrynin, G. Fridman, G. Friedman, and A. Fridman, "Physical and biological mechanisms of direct plasma interaction with living tissue," *New J. Phys.*, vol. 11, pp. 1–26, Nov. 2009.

[13] G. Fridman *et al.*, "Comparison of direct and indirect effects of non-thermal atmospheric-pressure plasma on bacteria," *Plasma Process. Polym.*, vol. 4, no. 4, pp. 370–375, 2007.

[14] L. F. Gaunt, C. B. Beggs, and G. E. Georghiou, "Bactericidal action of the reactive species produced by gas-discharge nonthermal plasma at atmospheric pressure: A review," *IEEE Trans. Plasma Sci.*, vol. 34, no. 4, pp. 1257–1269, Aug. 2006.

[15] J. E. Foster, G. Adamovsky, S. N. Gucker, and I. M. Blankson, "A comparative study of the time-resolved decomposition of methylene blue dye under the action of a nanosecond repetitively pulsed DBD plasma jet using liquid chromatography and spectrophotometry," *IEEE Trans. Plasma Sci.*, vol. 41, no. 3, pp. 503–512, Mar. 2013.

[16] J. Foster, B. S. Sommers, S. N. Gucker, I. M. Blankson, and G. Adamovsky, "Perspectives on the interaction of plasmas with liquid water for water purification," *IEEE Trans. Plasma Sci.*, vol. 40, no. 5, pp. 1311–1323, May 2012.

[17] M. A. Malik, "Water purification by plasmas: Which reactors are most energy efficient?" *Plasma Chem. Plasma Process.*, vol. 30, no. 1, pp. 21–31, 2010.

[18] S. J. Macgregor, J. M. Koutsoubis, and S. M. Turnbull, "The design and operation of a compact high-voltage, high pulse repetition frequency trigger generator," *Meas. Sci. Technol.*, vol. 9, no. 11, pp. 1899–1905, 1998.

[19] Z. Machala, M. Morvová, E. Marode, and I. Morva, "Removal of cyclohexanone in transition electric discharges at atmospheric pressure," *J. Phys. D, Appl. Phys.*, vol. 33, no. 24, pp. 3198–3213, 2000.

[20] M. Janda, V. Martišovitš, and Z. Machala, "Transient spark: A dc-driven repetitively pulsed discharge and its control by electric circuit parameters," *Plasma Sour. Sci. Technol.*, vol. 20, no. 3, pp. 035015-1–035015-10, 2011.

[21] Z. Machala, E. Marode, M. Morvová, and P. Lukáč, "DC glow discharge in atmospheric air as a source for volatile organic compounds abatement," *Plasma Process. Polym.*, vol. 2, no. 3, pp. 152–161, 2005.

[22] Z. Machala *et al.*, "DC discharges in atmospheric air for bio-decontamination—Spectroscopic methods for mechanism identification," *Eur. Phys. J. D*, vol. 54, no. 2, pp. 195–204, 2009.

[23] Y. Minamitani, S. Shoji, Y. Ohba, and Y. Higashiyama, "Decomposition of dye in water solution by pulsed power discharge in a water droplet spray," *IEEE Trans. Plasma Sci.*, vol. 36, no. 5, pp. 2586–2591, Oct. 2008.

[24] E. Sysolyatina *et al.*, "Role of the charged particles in bacteria inactivation by plasma of a positive and negative corona in ambient air," *Plasma Process. Polym.*, vol. 11, no. 4, pp. 315–334, 2014.

[25] E. Stoffels, Y. Sakiyama, and D. B. Graves, "Cold atmospheric plasma: Charged species and their interactions with cells and tissues," *IEEE Trans. Plasma Sci.*, vol. 36, no. 4, pp. 1441–1457, Aug. 2008.

[26] Y. Gorbanev, D. O'Connell, and V. Chechik, "Non-thermal plasma in contact with water: The origin of specie," *Chem.-Eur. J.*, vol. 22, no. 10, pp. 3496–3505, 2016.

[27] J. L. Brisset, J. Lelievre, A. Doubla, and J. Amouroux, "Interactions with aqueous solutions of the air corona products," *Rev. Phys. Appl.*, vol. 25, no. 6, pp. 535–543, 1990.

[28] R. Zhang, C. Zhang, X. Cheng, L. Wang, Y. Wu, and Z. Guan, "Kinetics of decolorization of azo dye by bipolar pulsed barrier discharge in a three-phase discharge plasma reactor," *J Hazard Mater.*, vol. 142, nos. 1–2, pp. 105–110, 2007.

[29] M. Selma and K. Takashima, "Decolorization of indigo carmine dye by spark discharge in water," *Int. J. Plasma Environ. Sci. Technol.*, vol. 2, no. 1, pp. 56–64, 2008.

[30] J. Gao *et al.*, "Plasma degradation of dyes in water with contact glow discharge electrolysis," *Water Res.*, vol. 37, no. 2, pp. 267–272, 2003.

[31] Y. Z. Wen, H. J. Liu, W. P. Liu, and X. Z. Jiang, "Degradation of organic contaminants in water by pulsed corona discharge," *Plasma Chem. Plasma Process.*, vol. 25, no. 2, pp. 137–146, 2005.

[32] A. T. Sugiarto, T. Ohshima, and M. Sato, "Advanced Oxidation Processes Using Pulsed Streamer Corona Discharge In Water," *Thin Solid Films*, vol. 407, nos. 1–2, pp. 174–178, 2002.

[33] S. Muradia, "Study of low-voltage pulsed plasma discharges inside water using a bubble-generating porous ceramic electrode for wastewater treatment," Ph.D. dissertation, Dept. Nanovision Technol., Shizuoka Univ., Shizuoka, Japan, 2013.

Sirui Li was born in Yunnan, China, in 1988. He received the B.Eng. (Hons.) and M.Sc. degrees in electronic and electrical engineering from the University of Strathclyde, Glasgow, U.K., in 2010 and 2011, respectively, where he is currently pursuing the Ph.D. degree in non-thermal plasma discharge for air treatment and surface decontamination.

Igor V. Timoshkin (M'07–SM'14) received the degree in physics from Moscow State University, Moscow, Russia, in 1992, and the Diploma and Ph.D. degrees from the Imperial College of Science, Technology and Medicine, London, U.K., in 2001.

He was a Researcher with Moscow State Agro-Engineering University, Moscow, and then with the Institute for High Temperatures of Russian Academy of Sciences before moving to ICSTM in 1997. He joined the Department of Electronic and Electrical Engineering, University of Strathclyde, Glasgow, U.K., in 2001, where he became a Reader in 2016. His current research interests include properties of solid and liquid dielectric materials, electronics of plasma discharges in condensed media, practical applications of electro-hydraulic and high-power ultrasound pulses, and bio-dielectrics and effects of electromagnetic fields on biological objects.

Michelle Maclean was born in Lewis, U.K., in 1980. She received the B.Sc. (Hons.) degree in microbiology and immunology and the Ph.D. degree in electronic and electrical engineering from the University of Strathclyde, Glasgow, U.K., in 2002 and 2006, respectively.

She is currently a Research Fellow with the Robertson Trust Laboratory for Electronic Sterilization Technologies, University of Strathclyde. Her current research interests include the development and application of novel electro-technologies for biological decontamination and sterilization applications in clinical and public health environments.

Dr. Maclean is a member of The Society for General Microbiology and The American Society of Microbiology.

Scott J. MacGregor (M'95) received the B.Sc. and Ph.D. degrees from the University of Strathclyde, Glasgow, U.K., in 1982 and 1986, respectively.

He is currently with the University of Strathclyde, where he became a Pulsed-Power Research Fellow in 1986, a Lecturer in pulsed-power technology in 1989, a Senior Lecturer in 1994, and a Reader and a Professor of High-Voltage Engineering in 1999 and 2001, respectively. He has been the Dean of Engineering with the University of Strathclyde since 2010. His current research interests include high-voltage pulse generation, high-frequency diagnostics, high-power repetitive switching, high-speed switching, electronic methods for food pasteurization and sterilization, generation of high-power ultrasound (HPU), plasma channel drilling, pulsed-plasma cleaning of pipes, and stimulation of oil wells with HPU.

Mark P. Wilson (M'10) was born in Stranraer, U.K., in 1982. He received the B.Eng. (Hons.), M.Phil., and Ph.D. degrees from the University of Strathclyde, Glasgow, U.K., in 2004, 2007, and 2011, respectively, all in electronic and electrical engineering.

He is currently a Teaching Associate with the University of Strathclyde, where he continues to investigate surface flashover of solids immersed in insulating oil.

Dr. Wilson is a member of the IEEE Nuclear and Plasma Sciences Society, from whom he received a Graduate Scholarship Award in 2011, the IEEE Dielectrics and Electrical Insulation Society, and the IET.

Martin J. Given (M'99–SM'11) received the Degree in physics from the University of Sussex, Brighton, U.K., in 1981, and the Ph.D. degree in electronic and electrical engineering from the University of Strathclyde, Glasgow, U.K., in 1996.

He is currently a Senior Lecturer with the Department of Electronic and Electrical Engineering, University of Strathclyde. His current research interests include, ageing processes and condition monitoring in solid and liquid insulation systems, high speed switching, and pulse power applications.

Tao Wang received the B.Eng. and M.Sc. degrees from Northeast China Dianli University, Jilin, China, in 1993 and 1996, respectively, and the Ph.D. degree from the University of Strathclyde, Glasgow, U.K., in 2005.

He then joined the Newland Entech as a Research Fellow developing high efficiency industrial ozone generator. He joined the Department of Electronic and Electrical Engineering, University of Strathclyde, as a Lecturer in 2010. His current research interests include non-thermal gas discharges and their applications in gas synthesis, water disinfection and advanced oxidation process in water.

John G. Anderson was born in Glasgow, U.K., in 1942. He received the B.Sc. degree in applied microbiology and the Ph.D. degree in fungal physiology from the University of Strathclyde, Glasgow, in 1968 and 1971, respectively.

He has been with the Department of Bioscience and Biotechnology, University of Strathclyde, since 1971, where he became a Professor of Microbiology and the Head of Department of Bioscience and Biotechnology. He is currently an Emeritus Professor with the University of Strathclyde. His current research interests include various aspects of food, biomedical, and environmental microbiology with interdisciplinary collaboration on the application of electro-technologies for electronic pasteurization and sterilization.